ABSTRACT

OVERBY, DAVID THOMAS. Stress-Strain Behavior of ASTM A706 Grade 80 Reinforcement. (Under the direction of Dr. Mervyn Kowalsky and Dr. Rudolf Seracino)

In the seismic design of reinforced concrete structures, the overstrength of the steel reinforcement plays a critical role in the structure's ability to dissipate energy inelastically as unaccounted for strength could lead to sudden, non-ductile modes of failure. Thus, knowledge of the expected mechanical properties of the reinforcement being used is extremely important. The current availability of ASTM A706 grade 80 rebar material test results is very limited in regards to both strength and strain parameters. In response to this issue, a research program was developed to determine the stress-strain behavior of ASTM A706 grade 80 high strength steel reinforcement.

Three types of tests were performed in pursuit of this objective: monotonic tensile tests, cyclic tests, and strain age tests. A total of 788 tensile tests of A706 grade 80 rebar were performed on all bar sizes No. 4 through No. 18 in the as-rolled condition. Additional tests of No. 5 and No. 7 bars were used to investigate the strain aging and cyclic performance of the steel. Steel was provided by three producing mills and multiple heats were tested from each mill. A non-contact 3D position measurement system was used to simultaneously evaluating strains over multiple gage lengths for the full duration of each test, including fracture of the bar.

Results generated by the tensile tests are used to develop recommendations for the yield strength, yield strain, strain at onset of strain hardening, tensile strength, and ultimate tensile strain based on the mean values obtained across all bar sizes. The Kolmogorov-Smirnov goodness-of-fit test is used to identify the underlying probability distributions of the material properties which have been presented graphically with the empirical cumulative

distribution functions in order to illustrate the variability in the data. The A706 grade 80 monotonic stress-strain curve is shown to have a proportionally consistent shape to the A706 grade 60 rebar and may be characterized by existing reinforcing steel models. No consistent trend related to strain aging was observed for any of the experimental treatments. An existing reinforcing steel model was shown to successfully characterize the shape of the cyclic stress-strain curve. Limitations of the testing equipment precluded identification of any specific relationship between cyclic load history and ultimate tensile strain.

© Copyright 2016 David Thomas Overby

All Rights Reserved

Stress-Strain Behavior of ASTM A706 Grade 80 Reinforcement

by
David Thomas Overby

A thesis submitted to the Graduate Faculty of
North Carolina State University
in partial fulfillment of the
requirements for the degree of
Master of Science

Civil Engineering

Raleigh, North Carolina

2016

APPROVED BY:

_____	_____
Rudolf Seracino, Ph.D.	James M. Nau, Ph.D.

_____
Mervyn J. Kowalsky, Ph.D.
Committee Chair

BIOGRAPHY

David Thomas Overby was born in Merrillville, IN; however, much of his early years were spent in the mountains of Pennsylvania where he developed a love for the outdoors and a fascination with knowing how things worked. Coupled with a desire to be continually learning, his interest in science and math ultimately led him to pursue a degree in Civil Engineering following graduation from Gospel Light Christian School in Walkertown, NC in May, 2010. Four years later, he received a Bachelor of Science in Civil Engineering from North Carolina State University. Desiring to expand on his knowledge, David continued his education into graduate school at North Carolina State University where he received a Master of Science in Civil Engineering with an emphasis on Structural Engineering in 2016. David intends to bring the experience and knowledge gained from his education with him into a career in structural engineering.

ACKNOWLEDGMENTS

I would very much like to thank my advisor, Dr. Mervyn Kowalsky, for his enthusiasm in structural and earthquake engineering and his willingness to be so engaged with his students in the projects that they pursue together. I appreciate his high standard of achievement and desire to do things both well and thoroughly. I would additionally like to thank Drs. Rudi Seracino and James Nau for being members of my committee and for the real-world perspective they are able to bring both to the classroom and the research to which they contribute.

I would be remiss not to gratefully acknowledge the faithful support of the staff and students at the CFL who contributed so extensively to the completion of this project. In particular, I would like to extend a hearty thanks to Greg Lucier, Jerry Atkinson, and Johnathan McEntire for constantly providing advice on how to use the equipment at the lab, fixing things when they broke, and their patience through numerous hours of performing the tensile tests. I am further indebted to Emrah Tasdemir for assisting in the design of the large bar test setup, Aaron Stroud for his efforts in helping test the large diameter bars, and Grayson Fulp for helping prepare the rebar specimens for testing.

Additional thanks go to the California Department of Transportation for their financial support and interest in the project, to the three producing mills (Cascade, Gerdau, and Nucor) who graciously donated reinforcing bars for this research, and the Concrete Reinforcing Steel Institute (CRSI) and Bethany Hennings who coordinated with the mills to acquire the steel and provided special access to the CRSI database of mill tensile test results.

Above all, I thank God who has given my life a purpose and meaning beyond itself.

TABLE OF CONTENTS

LIST OF TABLES x

LIST OF FIGURES xii

1. INTRODUCTION 1

1.1. Background 1

1.2. Research Objective 4

1.3. Scope 6

1.3.1. Tensile Tests 6

1.3.2. Strain Age Tests 6

1.3.3. Cyclic Tests 7

1.4. Overview of Report Contents 7

2. LITERATURE REVIEW 10

2.1. A706 Grade 80 Rebar in Design Standards 10

2.1.1. ACI 318-14 10

2.1.2. Caltrans Seismic Design Criteria 10

2.1.3. AASHTO LRFD Bridge Design Specification 11

2.1.4. AASHTO Guide Specification for LRFD Seismic Bridge Design 11

2.1.5. WSDOT Bridge Design Manual 12

2.1.6. ODOT Bridge Design and Drafting Manual 12

2.1.7. Alaska DOT 12

2.2. Existing A706 Grade 80 Experimental Data 12

2.2.1. Research Data 14

2.2.1.1. Rautenberg et al. (2013) 14

2.2.1.2. WJE RGA 04-13 Report (2013) 15

2.2.1.3. GCR 14-917-30 (2014) 19

2.2.1.4. Trejo, Barbosa, and Link. (2014) 21

2.2.2. Mill and CRSI Data 23

2.3. Statistical Studies of Rebar Test Results 27

2.3.1. Allen (1972) 27
2.3.2. Mirza and MacGregor (1979) 28
2.3.3. Nowak and Szerszen (2003) 29
2.3.4. Bournonville et al. (2004) 29
2.4. Strain Aging Literature 31
2.4.1. Introduction to Strain Aging 31
2.4.2. Relevant Papers on Strain Aging 34
2.4.2.1. Pussegoda (1978) 34
2.4.2.2. Lim (1991) 36
2.4.2.3. Restrepo-Posada et al. (1994) 38
2.4.2.4. Momtahan et al. (2009) 39
2.4.2.5. Summary of Strain Aging Literature 41
2.5. Cyclic Testing Literature 43
2.5.1. Existing Material Models 45
2.5.1.1. Giuffre-Pinto (1970); Menegotto-Pinto (1973) 45
2.5.1.2. Filippou et al. (1983) 47
2.5.1.3. Monti-Nuti (1992) 48
2.5.1.4. Chang and Mander (1994) 49
2.5.1.5. Dhakal and Maekawa (2002) 50
2.5.2. Summary of Cyclic Testing Literature 51
3. EXPERIMENTAL PROGRAM 53
3.1. Chapter Overview 53
3.2. Materials 53
3.3. Equipment 56
3.3.1. Testing Equipment 56
3.3.2. Instrumentation 60
3.4. Tensile Testing 63
3.4.1. Test Matrix 63
3.4.2. Specimen Preparation 65

3.4.3. Test Parameters 67
3.4.4. Calibration of Custom Testing Rig 72
3.5. Strain Age Testing 76
3.5.1. Test matrix 76
3.5.2. Specimen Preparation 76
3.5.3. Testing Parameters 78
3.6. Cyclic Testing 79
3.6.1. Test Matrix 79
3.6.2. Specimen Preparation 81
3.6.3. Test Parameters 81
4. RESULTS 83
4.1. Chapter Overview 83
4.2. Tensile Testing 84
4.2.1. Determination of Stress-Strain Parameters 84
4.2.1.1. Modulus of Elasticity 85
4.2.1.2. Yield Strength 85
4.2.1.3. Yield Strain 86
4.2.1.4. Onset of Strain Hardening 86
4.2.1.5. Tensile Strength and Ultimate Tensile Strain 87
4.2.2. Statistical Methods 87
4.2.3. Expected Mechanical Properties 92
4.2.3.1. Modulus of Elasticity 92
4.2.3.2. ADM Yield Strength 94
4.2.3.3. EUL Yield Strength 97
4.2.3.4. OM Yield Strength 100
4.2.3.5. Yield Strain 103
4.2.3.6. Strain at Onset of Strain Hardening 106
4.2.3.7. Tensile Strength 109
4.2.3.8. Ultimate Tensile Strain 112
4.2.3.9. Tensile to Yield Ratio 115

4.2.3.10. Summary of Tensile Test Results 118
4.2.4. Shape of the Strain Hardening Curve 119
4.3. Strain Age Testing 124
4.3.1. Impact of Aging Period 125
4.3.2. Impact of Pre-Strain Level 129
4.3.3. Impact of Bar Size 133
4.3.4. Impact of Temperature 136
4.4. Cyclic Testing 139
4.4.1. Model Comparison 140
4.4.2. Effects of Load History on Ultimate Tensile Strain 141
4.4.2.1. Test ID: 12544 145
4.4.2.2. Test ID: 12547 146
4.4.2.3. Test ID: 12548 147
4.4.2.4. Test ID: 12549 148
4.4.2.5. Test ID: 125410 150
4.4.2.6. Test ID: 125411 151
4.4.2.7. Test ID: 12746 152
4.4.2.8. Summary Table 154
5. DISCUSSION 155
5.1. Tensile Tests 155
5.1.1. Comparison with Literature Results 155
5.1.2. Comparison with Mill and CRSI Data 158
5.1.2.1. Yield Strength 158
5.1.2.2. Tensile Strength 159
5.1.2.3. Percent Elongation at Fracture 160
5.1.2.4. Tensile-to-Yield Ratio 161
5.1.3. Analysis of Variabilities 163
5.1.3.1. Mills 163
5.1.3.2. Heats 165
5.1.3.3. Twenty-foot Bars 165

5.1.3.4. Heats by Bar Size 166
5.1.3.5. Summary 167
5.1.4. Parameter Interactions 168
5.1.4.1. f_{ye} vs ε_{sh} 169
5.1.4.2. f_{ye} vs f_{ue} 170
5.1.4.3. f_{ye} vs ε_{su} 171
5.1.4.4. f_{ue} vs ε_{su} 172
5.1.4.5. ε_{sh} vs ε_{su} 173
5.1.4.6. percent elongation vs ε_{su} 174
5.1.5. Yield Strengths Falling Below 80 ksi 177
5.1.6. Variability in Strain Over Bar Length 178
5.1.7. Future Tensile Testing 181
5.1.7.1. Effect of Testing 1 Specimen per Bar 181
5.1.7.2. Effect of Testing 1 Specimen per Bar per Heat 182
5.2. Strain Age Tests 183
5.2.1. Comparison with Literature Results 183
5.2.2. Future Strain Age Testing 184
5.3. Cyclic Tests 185
5.3.1. Future Cyclic Testing 185
6. CONCLUSIONS 187
6.1. Summary 187
6.2. Recommendations 189
7. REFERENCES 190
APPENDICES 197
8. Appendix A: Summary of Bar Sizes by Heat and Mill 198
8.1. Mill 1 198
8.2. Mill 2 198
8.3. Mill 3 198

9. Appendix B: Determination of Stress-Strain Parameters 199
9.1. Modulus of Elasticity 199
9.2. Yield Strength 200
9.3. Onset of Strain Hardening 200
10. Appendix C: Mill Cumulative Distribution Functions 201
10.1. ADM Yield Strength 201
10.2. Yield Strain 202
10.3. Onset of Strain Hardening 203
10.4. Tensile Strength 204
10.5. Ultimate Tensile Strain 205
10.6. Tensile-to-Yield Ratio 206
11. Appendix D: Heat Cumulative Distribution Functions 207
11.1. Yield Strength 207
11.2. Yield Strain 209
11.3. Onset of Strain Hardening 211
11.4. Tensile Strength 213
11.5. Ultimate Tensile Strain 215
12. Appendix E: 2” vs 8” Gage Length Comparison 217
12.1. Yield Strain 217
12.2. Onset of Strain Hardening 217
12.3. Ultimate Tensile Strain 218
13. Appendix F: Comparison of Yield Strength Determination Methods 219
14. Appendix G: Summary of Yield Behaviors 220
15. Appendix H: Strain-aging Stress-strain Curves 221
16. Appendix I: Additional No. 7 bar cyclic test 235
17. Appendix J: Test Photos 236

LIST OF TABLES

Table 2-1. Stress-strain data from Rautenberg et al. (2013) 15
Table 2-2. Stress-strain data provided in NIST GCR Report (2014) 20
Table 2-3. Material test results for A706 grade 80 rebar used in Trejo et al. (2014) 21
Table 2-4. Statistical summary of stress data for all A706 grade 80 and Dual A615/A706 grade 80 rebar (CRSI, 2013) 24
Table 2-5. Cascade Steel mill data referenced in Trejo et al. (2014) 27
Table 2-6. Impact of vanadium content on strain aging susceptibility of mild (grade 275) New Zealand bars (Pussegoda, 1978) 35
Table 2-7. Impact of titanium content on strain aging susceptibility of mild (grade 275) New Zealand bars for a range of pre-strain levels (Pussegoda, 1978) 36
Table 2-8. Extent of strain-aging following a 5% pre-strain as presented in Lim (1991) 37
Table 2-9. Percent increase in yield strength of New Zealand grade 300 reinforcing steel as a function of pre-strain level and duration of aging period (Momtahan et al., 2009) 41
Table 2-10. Cyclical load history used in Monti and Nuti (1992) 49
Table 3-1 Partial mill chemical compositions (including vanadium content) demonstrating conformity with ASTM requirements 55
Table 3-2. As-stamped type and grade of steel by producing mill and bar size 56
Table 3-3. Tensile test matrix illustrating number of tests performed 64
Table 3-4. Results from the additional 9 No. 11 and 9 No. 14 bar tests used to develop adjustment factors 76
Table 3-5. Number of strain age tests by bar size and aging period. Three pre-strain levels were evaluated for each category: 0.0075, 0.0150, and 0.0300 76
Table 3-6. Cyclic test matrix 80
Table 4-1. Complete list of parameters determined for each tensile test 85
Table 4-2. Probability distributions found to be acceptable fits to each parameter from the KS test at a 5% significance level in order of accuracy 89
Table 4-3. Shape parameter values used to define the fitted probability distributions 90
Table 4-4. Summary of tensile testing results and design recommendations by parameter (1 ksi = 6.9 MPa). 119
Table 4-5. Summary of tensile testing means and standard deviations by bar size (1 ksi = 6.9 MPa) 119
Table 4-6. Ultimate tensile strain occurring during tensile test following cyclic loading 154
Table 5-1. Percent difference between experimental and mill-based data 162
Table 5-2. Mill averages and variability between mills 164
Table 5-3. Mill coefficients of variation and average CV across the mills 164
Table 5-4. Coefficients of variation of averages - variability "between" (heats from a common mill for each bar size) 167
Table 5-5. Averages of coefficient of variation - variability "within" (a heat for a given bar size) 167
Table 5-6. Coefficients of variation of averages - variability "between" 168
Table 5-7. Averages of coefficient of variation - variability "within" 168

Table 5-8. Mill 3 Heat 7 mean yield strengths by bar size 178
Table 5-9. Average variabilities in the six strain values recorded for each parameter from each test..... 180
Table 5-10. Impact on recommendations considering only 1 specimen per 20' bar..... 182
Table 5-11. Impact on recommendations considering only 1 specimen per 20’ bar and 1 20’ bar per heat..... 183
Table 6-1. Recommendations for A706 grade 80 monotonic stress-strain parameters 189

LIST OF FIGURES

Figure 1-1. Illustration of trend for increased steel strength to associate with reduced ductility 2
Figure 1-2. Illustration of need for manufactures to produce steel with yield strength well above the minimum allowable 4
Figure 1-3. Explanation of monotonic stress-strain parameters 5
Figure 2-1. Stress-strain curves for three No. 7 bars from Rautenberg et al. (2013) 15
Figure 2-2. Grades 60 and 80 stress-strain curves for ASTM A615 and A706 reinforcing steel from WJE (2013) report having distinct yield plateaus 17
Figure 2-3. A615 and A706 grade 80 stress-strain curves from WJE (2013) report exhibiting a “roundhouse” curve 18
Figure 2-4. Dual A615/A706 grade 80 coiled rebar stress-strain curve from WJE (2013) report exhibiting a "roundhouse" curve 18
Figure 2-5. Stress-strain curves of No. 8 and No. 18 bars referenced in NIST GCR Report (2014). Original source: Nucor Steel Seattle, Inc. 20
Figure 2-6. Stress-strain curves of three No. 3 bars (Trejo et al. 2014) 22
Figure 2-7. Stress-strain curves of three No. 5 bars (Trejo et al. 2014) 23
Figure 2-8. Stress-strain curves of three No. 6 bars (Trejo et al. 2014) 23
Figure 2-9. Distribution of all A706 grade 80 and Dual A615/A706 grade 80 test results by bar size (CRSI, 2013) 25
Figure 2-10. Distribution of all A706 grade 80 and Dual A615/A706 grade 80 test results by production year (CRSI, 2013) 25
Figure 2-11. Yield strength normal distribution for all A706 grade 80 and Dual A615/A706 grade 80 rebar (CRSI, 2013) 26
Figure 2-12. Tensile strength normal distribution for all A706 grade 80 and Dual A615/A706 grade 80 rebar (CRSI, 2013) 26
Figure 2-13. Schematic illustration of strain aging showing increased yield strength (ΔY), increased tensile strength (ΔU), reduced ductility ($\Delta\varepsilon$), and reemergence of the yield plateau. Adapted from Lim (1991). 32
Figure 2-14. Illustration of strain aging effect on yield strength and the Bauschinger effect (Restrepo-Posada, 1994) 39
Figure 2-15. Impact of aging period on yield strength resulting from a pre-strain of $10\varepsilon_y$ (Momtahan et al., 2009) 41
Figure 2-16. Coupon test of 10 mm diameter bar having symmetric tension/compression cycles used to calibrate Giuffre-Pinto (1970) material model 47
Figure 2-17. Comparison of Dhakal and Maekawa (2002) model, including buckling, with test data from Monti and Nuti (1992) 51
Figure 3-1. Relative sizes of No. 4 (left) through No. 18 bars (right) provided by mills 54
Figure 3-2. Single 30" test specimen cut from one of three 20-foot straight bars (No. 7 shown) and labelled according to developed numbering scheme. 54

Figure 3-3. Crossheads of MTS machine used to test No. 4 through No. 10 bars (No. 10 bar shown) 57
Figure 3-4. Custom testing rig designed to test No. 11, 14, and 18 bars 59
Figure 3-5. Wedge-chuck system used to anchor No. 11, 14, and 18 bars (tested No. 18 bar shown) 59
Figure 3-6. Interface between bar and wedge grips 59
Figure 3-7. Epsilon class B1 2” gage length extensometer used to record strains during No. 4 through No. 10 bar tests (No. 4 bar shown) 60
Figure 3-8. Single gage length of Optotrak markers on a No. 7 bar 61
Figure 3-9. Test setup showing MTS machine, extensometer, and Optotrak camera aimed at test specimen 62
Figure 3-10. Illustration of 3 heats, 3 20-foot bars, and 3 individual test specimens from a single mill (No. 7 bars shown) 63
Figure 3-11. No. 18 bar wedges undamaged (left) and after testing Mill 1 bars (right) 64
Figure 3-12. Numbering scheme used to uniquely identify each test specimen 66
Figure 3-13. Location and spacing of Optotrak markers on a No. 4 bar and illustration of six 2" and three overlapping 8" gage lengths 67
Figure 3-14. Back-calculated load rate of a No. 8 bar tested in the MTS machine confirming the specified 1 in/min displacement rate 69
Figure 3-15. Wedge-seating phenomenon observed in No. 11-No. 18 bar tests 71
Figure 3-16. Results of single No. 11 bar test showing impact of neglecting losses resulting from location the load cell away from the test specimen 73
Figure 3-17. Modified test setup with one 200-kip load cell in-line with the test specimen and another 200-kip load cell on a separate jack connected to the same hydraulic source 74
Figure 3-18. Relationship between the on-bar load cell and the off-bar load cell forces for 9 No. 11 and 9 No. 14 bar tests 75
Figure 3-19. No. 7 strain-age test bars returning to ambient temperatures after removing from the freezer. Visible ice formation from moisture in the laboratory air. 78
Figure 3-20. No. 7 bar in MTS machine prior to testing 82
Figure 4-1. Partially plotted stress-strain curve (left) and distribution of strain over instrumented region at that instant (right) 91
Figure 4-2. Modulus of elasticity empirical CDFs including all bar sizes 93
Figure 4-3. Modulus of elasticity empirical CDFs for individual bar sizes 94
Figure 4-4. ADM yield strength beta and empirical CDFs including all bar sizes 96
Figure 4-5. ADM yield strength empirical CDFs for individual bar sizes 97
Figure 4-6. EUL yield strength empirical CDFs including all bar sizes 99
Figure 4-7. EUL yield strength empirical CDFs for individual bar sizes 100
Figure 4-8. OM yield strength empirical CDFs including all bar sizes 102
Figure 4-9. OM yield strength empirical CDFs for individual bar sizes 103
Figure 4-10. Yield strain gamma and empirical CDFs including all bar sizes 105
Figure 4-11. Yield strain empirical CDFs for individual bar sizes 106
Figure 4-12. Strain at onset of strain hardening empirical CDFs including all bar sizes (lognormal distribution shown for reference purposes only) 108

Figure 4-13. Strain at onset of strain hardening empirical CDFs for individual bar sizes ... 109
Figure 4-14. Tensile strength lognormal and empirical CDFs including all bar sizes 111
Figure 4-15. Tensile strength empirical CDFS for individual bar sizes 112
Figure 4-16. Ultimate tensile strain Weibull and empirical CDFs including all bar sizes ... 114
Figure 4-17. Ultimate tensile strain empirical CDFs for individual bar sizes 115
Figure 4-18. Tensile-to-yield ratio gamma and empirical CDFs including all bar sizes..... 117
Figure 4-19. Tensile-to-yield ratio empirical CDFs for individual bar sizes..... 118
Figure 4-20. A706 grade 80 stress-strain curves for all tensile tests 121
Figure 4-21. Overlay of King Model on all stress-strain curves using recommended parameter values (King et al., 1986)..... 122
Figure 4-22. Overlay of Raynor Model on all stress-strain curves using recommended parameter values (Raynor et al., 2002) 123
Figure 4-23. Overlay of an A706 grade 60 curve on all experimental stress-strain curves.. 124
Figure 4-24. Impact of aging period on tensile strength of No. 5 bars 126
Figure 4-25. Impact of aging period on tensile strength of No. 7 bars 127
Figure 4-26. Impact of aging period on ultimate tensile strain of No. 5 bars..... 128
Figure 4-27. Impact of aging period on ultimate tensile strain of No. 7 bars..... 129
Figure 4-28. Impact of pre-strain level on tensile strength of No. 5 bars 130
Figure 4-29. Impact of pre-strain level on tensile strength of No. 7 bars 131
Figure 4-30. Impact of pre-strain on ultimate tensile strain of No. 5 bars..... 132
Figure 4-31. Impact of pre-strain on ultimate tensile strain of No. 7 bars..... 133
Figure 4-32. Impact of bar size on tensile strength after strain aging..... 135
Figure 4-33. Impact of bar size on ultimate tensile strain after strain aging 136
Figure 4-34. Impact of temperature on tensile strength of No. 7 bars 138
Figure 4-35. Impact of temperature on ultimate tensile strain of No. 7 bars 139
Figure 4-36. Comparison of cyclic test of No. 7 bar with OpenSees Reinforcing Steel Material (Mazzoni et al. 2007) model..... 141
Figure 4-37. Strain history of a No. 5 bar (12547) tested in force-control mode showing obvious strain "drifting"..... 142
Figure 4-38. Stress history of the same No. 5 bar tested in force-control mode showing constant stress while strains “drifted”..... 143
Figure 4-39. Unexpected buckled shape of a No. 7 bar tested in pure compression ($L/d_{bl} = 5$) 144
Figure 4-40. Buckled shapes of No. 7 bars tested in pure compression ($L/d_{bl} = 8$ to $L/d_{bl} = 4$) indicating poor fixity of the boundary conditions (MTS machine grips) 145
Figure 4-41. Cyclic test of a No. 5 bar (12544) followed by tensile test to failure 146
Figure 4-42. Cyclic test of a No. 5 bar (12547) followed by tensile test to failure 147
Figure 4-43. Cyclic test of a No. 5 bar (12548) followed by tensile test to failure 148
Figure 4-44. Cyclic test of a No. 5 bar (12549) followed by tensile test to failure 149
Figure 4-45. Cyclic test of a No. 5 bar (125410) followed by tensile test to failure 150
Figure 4-46. Cyclic test of a No. 5 bar (125411) followed by tensile test to failure 152
Figure 4-47.Cyclic test of a No. 7 bar (12746) followed by tensile test to failure 153
Figure 5-1. WJE (2013) stress-strain curves superimposed over project data..... 156

Figure 5-2. GCR (2014) stress-strain curves superimposed over project data (plotted up to ε_{su}) 157
Figure 5-3. Trejo et al. (2014) stress-strain curves superimposed over project data (plotted up to ε_{su}) 157
Figure 5-4. Empirical CDFs comparing project, CRSI, and mill certificate yield strength data 159
Figure 5-5. Empirical CDFs comparing project, CRSI, and mill certificate tensile strength data 160
Figure 5-6. Empirical CDFs comparing project, CRSI, and mill certificate elongation at fracture data 161
Figure 5-7. Empirical CDFs comparing project, CRSI, and mill certificate tensile-to-yield ratio data 162
Figure 5-8. Interaction between yield strength and onset of strain hardening strain 170
Figure 5-9. Interaction between yield strength and tensile strength 171
Figure 5-10. Interaction between yield strength and ultimate tensile strain 172
Figure 5-11. Interaction between tensile strength and ultimate tensile strain 173
Figure 5-12. Interaction between strain at the onset of strain hardening and ultimate tensile strain 174
Figure 5-13. Interaction between Optotrak-based percent elongation at fracture and ultimate tensile strain measurements 175
Figure 5-14. Change in variation between gage lengths with increasing strain 180

1. INTRODUCTION

1.1. Background

The basic principles of seismic design follow the capacity design philosophy as outlined by Paulay and Priestley (1992) that consists of three steps: (1) Locations of inelastic action are chosen; (2) The chosen locations are detailed to sustain the deformation demands expected during the design basis earthquake; and (3) All other elements of the system are protected against inelastic action. In the case of seismic design of reinforced concrete bridges, locations of inelastic action occur in the columns, while all other actions in the column (i.e. shear), and all other elements in the bridge (i.e., footing, cap-beams, joints, superstructure) are protected against failure. This role is switched in the case of reinforced concrete frames such that the columns are designed to remain elastic while the beams dissipate energy though plastic hinge formation. In all cases, it is the reinforcing steel that acts as the critical link between a ductile response and a brittle failure. As a consequence, reinforcing steel used in seismic applications must possess large inelastic strain capacity (ductility) as well as sufficient strain hardening to ensure the spread of plasticity over the plastic hinge and reduce the maximum strains occurring at a given point. Furthermore, strength properties should be tightly controlled to ensure efficiency in design by limiting the overstrength factor for the design of capacity protected members and actions.

In regions where high seismicity requires large quantities of reinforcing steel to ensure adequate ductility, congestion at joints is a major problem. The use of high strength reinforcing steel in these cases offers a potential solution to this problem; however, as

illustrated in Figure 1-1, one of the concerns associated with the use of high strength rebar in seismic design is the general trend that as the strength of the steel increases, its maximum elongation capacity reduces, a trend which could undermine its potential benefits. As such, numerical test data must be available to validate its use.

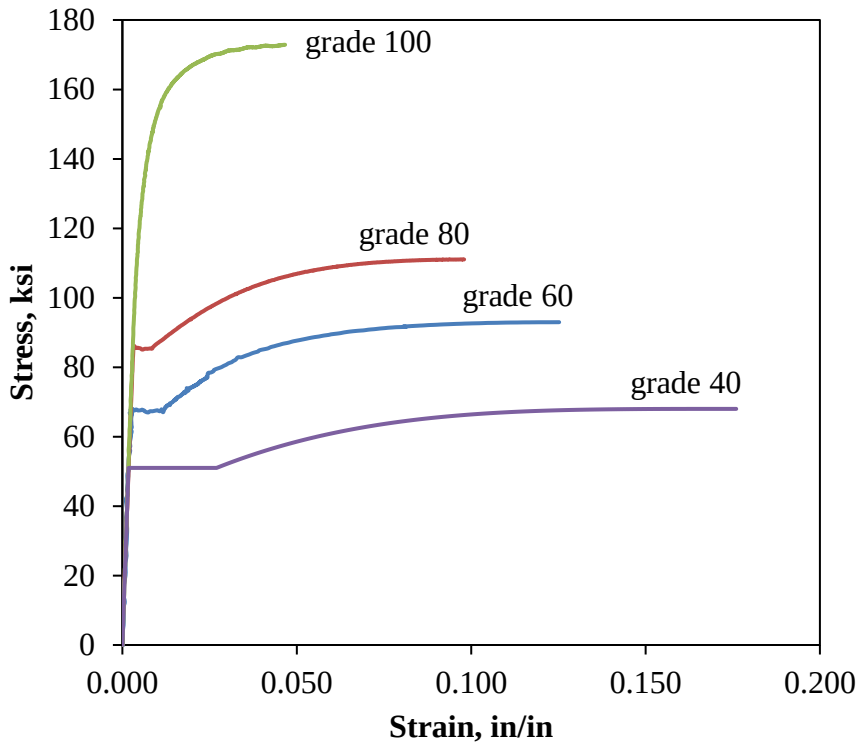

Figure 1-1. Illustration of trend for increased steel strength to associate with reduced ductility

Currently, the two most common designations for reinforcing steel in the US are ASTM A615 and ASTM A706. The less tightly controlled material properties of A615 reinforcement (ASTM A615, 2016) make it an undesirable choice in the context of seismic design. Conversely, A706 reinforcement must adhere to specific requirements regarding not only minimum, but also maximum yield strength as well as sustain larger elongations and

meet specific chemical composition requirements (ASTM A706, 2016). As a consequence, ASTM A706 steel is routinely specified for members expected to form plastic hinges, and is often used for all reinforcing steel in high seismic regions.

Prior to December 2009, the only grade of rebar available in the A706 specification was grade 60. Since that time, ASTM has included requirements for an 80 ksi (550 MPa) steel (A706 grade 80) in the A706 specification. The grade designation denotes the minimum allowable yield strength of the steel.

Because grade requirements are specified in terms of a minimum allowable value, it follows that actual reinforcing steel strengths should be higher than their specified values as producing mills must maintain an average strength that is safely above the minimum in order to remain profitable (Figure 1-2). Failure to account for this material overstrength in seismic design could lead to failure of capacity protected members due to unexpectedly high moment demands arising from the increased strength of the adjoining member provided by the steel reinforcement. Conservative material overstrength factors may be used to account for this behavior where actual (expected) material properties are unavailable; however, this leads to inefficient design with excess reinforcement that complicates construction and increases cost.

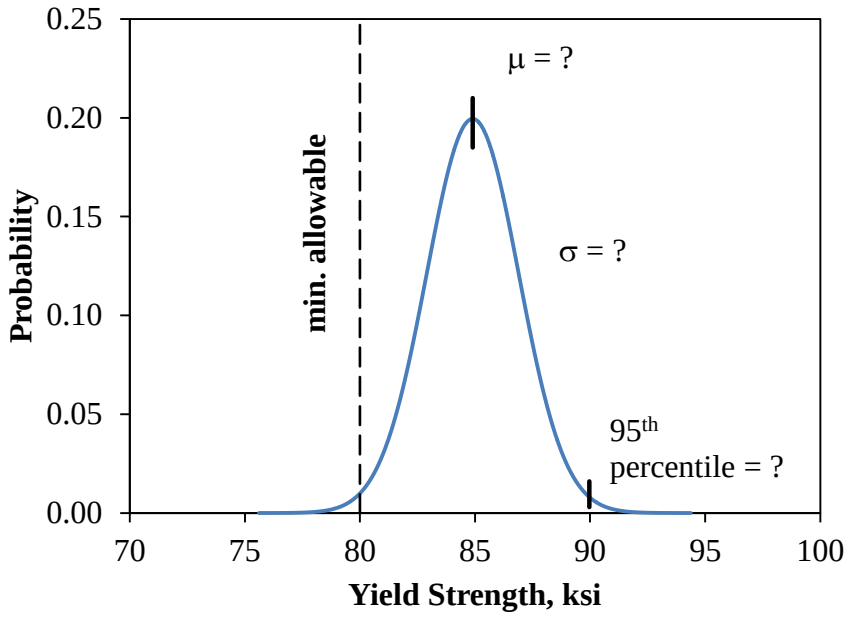

Figure 1-2. Illustration of need for manufactures to produce steel with yield strength well above the minimum allowable

1.2. Research Objective

Given the potential benefits of using A706 grade 80 rebar in seismic design, and considering the current limitations hindering its ready use in this context, the research presented in this paper aims to expand the existing knowledge base on the stress-strain behavior of A706 grade 80 rebar. The following items are identified as critical elements to be addressed in fulfilment of this task:

1. Determine the expected (mean) values of all parameters necessary to define the monotonic stress-strain curve (Fig. 1-3):
   - modulus of elasticity
   - yield strength

- yield strain
- strain at onset of strain hardening
- tensile strength
- ultimate tensile strain

2. Demonstrate the shape of the monotonic stress-strain curve
3. Evaluate the ability of existing monotonic and cyclic reinforcing steel models to accurately characterize the stress-strain curve when defined by the expected parameter values
4. Identify susceptibility to the strain-aging phenomenon and any contributing factors
5. Investigate the impact of cyclic load history on the ultimate tensile strain parameter

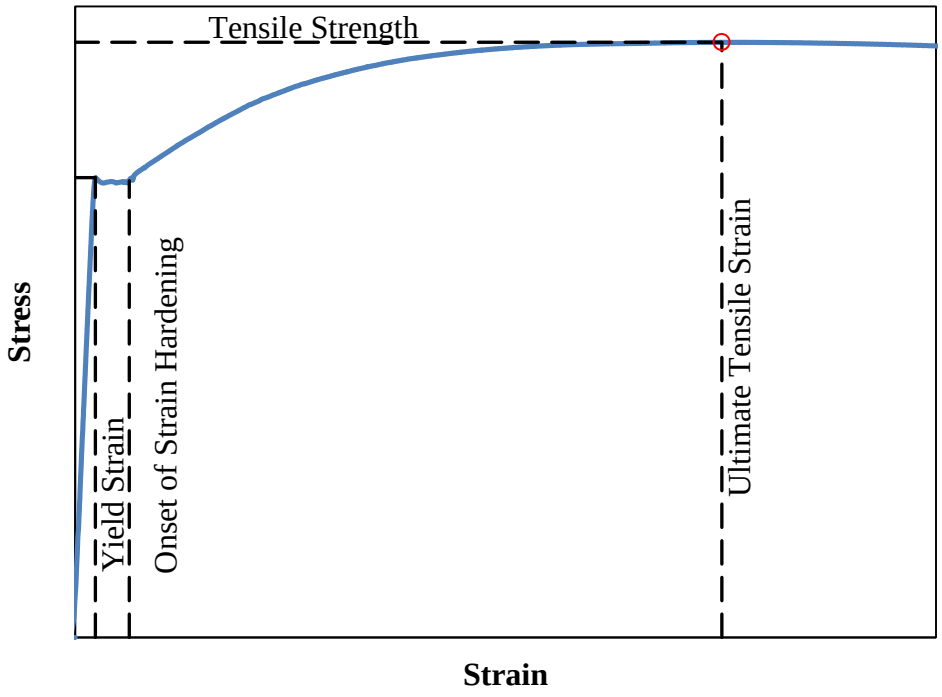

Figure 1-3. Explanation of monotonic stress-strain parameters

1.3. Scope

The research objectives presented above are addressed through the experimental testing and post-processing statistical analysis of A706 grade 80 rebar in the as-rolled condition at North Carolina State University Constructed Facilities laboratory. The reinforcing steel used in the research originated from three west coast producing mills: Cascade Steel Rolling Mills (McMinnville, OR), Gerdau Ameristeel (Rancho Cucamonga, CA), and Nucor Steel Seattle (Seattle, WA). Each mill provided three heats (batches) of bars for each of the ten major bar sizes: No. 4 through No. 18. Three types of tests were performed in pursuit of the research objectives: monotonic tensile tests, cyclic tests, and strain age tests.

1.3.1. Tensile Tests

The tensile testing program constituted the majority of the research effort in terms of number of tests and level of analysis of the findings. A total of 788 tests were performed in order to represent a statistically-defendable sampling from all of the mills, heats, and bar sizes provided. This portion of the research served to address objectives 1, 2, and 3.

1.3.2. Strain Age Tests

A subset of the reinforcing bars was used to evaluate the strain aging performance of the steel. In total, 39 tests were performed on No. 5 and No. 7 bars in order to evaluate the effect of bar size, pre-strain level, aging period, and temperature on the strain aging behavior of A706 grade 80 rebar. This portion of the research served to address objective 4.

1.3.3. Cyclic Tests

An additional subset of bars was used to evaluate the cyclic stress-strain behavior of the steel. A total of 13 tests were performed on No. 5 and No. 7 bars in order to address objectives 3 and 5.

1.4. Overview of Report Contents

Chapter 1 introduces the subject of A706 grade 80 rebar and gives context to the research presented in the following chapters. Specifically, it describes the role of reinforcing steel in seismic design, the advantages of using high strength rebar, the history of A706 grade 80 rebar, and its current place in the role of seismic design. Also presented are the research objectives and scope of the project.

Chapter 2 summarizes relevant background literature used to substantiate the research effort, direct its approach, and evaluate its findings. First, a review of the limitations on A706 grade 80 rebar in current design standards is used to illustrate the need for the present research. Following this, an overview of the existing papers, reports, and databases containing A706 grade 80 experimental data is presented to further demonstrate the need for the current research as well as provide a point of reference for evaluating the experimental findings. A third section focuses on previous approaches to the statistical analysis of rebar tensile test data. The literature findings presented in this section are used to direct the methods employed in evaluating the data generated from the experimental tests and evaluating it for anomalies. The chapter concludes with an introduction to strain aging and how it has been previously studied with regards to reinforcing steel as well as an overview of

currently available cyclic material models, how they were defined, and which parameters are necessary to defining each one.

Chapter 3 covers all aspects of the experimental testing portions of the project. Included in this chapter is a detailed presentation of the material that was tested as well as a thorough description of the equipment and instrumentation used in the testing. Procedures specific to each of the three types of tests (tensile, strain age, and cyclic) are described in their own section. These sections each contain details such as test matrix, parameters investigated, specimen preparation, and testing procedure.

Chapter 4 presents the results of the experimental testing portions of the project broken down according to the three types of tests performed. Included is a description of how each of the tensile test parameters where determined and what statistical methods were employed in aggregating and evaluating the test results which have been presented as empirical and best-fit cumulative distribution functions to demonstrate the variability in the data. The shape of the monotonic stress-strain curve is presented graphically and compared with existing material models calibrated with the test results. The impact of aging period, pre-strain level, bar size, and temperature on the strain aging performance is also presented graphically. The chapter concludes with a section addressing the cyclic behavior of the steel.

Chapter 5 discusses the results presented in Chapter 4 in the context of existing test data found in the literature and additionally explores trends and anomalies observed in the test results. Specifically, this includes a comparison of the literature monotonic stress-strain curves with those obtained from the tensile tests, a comparison of the tensile test results with available mill certificate reports, an assessment of the variability in test results occurring

between the three mills, the heats within a mill, and the individual lengths of bar within a heat. Also included is an investigation of the correlation between monotonic stress-strain parameters, a summary of test results failing to meet the ASTM requirements, and an observation on how strains vary over the length of bar in a tensile test. A few comments are offered based on the results of the strain aging and cyclic test results in order to relate them back to the literature review findings. The chapter closes with a proposal for future work in the areas of tensile testing, strain age testing, and cyclic testing of A706 grade 80 rebar based on the research findings.

Chapter 6 summarizes the conclusions from the research, including final recommendations on the monotonic stress-strain curve parameter values, and relates the findings back to the initial research objectives.

2. LITERATURE REVIEW

2.1. A706 Grade 80 Rebar in Design Standards

The overall lack of experimental data on A706 grade 80 rebar in the literature is reflected in the hesitancy of design codes to allow its use in regions expected to form plastic hinges. In some cases, the use of A706 grade 80 reinforcement is directly restricted while in others it is passively restricted by setting upper limits on yield strength that are below 80 ksi (550 MPa). A brief summary of the guidelines (or lack thereof) for use of A706 grade 80 steel in design codes is presented below.

2.1.1. ACI 318-14

ACI 318-14 Section 20.2.2 limits deformed reinforcement used in special seismic systems to be of grade 60 or lower "because of insufficient data to confirm applicability of existing code provisions for structures using the higher grade [A706 grade 80]" (ACI 318-14). However, the commentary to Section 18.2.6 makes provision for higher grades where sufficient test data is available to support their use: "Section 18.2.1.7 permits alternative material such as ASTM A706 Grade 80 if results of tests and analytical studies are presented in support of its use" (ACI 318-14).

2.1.2. Caltrans Seismic Design Criteria

Section 3.2 of the Caltrans SDC 1.7 limits the range in yield stress of ASTM A706 reinforcement to between 60 ksi and 78 ksi. The use of ASTM A706 grade 80 reinforcing steel is not directly addressed.

2.1.3. AASHTO LRFD Bridge Design Specification

Based on research by Shahrooz et al. (2011), the AASHTO LRFD Bridge Design Specification (AASHTO 2014) permits the use of reinforcing steel with specified minimum yield strength of up to 100 ksi (690 MPa) for all elements and connections in Seismic Zone 1 where permitted by specific articles. Section C5.4.3.3 states that "Reinforcing steels with a minimum specified yield strength between 75.0 and 100 ksi may be used in seismic applications, with the Owner's approval, only as permitted in the *AASHTO Guide Specifications for LRFD Seismic Bridge Design*" (AASHTO 2014). This implies that A706 grade 80 reinforcing steel is permissible, subject to specific constraints.

2.1.4. AASHTO Guide Specification for LRFD Seismic Bridge Design

Section 8.4.1 of the AASHTO Guide Spec. for LRFD Seismic Bridge Design (AASHTO 2011) states that "ASTM A 706 Grade 80 reinforcing steel may be used in capacity-protected members as specified in Article 8.5 but shall not be used in members where plastic hinging is expected". It is further stated in the accompanying commentary that this allowance was made due to the strength control and elongation characteristics of A706 grade 80 reinforcement, and that it has not been permitted on plastic hinge regions due, in part, to a lack of stress-strain data. Only ASTM A615 grade 60 (in seismic design categories B and C, with the owner's approval) or A706 grade 60 reinforcing steel is allowed in members expected to form a plastic hinge.

2.1.5. WSDOT Bridge Design Manual

The Washington Department of Transportation Bridge Design Manual (WSDOT 2015) Section 5.1.2 permits the unrestricted use of A706 grade 80 reinforcement in regions having Seismic Design Category (SDC) A, but limits its use to only capacity protected members for SDCs B, C, and D.

2.1.6. ODOT Bridge Design and Drafting Manual

Section 1.5.5.1.17 of the Oregon Department of Transportation Bridge Design and Drafting Manual is specifically devoted to the use of ASTM A706 grade 80 reinforcement (ODOT 2015). The manual states that A706 grade 80 reinforcement may not be used in members designed for plastic seismic performance such as bridge columns due to limited experimental testing.

2.1.7. Alaska DOT

The Alaska DOT currently uses A706 grade 60 rebar for the design of members expected to form a plastic hinge; however, A706 grade 80 has been specified for capacity protected members in accordance with the AASHTO specifications (Elmer Marx, AKDOT, personal communication, April 1, 2016).

2.2. Existing A706 Grade 80 Experimental Data

Just five reports were found to include material test results on A706 grade 80 steel either in tabulated or graphical form. Of the five reports, only two unique datasets could be confirmed: one consisting of three No. 7 bar tests (Rautenberg et al., 2013) and one consisting of three No. 3, three No. 5, and three No. 6 bar tests (Trejo et al., 2014). The

earliest of the five reports was completed in 2013, two were completed in March of 2014, and the most recent paper was published in June of 2015. This is not surprising considering the relatively recent introduction of grade 80 rebar into the ASTM A706/A706M specification in 2009.

The available experimental data is further limited in that only a few bar sizes have been considered and that strains have generally not been provided to accompany the included yield and tensile strength data. This is particularly true with data provided by the producing mills as they generally lack the necessary equipment required to capture strains. It should also be considered that because data obtained from producing mills does not necessarily stem from ideal laboratory conditions using appropriate, carefully calibrated measurement equipment and trained personnel, it should not be used for design purposes. This limitation extends to the Concrete Reinforcing Steel Institute (CRSI) Mill Databases which, while offering insight into the increased use and testing of A706 grade 80 rebar between 2011 and 2013, are composed of submitted mill test results.

By consequence of the extremely limited amount of data found in the available literature, what does exist is not sufficient to generate recommendations on the material properties of A706 grade 80 rebar. Rather, these findings simply served as reference points to validate trends and identify anomalies arising during the testing phase of the project. A graphical comparison of the literature-based stress-strain curves with the experimental curves generated through this project is presented in Chapter 5.

2.2.1. Research Data

2.2.1.1.Rautenberg et al. (2013)

Rautenberg et al. (2013) presented the findings of a study on the applicability of high-strength reinforcement in reinforced concrete columns resisting lateral earthquake loads. The primary goal of the research, which was based on testing conducted as part of Rautenberg's PhD dissertation at Purdue in 2011 (Rautenberg, 2011), was to evaluate the 60 ksi limit imposed by the American Concrete Institute (ACI) on the yield strength of rebar used in regions expected to form plastic hinges (ACI 318-11). A total of 8 columns consisting of either ASTM A706 grade 60, A706 grade 80, or A1035 grade 120 longitudinal reinforcement were considered in the analysis. Material testing was conducted for the purpose of calibrating numerical models of full-scale buildings subjected to strong ground motions. Of particular interest are the tensile tests that were performed on three A706 grade 80 No. 7 bars. The test specimens all originated from the same heat and were tested in a Baldwin 120-kip capacity universal testing machine upgraded with Instron control and data acquisition equipment. An Instron extensometer having two inch gauge length was used to acquire the strains. Tests were performed in compliance with ASTM A370 (2009). Data from the tests, which is publicly available on the NEES website (NEES, 2009), is presented in Table 2-1.

Table 2-1. Stress-strain data from Rautenberg et al. (2013)

Specimen Number	Yield Strength		Tensile Strength		Elong. % in 8 inch
	Stress, ksi	Strain, in/in	Stress, ksi	Stress, ksi	
7a	83	---	119	---	11.7
7b	83	---	117	---	15.6
7c	84	---	118	---	14.8

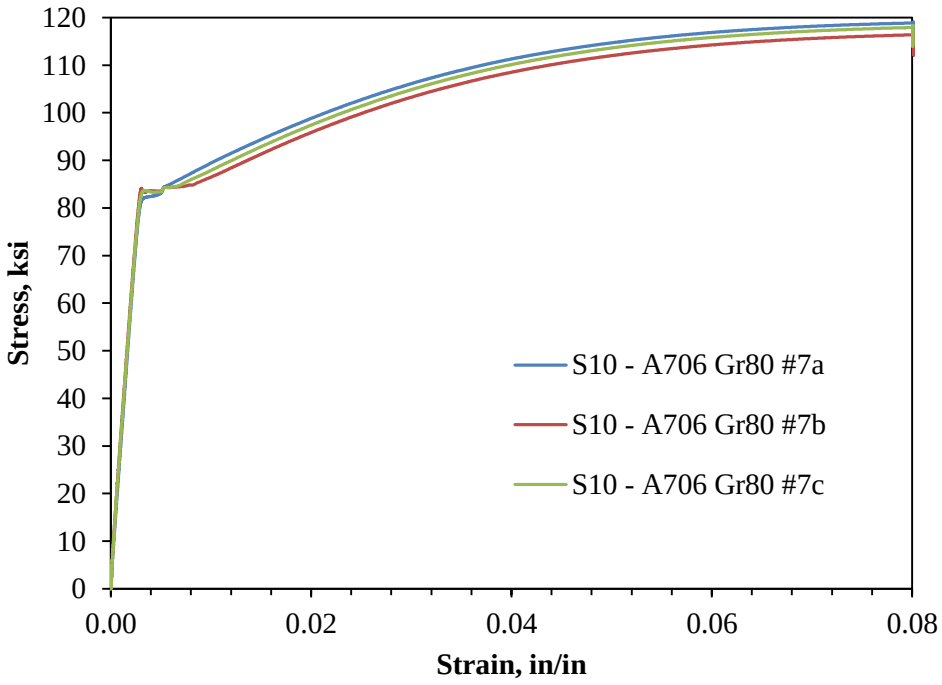

Figure 2-1. Stress-strain curves for three No. 7 bars from Rautenberg et al. (2013)

2.2.1.2.WJE RGA 04-13 Report (2013)

A report submitted to the Charles Pankow Foundation in late 2013 by Wiss, Janney, Elstner and Associates, Inc. (WJE, 2013) seeking to determine if it would be appropriate for

ACI to revise the ACI 318-14 required method for measuring the yield strength of nonprestressed reinforcement without a well-defined yield point from the extension under load (EUL) method at a strain of 0.0035 to the offset method (OM) at an offset strain of 0.2 percent, presented a number of monotonic stress-strain curves for A706 grade 80 rebar. While tabulated values of stress and strain were not provided as part of the report, the general shape of the curves can be insightful. Data used to define the curves originated from the 2012 and 2013 CRSI Mill Databases, the archives of the WJE laboratory, and testing at a university research laboratory. Because the CRSI Mill Databases are composed of data provided by producing mills, they only contain data on yield strength, tensile strength, and percent elongation at fracture. The question of how WJE could have used this data to produce curves without the necessary strains is answered by noting that CRSI coordinated the collection of industry-recorded stress-strain curves specifically for their project.

Several of the stress-strain curves presented in the WJE (2013) report exhibit distinct yield plateaus (Fig. 2-2) while others have a more "roundhouse" distribution (Figures 2-3 and 2-4). It should be noted that while Figure 2-2 includes curves for A615 grades 60 and 80 and A706 grades 60 and 80 bars, the report did not distinguish between specifications for either of the grades. Similarly, Figure 2-3 presents curves for both A615 and A706 grade 80 bars but does not clarify which are A615 and which are A706. According to the report, 98% of the straight bar curves had a well-defined or sharp yield point while all of the coiled bar curves had the "roundhouse" distribution. Additionally, the coiled reinforcing bar curves had distinctly lower elastic moduli – on the order of 21,000-22,000 ksi. Black dashed lines are

actual tests while red solid lines represent “normalized” stress-strain relations generated to have ideal properties.

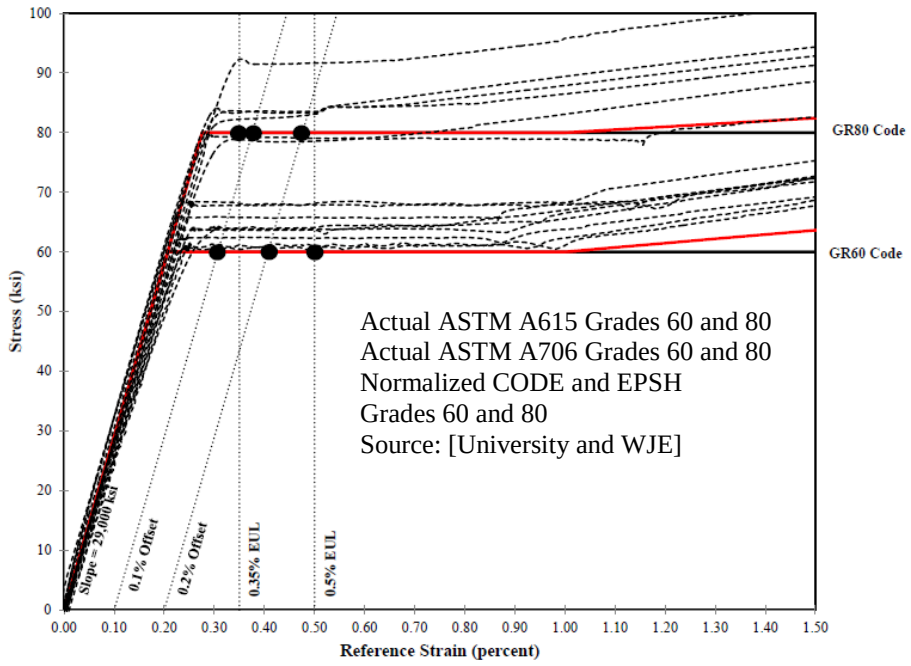

Figure 2-2. Grades 60 and 80 stress-strain curves for ASTM A615 and A706 reinforcing steel from WJE (2013) report having distinct yield plateaus

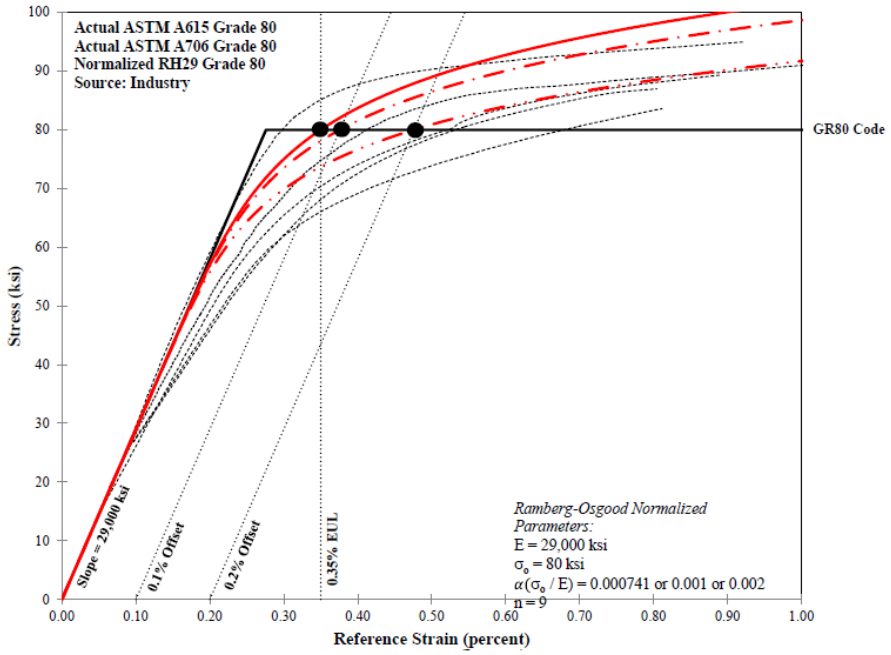

Figure 2-3. A615 and A706 grade 80 stress-strain curves from WJE (2013) report exhibiting a "roundhouse" curve

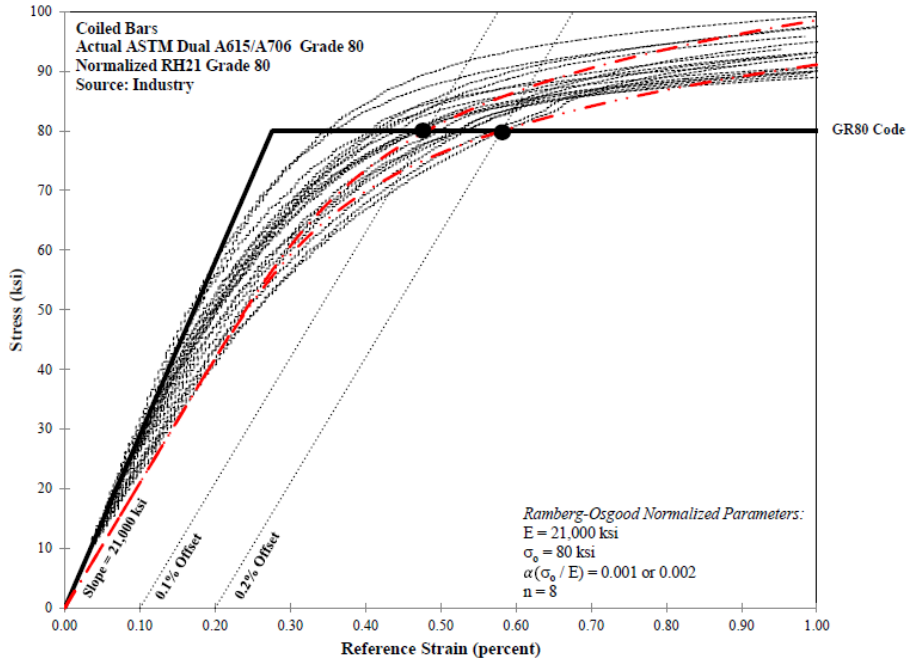

Figure 2-4. Dual A615/A706 grade 80 coiled rebar stress-strain curve from WJE (2013) report exhibiting a "roundhouse" curve

2.2.1.3.GCR 14-917-30 (2014)

A detailed report produced by the National Earthquake Hazards Reduction Program (NEHRP) Consultants Joint Venture (GCR, 2014) in March 2014 focused on the use of high-strength reinforcement (f_y greater than 60 ksi) in special moment frames and special structural walls. A parametric study of four building models reinforced with grades 60, 80, and 100 longitudinal reinforcement subjected to actual recorded ground motions revealed that the different grades offered comparable performance in the considered earthquakes. Results from the study were used to validate a proposal to ACI recommending A706 Grade 80 reinforcement be allowed in special moment frames and structural walls. Reinforcing steel data was provided by Nucor Steel Seattle, Inc. and the 2011 and 2012 CRSI Mill Databases.

While no numerical stress-strain data was provided in the report, the stress-strain curve of a No. 8 and a No. 18 bar was provided courtesy of the steel mill (Fig. 2-5). Based on the graph, the No. 18 bar barely meets the minimum allowable yield strength of 80 ksi when a 2% offset line is used to define the yield point. Past research has indicated a possibility for larger diameter bars to have lower strengths, presumably due to factors associated with the manufacturing process such as reduced grain refinement and different cooling rates and times (Lim, 1991); however, other research suggests that this is not the case (Mirza and MacGregor, 1979; Nowak and Szerszen, 2003). It is unclear whether such factors influenced the results of the present research. Nonetheless, the nature of the curves offers an interesting point of comparison with test results obtained during the experimental phase of the current project (Section 5.1.1.). Despite their differences in yield and tensile strength, both bars

seemingly surpass the minimum tensile to yield ratio of 1.25. The strain at peak stress was approximately 10% for both bar sizes.

Table 2-2. Stress-strain data provided in NIST GCR Report (2014)

Bar Size	Yield Strength		Tensile Strength		Elong. % in 8 inch
	Stress, ksi	Strain, in/in	Stress, ksi	Strain, in/in	
No. 8	---	---	---	---	14
No. 11	---	---	---	---	14.4
No. 18	---	---	---	---	---

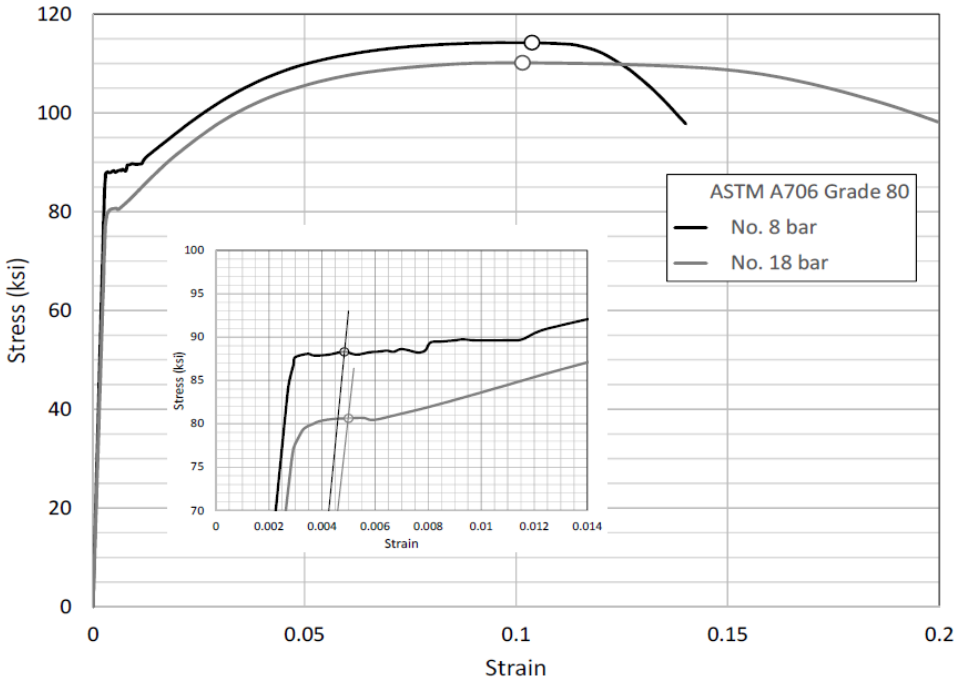

Figure 2-5. Stress-strain curves of No. 8 and No. 18 bars referenced in NIST GCR Report (2014). Original source: Nucor Steel Seattle, Inc.

2.2.1.4.Trejo, Barbosa, and Link. (2014)

Trejo et al. (2014) presented the results of a study on the seismic performance of 24-inch diameter circular reinforced concrete bridge columns constructed with A706 grade 80 reinforcement. A total of six of these half-scale columns were constructed and tested using either No. 5 or No. 6 longitudinal reinforcement, No. 3 transverse reinforcement, and either A706 grade 60 or A706 grade 80 steel. The study concluded that, among other things, columns reinforced with grade 80 rebar exhibited equal or greater maximum drift ratio compared to those with grade 60 rebar, both grades of steel resulted in similar column lateral displacement and ductility, and that columns reinforced with grade 60 rebar showed higher total energy dissipation as a result of their higher area of steel. Column failure mode (bar fracture due to buckling of longitudinal bars) was consistent across both grades of steel. The tensile test data presented in the report and reproduced below (Table 2-3) is the most detailed summary of the mechanical characteristics of A706 grade 80 reinforcing bars found in any of the other reports. This same data appears in a more recent paper by the same authors (Barbosa et al., 2015).

Table 2-3. Material test results for A706 grade 80 rebar used in Trejo et al. (2014)

Bar Size	Yield Point (0.2% offset)		Yield Point (0.0035 EUL)		Tensile Strength		Onset of Strain Harding		Ultimate Strain		Elong. % in 8 inch
	Stress, ksi	Strain, in/in	Stress, ksi	Strain, in/in	Stress, ksi	Strain, in/in	Stress, ksi	Strain, in/in	Stress, ksi	Strain, in/in	
No. 3	85.6	0.0055	73.3	0.0035	120.5	0.0947	N.A.	N.A.	85.2	0.1378	13
No. 5	86.2	0.0051	85.4	0.0035	114.3	0.1066	85.9	0.0084	86.8	0.1555	14
No. 6	86.1	0.0048	84.3	0.0035	114.0	0.1225	85.5	0.0098	93.9	0.1893	15

The tabulated stresses and strains presented in Table 2-3 are the average of 3 tests for each bar size. The No. 3 bars originated as coils, and the No. 5 and No. 6 bars were both produced from the same heat in 20 ft. straight lengths. Strain data up to necking was retrieved with a two inch gauge length extensometer. The onset of strain hardening was taken to be the point where the stress-strain curve begins to achieve a positive slope after the initial yield point. The ultimate stress and strain are the values obtained just before fracture.

The stress-strain curves of three No. 3 bar tests, three No. 5 bar tests, and three No. 6 bar tests were included in the report by Trejo et al. (2014). These curves have been reproduced in Figures 2-6 through 2-8. The "roundhouse" nature of the No. 3 bar curves follows what is typically seen in coiled reinforcing bars which undergo cold working as a result of the coiling and uncoiling process. The No. 5 and No. 6 bars both exhibited sharp-kneed yield points followed by a yield plateau. The strain at maximum stress averaged about 11.4 percent and the strain at the onset of strain hardening averaged about 0.9 percent.

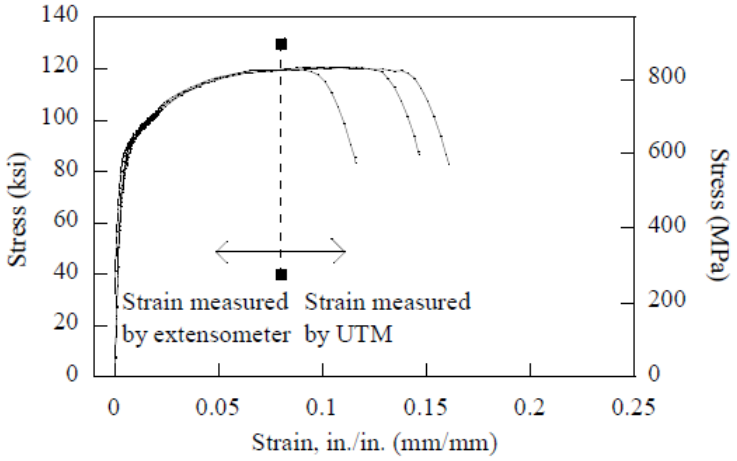

Figure 2-6. Stress-strain curves of three No. 3 bars (Trejo et al. 2014)

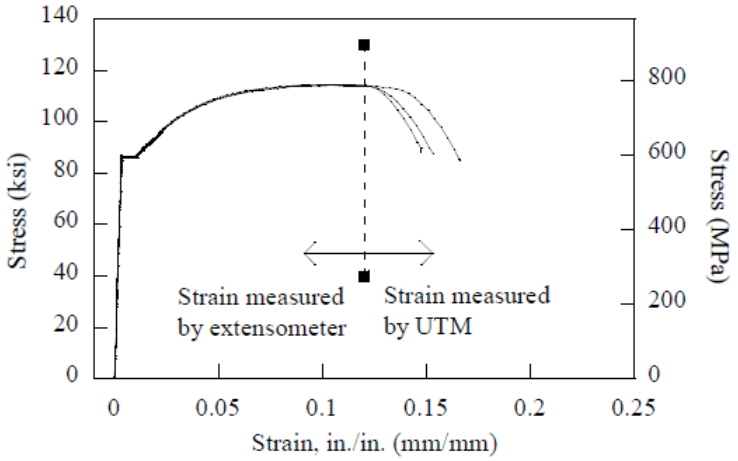

Figure 2-7. Stress-strain curves of three No. 5 bars (Trejo et al. 2014)

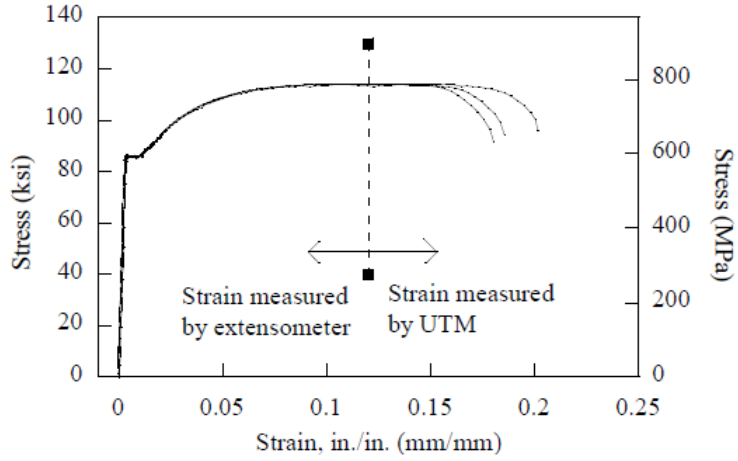

Figure 2-8. Stress-strain curves of three No. 6 bars (Trejo et al. 2014)

2.2.2. Mill and CRSI Data

The Concrete Reinforcing Steel Institute (CRSI) maintains an unpublished database of certified mill test report data that is made available upon special request for research purposes. CRSI provided the current research project with access to over 253,000 tensile test

results taken between 2011 and 2013. Data on yield strength, tensile strength, and percent elongation at fracture of all included types and grades of reinforcing steel is available in the database; however, the data is limited in that it does not include the associated strains. ASTM A706 grade 80 steel accounted for just 148 of the 253,000 plus tensile tests results and ASTM Dual A615/A706 grade 80 accounted for 76 of the tensile test results. Pertinent statistical data from the databases is summarized below (Table 2-4).

Table 2-4. Statistical summary of stress data for all A706 grade 80 and Dual A615/A706 grade 80 rebar (CRSI, 2013)

		Yield Strength, ksi				Tensile Strength, ksi			
Type	Entries	Min	Max	Mean	St. Dev.	Min	Max	Mean	St. Dev.
A706 grade 80	148	80.4	95.8	86.9	3.17	107.7	126.6	114.5	3.72
Dual A615/A706 grade 80	76	80.8	97.5	85.3	3.49	110.1	124.5	116.1	2.81

A surprising observation about the distribution of bar sizes in the databases is that a large quantity (61%) of the A706 grade 80 bars are for sizes No. 11 through No. 18 (Fig. 2-9). Figure 2-10 illustrates the obvious increase in production of A706 grade 80 and Dual A615/A706 grade 80 reinforcing steel between 2011 and 2013. The normalized distributions provided in Figures 2-11 and 2-12 show a tendency of Dual A615/A706 grade 80 coiled reinforcement to have a lower mean yield strength and higher mean tensile strength than straight reinforcement. Note that the normalized distributions are for the percent of total A706 grade 80 and Dual A615/A706 grade 80 not the entire 253,000 plus-entry database. As summarized in Table 2-4, the average yield strength of all of the A706 grade 80 bars is 86.9 ksi, and the average tensile strength is 114.5 ksi. Similarly, the average yield strength of all

of the Dual A615/A706 grade 80 bars is 85.3 ksi, and the average tensile strength is 116.1 ksi.

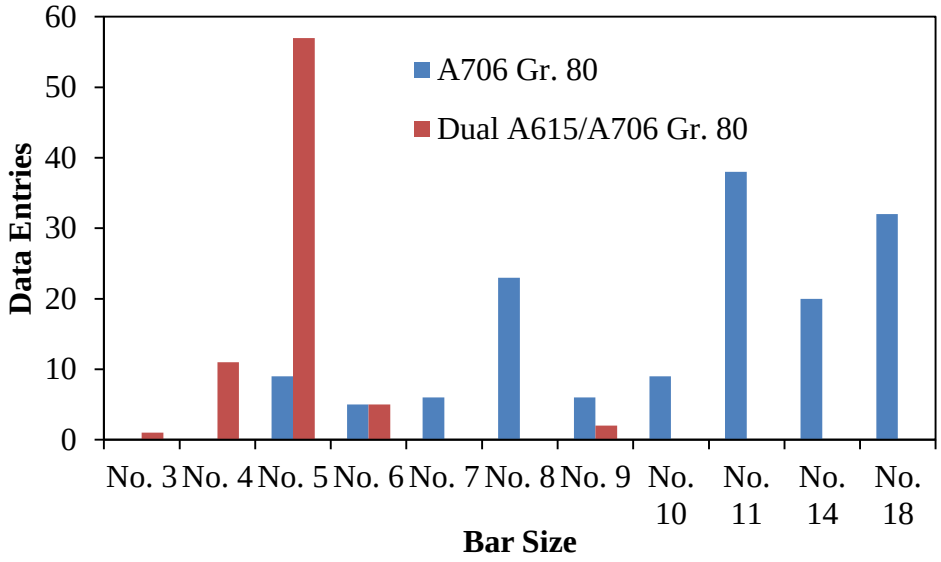

Figure 2-9. Distribution of all A706 grade 80 and Dual A615/A706 grade 80 test results by bar size (CRSI, 2013)

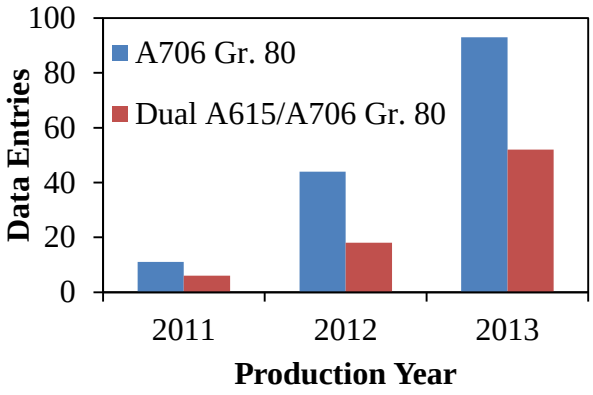

Figure 2-10. Distribution of all A706 grade 80 and Dual A615/A706 grade 80 test results by production year (CRSI, 2013)

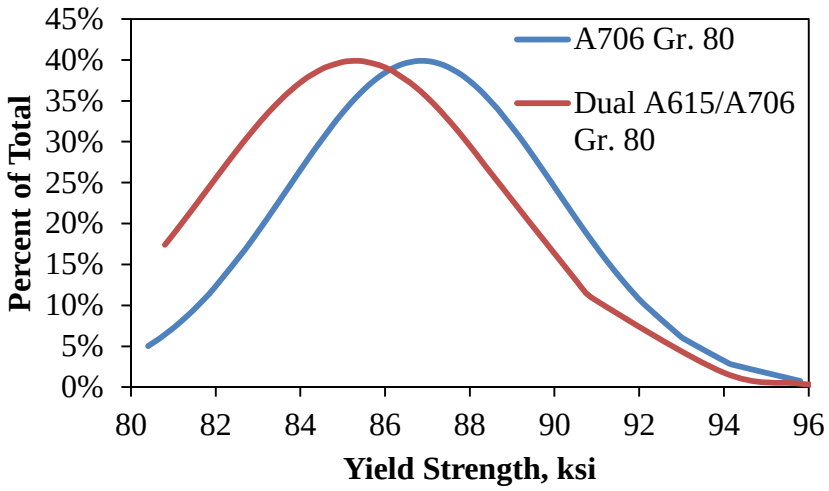

Figure 2-11. Yield strength normal distribution for all A706 grade 80 and Dual A615/A706 grade 80 rebar (CRSI, 2013)

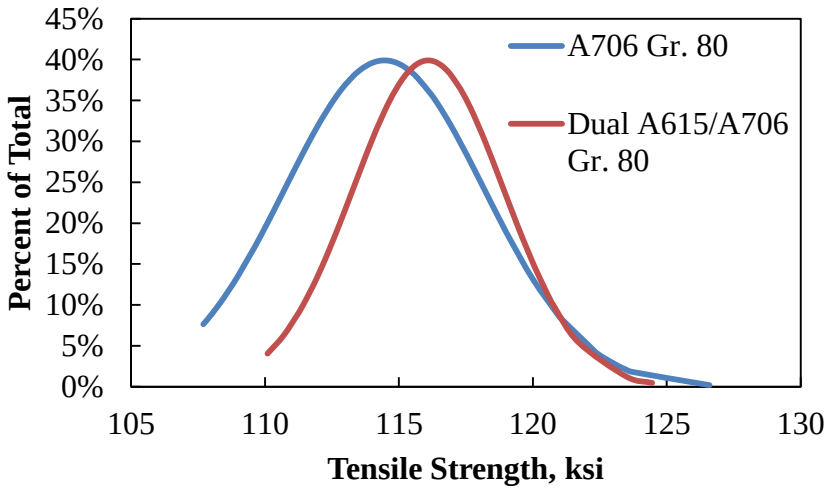

Figure 2-12. Tensile strength normal distribution for all A706 grade 80 and Dual A615/A706 grade 80 rebar (CRSI, 2013)

In addition to the mill data provided in the CRSI database, the report by Trejo et al. (2014) also included mill test results provided with the steel received as part of that research project. The data from that producing mill is provided in Table 2-5. Besides representing additional data points, these results offer insight into the way mill test results compare

against laboratory test results. A comparison of Tables 2-3 and 2-5 illustrates the trend for mill-measured strength values to be higher and percent elongation at fracture values to be lower than research laboratory test results. As will be seen in Chapter 5, this trend also held true for the results obtained as part of the current research project. Note that the method by which the producing mill obtained the yield strength data was not clarified in the report.

Table 2-5. Cascade Steel mill data referenced in Trejo et al. (2014)

Bar Size	Yield Strength		Tensile Strength		Elong. % in 8 inch
	Stress, ksi	Strain, in/in	Stress, ksi	Strain, in/in	
#3	96.5	---	124.0	---	23
#5	87.5	---	114.0	---	13
#6	88.0	---	115.0	---	14

2.3. Statistical Studies of Rebar Test Results

2.3.1. Allen (1972)

Allen (1972) conducted a statistical analysis of reinforcing bar mechanical properties based on two samples of Canadian-manufactured rebar test results. The smaller sample originated from a research facility and consisted of 102 tests on No. 3, 5, 8, 11, and 14 grade 40 bars representing 5 different heats. The larger sample originated from a Canadian manufacturing plant and consisted of 132 tests on No. 5 through No. 14 grade 60 bars where each test represented a different heat. Relevant findings from the paper were the distribution of the test results and the variability between and within heats. Specifically, it was noted that

the ultimate tensile strength was approximately normally distributed. The coefficient of variation (COV) for bars tested within a heat ranged from 2-3% for the yield strength and about 1% for the ultimate tensile strength. The variation across heats within a mill was noted to be higher with COV's of 7-8% for the yield strength and around 3% for the ultimate tensile strength.

2.3.2. Mirza and MacGregor (1979)

Mirza and MacGregor (1979) compiled nearly 4000 tensile test results from over 13 sources (mill and laboratory), including three different grades (40, 50, and 60) and nine different bar sizes (No. 3, 4, 5, 6, 8, 10, 11, 14, and 18) in order to investigate the variability in reinforcing steel mechanical properties, specifically the yield strength, tensile strength, and modulus of elasticity. While a number of sources of variability were considered, the two that are most relevant to this paper are the variability in the strength of the material and the effect of bar diameter. It was shown that the yield strength COV's ranged from 1-4% for individual bar sizes from a single source and from 5-8% for individual bar sizes considering all sources. Similarly, the yield strength COV's ranged from 4-7% considering all bar sized from a single source, and from 8-12% considering all bars sizes across all the supports. They concluded that, at least for grade 60 steel, the larger diameter bars (No. 14 and 18) did not show lower yield strength than the smaller bars.

In addition to presenting their findings in terms of the means and coefficients of variation, the authors also evaluated the ability of a number of probability distributions to characterize the spread of the data. More specifically, they investigated normal, lognormal,

modified lognormal, beta, and Pearson system distributions. The general conclusion was that the yield strength and tensile strength could be described by a normal distribution between the 5th and 95th percentile, but that the beta distribution offered the most comprehensive fit to the data. The authors noted that a likely reason for the non-normal behavior at the lower probabilities could be attributed to mill test results not including tests that failed to meet the minimum grade requirement, therefore, in a sense, biasing the available data. A normal distribution was used to characterize the modulus of elasticity data. It should be noted that there was no indication given as to how the different probability distributions were evaluated other than through visual inspection.

2.3.3. Nowak and Szerszen (2003)

As part of an effort to develop appropriate resistance models for calibration of the ACI 318 Code, Nowak and Szerszen (2003) assembled the results of 416 industry-based tensile test results of grade 60 rebar ranging in size from No. 3 to No. 11. A component of the investigation was to identify a suitable probability distribution to characterize the yield strength of the data in order to run Monte Carlo simulations to develop the resistance models. The authors concluded that a normal distribution suitably described the yield strength data. The COV's varied from 3.5 to 6.5 percent. The only technique described in the paper for evaluating the probability distribution fits was the use of normal probability paper.

2.3.4. Bournonville et al. (2004)

Bournonville et al. (2004) performed a statistical evaluation of the mechanical properties and weight of reinforcing bars produced by twenty-nine United States mills in the

year 1997. A total of 23,768 heats of bars were represented in the analysis. The study included bar sizes No. 3 through No. 18 and specifications A615 grades 40, 60, and 75, A616 grade 60, and A706 grade 60. Of interest to the present research on A706 grade 80 rebar are the findings related to the A706 bars and the grade 75 bars.

The authors concluded that less than 0.1% of heats failed to meet the minimum ASTM standards for both yield strength and tensile strength. They also concluded that the normal and beta distributions could be used to characterize the yield and tensile strengths of A615 grade 75, A616 grade 60, and A706 grade 60 rebar. It should be noted, however, that while the report clarified the method of fitting the beta distribution to the test data, it did not indicate how the distributions were deemed reliable fits to the data other than through visual inspection using normal probability plots. A more robust approach would have used an appropriate goodness-of-fit test and a desired significance level.

Other relevant findings from the report where that the A615 grade 60 bars showed an increase in yield strength with an increase in bar size but a general decrease in tensile strength with increasing bar size. No such trend was observed in either the A706 grade 60 bars or higher strength A615 grade 75 bars. The overall (across all the mills) coefficients of variation for the A706 grade 60 bar yield and tensile strengths were 4 to 6 percent and 3 to 6 percent respectively.

2.4. Strain Aging Literature

2.4.1. Introduction to Strain Aging

Strain aging can be defined as the process by which a reinforcing bar develops increased strength and reduced ductility over time following inelastic deformation. This behavior arises as a result of dislocation pinning at the molecular level in which small, interstitial atoms like carbon and nitrogen are freed through plastic deformation of the material and allowed to migrate through the crystal structure until they accumulate at dislocation sites (irregularities in the molecular structure), preventing further slipping of the crystal planes (Cottrell and Bilby, 1949). The increased resistance to sliding of the crystal planes is seen as an increase in strength (both yield and ultimate) and reduction in ductility of the material (Figure 2-13). As illustrated in the figure, an additional indicator of strain aging is the reemergence of the yield plateau.

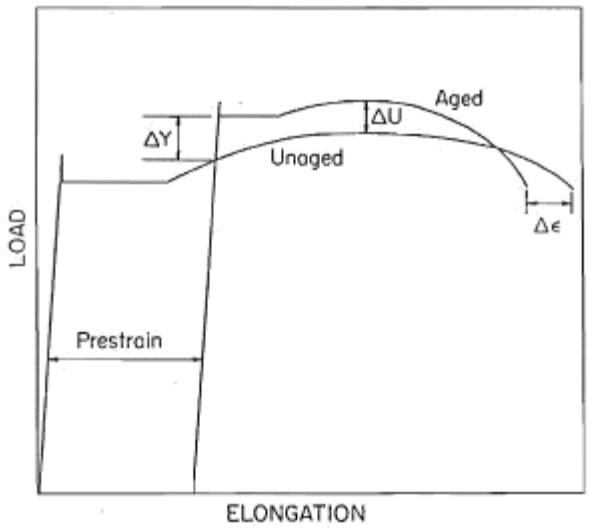

Figure 2-13. Schematic illustration of strain aging showing increased yield strength (ΔY), increased tensile strength (ΔU), reduced ductility (Δε), and reemergence of the yield plateau. Adapted from Lim (1991).

It is important to note that this process is separate from any increase in strength arising through other phenomenon such as cold working or strain hardening. Whereas the strength increase in these cases is the result of an increased number of dislocation sites, the strength increase due to strain aging is the result of an increased utilization of the dislocation sites that already exist as they accumulate migrating interstitial atoms over the course of time. It follows, then, that the susceptibility of a metal to the strain aging phenomenon is heavily dependent of the chemical composition of the material. The literature on strain aging can therefore generally be identified as addressing two broad categories: 1) identification of the chemical combinations that would render a steel strain-age-susceptible and 2) identification of external factors that would influence the severity of the susceptibility.

Strain aging has been previously studied in the context of earthquake structural engineering as its ability to impact reinforcing steel strength and ductility over time could have significant implications on the capacity design philosophy in which the ability of a structure to dissipate energy through inelastic deformation (plastic hinge formation) is reliant on a specified hierarchy of strength. Within this approach, locations of inelastic action are specifically chosen and detailed to ensure ductile response while other members are chosen to remain elastic to protect against brittle failure modes such as shear failure. These capacity protected members are designed for the maximum overstrength moments from the adjacent beams (in frames) or columns (in bridges).

As a primary goal of this methodology is to prevent collapse of the structure, it is often possible that repair methods may be implemented to restore the function of the structure following a seismic event inducing damage. Should the calculated capacity of the repaired structure neglect the increased strength and reduced ductility of the plastically-strained reinforcing steel, a subsequent seismic event may lead to unanticipated failure of capacity protected members due to strain aging of the reinforcing steel. One examples of this would include shear failure of columns in frames or bent caps in bridges as a result of higher input moments from the adjoining members arising from an increase in the rebar strength. Another example of the negative impacts of strain aging on the capacity design philosophy would include loss of confinement due to reduced ductility and subsequent early fracture of the transverse reinforcing steel.

As illustrated in Chapter 1, there is a general trend for increased steel strength to be accompanied by reduced steel ductility (as part of the metallurgical process). As such, the

anticipated reduced ductility of A706 grade 80 rebar as compared to A706 grade 60 rebar means that its susceptibility to strain aging must be investigated and understood prior to its use in members expected to dissipate energy through inelastic deformation (or at least before repair of such members following a seismic event).

2.4.2. Relevant Papers on Strain Aging

2.4.2.1.Pussegoda (1978)

Pussegoda (1978) conducted a detailed investigation on the impact of chemical composition on strain aging susceptibility of steel reinforcing bars. In particular, the study specifically focused on the use of two alloying elements, titanium and vanadium, to mitigate strain aging effects as these elements were established to be strong nitride forming compounds. Fourteen New Zealand grade 275 bars were manufactured with varying percentages of vanadium (approx. 0 to 0.1%), tested to 5% pre-strain ($36\varepsilon_y$, assuming E_s=200000 MPa), and then artificially aged at 100° C for 3 hours in order to determine the quantity of vanadium needed to prevent strain aging. The temperature and duration of the artificial aging period were derived using Hundy's equation (Hundy, 1954) to simulate the effects of natural aging at 15° C for 9 months. An additional set of 15 grade 275 bars, 6 having no titanium and 9 having 0.03% titanium, were tested to varying levels of pre-strain (2.5 to 15%) to simultaneously investigate the effect of pre-strain level on degree of strain aging as well as the ability of titanium to hinder strain aging. Artificial aging at 100° C for 3 hours was again used to simulate natural strain aging over 9 months.

The tests that were conducted established several things that may be relevant to the present discussion. First, it was concluded that a vanadium content of 0.06% was sufficient to effectively eliminate strain aging in the steel, which had a nitrogen content 0.005-0.006 percent. As illustrated in Table 2-6, bars with only trace quantities of vanadium saw as high as a 20 percent increase in yield strength, whereas this value was reduced to 4 percent in the vanadium-enriched bars. Increasing the vanadium content beyond 0.06% had no further effects on strain aging.

Table 2-6. Impact of vanadium content on strain aging susceptibility of mild (grade 275) New Zealand bars (Pussegoda, 1978)

	Approx. 0% V		0.06% V	
	Actual Change	Percent Increase	Actual Change	Percent Increase
ΔY	63 MPa (9 ksi)	20%	13 MPa (1.9 ksi)	4%
ΔU	38 MPa (5.5 ksi)	8%	1 MPa (0.1 ksi)	0.2%
ΔEl (%)	-7.5	-21%	0.5	2%

The second set of tests demonstrated that titanium could also be used as a means of preventing strain aging, as illustrated in Table 2-7. The main findings from these tests were that increasing the level of pre-strain in normal grade 275 bars (no added titanium) did not increase the yield strength after aging; however, it did increase the tensile strength and reduced the percent elongation. It was also shown that a pre-strain above 10% actually saw a reduction in strain aging rather than an increase.

Table 2-7. Impact of titanium content on strain aging susceptibility of mild (grade 275) New Zealand bars for a range of pre-strain levels (Pussegoda, 1978)

	0% Ti		0.035% Ti	
	Actual Change	Percent Increase	Actual Changes	Percent Increase
ΔY	57-61 MPa (8.3-8.8 ksi)	21-22%	9-22 MPa (1.3-3.2 ksi)	3-7%
ΔU	27-61 MPa (3.9-8.8 ksi)	6-14%	1-11 MPa (0.15-1.6 ksi)	0-2%
ΔEl (%)	-6.0 to -10.0	-15 to -25%	0 to -1.0	0 to -3%

2.4.2.2.Lim (1991)

Lim (1991) investigated the distribution of mechanical properties of two grades of New Zealand steel (grade 300 and 430) and used multiple linear regression to compare the mechanical properties with the determined chemical compositions. A total of 180 test results were evaluated. All bars were received from a single mill; however, each test represented a different batch of steel. The impact of strain aging was studied by testing an additional bar from each batch to a strain of 5% ($33\varepsilon_y$ and $23\varepsilon_y$ for grades 300 and 430, respectively, assuming E_s=200000 MPa) and then artificially aging the specimen for 3 hours at 100° C to theoretically simulate one year of natural strain aging at an ambient temperature of 15° C, according to Hundy's Equation (Hundy, 1954). Note that this same treatment was equated to 9 months of natural strain aging at an ambient temperature of 15° C in Pussegoda (1978). This discrepancy may be explained by a difference in the estimated quantity of interstitial carbon or nitrogen used in solving the equation. The extent of strain aging was evaluated

using three parameters: ΔY, ΔU, and ΔEl which are the increase in yield strength, increase in ultimate tensile strength, and reduction in percent elongation at fracture, respectively.

The findings from the report can be broken into two categories: the severity of strain aging and the impact of chemical composition on strain aging. Table 2-8 summarizes the severity of strain aging observed in the tests. From the table, it is evident that the lower yield strength steel suffered more from the effects of strain aging. The authors attributed this behavior to the higher vanadium content of the higher strength, grade 430 steel (0.04% versus 0.003%) as it is known to inhibit the migration of free nitrogen through the formation of vanadium nitride.

Table 2-8. Extent of strain-aging following a 5% pre-strain as presented in Lim (1991)

	Grade 300 (44 ksi)	**Grade 430 (62 ksi)**
$\mathbf{\Delta Y_{avg}}$	48.9 MPa (7.1 ksi)	20.6 MPa (3.0 ksi)
$\mathbf{\Delta U_{avg}}$	68.7 MPa (10.0 ksi)	49.6 MPa (7.2 ksi)
$\mathbf{\Delta El_{avg}}$	5.1%	2.28%

While the regression analysis was only performed on the grade 430 steel due to limited chemical data for the grade 300 steel, it did conclude that vanadium content was strongly correlated with ΔY. Unfortunately, the conclusiveness of the analysis suffered from the fact that no nitrogen percentages were available, meaning that a critical ratio between the two elements could not be determined. Nonetheless, it was proposed from the analysis that strain aging could have been eliminated at a vanadium content of 0.08 percent.

Several other observations from the report are relevant to the present research. A comparison of the tensile test results from the producing mill with laboratory results of the same steel showed that mill tests consistently demonstrated higher yield and tensile strengths of 20-30 MPa (2.9-4.4 ksi) and 33 MPa (4.8 ksi), respectively. This variation was largely attributed to differences in strain rates. Also observed was the trend for larger diameter bars to have reduced strength and ductility as compared to smaller diameter bars, which is thought to arise from the finer grain size of the smaller diameter bars that results from additional rolling at the mill and faster cooling .

2.4.2.3.Restrepo-Posada et al. (1994)

As part of an investigation into the effects of cyclic loading, bar deformation, and strain rate on the stress-strain behavior of two grades of New Zealand reinforcing steel (grades 300 and 430), Restrepo-Posada et al. (1994) also studied the strain aging behavior of both grades of rebar. In total, four strain-age tests were conducted for each grade, two having the pre-strain within the yield plateau, and two with the pre-strain point at the onset of strain hardening. Each set of two was composed of one uniaxial test and one cyclic test having a single reversal loop following the pre-strain. Two aging periods were evaluated: 37 days and 147 days. The bars were naturally aged at an ambient 68° F (20° C).

The tests concluded that the grade 300 steel was susceptible to strain aging while the grade 430 steel was not. This matches the findings by Lim (1991). The difference was attributed to the respective vanadium contents of the two steels which were zero and 0.04 percent, respectively. Observed signs of strain aging in the grade 300 steel included increased

yield strength, reemergence of the yield plateau in monotonic tests, dissipation of the Bauschinger effect in cyclic tests, and reduced ductility. Figure 2-14 illustrates several of these effects. The majority of the strain aging seemingly occurred within the first 37 days as there was little difference with the 147 day tests in terms of the increase in yield strength. The highest measured increase in yield strength was 21 percent. The increase in the ultimate tensile strength across the different tests was insignificant at about 1 percent; however, there was a clear reduction in ductility.

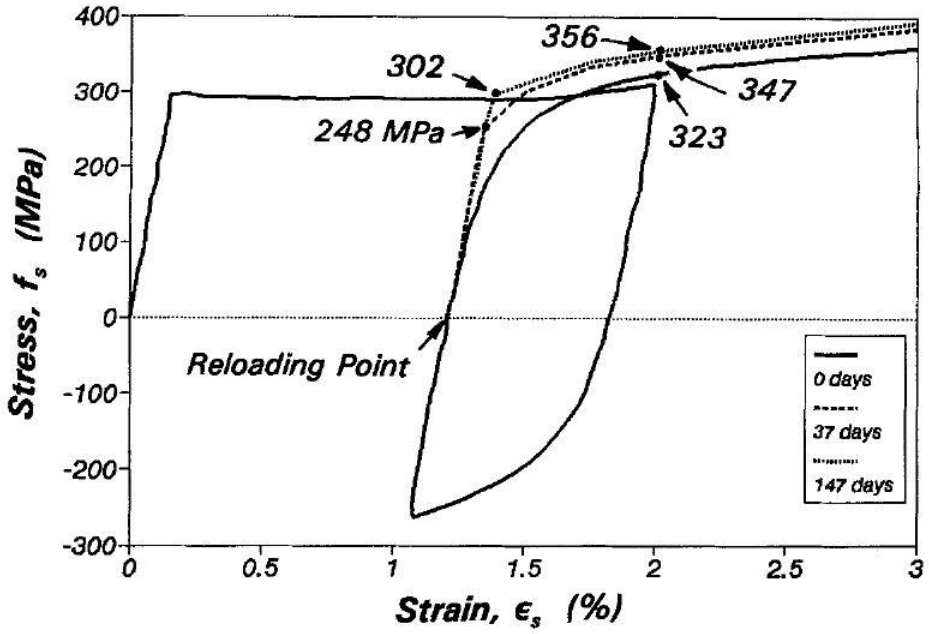

Figure 2-14. Illustration of strain aging effect on yield strength and the Bauschinger effect (Restrepo-Posada, 1994)

2.4.2.4.Momtahan et al. (2009)

Momtahan et al. (2009) studied the influence of pre-strain level and aging time on the strain aging behavior of grade 300 New Zealand reinforcing steel. In total, 53 16MM (No. 5) bars were tested monotonically to one of four pre-strain levels ($2\varepsilon_y$, $5\varepsilon_y$, $10\varepsilon_y$, and $15\varepsilon_y$) and

aged for one of five durations (3, 7, 15, 30, and 50 days) before being retested to capture the increase in yield strength. The pre-strain levels were chosen to represent the maximum strains the longitudinal bars could be anticipated to experience before repair of the structure became unrealistic, at which point the potential effects of strain aging would be inconsequential. The aging periods were chosen somewhat arbitrarily, though, based on the previous work by Restrepo-Posada et al. (1994). Bars were stored at 50° F (10° C) for each of the aging periods to simulate anticipated service condition temperatures.

A summary of the results from the investigation is provided in Table 2-9. In short, no distinguishable strain aging occurred within the first 15 days for the $2\varepsilon_y$, $5\varepsilon_y$, and $10\varepsilon_y$ pre-strain levels ($15\varepsilon_y$ bars were only tested at 30 and 50 days). As seen in Figure 2-15, there was a distinguishable increase in the steel yield strength with increasing aging period; however, as the increases are so small (less than 5%) for the lower pre-strain levels, it is difficult to distinguish them from the typical bar-to-bar variability. Nonetheless, it was clearly evident that increasing the aging period increased the severity of strain aging. It was also clearly demonstrated that increasing the level of pre-strain increased the severity of strain aging. This characteristic has been attributed to the increased dislocation density that results from plastic deformation, meaning that the interstitial atoms have less distance to travel before encountering and pinning the dislocations. Finally, the authors stated that there did not seem to be any increase in ultimate tensile strength.

Table 2-9. Percent increase in yield strength of New Zealand grade 300 reinforcing steel as a function of pre-strain level and duration of aging period (Momtahan et al., 2009)

	3 days	7 days	15 days	30 days	50 days
$2\varepsilon_y$	< 1%	none	< 3%	< 3%	< 3%
$5\varepsilon_y$	< 1%	none	< 3%	< 3%	< 5%
$10\varepsilon_y$	none	< 3%	< 3%	< 5%	13%
$15\varepsilon_y$	N/A	N/A	N/A	~ 25%	25%

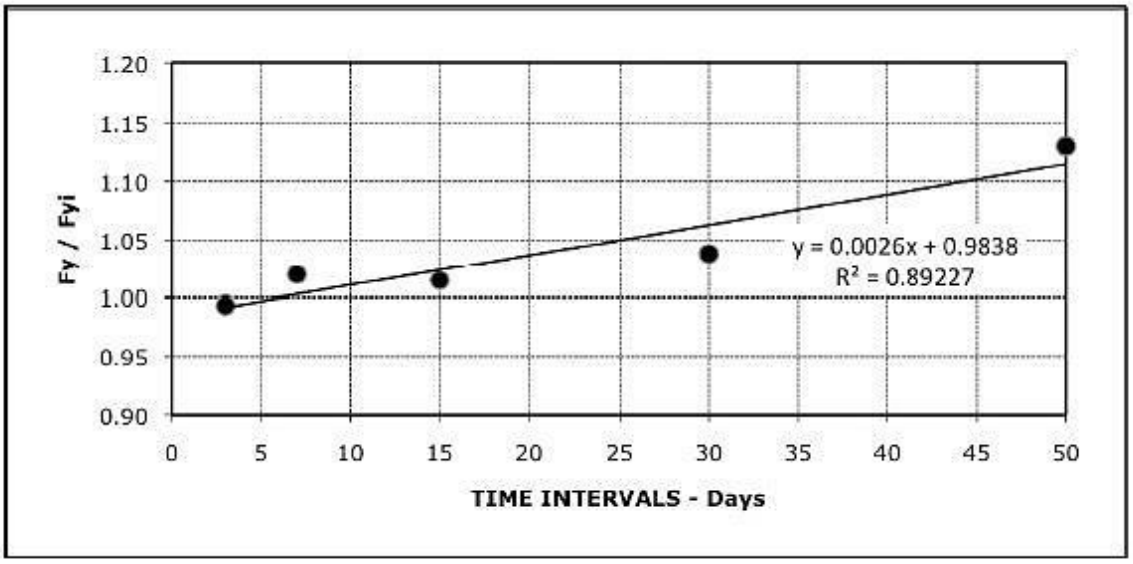

Figure 2-15. Impact of aging period on yield strength resulting from a pre-strain of $10\varepsilon_y$ (Momtahan et al., 2009)

2.4.2.5.Summary of Strain Aging Literature

The foregoing presentation of existing research on the topic of strain aging as it pertains to reinforcing steel serves as a point of reference in identify the most important variables to consider in an investigation of the strain aging phenomenon and how it may affect A706 grade 80 rebar. In particular, it is evident that chemical composition plays a

significant role in the ability of a given type of steel to be affected by strain aging. As was described at the beginning of this section, strain aging takes place through the pinning of molecular slip planes by small, interstitial elements such as nitrogen and carbon. It has been explained in Pussegoda (1978) that nitrogen is the main participant in strain aging below 100° C while carbon assumes this role at higher temperatures. The process of diffusion and pinning can be hindered through the addition of nitride forming elements to the steel. While numerous elements are capable of performing this function, the research consistently points towards vanadium as the element of choice as it not only reduces strain aging but also contributes to higher yield strength, lower variability in yield strength, and acceptably high ductility (Milbourn and Yu, 2010) without the adverse side effects and production costs of many of the other nitride forming elements (Pussegoda, 1978) which make it ideal for use in a seismic steel such as A706 grade 80.

While there seems to be a consensus on which elements affect strain aging, the literature was somewhat divided on the relative proportions of those elements. Pussegoda (1978) demonstrated that a vanadium content of 0.04-0.06% was sufficient to reduced strain aging to negligible levels in a grade 275 reinforcing steel having 0.0056% nitrogen. This would suggest a V/N ratio between 7:1 and 10:1. Lim (1991) speculated that a vanadium content of 0.08% would have prevented strain aging in a grade 430 steel; however, a V/N ratio could not be established as the nitrogen content of the steel was unknown. It has elsewhere been suggested that a V/N ratio of 4:1 is sufficient to reduce strain aging to insignificant levels (Russwurm and Wille, 1995).

The impact of external variables such as aging time and level of pre-strain on the extent of strain aging has also been investigated though the results are more difficult to interpret. Some studies relied on artificial aging through a sustained heat treatment after plastic deformation, while others allowed the steel to age naturally at ambient temperatures. Furthermore, the grades of steel evaluated ranged from 275 MPa (40 ksi) to 430 MPa (63 ksi) which, in addition to being varied, all fall below the 550 MPa limit of A706 grade 80 rebar. Nonetheless, Pussegoda (1978) and Momtahan et al. (2009) concluded that increasing the level of pre-strain increased the extent of strain aging in the steel they studied. Further, Restrepo-Posada et al. (1994) and Momtahan et al. (2009) demonstrated that the impact of strain aging increased with increased aging time (up until a point).

2.5. Cyclic Testing Literature

As described at the beginning of this chapter, a limited number of papers have presented experimental findings related to the monotonic stress-strain behavior of A706 grade 80 rebar. While this information is extremely useful, actual reinforcing bars in a reinforced concrete member will experience cyclical demands during an earthquake attack. As these demands expose unique characteristics of the steel such as fatigue and buckling behavior, it is necessary to investigate the cyclic performance of A706 grade 80 rebar in order to more fully complete the picture of its stress-strain behavior. At the time of this research, there does not appear to be anything in the literature specifically investigating the cyclic stress-strain behavior of A706 grade 80 rebar.

As such, the literature presented in this section does not relate directly to A706 grade 80 rebar, but rather serves to support the two objectives of the cyclic testing program outlined in Chapter 1 and summarized below:

- Identify if there is anything unique about the A706 grade 80 cyclic stress-strain behavior that would not be captured by existing material models
- Investigate the effect of inelastic cycling on the tensile ductility of the steel

The first objective requires both knowledge of existing material models and availability of A706 grade 80 cyclic test data. The second objective simply requires cyclic and monotonic experimental test data. While knowledge of existing material models currently being used in computational programs is easily obtained, acquisition of the necessary experimental test data is not as readily obtainable as there is currently no standard in place for cyclic testing of reinforcing bars. As such, the cyclic testing program must draw on the work of previous researchers studying other grades of steel as well as a rational understanding of the demands experienced by a reinforcing bar in a concrete member during an earthquake.

Based on the foregoing discussion, the following papers have been presented as they represent currently available cyclic material models and modifications to those models to include additional features such as low cycle fatigue and buckling. Emphasis is placed on the parameters necessary to define the models, the purpose of those parameters, the intuition behind the model, and the experimental procedures used in obtaining the test data used to calibrate the models.

2.5.1. Existing Material Models

2.5.1.1.Giuffre-Pinto (1970); Menegotto-Pinto (1973)

Many of the modern cyclic reinforcing steel models can be identified as modifications of the Giuffre-Pinto (1970) cyclic steel model. For this reason, a brief overview of their model is presented as foundational to understanding the abilities and limitations of the more recent models. The Giuffre-Pinto cyclic steel model can be seen as an extension of the monotonic material model developed by Goldberg and Richard (1963) to cyclic applications by redefining the stress and strain variables according to the Ramberg-Osgood (1943) approach. Despite drawing on the Ramberg-Osgood model, which is a $\varepsilon=f(\sigma)$ model, the Giuffre-Pinto model is defined as a $\sigma=f(\varepsilon)$ cyclic model, which makes it preferable for implementation in displacement-based methods – a characteristic that explains its widespread presence in modern computational programs. The model proposed by Giuffre and Pinto offered an improvement over existing models in that it could be used to characterize features such as the Bauschinger effect, impact of plastic excursion on the shape of the cyclic loops, and hardening and softening behavior. The generalized equation is presented below as Eqn. 2-1. The parameter R varies as a function of the plastic excursion (η) and may be modified by the input parameters A1 and A2 in order to define the curvature of the reversals as well as account for the Bauschinger effect. The parameter A may be used to define the rate of softening or hardening of the steel. Thus there are six parameters necessary to define this model: σ_0, ε_0, R_0, A1, A2, and A. A coupon test of a mild steel bar (d=10 mm) undergoing

symmetric tension and compression cycles was used to calibrate the model parameters (Figure 2-16).

Equation 2-1

$$\bar{\sigma} = \frac{\bar{\varepsilon}}{[1 + |\bar{\varepsilon}|^{R(\eta)}]^{1/R(\eta)}} + A\bar{\varepsilon}$$

Equation 2-2

$$R(\eta) = R_0 - \frac{A_1\eta}{A_2 + \eta}$$

Although the above equation first appears in this form in Giuffre-Pinto (1970), it is generally referred to as the Menegotto-Pinto (1973) equation in the literature and software manuals. This discrepancy may owe to the fact that the 1970 appearance occurs in an Italian journal while the first appearance of the model in the English literature seems to have been in the 1973 article where the equation takes a slightly different form:

Equation 2-3

$$\sigma^* = \frac{(1-b)\varepsilon^*}{(1 + \varepsilon^{*R(\xi)})^{1/R(\xi)}} + b\varepsilon^*$$

Despite the advantages offered by the model defined in Equations 2-1 and 2-3, there are several limitations that have been addressed by later researchers. Specifically, the model does not provide a way to define a yield plateau following the initial yield point, it does not account for buckling, it does not account for low-cycle fatigue, and it does not include isotropic hardening.

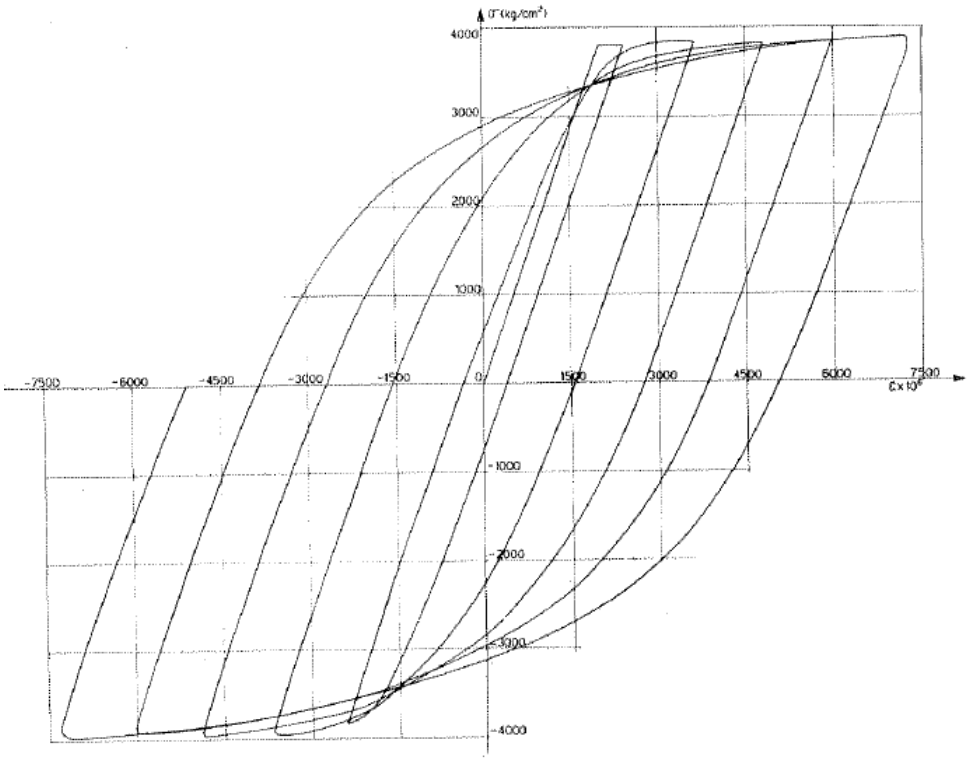

Figure 2-16. Coupon test of 10 mm diameter bar having symmetric tension/compression cycles used to calibrate Giuffre-Pinto (1970) material model

2.5.1.2.Filippou et al. (1983)

An improvement to the Giuffre-Pinto (1970) model came when Filippou et al. (1983) implemented an isotropic hardening rule (Eqn. 2-4) based on the work by Stanton and McNiven (1979). This was accomplished through the introduction of two new parameters (A3 and A4) to the Menegotto-Pinto (1973) formulation. While the previous formulation of the model was adequately suited to structural steel in which symmetric tensile and compressive stresses and strains could be expected, the improved formulation addresses the fact that reinforcing steel in a reinforced concrete member subjected to reverse cyclic loading

will experience unbalanced tension and compression strain histories due to the presence of the concrete and closure of the cracks. This is accomplished by allowing for a shift in the yield asymptote as a function of the maximum achieved plastic strain – a feature which gives the model the ability to properly characterize reversals from partial unloading as well as prediction of isotopic hardening.

Equation 2-4

$$\frac{\sigma_{st}}{\sigma_y} = a_3\left(\frac{\epsilon_{max}}{\epsilon_y} - a_4\right)$$

Calibration of the model was achieved through comparison with the cyclic rebar test results presented in Ma et al. (1976). The tests consisted of six machined No. 5 and No. 6 bars (grade 60) tested using load histories representative of what would be experienced in the top and bottom bars in actual reinforced concrete beams. One of the rebar specimens was tested using an arbitrary load history. While this addition to the Menegotto-Pinto model does not account for buckling or low-cycle fatigue, it does appear as an option in many of the later modifications to the model.

2.5.1.3.Monti-Nuti (1992)

The modification of the Menegotto-Pinto (1973) model to include an isotropic hardening rule by Filippou et al. (1983) was expanded on by Monti and Nuti (1992) to include two additional hardening rules as well as the ability to capture post-buckling softening. The improved model retained the Menegotto-Pinto model parameters R_0, A_1, A_2, and b^+ while replacing the added parameters A_3 and A_4 with a single new parameter, P, which is calibrated based on cyclic test results. Calibration of the model was based on tests of

16, 20, and 24 mm diameter rebar (approximately No. 5, 6, and 7) of grade 440 MPa having L/D ratios of 5, 8, and 11. Five different load histories were evaluated (Table 2-10): two random, one symmetrical, and two nonsymmetrical. The paper did not clarify how the specific tension-compression strain pairs were selected.

Table 2-10. Cyclical load history used in Monti and Nuti (1992)

Test	Strain History (percent strain)
A1, C1	+0.5 -0.5; +2.5 -1; +2 +0.4; +4 +1; +3 +1.5; +4
A2, C2	+1 0; +1.5 -0.5; +2 -0.5; +4 +1.5; +3 +0.5; +4
A3, C3	3(+1 -1); 2(+2 -1); 4(+2 -2)
A4, C4	2(+3 -1); 2(+2 -1); 4(+3 -1)
C5	+1 -1; +2 -1; +3 -1; +4 -3

2.5.1.4.Chang and Mander (1994)

Chang and Mander (1994) presented another modification of the Menegotto-Pinto (1973) model, based on the work by Mander (1983), in which the Coffin-Manson (1955) fatigue life model was incorporated to predict bar fracture. Other features of their formulation included modeling of the monotonic envelope branch to include a yield plateau defined between the yield strain (ε_y) and the strain at the onset of strain hardening (ε_{sh}). An implicitly defined scaling factor allowed the envelope branch to be adjusted in order to account for strength degradation after each reversal based on the plastic deformation, similar to the shifting approach used by Filippou et al. (1983).

Despite the fact that ten different rules are used to define the loop shapes, depending on whether the reversal took place from the envelope curve or part way through a returning branch, the model benefits from the fact that it may be completely defined using parameters

obtained from a monotonic tensile test: f_y, E_s, ε_{sh}, E_{sh}, f_{su}, and ε_{su}. This feature is achieved through implicit formulation of many of the cyclic parameters. Cyclic test results available in Kent and Park (1973), Ma et al. (1976), and Panthaki (1991) were used to calibrate the model. While the Chang and Mander (1994) model does not include buckling, it is available in current analysis programs.

2.5.1.5.Dhakal and Maekawa (2002)

A more recent modification of the Menegotto-Pinto (1973) model to include post-buckling behavior has been proposed by Dhakal and Maekawa (2002). The proposed model combines the Mander (1983) tension envelope curve formulation and the Menegotto-Pinto (1973) reversal rules with a post-buckling softening formulation developed by the authors to form a path-dependent cyclic material model. The aim of the new model was to address the limited scope of the existing models, such as the one proposed by Monti and Nuti (1992), which had been calibrated based on limited tests of only a few L/D ratios and steel strengths.

A defining feature of the proposed model was the ability to predict the post-buckling softening curve as a function of just the bar free length (L), the bar diameter (D), and the square root of the yield strength (f_y). Verification of the final model was performed using the experimental cyclic tests presented in Monti and Nuti (1992).

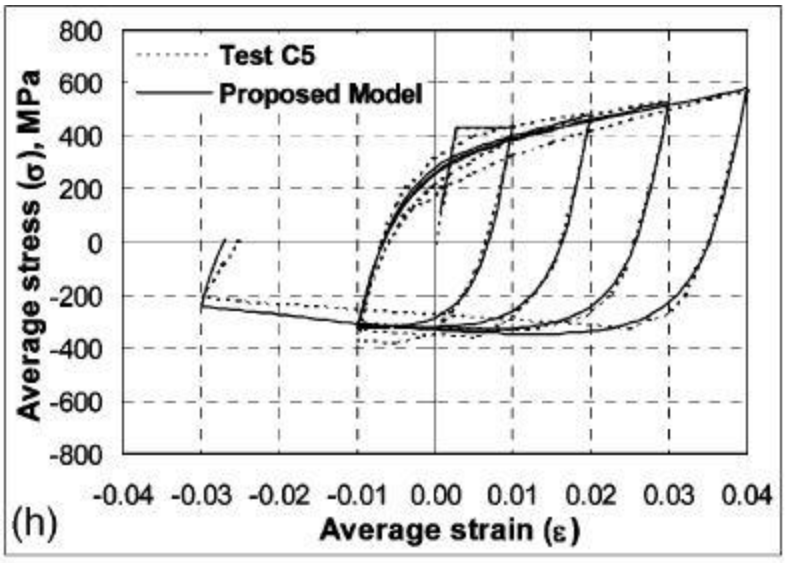

Figure 2-17. Comparison of Dhakal and Maekawa (2002) model, including buckling, with test data from Monti and Nuti (1992)

2.5.2. Summary of Cyclic Testing Literature

The above reports illustrate the importance of capturing the cyclic stress-strain performance of reinforcing steel used in reinforced concrete members expected to sustain earthquake-induced forces. Further illustrated is the trend towards increasingly comprehensive models that are able to retain as simplified a formulation as possible. Critical elements of the above models include capturing the Bauschinger effect, strength degradation through implementation of various hardening rules, and the ability of the model to predict the hysteretic behavior of the steel following reversals from any point on the curve. More recent models have implemented equations for predicting the effects of buckling as well as fatigue and subsequent fracture (Mendes and Castro, 2014).

While all of the models presented above referenced experimental test results for verification, there did not seem to be a consistent trend in how the experimental tests should be conducted. The nature of the strain histories varied from symmetrical tension/compression pairs between set strain limits, to nonsymmetrical tension/compression pairs, to random tension/compression pairs. Filippou et al. (1983) specifically chose tension/compression pairs representative of those experienced by top and bottom bars in reinforced concrete beams. An attempt more along the lines of this approach has been followed in the current project.

3. EXPERIMENTAL PROGRAM

3.1. Chapter Overview

Presented in this chapter is a detailed explanation of the experimental portion of the research that was conducted in pursuit of the research objectives outlined in Chapter 1. Particulars related to the material that was tested are presented first, followed by an overview of the instrumentation and test setups used to collect the experimental data. Following this is a breakdown of each of the three test types (monotonic tensile, strain age, and cyclic) summarizing the variables in the test matrix, preparation of the test specimens, and specific parameter values related to performing the tests.

3.2. Materials

Reinforcing steel for the project was received from three different producing mills. Each mill provided reinforcing bars from all sizes No. 4 through No. 18 (Fig. 3-1). In addition, each mill provided steel such that three different heats were represented for each of the ten bar sizes. Note that this is not to say that each mill only provided three different heats of steel. Appendix A provides a breakdown of the different bar sizes and heats for each mill. For each combination of heat and bar size, each mill provided, at minimum, three twenty-foot lengths of straight rebar. In some cases, additional twenty-foot bars were provided for a given heat and bar size. Individual test specimens for the different types of testing were cut from these twenty-foot bars (Fig. 3-2).

Figure 3-1. Relative sizes of No. 4 (left) through No. 18 bars (right) provided by mills

Figure 3-2. Single 30" test specimen cut from one of three 20-foot straight bars (No. 7 shown) and labelled according to developed numbering scheme.

Accompanying the shipments, each mill provided a certificate of compliance with the ASTM A706/A706M mechanical and chemical composition requirements. Included in these certificates were representative values of yield strength, tensile strength, and percent elongation at fracture for each heat of steel provided. Also provided with the steel were the results of a chemical analysis on each of the heats that listed the alloying elements included

and their respective percentages. According to these mill-supplied chemical compositions, each heat of steel being provided met the A706 requirements (Table 3-1). Similarly, each heat qualified as A706 grade 80 on the basis of the mechanical properties provided in the mill certificates.

Table 3-1 Partial mill chemical compositions (including vanadium content) demonstrating conformity with ASTM requirements

Element	Mill 1 Average	Mill 2 Average	Mill 3 Average	ASTM Max Allowable
C%	0.27	0.28	0.28	0.30
Mn%	1.35	1.29	1.28	1.50
P%	0.016	0.020	0.010	0.035
S%	0.022	0.030	0.040	0.045
Si%	0.20	0.27	0.21	0.50
V%	0.10	0.08	0.13	N/A
CE%	0.51	0.52	0.51	0.55

Due to constraints in cost and time associated with changing out the rollers at the steel mills, only a portion of the bars provided to the research project were actually stamped A706 grade 80, despite meeting the required mechanical and chemical compositions as per the mill certificates. Table 3-2 provides a summary of the different markings on the bars according to mill and bar size. As will be discussed later in this chapter, special care was taken to ensure that each rebar test specimen could be traced back to the exact twenty-foot bar from which it originated. This included a record of each bar's grade stamp and associated heat number and predicted mechanical and chemical properties.

Table 3-2. As-stamped type and grade of steel by producing mill and bar size

Bar Size	Mill 1		Mill 2		Mill 3	
	Type	**Grade**	**Type**	**Grade**	**Type**	**Grade**
No. 4	A615	60	A615	60	A615	60
No. 5	A615	60	A615	60	A615	60 and 80
No. 6	A615	60	A615	60	A615	60
No. 7	A706	80	A615	60	A615	60
No. 8	A706	80	A615	60	A615	75
No. 9	A706	80	A615	60	A615	60 and 75
No. 10	A706	80	A615	60	A615	75
No. 11	A706	80	A615	75	A615	75
No. 14	A706	80	A615	75	A615	75
No. 18	A706	80	A615	75	A615	75

All heats met ASTM A706 grade 80 chemical and mechanical requirements according to the mill certificates provided with the steel

3.3. Equipment

3.3.1. Testing Equipment

Two different test setups were used to perform the experimental testing. A commercially available MTS universal testing machine was used to perform the tensile tests of the No. 4 through No. 10 bars and all of the cyclic and strain age tests while a custom-built testing rig was fabricated in-house to perform the No. 11 through No. 18 bar tensile tests.

The MTS universal testing machine (Figure 3-3) is capable of performing tensile or cyclic testing and may be operated in one of three control modes: force control, displacement control, or strain control. The maximum pull capacity of 200 kips would have permitted the testing of up to a No. 11 grade 80 bar, but the maximum grip size available could only accommodate the diameter of a No. 10 bar.

Figure 3-3. Crossheads of MTS machine used to test No. 4 through No. 10 bars (No. 10 bar shown)

Because of the limitations of the MTS machine just described, the custom-built testing rig shown in Fig. 3-4 was designed to complete the tensile testing of the No. 11 through No. 18 bars. Three 200-kip double-acting hydraulic jacks provided the test setup with a total capacity of 600 kips. The jacks were operated by an electric hydraulic pump and reacted at either end against one of two 5" thick grade 50 hexagonal steel plates. The reinforcing bars were anchored at the top and bottom of the test setup using a wedge-chuck system which allowed the forces from the jacks to be transferred through the plates to the test specimen which passed through a 3" diameter hole at the center of the plates. An advantage

of this system is that the entire test setup was self-reacting and able to simple sit on the laboratory floor. A disadvantage was that only tensile tests could be performed.

Forces were obtained by a single 200 kip load cell located separate from the main setup on a fourth 200-kip jack. This configuration resulted from the need to record forces in excess of 480 kips with a 200-kip cell which would be damaged if placed directly in line with a No. 14 or 18 bar. Rather than place the load cell on one of the three jacks surrounding the bar, which would require equal-height spacers on the other two jacks, it was placed on a fourth jack physically separated from the setup but still connected to the hydraulic pump. This fourth jack reacted against a high-strength threaded rod sized to take the full capacity of the jack. Theoretically, the fourth jack would produce the same force as the other three jacks as a consequence of being the same size and connected to the same hydraulic source; however, complicating issues of frictional losses caused this theory to break down. As a result, the force readings from the load cell had to be artificially reduced to account for losses between the two systems. This is described in further detail in Section 3.4.4.

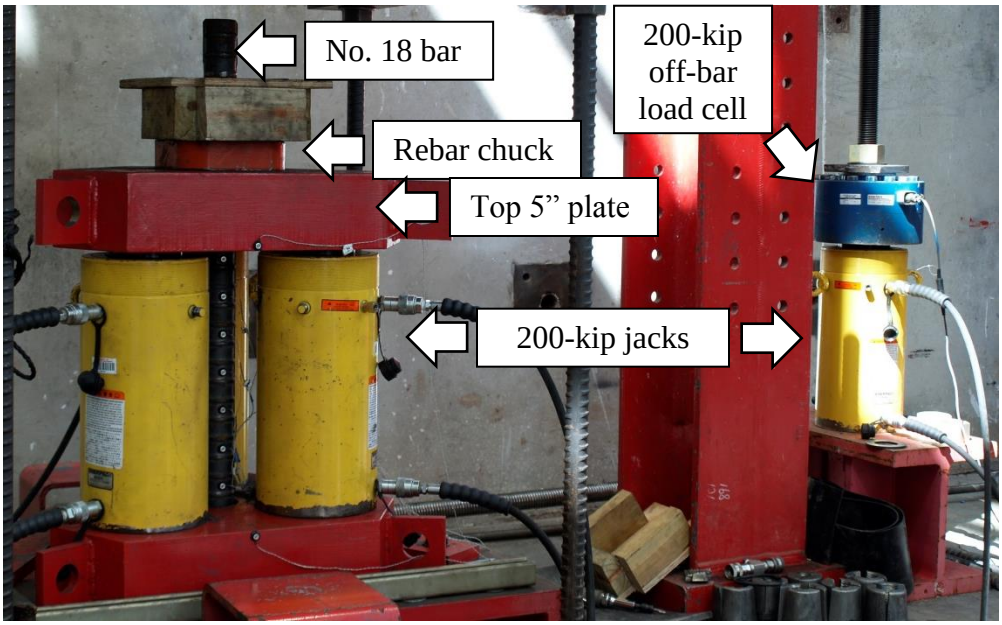

Figure 3-4. Custom testing rig designed to test No. 11, 14, and 18 bars

Figure 3-5. Wedge-chuck system used to anchor No. 11, 14, and 18 bars (tested No. 18 bar shown)

Figure 3-6. Interface between bar and wedge grips

3.3.2. Instrumentation

An Epsilon Class B1 2 inch gage length extensometer (Fig. 3-7) was used to record strains for all No. 4 through No. 10 bar tests. An Epsilon Class B1 1.4" gage length extensometer was used to record strains on several of the cyclic bar tests. ASTM A370 "Standard Test Methods and Definitions for Mechanical Testing of Steel Products" recommends that a class B1 extensometer be used to record strain during tensile tests (ASTM A370, 2015). In addition to the extensometer, an Optotrak system was used to calculate strains on all tests.

Figure 3-7. Epsilon class B1 2" gage length extensometer used to record strains during No. 4 through No. 10 bar tests (No. 4 bar shown)

The Optotrak system is a 3D noncontact position measurement system capable of simultaneously tracking the location of up to 512 target LEDs or "markers" with an RMS accuracy of up to 0.1 mm and a resolution of 0.01 mm (NDI, 2011). The entire system operates in the infrared spectrum in which markers flash IR light at a predefined frequency of

up to 4600 Hz and, depending on the number of markers used, can be recorded at a frame rate as high as 2000 Hz. The outputs from the Optotrak are the x-y-z coordinates of each marker relative to a pre-defined origin at each frame record.

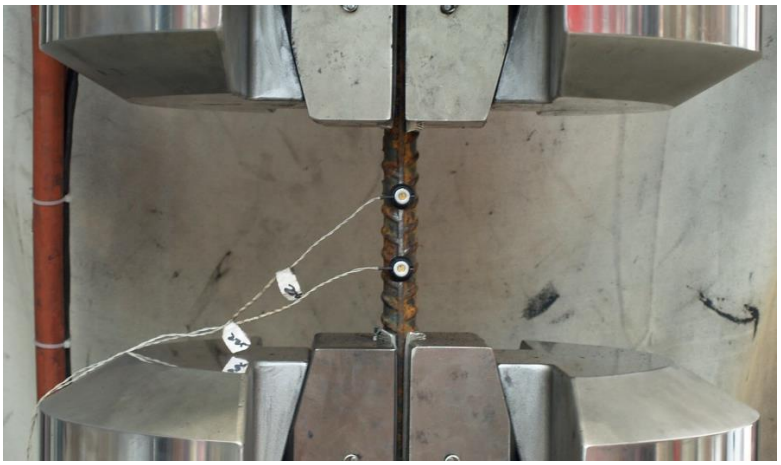

Figure 3-8. Single gage length of Optotrak markers on a No. 7 bar

The distance between any two markers at a given instant in time can be calculated using the 3D Pythagorean Theorem. Strains are then calculated by taking the change in distance between any two markers divided by the initial distance between them. Because the Optotrak is capable of tracking multiple markers simultaneously, therefore allowing multiple gage lengths to be established on a single test specimen, it is possible to assess the distribution of strain over the entire instrumented region of the specimen at each reading of the data. Furthermore, it is possible to develop a stress-strain curve for each gage length as the strains within a given gage length are necessarily unique to that gage length. The application of this additional data is discussed in further detail in Chapter 4.

Another key advantage of the Optotrak is the ability to keep the markers in place through fracture which becomes increasingly detrimental to the extensometer as bar size increases. As a result, it is possible to record the strain at the instant of fracture. Furthermore, when compared to strain gages, the ability to measure large strains is significantly enhanced. For these reasons, final recommendations related to strains have been based on the Optotrak system measurements.

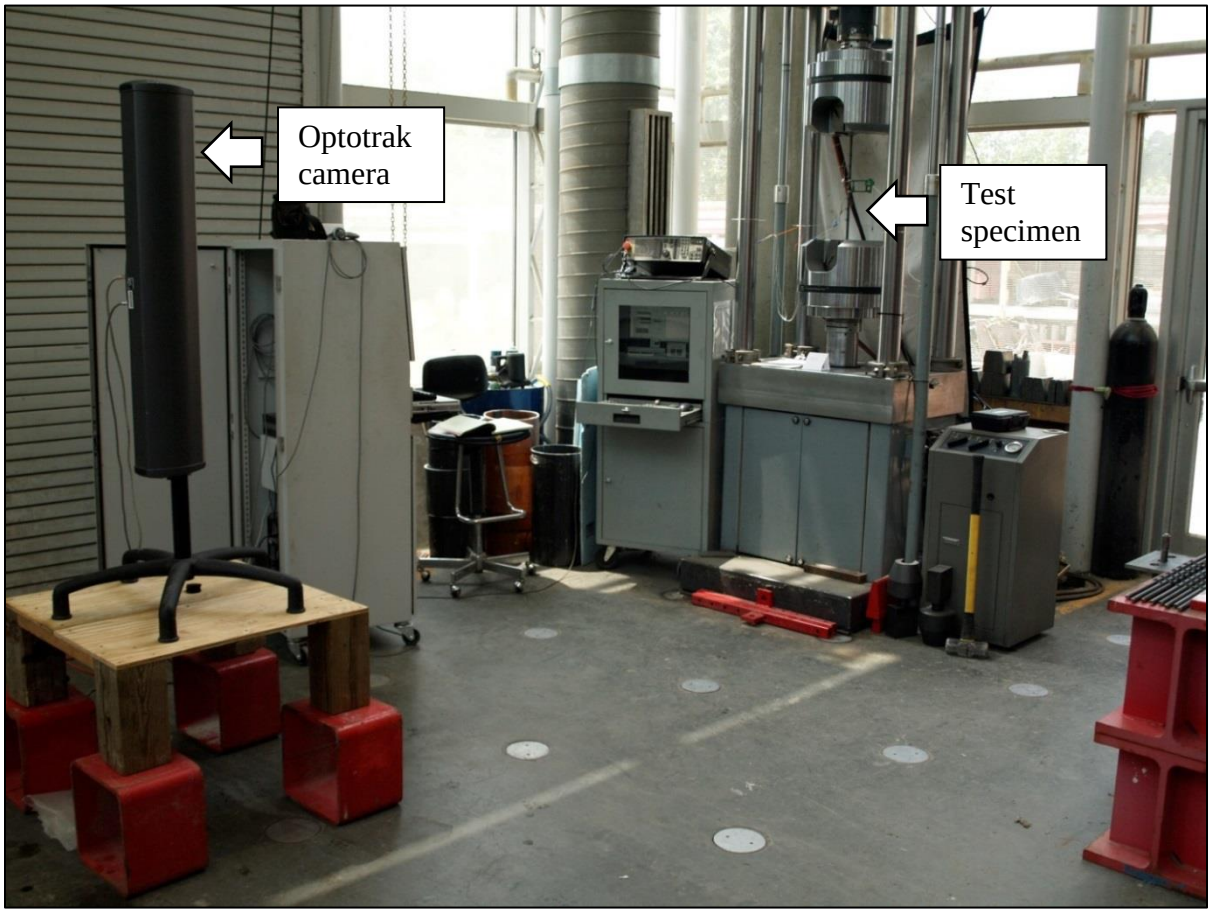

Figure 3-9. Test setup showing MTS machine, extensometer, and Optotrak camera aimed at test specimen

3.4. Tensile Testing

3.4.1. Test Matrix

Table 3-3 summarizes the tensile testing matrix. A total of 788 monotonic tensile tests on the ten major imperial bar sizes (No. 4 through No. 18) were conducted on A706 grade 80 rebar manufactured by three different producing mills. Each mill provided bars from three different heats for each of the 10 sizes. Within each heat and bar size, three specimens were cut from each of three individual 20-foot lengths of bar (Fig. 3-10).

Figure 3-10. Illustration of 3 heats, 3 20-foot bars, and 3 individual test specimens from a single mill (No. 7 bars shown)

The total possible number of tests amounted to 810, but only 59 of the anticipated 81 No. 18 bar tests were performed due to an incompatibility of the test setup with the

transverse ribs on the bars from one of the mills. The 22 remaining tests were not performed due to incompatibility of the testing grips with the horizontal ribs on a subset of the No. 18 bars (all from the same mill) which inevitably resulted in cracking and fracture of the wedge grips in the direction of the teeth after one to two tests (Fig. 3-11). Nonetheless, of the 27 Mill 1 No. 18 bar specimens that posed this problem, five representative samples were able to be tested. All tests were conducted with the bars in the as-rolled condition.

Table 3-3. Tensile test matrix illustrating number of tests performed

Bar Size	Mills	Heats	20' bars	Specimens	Tests
No. 4	3	3	3	3	81
No. 5	3	3	3	3	81
No. 6	3	3	3	3	81
No. 7	3	3	3	3	81
No. 8	3	3	3	3	81
No. 9	3	3	3	3	81
No. 10	3	3	3	3	81
No. 11	3	3	3	3	81
No. 14	3	3	3	3	81
No. 18	3	3	3	3	59
Total Number of Tensile Tests					788

Figure 3-11. No. 18 bar wedges undamaged (left) and after testing Mill 1 bars (right)

3.4.2. Specimen Preparation

Each test specimen was labelled with a unique identification number to denote its exact place in the testing matrix and to ensure that test results could later be organized on the basis of mill, heat, or even single twenty-foot bar. Figure 3-12 illustrates the numbering scheme. The first number in the sequence represented the producing mill. As there were three mills providing steel, this number was always a 1, 2, or 3. The second number indicated from which of that mill's heats the bar originated. As stated previously, there were more than three heats of steel per mill, however, only three of these could be represented by a given bar size. This number ranged from1 to 9 depending on the mill (See Appendix A). The middle number denoted the bar size and therefore ranged from 4 to 18 to correspond to one of the ten bar sizes considered. The fourth number indicated from which of the three twenty-foot bars in a particular heat the specimen was cut and varied from 1 to 3 accordingly. The final number identified the specific test specimen and also varied from 1 to 3. An advantage of this numbering scheme is that it offered a concise way of representing mill names and lengthy heat ID's as a single number. Furthermore, it provided unique file names for each test that could easily be referenced either manually or by computer program.

Figure 3-12. Numbering scheme used to uniquely identify each test specimen

Individual test specimen lengths were determined according to ASTM A370 "Standard Test Methods and Definitions for Mechanical Testing of Steel Products" which specifies a required minimum distance of two bar diameters between the grip-bar interface and the nearest gage mark (ASTM A370, 2015). Thus, the minimum length of a test specimen is a function of its diameter and the desired number and size of the gage lengths. All specimens were cut to allow for six 2" gage lengths in order to take advantage of the Optotrak capabilities.

A spacing of 2" was chosen for the Optotrak markers in order to be consistent with the 2" gage length of the extensometer. Including six of these 2" gage lengths inherently offered a way of measuring strains over three overlapping 8" gage lengths (Fig. 3-13) as strains can be calculated between any two markers regardless of whether or not they are adjacent. Including three 8" gage lengths increased the likelihood that fracture could be captured in an instrumented region of the test specimen. Additionally, the ability to provide strain data in terms of an 8" gage length offered compatibility with existing test data also in terms of an 8" gage length. As indicated by the results presented in Appendix E, little

difference existed between 2” and 8” gage length measurements. Final recommendations related to strains have, therefore, been based on the 2” gage length data.

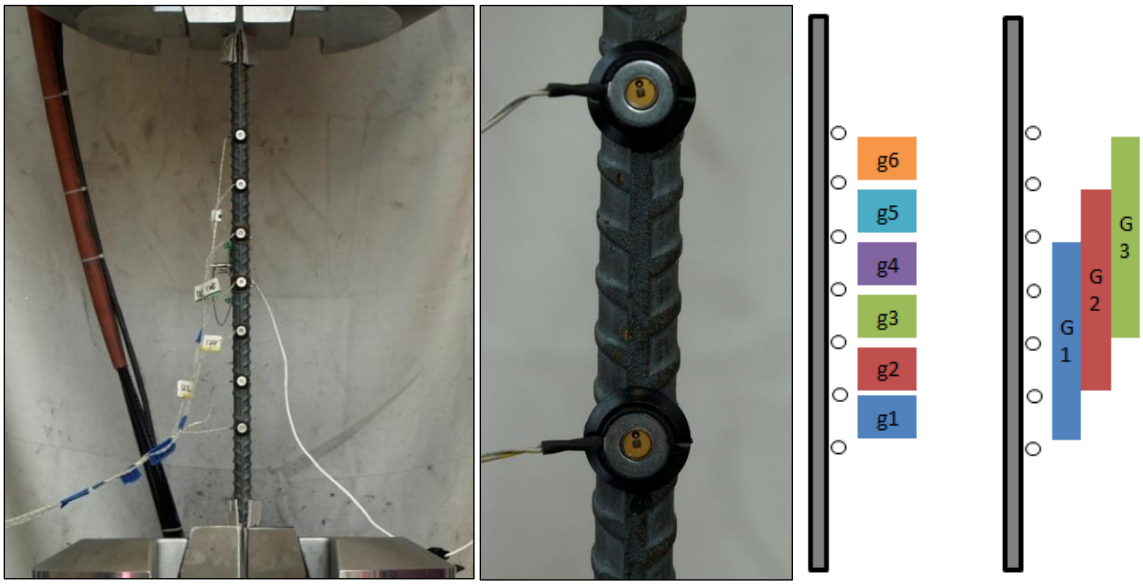

Figure 3-13. Location and spacing of Optotrak markers on a No. 4 bar and illustration of six 2" and three overlapping 8" gage lengths

A single specimen length of 30 inches was used for all bar sizes No. 4 through No. 10, while a longer specimen length of 48 inches was used for the No. 11 through No. 18 bars to accommodate the dimensions of the custom testing rig. In all cases, the chosen lengths exceeded the minimum allowable lengths for the number of gage lengths used.

3.4.3. Test Parameters

The No. 4 through No. 10 bars were tested in displacement control at a rate of 1 in/min in order to satisfy the testing speed requirements of ASTM specification A370 which specifies an upper and lower pre-yield and post-yield testing speed as a function of the free length of the bar. As stated previously, a single specimen length of 30 inches was used for all

No. 4 through No. 10 tests. This corresponded to a bar free length of approximately 20 inches. Rather than select a single pre-yield speed and a different post-yield speed, which causes a momentary fluctuation in the force-displacement response at the change in load rate and necessarily adds a level of subjectivity to the test, the constant displacement rate of 1 in/min was applied for the full duration of each test. Initially, all tests were taken until fracture of the bar; however, tests conducted later in the testing program were stopped prior to fracture if necking occurred outside of the instrumented region. This prevented unnecessary wear on the testing equipment as no further useable data would have been acquired in these cases. A compilation of fractured and necked bar photos is included in Appendix J.

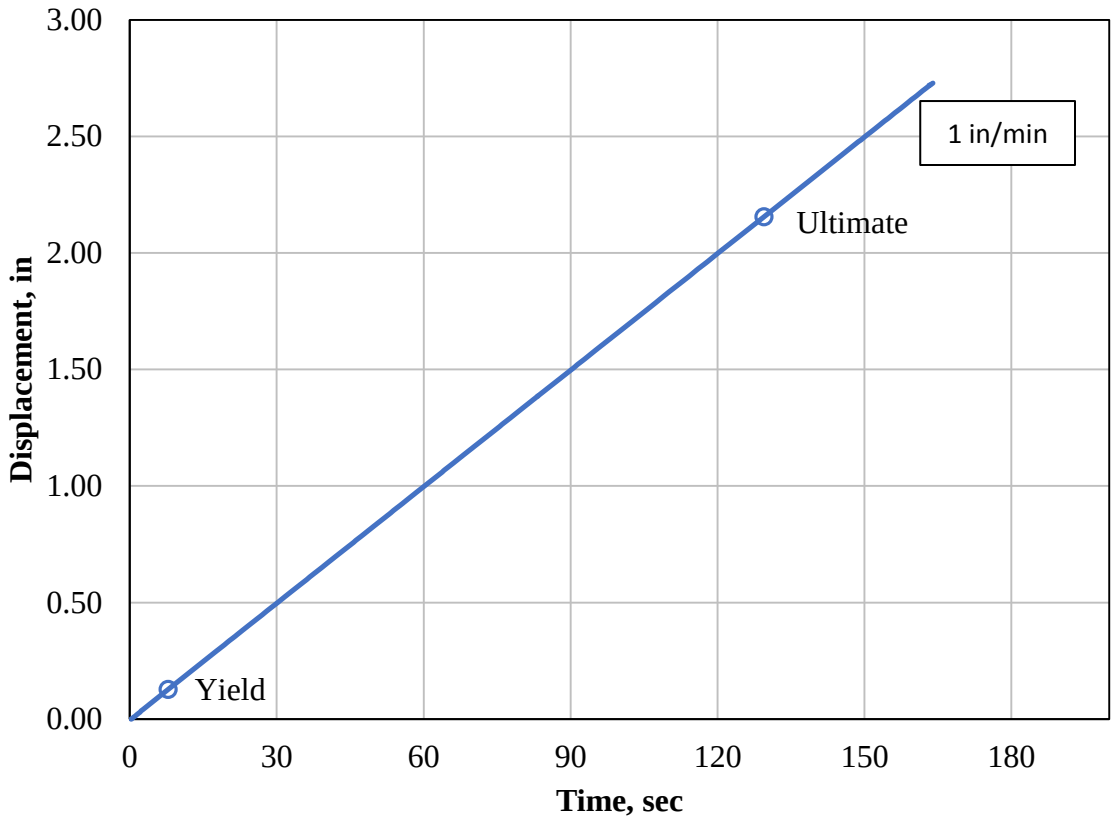

Figure 3-14. Back-calculated load rate of a No. 8 bar tested in the MTS machine confirming the specified 1 in/min displacement rate

The No. 11 through No. 18 bars were tested at a displacement rate proportional to the flowrate of the electric hydraulic pump used to power the three 200-kip jacks. Unlike the MTS machine, the custom testing rig lacked a servomechanism to auto-regulate the displacement rate, and, as a consequence, possessed no means to specify a desired load rate before the test. Rather, the load rate had to be measured during the test and then calculated afterwards. This was achieved by placing an Optotrak marker on each of the plates such that their relative displacement could be tracked with time (See Fig. 3-4).

Performing this calculation for a number of tests revealed a consistent plate displacement rate of 0.3 in/min. Seating of the wedge grips inhibited this constant displacement rate from being translated directly to the bar, as described in the next paragraph. Instead it was observed that the bars elongated according to a bilinear displacement rate that was initially much slower than the displacement rate of the plates, but picked up speed following yielding, a phenomenon that has been identified as wedge seating.

Wedge seating describes the process by which the toothed wedge grips used to anchor the test specimens on either end of the 5" reaction plates progressively bite deeper into the bar (Fig. 3-6) and are consequently allowed to slide farther down into the chuck over the course of the test. Because initially the resistance of the bar to elongating is very high (slope of the elastic force-displacement curve much greater than the inelastic portion), the majority of the wedge seating (biting and sliding) occurs prior to yielding (Fig. 3-15); however, following yielding, the stiffness of the bar essentially drops to zero (the yield plateau) and the wedges do not displace while the bar does so under nearly constant force. This explains the blip in the wedge seating and bar elongation curves immediately after yielding as seen in Figure 3-15. Note that the "wedge seating" curve (which denotes the rate of wedge seating) was obtained by taking the difference between the displacement rate of the plates and the elongation rate of the bar. Following the onset of strain hardening, the bar again has resistance to elongation, albeit at a reduced, nonlinear rate corresponding to the shape of the strain hardening curve. As a consequence, little additional wedge seating occurs and the bar elongates at nearly the same rate as the plates displace. Thus, initially, the displacement rate

of the bar is slower than that of the plates, but following yielding they are essentially the same at about 0.3 in/min.

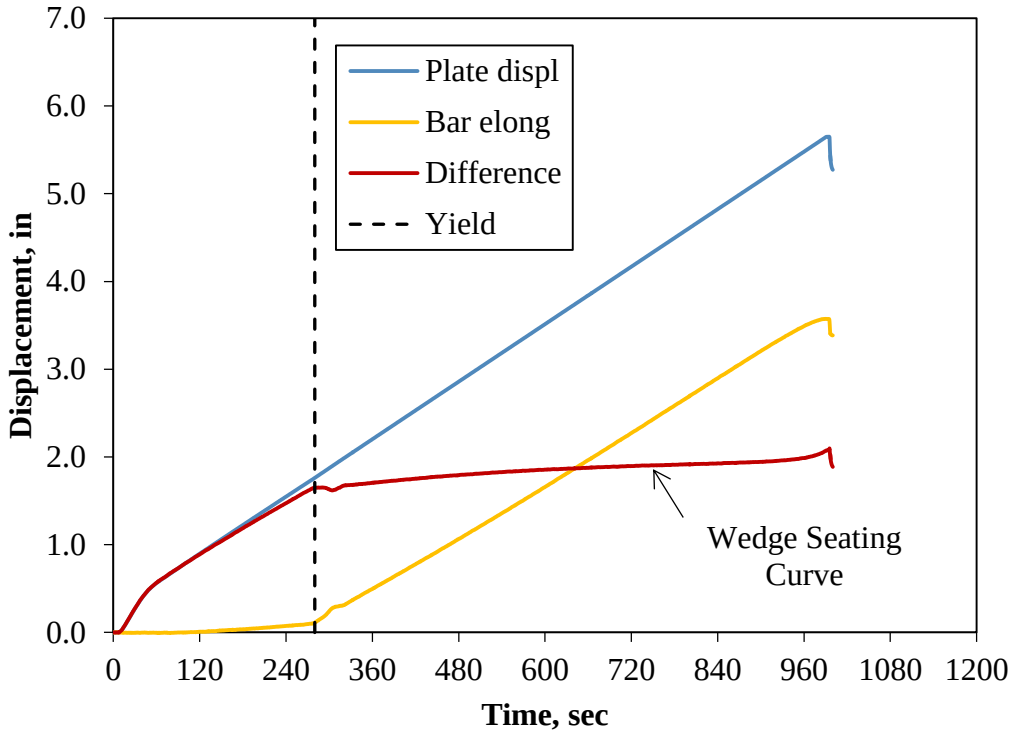

Figure 3-15. Wedge-seating phenomenon observed in No. 11-No. 18 bar tests

As a result of the wedge seating phenomenon and the associated bilinear load rate, bars tested in the custom testing rig inherently experienced a bilinear strain rate. The dimensions of the custom testing rig dictated that each specimen have a free length of 33" between the wedge grips. This distance provided adequate length to accommodate the six 2" gage lengths and satisfy the testing speed requirements of ASTM specification A370. As stated previously, each of the No. 11, 14, and 18 bar specimens was 48" in length.

Due to the more violent nature of fracture of the larger bars and the nature of the wedge-chuck system, very few of the No. 11, 14, and 18 bars were tested completely to fracture. Instead, tests were stopped once the force readings showed a steady drop indicating that the ultimate tensile point had been reached and the bar had begun necking.

In all cases, stresses were determined by dividing the recorded forces on the test specimen by the nominal cross-sectional area in accordance with ASTM A370. The No. 4 through No. 10 bar forces were obtained from the MTS machine's built-in load cell. The No. 11 through No. 18 bar forces were recorded using the 200-kip load cell shown in Fig 3-4.

3.4.4. Calibration of Custom Testing Rig

As stated previously, the initial configuration of the load cell away from the bar served as a way to indirectly measure bar forces in excess of 200 kips using a single 200 kip load cell. Theoretically, the force at the load cell would be exactly one third of the force on the bar assuming each of the four identical jacks receives the same pressure from the hydraulic pump. In actuality, the three jacks loading the bar do not receive the same pressure as the single jack with the load cell. As a result, the force applied to the load cell does not correspond to exactly one third of the force experienced by the test specimen. This fact is illustrated in Figure 3-16.

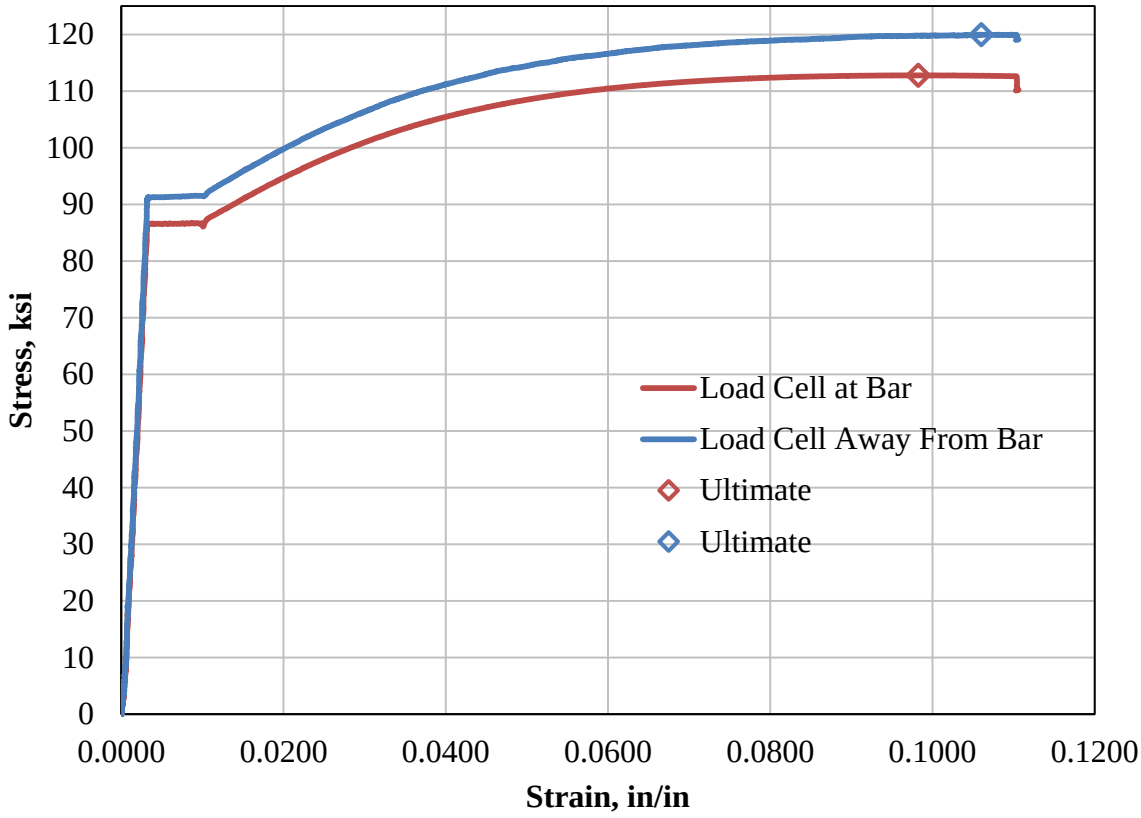

Figure 3-16. Results of single No. 11 bar test showing impact of neglecting losses resulting from location the load cell away from the test specimen

In order to account for these losses, a relationship between the force applied to the load cell and the force experienced by the test specimen was obtained by performing a subset of tests in which a second 200 kip load cell was placed directly in-line with the test specimen (Fig. 3-17). Preliminary tests of a No. 9 bar, a No. 11 bar, and a No. 14 bar using this modified test setup revealed a consistent five to six percent difference in the forces recorded by the two load cells after about 50 kips regardless of bar size. The tests also revealed that the off-bar load cell tended to register the maximum force 30-50 seconds after the on-bar load cell. The ultimate tensile strains associated with this 30-50 second delay differed by

about 6.5% with the higher strain values corresponding to the delayed max force. This phenomenon arises from the fact that the Optotrak strain data is paired with the load cell data by matching record counts.

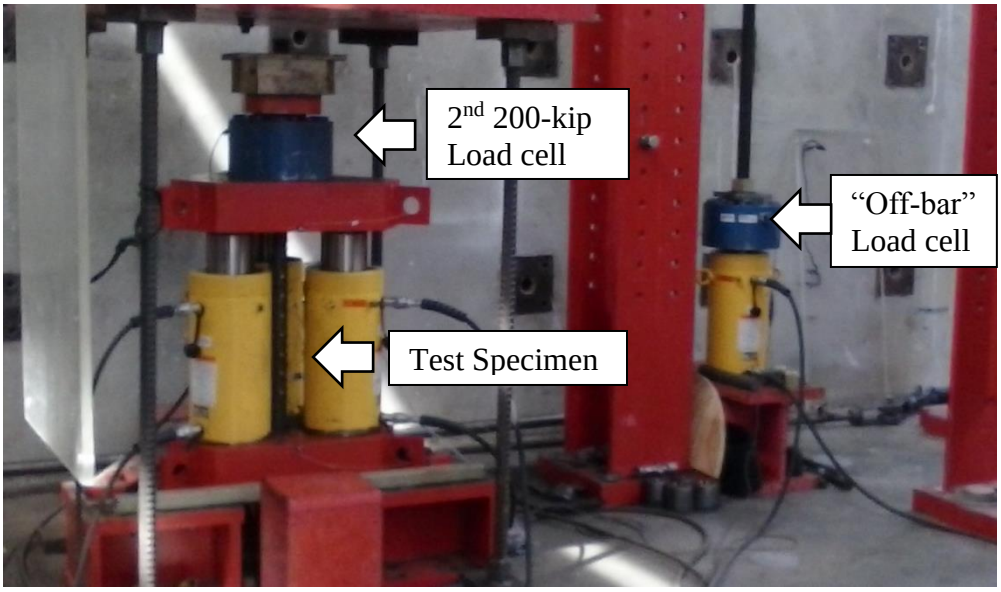

Figure 3-17. Modified test setup with one 200-kip load cell in-line with the test specimen and another 200-kip load cell on a separate jack connected to the same hydraulic source

An additional, more thorough series of tests on nine No. 11 bars and nine No. 14 bars was used to confirm the trend observed in the three tests just described. One test specimen was taken from each heat of each mill (18 total specimens) and tested in the modified test setup that included both 200 kip load cells, one in-line with the bar and one separate from the bar. These tests confirmed that the percent error between the two load cells followed a consistent trend regardless of bar size. The results of these tests are presented in Figure 3-18. Note that the tests could only be conducted up to a force of 230 kips before risking permanent damage to the load cell in-line with the bar. This upper limit allowed testing of the

No. 11 bars fully to ultimate but required the No. 14 bar tests to be stopped during the strain hardening region.

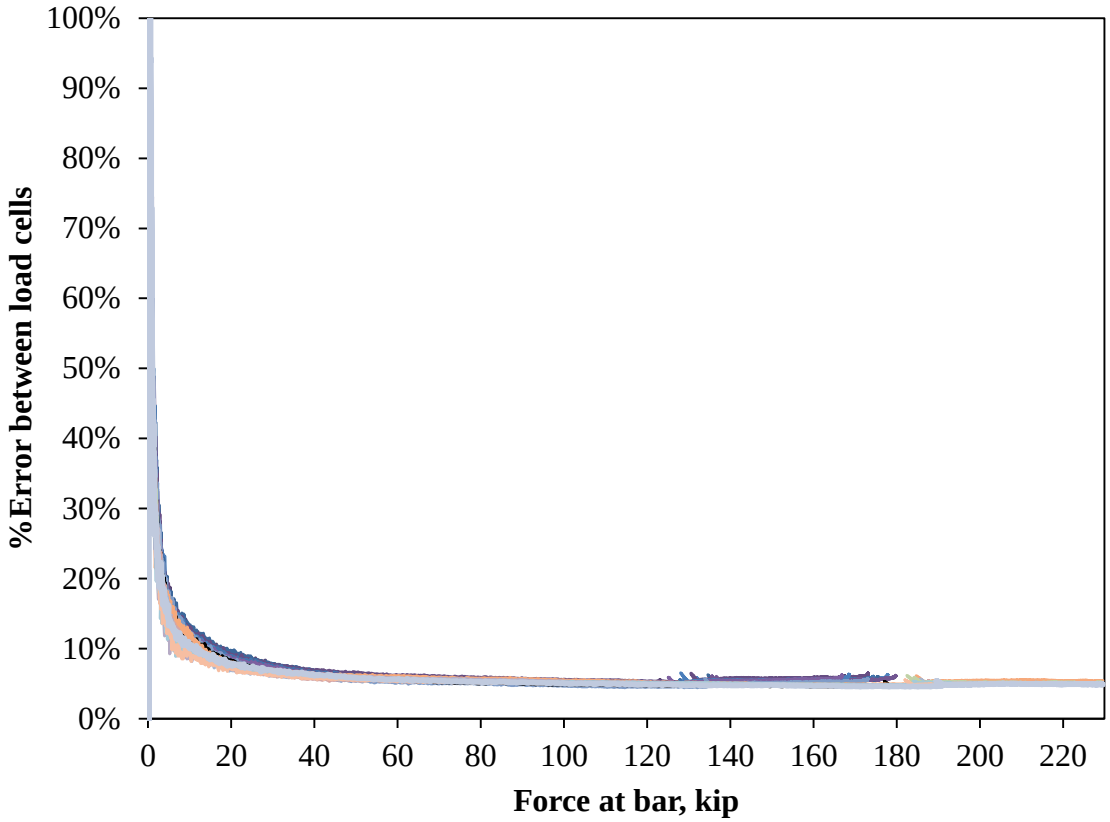

Figure 3-18. Relationship between the on-bar load cell and the off-bar load cell forces for 9 No. 11 and 9 No. 14 bar tests

Table 3-4 summarizes the average percent errors for the three affected parameters. Based on these values, the following reductions were applied to the No. 11, 14, and 18 bar data collected using the off-bar load cell: a 5% reduction in the expected yield strength values, a 6% reduction in the expected tensile strength values, and a 6.5% reduction in the expected ultimate tensile strain values.

Table 3-4. Results from the additional 9 No. 11 and 9 No. 14 bar tests used to develop adjustment factors

	f_{ye}	$f_{ye\ off\text{-}bar}$	%Error	f_{ue}	$f_{ue\ off\text{-}bar}$	%Error	ε_{su}	$\varepsilon_{su\ off\text{-}bar}$	%Error
Average	83.2	87.5	**5.07%**	110.9	117.8	**6.27%**	0.0999	0.1064	**6.54%**
St. Dev.	2.5	2.6	0.3%	2.9	3.1	0.2%	0.0031	0.0050	3.1%

3.5. Strain Age Testing

3.5.1. Test matrix

A total of 30 strain aging tests consisting of two bar sizes (No. 5 and No. 7) were conducted for 3 separate pre-strain levels and 5 aging periods. An additional 9 tests were conducted on just No. 7 bars, using the same pre-strain levels, in order to investigate the impact of storing the bars at subfreezing temperatures on the rate of strain aging. The complete test matrix is presented in Table 3-5.

Table 3-5. Number of strain age tests by bar size and aging period. Three pre-strain levels were evaluated for each category: 0.0075, 0.0150, and 0.0300

	48 hours	10 days	30 days	60 days	6 months
No. 5	3	3	3	3	3
No. 7	3	3	3	3	3
No. 7 (freezing)	--	--	3	3	3

3.5.2. Specimen Preparation

In the case of the strain age testing, all of the test specimens originated from the same mill and heat. The purpose of this restriction was to better isolate the variables being considered: bar size, aging period, and pre-strain level. Mill 1 heat 1 was selected for the strain age testing based on the results of the tensile testing program which revealed this

particular heat to have the lowest variability in test results as well as a representative yield plateau length.

While bar sizes No. 5, 7, and 9 were initially planned for the strain aging tests, a damaged part in the MTS machine's grip pressure mechanism precluded the No. 9 bars from the testing program as they required a grip pressure in excess of the machine's reduced capabilities. The selected aging periods of 48 hours, 10 days, 30 days, 60 days, and 6 months were chosen based on the findings of the literature review in which previous researchers observed strain aging in bars aged 37 days (Restrepo-Posada et al., 1994). The first pre-strain level of 0.0075 was chosen to correspond to the end of the yield plateau and the onset of strain hardening in the Mill 1 heat 1 bars. The second pre-strain level of 0.0150 was chosen to be representative of the strain that might realistically be experienced by a longitudinal reinforcing bar during an earthquake not causing collapse or total loss of the structure. In other words, a strain corresponding to a level of damage in the structure that would likely be repaired. The final pre-strain level was chosen as an upper bound value beyond which repair of the structure would likely be impractical. The low temperature tests were meant as a way to identify the temperature-susceptibility of strain aging. As such, the bars were aged at approximately -15° F, but still tested at ambient temperatures.

A specimen length of 24" was chosen for the strain age tests. This corresponded to a bar free length of 14" which allowed room for 5 Optotrak markers to create four 2" gage lengths (Fig. 3-19). Using a shorter specimen length than in the tensile tests served as a way to maximize the use of the remaining rebar, particularly since all of the specimens were taken from the same heat and mill. Furthermore, all of the 48 hour and 10 day test specimens

originated from the same 20’ bar, while the 30 day, 60 day, and 6 month specimens all originated from a second 20’ bar from the same heat. The specimens for the low temperature test were taken from a third 20’ bar, also from Mill 1 Heat 1. The same identification scheme of mill, heat, bar size, bar number, and specimen number used to track the tensile test specimens was additionally used for the strain age specimens to allow comparisons between the two datasets where applicable.

Figure 3-19. No. 7 strain-age test bars returning to ambient temperatures after removing from the freezer. Visible ice formation from moisture in the laboratory air.

3.5.3. Testing Parameters

As a result of the shorter specimen length, a lower testing speed could be used for the strain age tests. All specimens were pre-strained at a rate of 0.3 in/min corresponding to the

upper bound pre-yield strain rate permitted by ASTM A370. A load rate of 0.7 in/min was used to re-test the specimens at the conclusion of the aging period.

The procedure for conducting the strain age tests was to initially test the bar to the desired pre-strain, pause the test, and then gradually release the force on the bar until it could be removed from the grips of the MTS machine. Following this, the bars were stored at ambient laboratory temperatures for the duration of the desired aging period. In the case of the low temperature tests, the bars were placed into a freezer upon completion of the pre-strain testing where they remained until the end of the aging period. At the conclusion of this period, the bars were again loaded into the testing machine and tested until failure. The low temperature bars where allowed a minimum of 1 hour to return to ambient temperatures before being retested. Chapter 4 presents the results from the tests.

3.6. Cyclic Testing

A limited number of cyclic tests on No. 5 and No. 7 bars were conducted with the primary purpose of evaluating the capability of existing rebar models to characterize the cyclic material behavior. A further intent of the cyclic testing program was to investigate the effect of cyclic load history on the ultimate tensile strain (strain at max stress). While difficulties with the gripping mechanism of the MTS machine greatly limited the scope of this portion of the research, informative results were still able to be obtained.

3.6.1. Test Matrix

Table 3-6 summarizes the cyclic tests that were performed. A total of ten No. 5 bars and three No. 7 bars were tested in the as-rolled condition using varying load histories and

numbers of cycles. Two of the No. 7 bars and two of the No. 5 bars were tested in manual control and given a random load history. The remaining specimens were tested in either displacement or force control mode with the intent of cycling between tensile and compressive strains considered to be representative of the actual strain history that a longitudinal reinforcing bar might undergo during an earthquake. Due to issues explained in Chapter 4, none of the force control or displacement control specimens actually attained the desired strain history due to complications with the testing grips. As a consequence, the table includes both the anticipated strain history and the actual train history occurring during the test.

Table 3-6. Cyclic test matrix

ID	Bar Size	L/d_{bl}	Control Mode	Anticipated Strain History # cycles (T, C)	Actual Strain History # cycles (T, C)
12541	5	6	displ.	20 (0.02, -0.005)	20 (0.015, -0.002)
12542	5	6	displ.	20 (0.02, -0.005)	20 (0.013, -0.002 to 0.004)
12543	5	6	displ.	20 (0.017, -0.005)	20 (0.02 to 0.024, 0.001 to 0.015)
12544	5	6	displ.	100 (0.01, -0.001)	100 (0.0025, -0.002)
12546	5	6	force	20 (0.01, -0.001)	20 (0.009, -0.002)
12547	5	6	force	100 (0.01, -0.001)	100 (0.0086 to 0.012, -0.003 to 0.0005)
12548	5	6	displ.	50 (0.02, 0.017)	60 (0.009, 0.0076)
12549	5	6	force	50 (0.02, $\varepsilon(\sigma=0)$)	50 (0.017 to 0.025, 0.013 to 0.021)
125410	5	6	manual	8 (0.01, 0.00) 2 (0.02, 0.01)	8 (0.01, 0.00) 2 (0.02, 0.00)
125411	5	6	manual	10 (0.01, 0.00) 10 (0.02, 0.01) 10 (0.03, 0.02)	10 (0.01, 0.00) 10 (0.02, 0.01) 10 (0.03, 0.02)
12746	7	6	displ.	10 (0.02, -0.005) 10 (0.02, -0.005)	10 (0.007, -0.003) 10 (0.02 to 0.01, -0.02 to -0.03)
Rand 1	7	6	manual	random	Fig. 4-36
Rand 2	7	6	manual	random	Appendix I

3.6.2. Specimen Preparation

Save for the two No. 7 bars tested manually, test specimens used to perform the cyclic tests were taken from the remaining Mill 1 heat 2 bars as this mill provided extra steel and the tensile tests showed comparatively low variability within this heat. Furthermore, each of the No. 5 bar test specimens originated from the same 20' length. Two of the No. 7 bar specimens originated from a common 20' length of bar. The test specimens were cut to provide an unbraced length between the MTS machine crossheads of 6 bar diameters. The same identification scheme of mill, heat, bar size, bar number, and specimen number used to track the tensile and strain age test specimens was used for the cyclic test specimens to allow for close comparison with the tensile test results.

3.6.3. Test Parameters

Due to the lack of requirements for performing tensile tests, as discussed in Chapter 2, the tensile testing speed requirements of ASTM A370 were translated into cycle frequency based on an equivalent monotonic rate of 0.7 in/min. While the majority of the tests were conducted for just 20 cycles, a few tests were performed for a greater number of cycles, as indicated in Table 3-6, as part of the effort to identify the effect of cycling on the monotonic strain at max stress.

Initially, all of the tests were conducted using the MTS machine's displacement control mode in which the desired strain history was first transformed into displacement limits based on the expected unbraced length of the bar. The bar was then tested between these displacement limits using a sinusoidal wave form at a cycle rate defined by the

specified frequency, as stated above. As will be presented in Chapter 4, this approach did not result in a consistent strain history. As such, later tests used a force-based load history in which the desired strain history was correlated with a theoretical force history based on the results of earlier tests in the project. The use of a direct strain-controlled cyclic load history in which readings from the extensometer would be used to internally control the MTS cross-head movement in real time was avoided as it risked damage to the extensometer in the event of slipping of the extensometer on the bar. Later tests were controlled manually by operating the MTS machine in a monotonic test mode using a slower displacement rate equivalent to 0.2 in/min and manually reversing the load direction at the desired stain limits which could be read in real time from the extensometer through the data acquisition. Several of the specimens were tested monotonically in tension following the cyclic loading to evaluate the impact of cycling on the ultimate tensile strain.

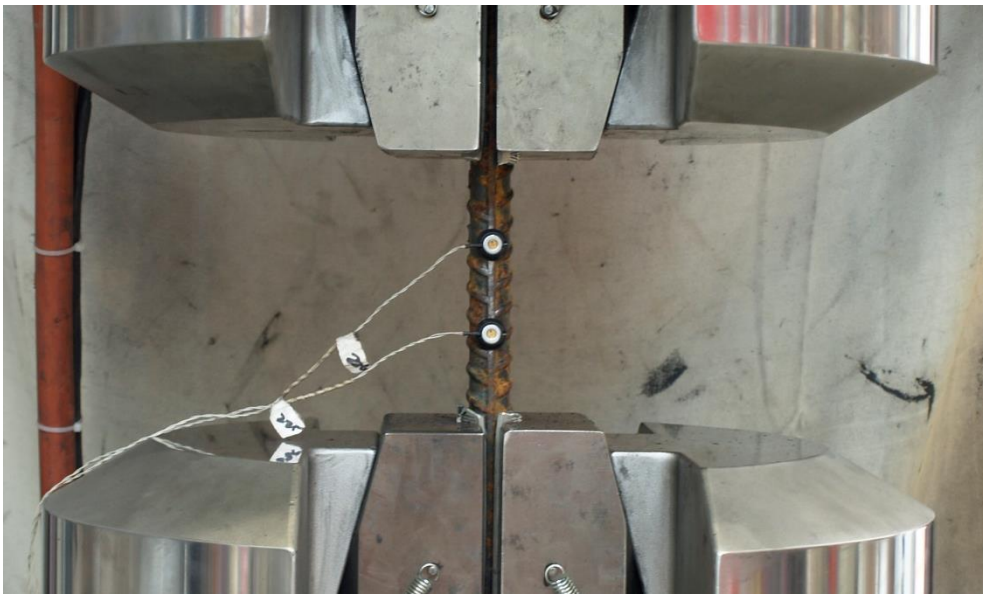

Figure 3-20. No. 7 bar in MTS machine prior to testing

4. RESULTS

4.1. Chapter Overview

Presented in this chapter are the findings of the experimental program just described. As with the previous chapter, each of the three types of tests are addressed independently. The presentation of the tensile test results opens with an explanation of which stress-strain parameters were evaluated and how they were determined. Following this is an overview of the statistical methods used in interpreting the findings and then a presentation of each of the stress-strain parameters in terms of the identified cumulative distribution functions including best-fit probability distributions. Relevant summary statistics of the tensile tests are provided in Section 4.2.3.10.

The strain aging section of this chapter presents the results of the 30 tests that were described in Chapter 3. A subsection is devoted to each of the four variables investigated for impact on strain-aging: impact of aging period, impact of pre-strain, impact of bar size, and impact of low temperature. Stress-strain curves from the tests have been located in Appendix H.

The chapter concludes with a presentation of the results of the cyclic testing program. Included in this is a presentation of a cyclic material model that has been fitted to one of the experimental stress-strain curves. Also included in the cyclic test results section is a presentation of the tests used to identify the impact of cyclic load history on the monotonic strain at max stress.

4.2. Tensile Testing

4.2.1. Determination of Stress-Strain Parameters

Each test generated two raw data files: one text file containing force data and one CSV file containing the Optotrak marker x-y-z coordinate data. Data was collected at a frequency of 8 Hz for the No. 4 through No. 10 bar tests and 2 Hz for the No. 11 through No. 18 bar tests. A slower recording rate was chosen for the large bar tests to account for the slower displacement rate produced by the electric hydraulic pump.

The two raw data files were compiled and processed in a single macro-enabled Excel workbook unique to each test in which forces were converted to stresses based on the nominal cross-sectional area of the bar and Optotrak marker coordinate data was converted to strain data using the procedure described in Chapter 3. A combination of VBA programs and Excel worksheet functions was used in these compiled individual test files to identify the values of the six parameters needed to define the monotonic stress-strain curve, as indicated in Section 1.2, within each gage length for each test. Table 4-1 provides a list of all the parameters for which values were determined for each test. These parameters were specifically selected as they correspond to transitional points on the monotonic stress strain curve, and many of them are necessary to defining existing material models. Parameters highlighted in bold were used to define the recommendations for the A706 grade 80 stress-strain curve presented in Chapter 5. The remainder of this section describes each of the parameters and how they were determined.

Table 4-1. Complete list of parameters determined for each tensile test

Modulus of Elasticity	Yield						Onset of Strain Hardening		Ultimate Tensile	
	ADM		EUL		0.2% OM					
E_s	$f_{y\ ADM}$	$\varepsilon_{y\ ADM}$	$f_{y\ EUL}$	$\varepsilon_{y\ EUL}$	$f_{y\ OM}$	$\varepsilon_{y\ OM}$	f_{sh}	ε_{sh}	f_u	ε_u

4.2.1.1.Modulus of Elasticity

The modulus of elasticity, E_s, was taken as the slope of the line passing between 0.2 times the top-of-the-knee yield strength and 0.8 times the top-of-the-knee yield strength. This was to ensure that the value obtained was an accurate representation of the actual linear portion of the stress-strain curve and not biased by any non-linearity in the curve at the start of the test or just before the top-of-the-knee yield point. A graphical illustration of this process has been provided in Appendix B.

4.2.1.2.Yield Strength

Three methods of determining the yield strength were evaluated: the Autographic Diagram Method or "top-of-the-knee" ($f_{y\ ADM}$), the Extension Under Load Method ($f_{y\ EUL}$), and the Offset Method ($f_{y\ OM}$). The Extension Under Load yield strength was taken as the value of stress corresponding to a strain of 0.0035. The Offset Method yield strength was taken as the value of stress corresponding to the intersection of the stress-stain curve with a 0.2% offset line running parallel to the linear elastic region of the curve. All three methods are permitted by ASTM A370. A graphical illustration of each has been provided in Appendix B.

4.2.1.3.Yield Strain

Three individual yield strains were identified for each test, one corresponding to each of the three determined yield strengths: the Autographic Diagram Method yield strain ($\varepsilon_{y\ ADM}$), the Extension Under Load yield strain ($\varepsilon_{y\ EUL}$), and the Offset Method yield strain ($\varepsilon_{y\ OM}$). The ADM yield strain was taken as the strain corresponding to the top-of-the-knee yield strength ($f_{y\ ADM}$). The EUL yield strain simply equaled 0.0035 by definition. The OM yield strain was identified as the value of strain corresponding to the intersection of the stress-strain curve with a 0.2% offset line running parallel to the linear elastic region of the curve.

4.2.1.4.Onset of Strain Hardening

The strain at the onset of strain hardening, ε_{sh}, was determined as the point at which a horizontal line passing through the 0.2% offset stress intersected a line tangent to the initial portion of the strain hardening curve. Specifically, the tangent line to the strain hardening curve was defined as the line passing between 1.02 times the 0.2% offset yield strength and 1.05 times the 0.2% offset yield strength. In specimens exhibiting well-defined yield plateaus, the 0.2% offset line consistently intersected the yield plateau thus making the horizontal line passing through this point analogous to the slope of the yield plateau. The stress at the onset of strain hardening was taken as the point on the actual stress-stain curve corresponding to the strain at the onset of strain hardening using interpolation as necessary. This approach was designed to reduce subjectivity in determining when the yield plateau ceased and when the strain hardening curve commenced as well as to speed up the processing of the data. A graphical illustration of this process has been provided in Appendix B.

4.2.1.5.Tensile Strength and Ultimate Tensile Strain

The tensile strength, f_u, was identified as the maximum value of stress occurring during the test; in other words, the point at which strain hardening ceased and necking initiated. The ultimate tensile strain, ε_u, was identified as the value of strain corresponding to the point of maximum stress. This is not to be confused with the value of strain at fracture.

4.2.2. Statistical Methods

Two primary approaches were taken to interpreting the body of data generated during the tensile testing program. The first approach was to describe the combined results for each of the parameters in terms of its summary statistics, specifically: mean, standard deviation, coefficient of variation, 5th percentile, and 95th percentile. A summary of these results is presented in Section 4.2.3.10. The second approach was to plot the cumulative distribution curves for each parameter and then evaluate the underlying probability distributions. This method accomplished several things: it provided a graphical means of illustrating the spread of the data, it provided a graphical way to identify trends or anomalies in the data, and most significantly it provided a resource for other researchers to use in the future. The remainder of this section expands on the latter of these two approaches.

Quantitatively, a cumulative distribution function (CDF) describes the percentage of data in a dataset that exists at or below a given value. Qualitatively, it serves as a graphical means of illustrating the distribution of the data in a dataset about its median. CDFs that are short and steep imply less variability in the data while CDFs that are long and sweeping imply higher variability in the data. It should be noted that this interpretation can be biased

by the scale used in generating the graph. The term *empirical* distribution function is used to describe the arrangement of the actual, raw measurements according to probability of exceedance. Several methods of organizing the empirical distribution of a dataset have been proposed; however, the method followed in this paper is presented in Equation 4-1. The equation was implemented indirectly through the PERCENTRANK.EXC function in EXCEL.

Equation 4-1

$$P_i = \frac{i}{(N+1)}$$

Knowledge of the underlying distribution of a dataset is beneficial in that it permits the dataset to be defined by a mathematical function that can be used to approximate values from the global dataset (in this case, all A706 grade 80 bars in existence) which is typically impossible to completely test. An example of where such findings are useful is in the area of probabilistic seismic risk assessment in which sampling techniques such as Latin Hypercube sampling are used within a Monte Carlo simulation to develop seismic fragility curves that take into consideration the expected material properties and their associated distributions. Thus, the ability to define the constitutive properties of the material as mathematical expressions is extremely useful.

Five probability distributions were analyzed for each of the primary monotonic stress-strain parameters in an effort to identify which underlying distributions described their empirical distributions. Specifically, the normal distribution, lognormal distribution, and beta distribution were selected based on the literature findings presented in Chapter 2. The gamma

and Weibull distributions were additionally investigated. It should be noted that a unique aspect of the current work is the consideration of the strain parameter distributions in addition to the strength parameter distributions.

Numerous methods of evaluating the likelihood that a dataset originates from a given distribution are available. For the purposes of this research, the Kolmogorov-Smirnov (KS) goodness-of-fit test was chosen and used to evaluate the distributions at a 5% significance level. The confidence intervals and maximum likelihood estimates for each parameter were obtained using the Matlab distribution fitting functions (*betafit*, *gamfit*, etc.). The final shape parameter values needed to define each distribution were obtained by varying the maximum likelihood estimates within the confidence intervals using the Solver command in EXCEL such that sum square of the error between the fitted distribution and the empirical data was minimized. The KS test was then performed on this fitted distribution to evaluate the quality of the fit. Table 4-2 indicates which probability distributions were found to be acceptable fits for each of the stress-strain parameters in order of accuracy. Table 4-3 provides the derived values of the shape parameters used to define the fitted distributions.

Table 4-2. Probability distributions found to be acceptable fits to each parameter from the KS test at a 5% significance level in order of accuracy

	Normal	**Lognormal**	**Beta**	**Gamma**	**Weibull**
f_y	-	-	1	2	-
ε_y	-	-	2	1	-
ε_{sh}	-	-	-	-	-
f_u	2	1	3	4	-
ε_u	-	-	-	-	1
f_u/f_y	-	-	2	1	-

Table 4-3. Shape parameter values used to define the fitted probability distributions

Parameter	Beta		Gamma		Weibull	
	alpha	**beta**	**alpha**	**beta**	**alpha**	**beta**
f_y	123.49	21.86	873.28	9.75E-04	-	-
ε_y	139.73	43151.61	141.74	2.28E-05	-	-
ε_{sh}	-	-	-	-	-	-
f_u	440.36	342.84	1001.69	5.61E-04	-	-
ε_u	-	-	-	-	21.72	0.0978

As previously stated, each test specimen was outfitted with six 2” gage lengths for recording strains. Recall that this additionally allowed strains to be calculated over any of three overlapping 8” gage lengths (Section 3.4.2). Due in part to variability in recording the data and in part to the fact that strains are not perfectly uniform throughout the entire length of bar (refer Section 5.1.6), there is some variability between gage lengths at a given strain recording as illustrated in Figure 4-1. As a result, six unique 2” gage length strains and three unique 8” gage length strains can be identified for every one recording of force. This translates into as many as nine values for the yield strain, onset of strain hardening, and ultimate tensile strain parameters for each test.

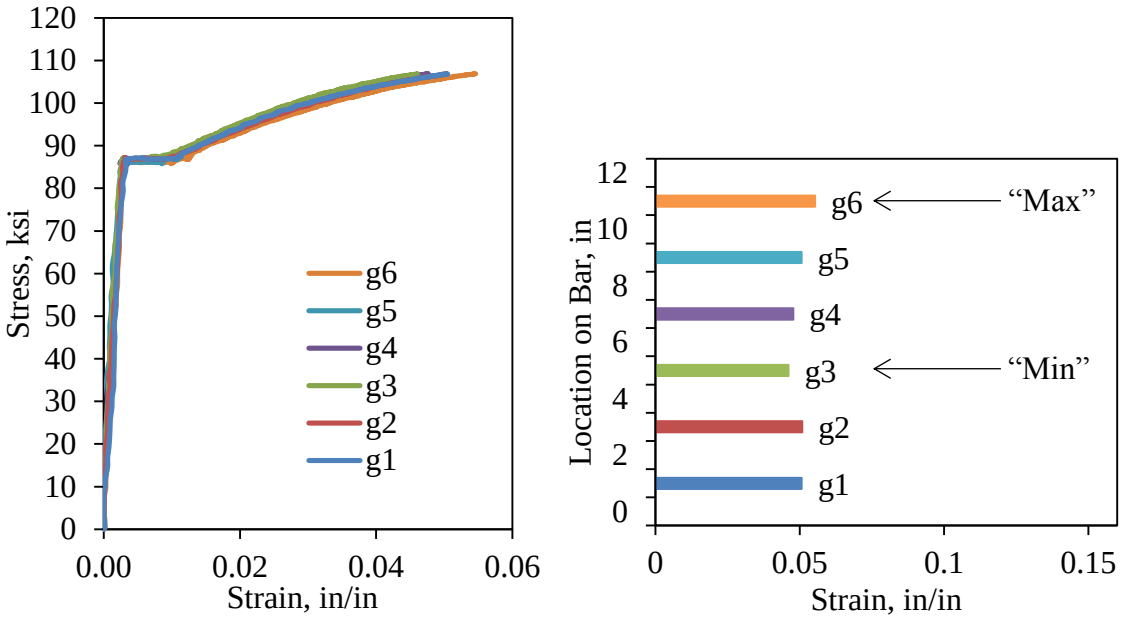

Figure 4-1. Partially plotted stress-strain curve (left) and distribution of strain over instrumented region at that instant (right)

Noting from Section 3.4.2 that little difference existed between 2" and 8" gage length measurements, this can be reduced to six values per parameter for each test by considering only the 2" gage length results. However, in order to plot the CDF curves for the strain-based parameters, it is desirable that each test be represented by only one data point.

As a result, four CDF curves have been plotted for all of the stress-strain parameters obtained from Optotrak strain data. One of the curves is composed entirely of the minimums of the six values from each test ("Min" CDF). Similarly, one of the curves is composed entirely of the maximums of the six values from each test ("Max" CDF). A third curve is obtained by taking the mean of the six values from each test ("Mean" CDF), and a fourth CDF curve is obtained by taking all six values from each test ("Total" CDF). Necessarily, this fourth curve includes on the order of six times as many data points as any of the other

three curves. As will be seen, the recommended values were ultimately taken from the CDF curves of the means and the min, max, and total CDF curves left for illustrative purposes only.

4.2.3. Expected Mechanical Properties

4.2.3.1.Modulus of Elasticity

As described in Section 4.2.1, the modulus of elasticity was defined as the slope of the linear elastic region of the stress-strain curve between 0.2 times the top-of-the-knee yield strength and 0.8 times the top-of-the-knee yield strength. This parameter was not evaluated for a best-fit probability distribution.

Figure 4-2 presents the empirical CDF curves for the modulus of elasticity considering all bar sizes. Because this parameter is indirectly based on Optotrak readings, there are four empirical distributions, as described in Section 4.2.2. The mean value of the empirical data is 27,888 ksi. The standard deviation and coefficient of variation are 1,601 ksi and 5.7% respectively. Also included in the graph is a modulus of elasticity value of 29,000 ksi for reference.

Figure 4-3 illustrates the breakdown of the modulus of elasticity data according to the mean CDFs for each bar size. The mean values ranged from 26,143 ksi to 28,894 ksi with the No. 14 bars having the lowest mean value and the No. 4 bars having the highest. There was no indication that the modulus of elasticity was influenced by bar size. Table 4-5 summarizes the mean values of each parameter according to bar size.

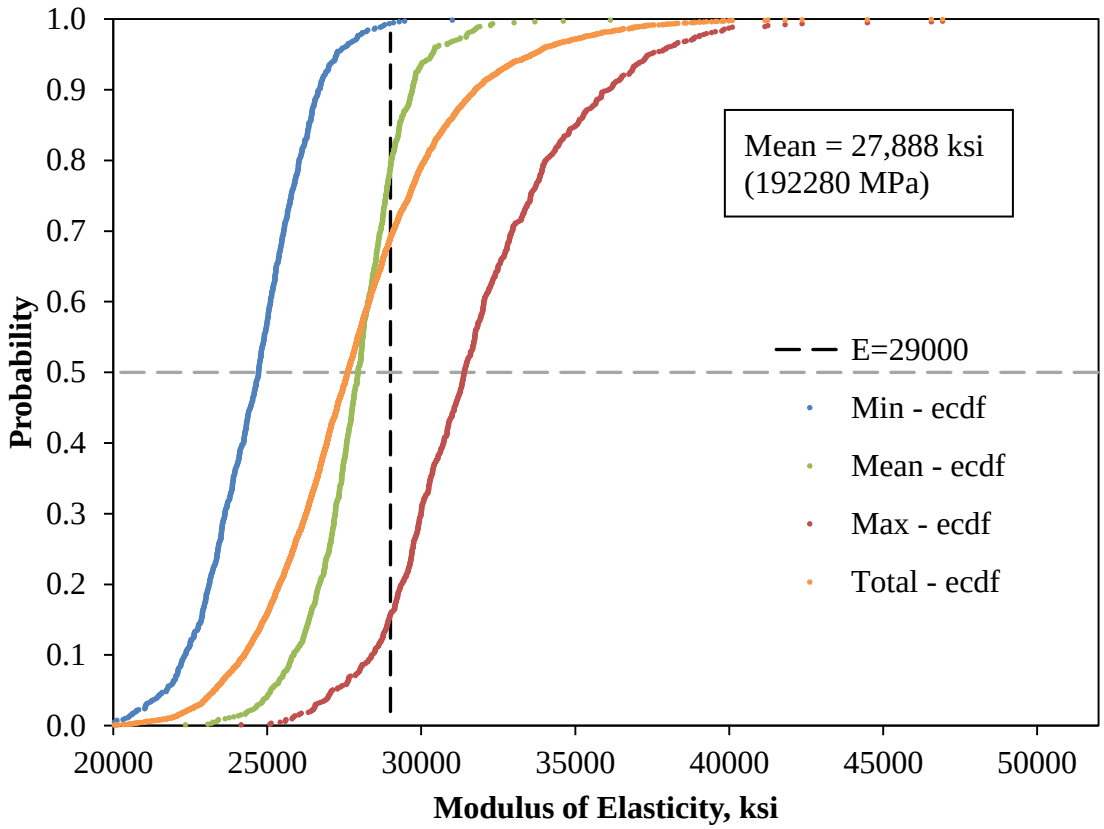

Figure 4-2. Modulus of elasticity empirical CDFs including all bar sizes

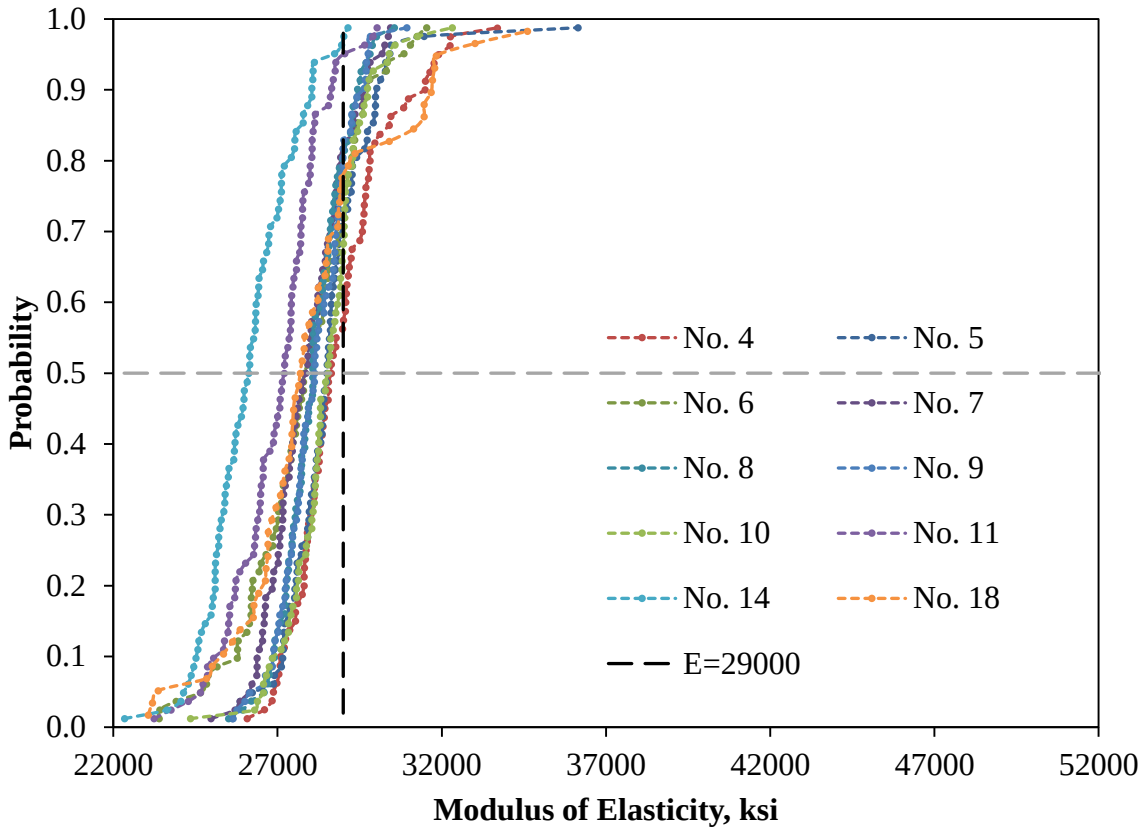

Figure 4-3. Modulus of elasticity empirical CDFs for individual bar sizes

4.2.3.2.ADM Yield Strength

As described in Section 4.2.1., the ADM yield strength corresponded to the upper yield strength or top-of-the-knee yield strength. Test specimens that did not exhibit well-defined yield plateaus (98 of 788 tests) were not included in this dataset. A summary of the different categories of yield behavior and percentages on how many tests fell in each category are provided in Appendix G. Additionally, a comparison of the 0.2% Offset Method yield strengths and the Autographic Diagram Method or top-of-the-knee yield strengths is

provided in Appendix F. As stated in Chapter 3, a 5% reduction was applied to the No. 11, 14, and 18 bar yield strengths to account for the losses occurring in the custom testing rig.

The beta and empirical CDF curves for the ADM yield strength considering all bar sizes are presented in Figure 4-4. The gamma and beta distributions were found to be acceptable fits to the yield strength data at a 5 percent significance level; however, the beta distribution was identified as the best fitting distribution based on the Kolmogorov-Smirnov statistic. This observation is consistent with the work by Bournonville et al. (2004) who found the beta distribution to be an acceptable fit for A706 grade 60 rebar.

The mean value of the empirical data is 85.0 ksi. The standard deviation and coefficient of variation are 3.0 ksi and 3.6% respectively. Also included in the graph are the ASTM minimum and maximum allowable yield strengths of 80 ksi and 98 ksi respectively (ASTM, 2016). Because this parameter is determined based on load cell readings as opposed to Optotrak readings, there is only one fitted and one empirical distribution.

From the figure, it is immediately apparent that several of the tests (48 out of 690 tests) fell below the ASTM lower limit of 80 ksi. While this behavior was limited solely to the No. 11, 14, and 18 bars (see Figure 4-5), it was demonstrated through additional testing that this was not a result of the adjustment factor previously described. A further observation of the testing was that different bar sizes originating from the same heat could have distinctly different yield strengths. This observation is presented in further detail in Chapter 5.

Figure 4-5 illustrates the breakdown of the ADM yield strength data according to bar size. These curves were not evaluated for best-fit probability distributions. The mean values ranged from 80.7 ksi to 88.0 ksi (556 MPa to 607 MPa) with the No. 18 bars having the

lowest mean value and the No. 4 bars having the highest. Table 4-5 summarizes the mean values of each parameter according to bar size.

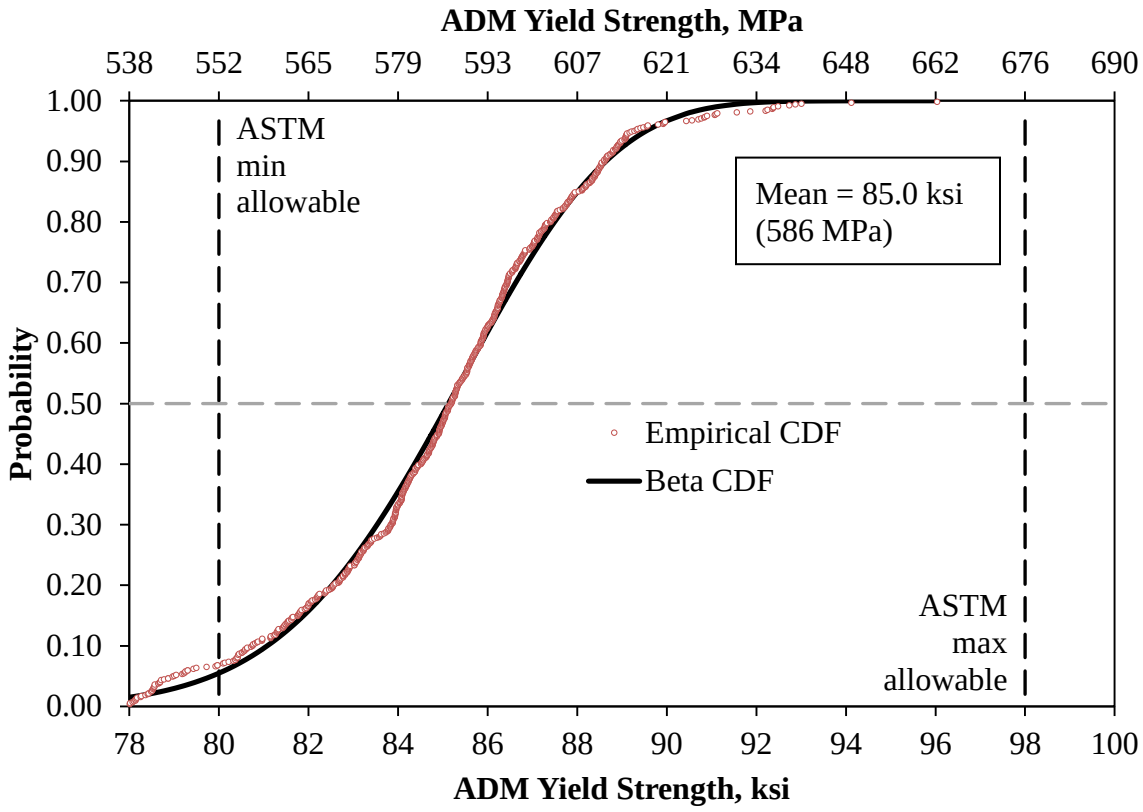

Figure 4-4. ADM yield strength beta and empirical CDFs including all bar sizes

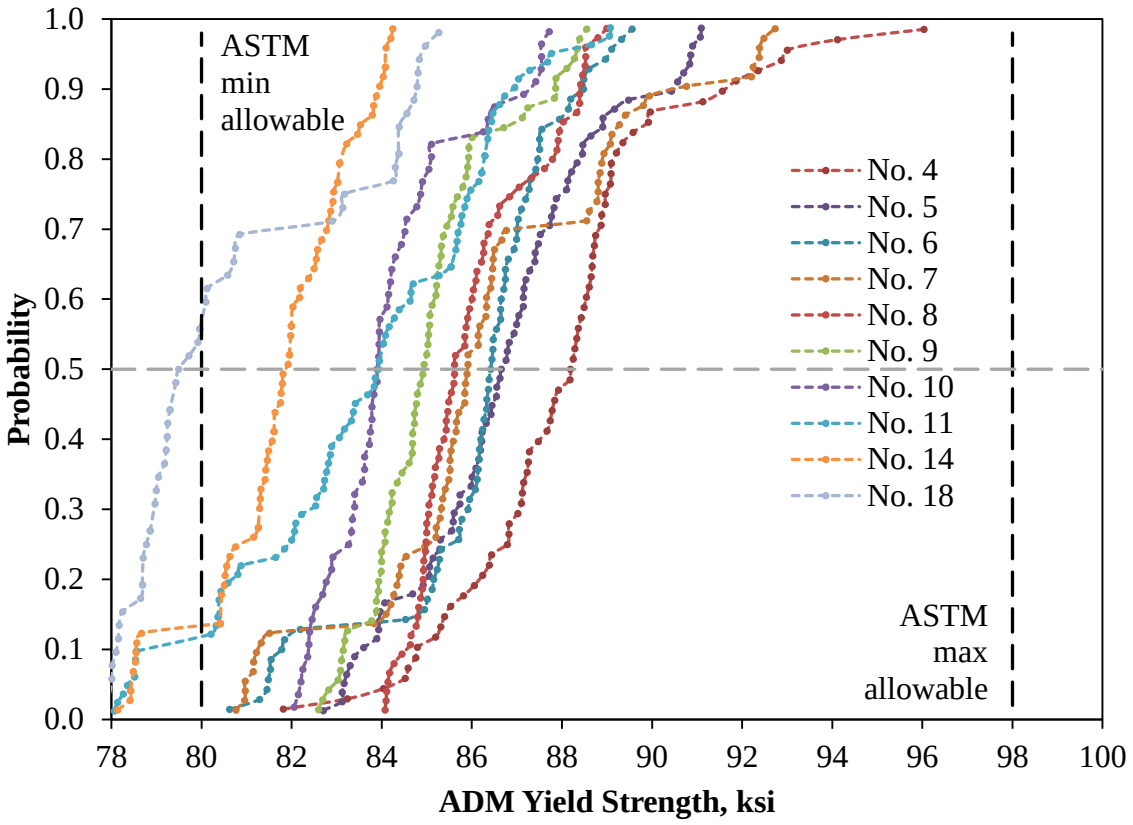

Figure 4-5. ADM yield strength empirical CDFs for individual bar sizes

4.2.3.3.EUL Yield Strength

As described in Section 4.2.1., the EUL yield strength was defined as the value of stress at a strain of 0.0035. All tests were included in this dataset, regardless of yield behavior. A summary of the different categories of yield behavior and percentages on how many tests fell in each category are provided in Appendix G. A 5% reduction was applied to the No. 11, 14, and 18 bar yield strengths to account for the losses occurring in the custom testing rig.

As this parameter was not used to prescribe recommendations for the yield strength, it was not evaluated for a best-fit probability distribution.

Figure 4-6 presents the empirical CDF curves for the EUL yield strength considering all bar sizes. Because this parameter is indirectly based on Optotrak readings, there are four empirical distributions, as described in Section 4.2.2. The mean value of the empirical data is 84.3 ksi. The standard deviation and coefficient of variation are 3.2 ksi and 3.8% respectively. Also included in the graph are the ASTM minimum and maximum allowable yield strengths of 80 ksi and 98 ksi respectively (ASTM, 2016).

As with the ADM yield strength CDF's, it is immediately apparent that several tests failed to meet the ASTM minimum yield strength requirements. This observation is presented in further detail in Chapter 5.

Figure 4-7 illustrates the breakdown of the EUL yield strength data according to bar size. Only the mean empirical CDF for each bar size is presented. The mean values of the mean empirical data, based on a 2" gage length, ranged from 80.5 ksi to 86.6 ksi with the No. 18 bars having the lowest mean value and the No. 4 bars having the highest. The general trend from the empirical CDF is that there is a decrease in median yield strength with increasing bar size. Table 4-5 summarizes the mean values of each parameter according to bar size.

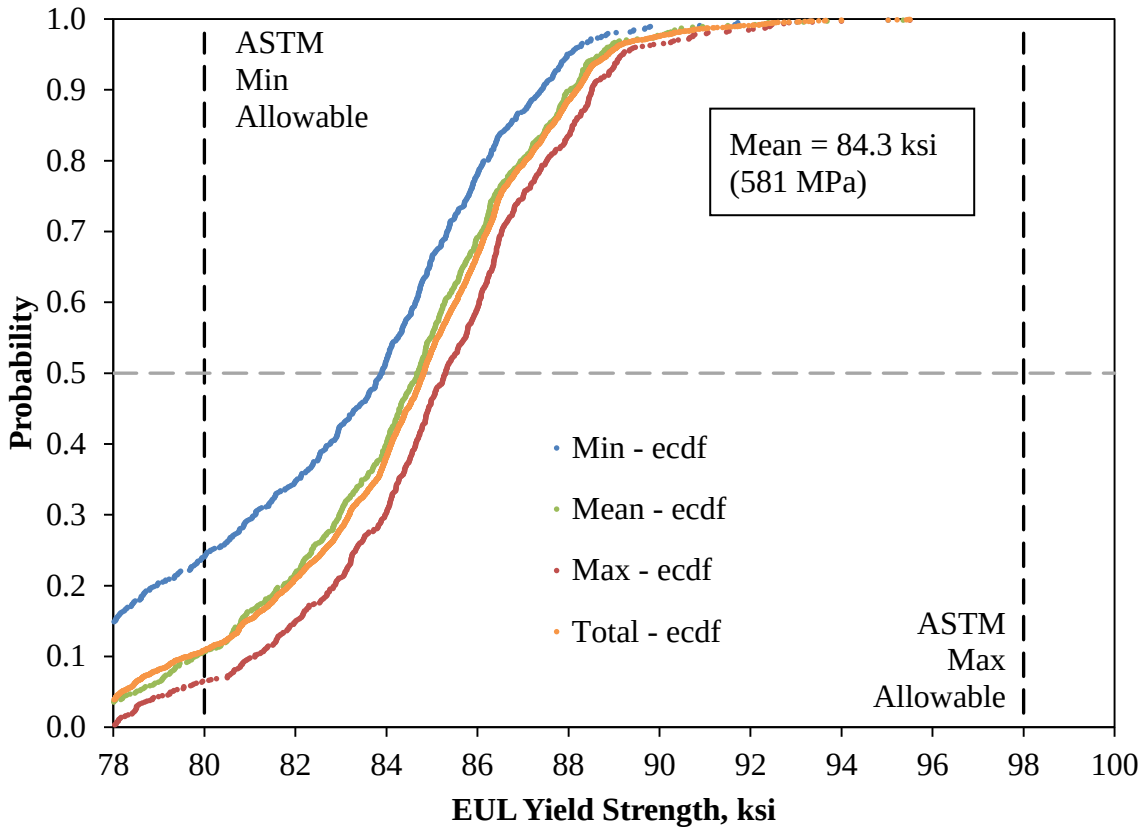

Figure 4-6. EUL yield strength empirical CDFs including all bar sizes

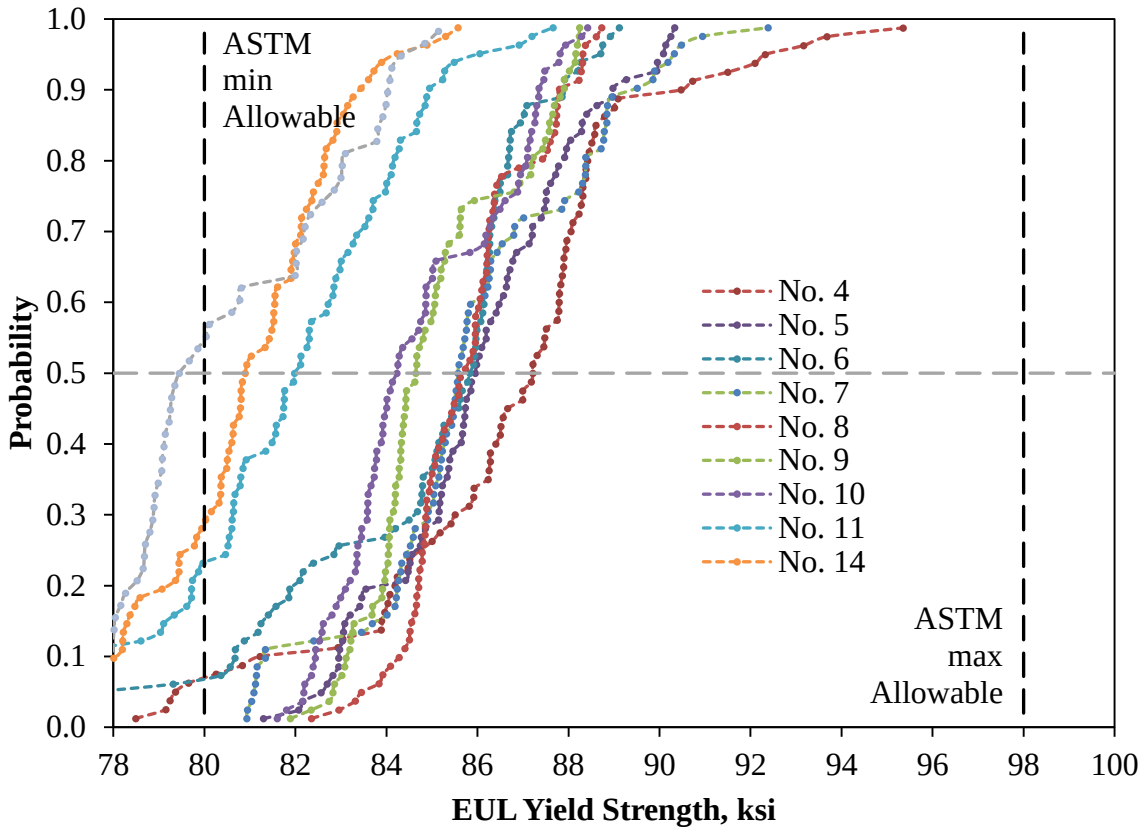

Figure 4-7. EUL yield strength empirical CDFs for individual bar sizes

4.2.3.4.OM Yield Strength

As described in Section 4.2.1, the OM yield strength was defined as the value of stress corresponding to the intersection of the stress-stain curve with a 0.2% offset line running parallel to the linear elastic region of the curve. All tests were included in this dataset, regardless of yield behavior. A summary of the different categories of yield behavior and percentages on how many tests fell in each category are provided in Appendix G. A 5% reduction was applied to the No. 11, 14, and 18 bar yield strengths to account for the losses occurring in the custom testing rig.

As this parameter was not used to prescribe recommendations for the yield strength, it was not evaluated for a best-fit probability distribution.

Figure 4-8 presents the empirical CDF curves for the OM yield strength considering all bar sizes. Because this parameter is indirectly based on Optotrak readings, there are four empirical distributions, as described in Section 4.2.2. The mean value of the empirical data is 85.1 ksi. The standard deviation and coefficient of variation are 2.9 ksi and 3.4% respectively. Also included in the graph are the ASTM minimum and maximum allowable yield strengths of 80 ksi and 98 ksi respectively (ASTM, 2016).

As with the ADM and EUL yield strength CDF's, it is immediately apparent that several tests failed to meet the ASTM minimum yield strength requirements. This observation is presented in further detail in Chapter 5.

Figure 4-9 illustrates the breakdown of the OM yield strength data according to bar size. Only the mean empirical CDF for each bar size is presented. The mean values of the mean empirical data, based on a 2" gage length, ranged from 81.2 ksi to 87.3 ksi with the No. 18 bars having the lowest mean value and the No. 4 bars having the highest. The general trend from the empirical CDF is that there is a decrease in median yield strength with increasing bar size. Table 4-5 summarizes the mean values of each parameter according to bar size.

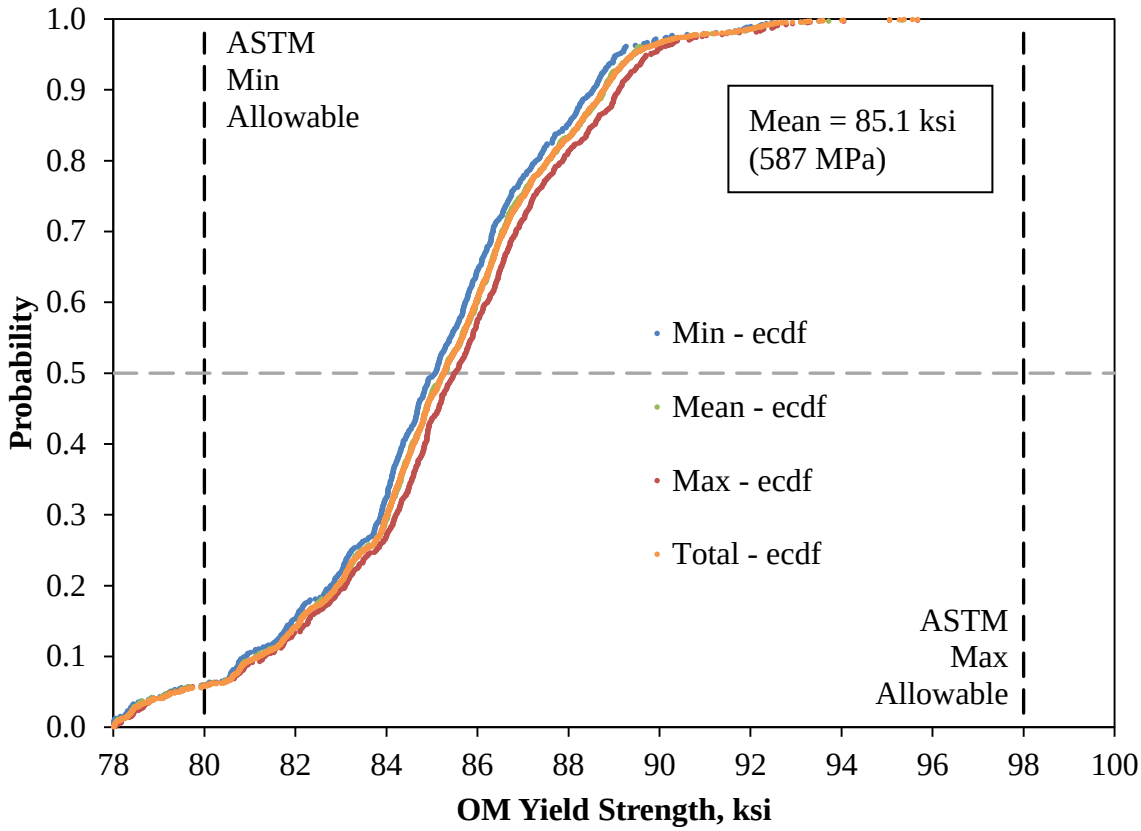

Figure 4-8. OM yield strength empirical CDFs including all bar sizes

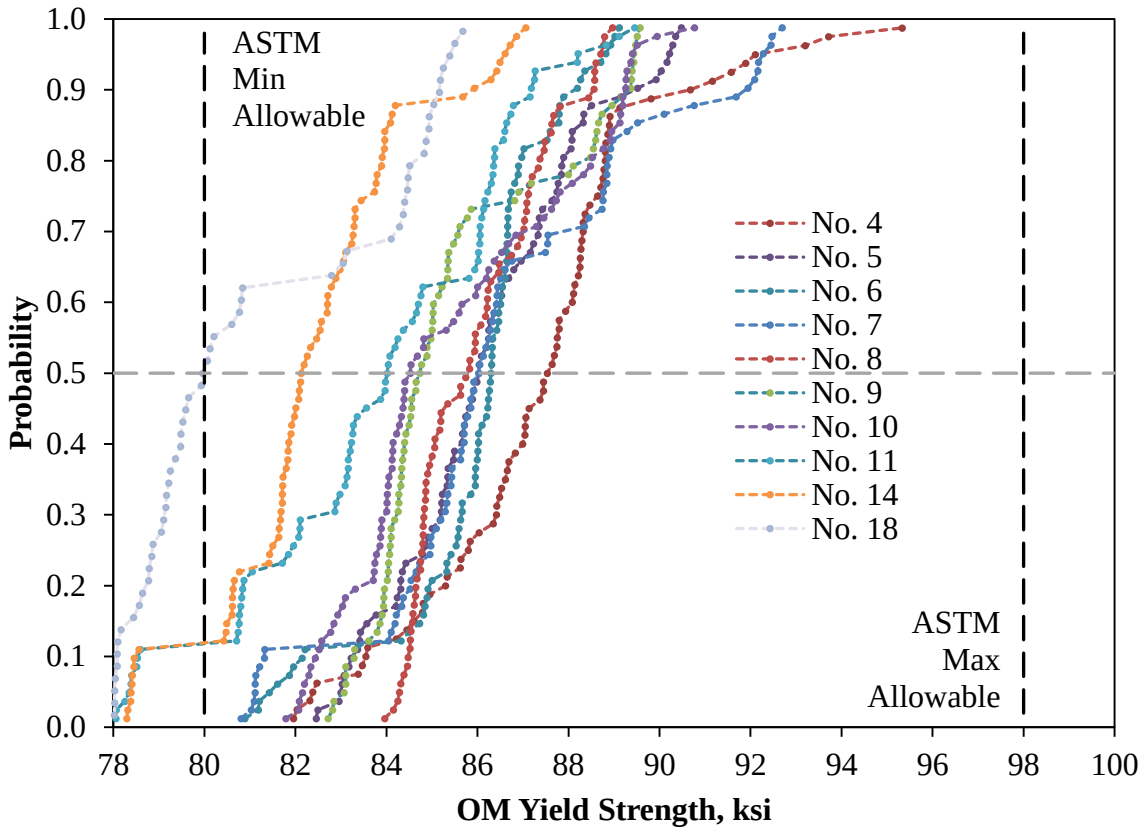

Figure 4-9. OM yield strength empirical CDFs for individual bar sizes

4.2.3.5. Yield Strain

As described in Section 4.2.1., the yield strain was identified as the value of strain corresponding to the stress at the top of the knee of the stress-strain curve at the onset of yielding. This method of determining yield strain was chosen rather than the strain corresponding to the intersection of the 0.2% offset line ($\varepsilon_{y\,OM}$) which always either passed through a point on the yield plateau or intersected the strain hardening curve when specimens exhibited short or nonexistent yield plateaus. In either case, the intersection met the stress-strain curve well after the steel had ceased to be linear elastic. Test specimens that did not

exhibit well-defined yield plateaus (98 of 788 tests) were not included in this dataset. A summary of the different categories of yield behavior and percentages on how many tests fell in each category is provided in Appendix G. Additionally, a comparison of the 2" vs 8" gage length results for the expected yield strain, onset of strain hardening, and the ultimate tensile strain is presented in Appendix E.

The gamma and empirical CDF curves for the expected yield strain are presented in Figure 4-10. The gamma and beta distributions were both found to be acceptable fits to the yield strength data at a 5 percent significance level; however, the gamma distribution was identified as the best fitting distribution based on the Kolmogorov-Smirnov statistic.

Because this parameter is determined based on Optotrak readings, there are four empirical distributions as described in Section 4.2.2. The gamma distribution was fitted to the mean empirical distribution. The mean value of the mean empirical data, based on a 2" gage length, is 0.0033 in/in. The corresponding standard deviation and coefficient of variation are 0.0003 in/in and 9% respectively.

Figure 4-11 illustrates the breakdown of the as-measured yield strain data according to the mean CDFs for each bar size. The mean values ranged from 0.0031 to 0.0034 with the No. 10 bars having the lowest mean value and the No. 14 bars having the highest. There is no indication that the yield strain was influenced by bar size. Table 4-5 summarizes the mean values of each parameter according to bar size.

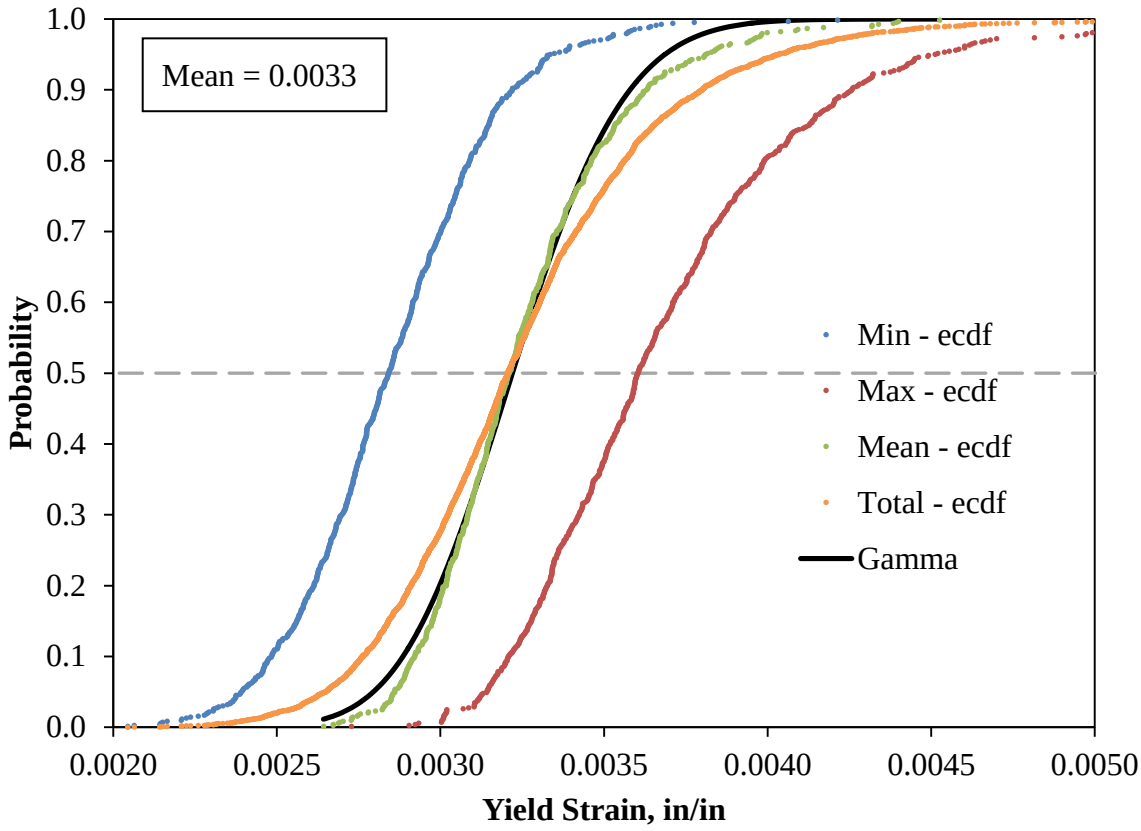

Figure 4-10. Yield strain gamma and empirical CDFs including all bar sizes

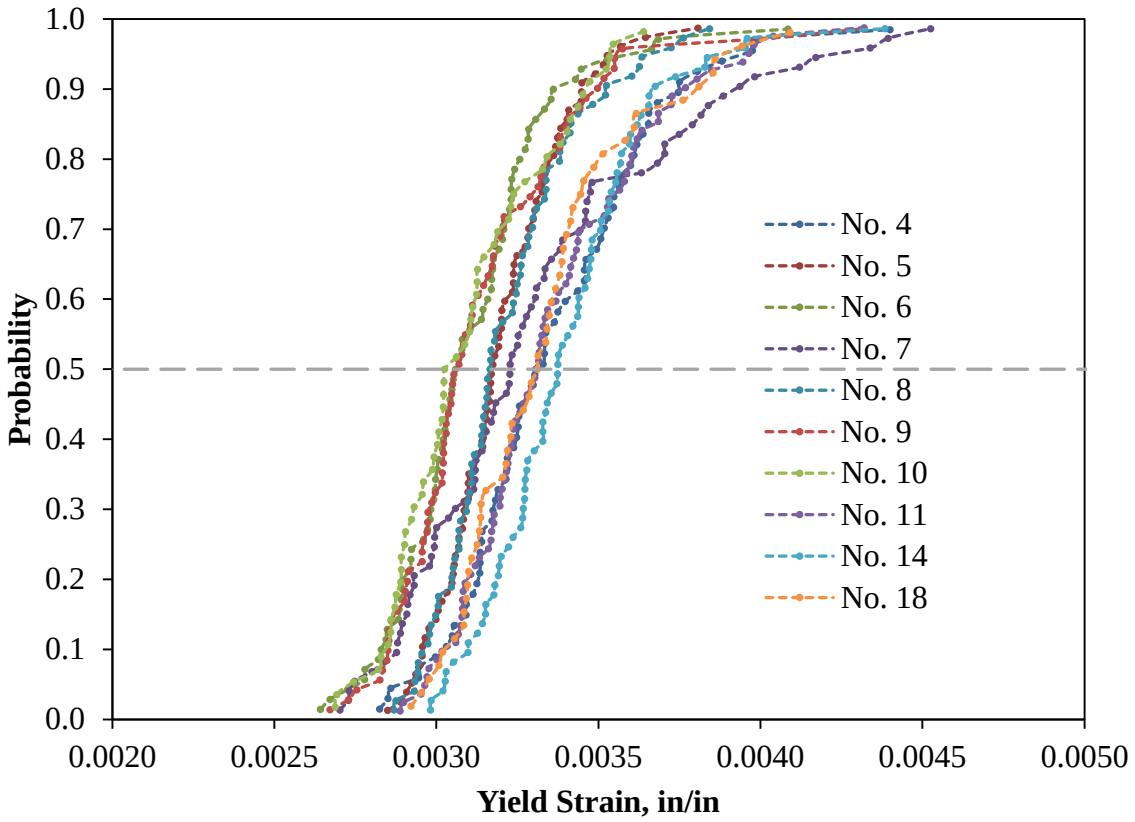

Figure 4-11. Yield strain empirical CDFs for individual bar sizes

4.2.3.6.Strain at Onset of Strain Hardening

As stated in Section 4.2.1., the onset of strain hardening was identified as the value of strain corresponding to the intersection of a horizontal line passing through the 0.2% Offset Method yield strength and the slope of the initial portion of the stain hardening curve. Test specimens that did not exhibit well-defined yield plateaus are included in this dataset because they still exhibited strain hardening. In these cases, the onset of strain hardening generally coincided with the intersection of the 0.2% offset line with the stress-strain curve.

The lognormal and empirical CDF curves for the onset of strain hardening are presented in Figure 4-12. Due to the bimodal shape of the empirical distribution, none of the considered probability distributions offered acceptable fits to the data at a 5% significance level. The lognormal distribution offered the closest fit despite failing the goodness-of-fit test and is therefore shown in Fig. 4-12 for reference purposes only.

Because this parameter is determined based on Optotrak readings, there are four empirical distributions as described in Section 4.2.2. The lognormal distribution was fitted to the mean empirical distribution for reference purposes. The mean value of the mean empirical data, based on a 2" gage length, is 0.0074 in/in. The corresponding standard deviation and coefficient of variation are 0.0019 in/in and 26% respectively.

The bimodal distribution of the empirical data illustrates the variability in yield plateau lengths which range anywhere from just past yielding to greater than 1% strain. The combined dataset indicates a decrease in yield plateau length as bar size increases from No. 6 to No. 10 (Fig. 4-13). This trend was not reflected in any of the mills individually; however, and was shown to result from a single mill having No. 6 bars with long yield plateaus and No. 10 bars with little to no yield plateaus (Appendix D). As a result, the No. 6 bars averaged the highest overall onset of strain hardening strains at 0.0085, and the No. 10 bars averaged the lowest overall onset of strain hardening strains at 0.0056. Considering this, there is no indication that the onset of strain hardening strain was influenced by bar size. Table 4-5 summarizes the mean values of each parameter according to bar size.

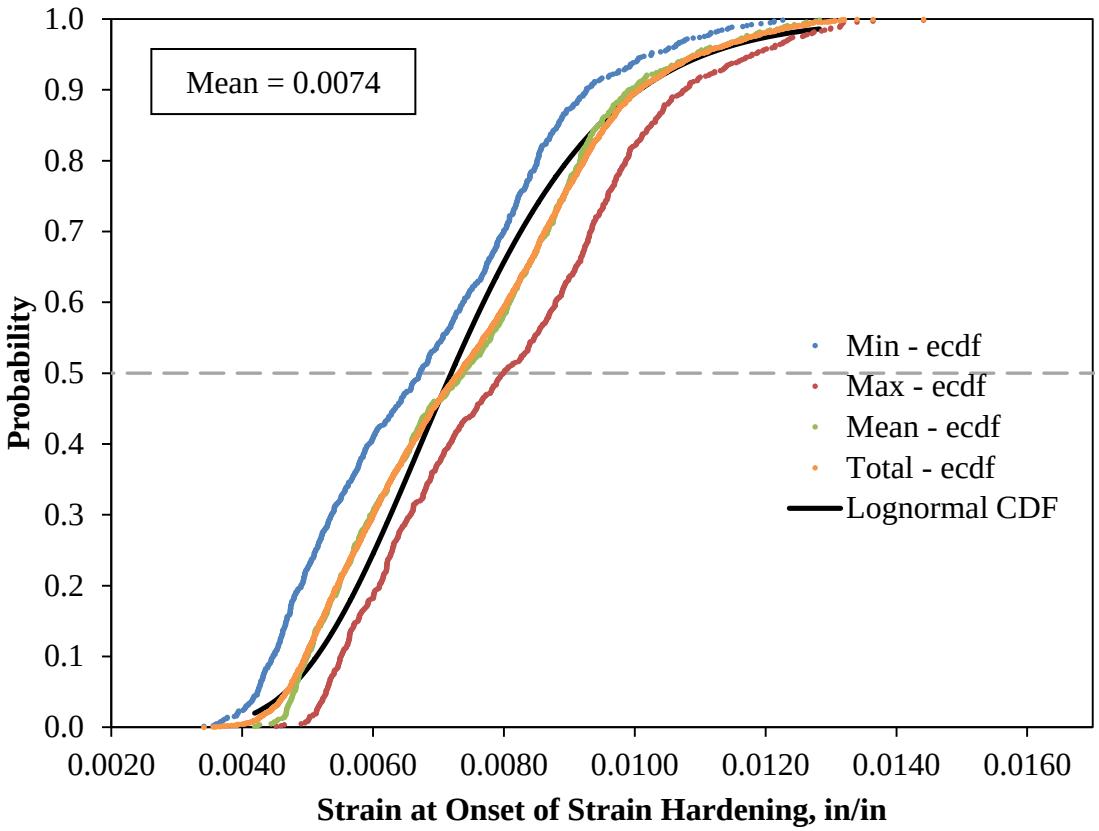

Figure 4-12. Strain at onset of strain hardening empirical CDFs including all bar sizes (lognormal distribution shown for reference purposes only)

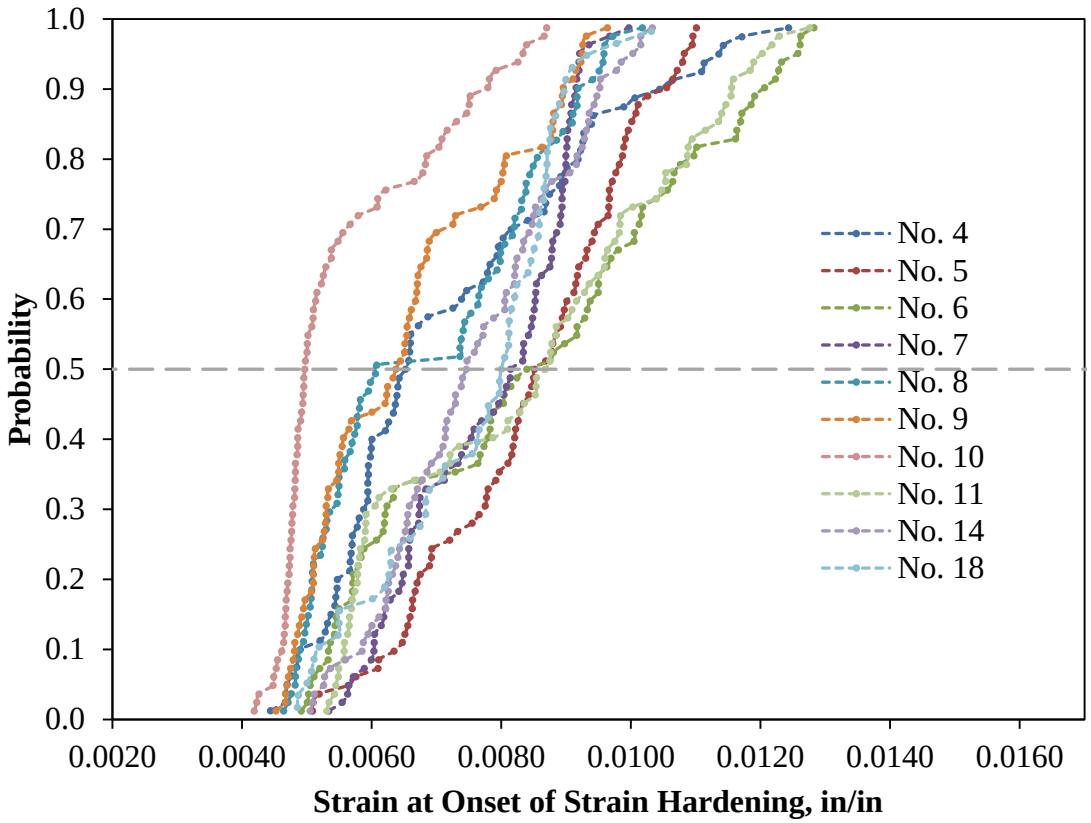

Figure 4-13. Strain at onset of strain hardening empirical CDFs for individual bar sizes

4.2.3.7.Tensile Strength

As stated in section 4.2.1., the tensile strength was identified as the maximum value of stress recorded during the test. This represents the point at which strain hardening transitions to strain softening or necking. As stated in Chapter 3, a 6% reduction was applied to the No. 11, 14, and 18 bar tensile strengths to account for the losses occurring in the custom testing rig. None of the tensile strength values fell below the ASTM lower limit of 100 ksi.

The lognormal and empirical CDF curves for the tensile strength are presented in Figure 4-14. The normal, lognormal, beta, and gamma distributions were found to be acceptable fits to the tensile strength data at a 5 percent significance level. The lognormal distribution was identified as the best fitting distribution based on the Kolmogorov-Smirnov statistic, though followed closely by the normal and the beta distributions.

The mean value of the empirical data is 112.5 ksi. The standard deviation and coefficient of variation are 3.6 ksi and 3.2% respectively. The value corresponding to the 95th percentile of the empirical data is 118.9 ksi. Also included in the graph is the ASTM minimum allowable tensile strength of 100 ksi (ASTM, 2016). Because this parameter is determined based on load cell readings as opposed to Optotrak readings, there is only one fitted and one empirical distribution.

Figure 4-15 illustrates the breakdown of the expected tensile strength data according to bar size. The mean values ranged from 107.6 ksi to 114.6 ksi with the No. 18 bars having the lowest mean value and the No. 10 bars having the highest. The adjustment to the No. 11, 14, and 18 bar data previously described revealed a consistent trend for these three sizes to have the lowest tensile strengths – a combined mean of 108.8 ksi versus a combined mean of 113.7 ksi for the No. 4 through No. 10 bars. There was no indication that bar size had any effect on tensile strength in the remaining sizes. Table 4-5 summarizes the mean values of each parameter according to bar size.

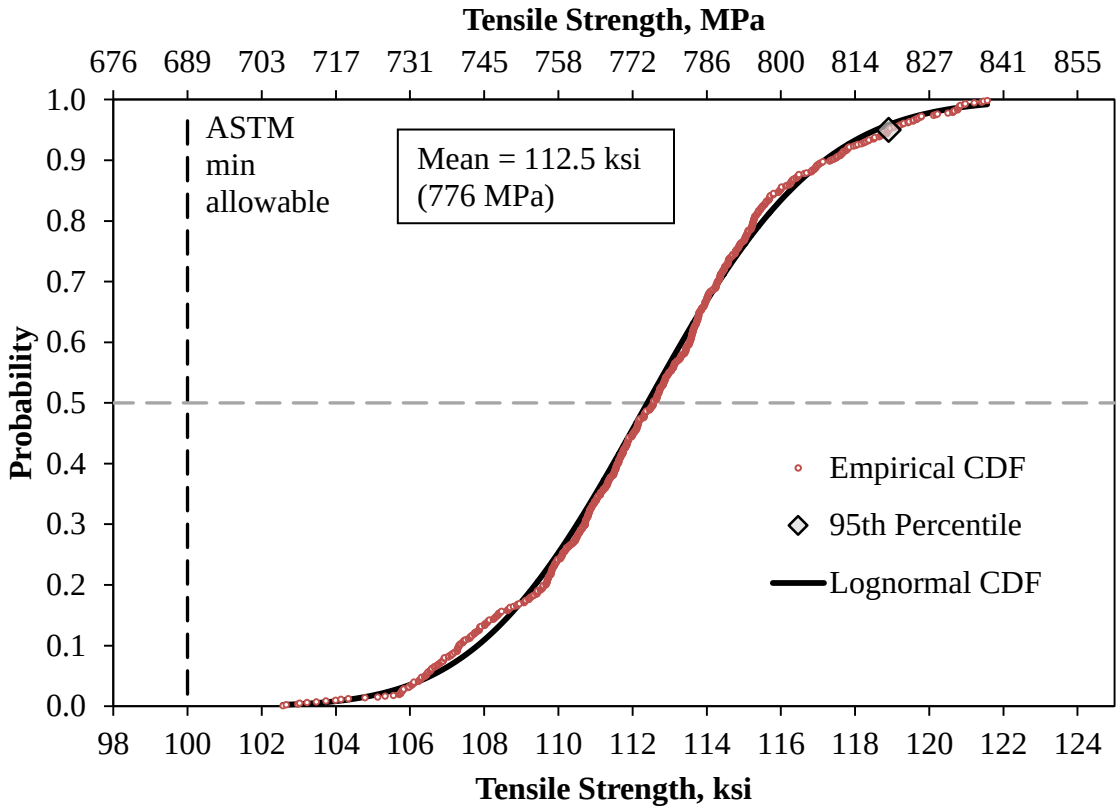

Figure 4-14. Tensile strength lognormal and empirical CDFs including all bar sizes

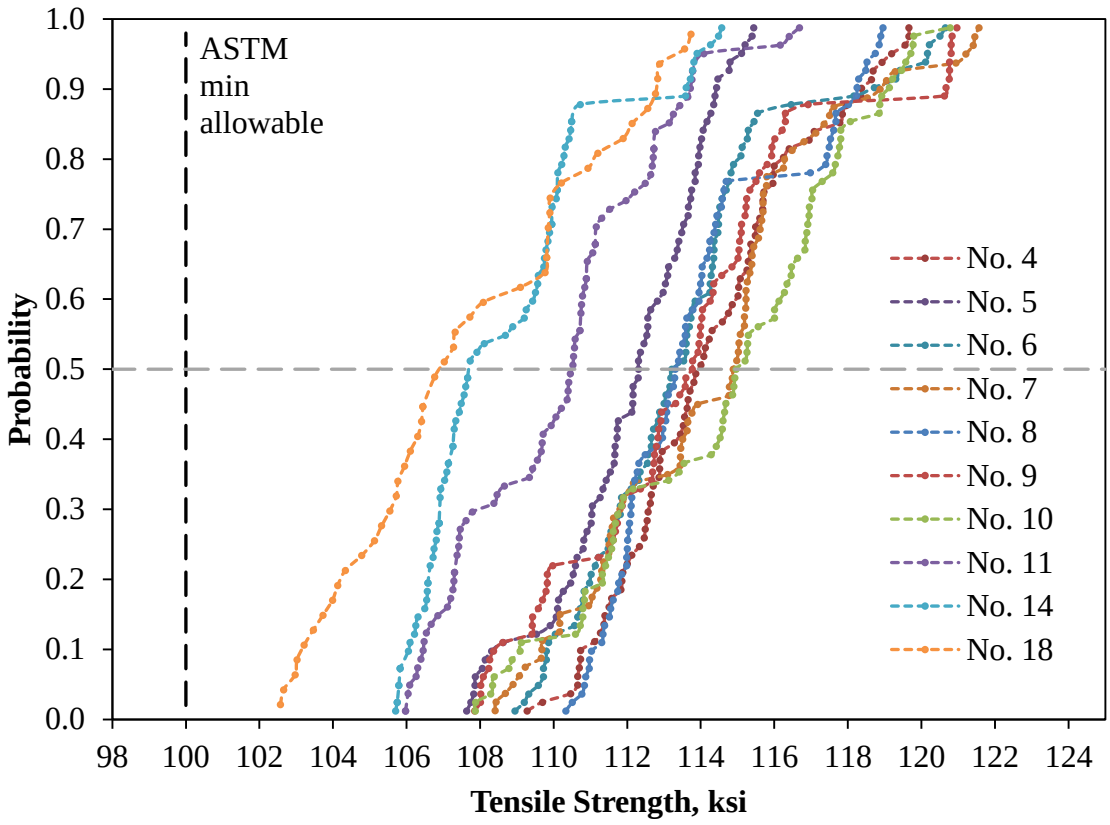

Figure 4-15. Tensile strength empirical CDFS for individual bar sizes

4.2.3.8.Ultimate Tensile Strain

As stated in Section 4.2.1., the ultimate tensile strain was identified as the value of strain corresponding to the maximum value of stress recorded during the test. This is not to be confused with the value of strain corresponding to rupture of the test specimen. As stated in Chapter 3, a 6.5% reduction was applied to the No. 11, 14, and 18 bar tensile strengths to account for the losses occurring in the custom testing rig.

The Weibull and empirical CDF curves for the ultimate tensile strain are presented in Figure 4-16. Only the Weibull distribution was found to be an acceptable fit to the ultimate tensile strain data at a 5 percent significance level.

Because this parameter is determined based on Optotrak readings, there are four empirical distributions as described in Section 4.2.2. The mean value of the mean empirical data is 0.0954 in/in. The corresponding standard deviation and coefficient of variation are 0.0055 and 5.8% respectively. The value corresponding to the 5th percentile of the empirical data is 0.0845 in/in.

Figure 4-17 illustrates the breakdown of the adjusted ultimate tensile strain data according to the mean CDFs for each bar size. The mean values ranged from 0.0922 to 0.0971 with the No. 4 bars having the lowest mean value and the No. 7 bars having the highest. There is no indication that the ultimate tensile strain was influenced by bar size. Table 4-5 summarizes the mean values of each parameter according to bar size.

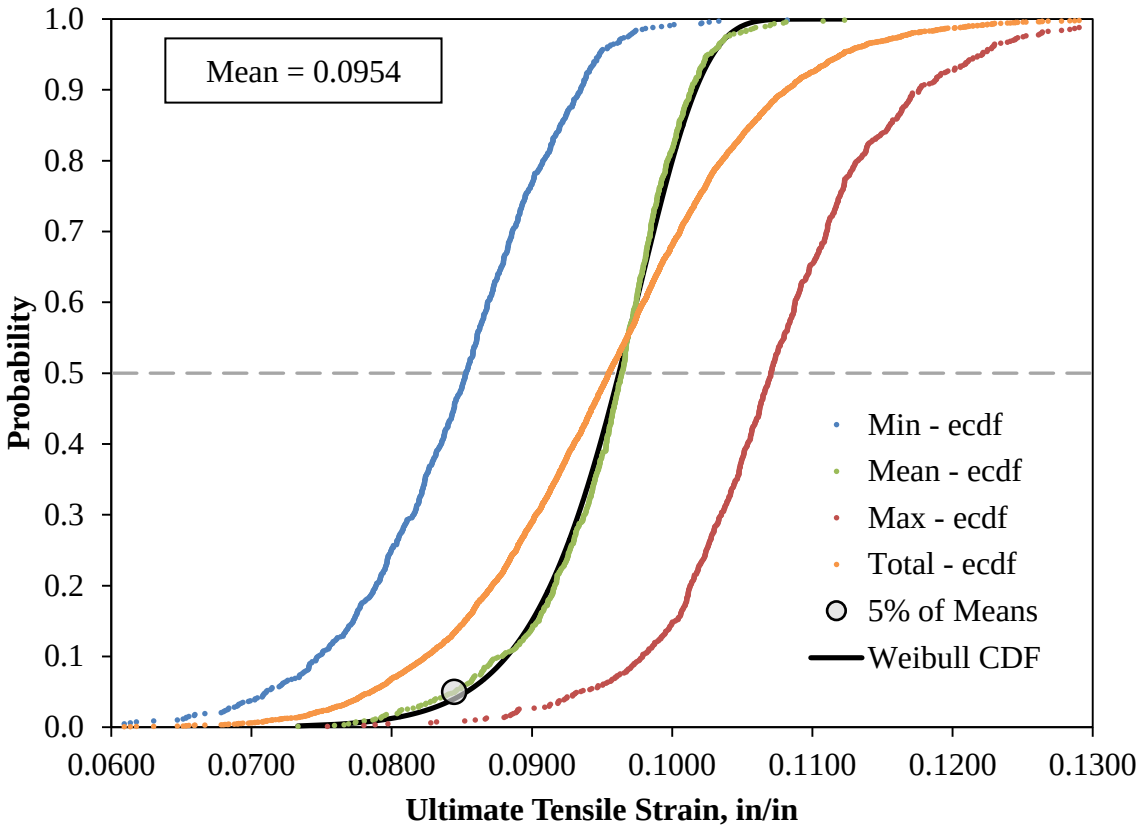

Figure 4-16. Ultimate tensile strain Weibull and empirical CDFs including all bar sizes

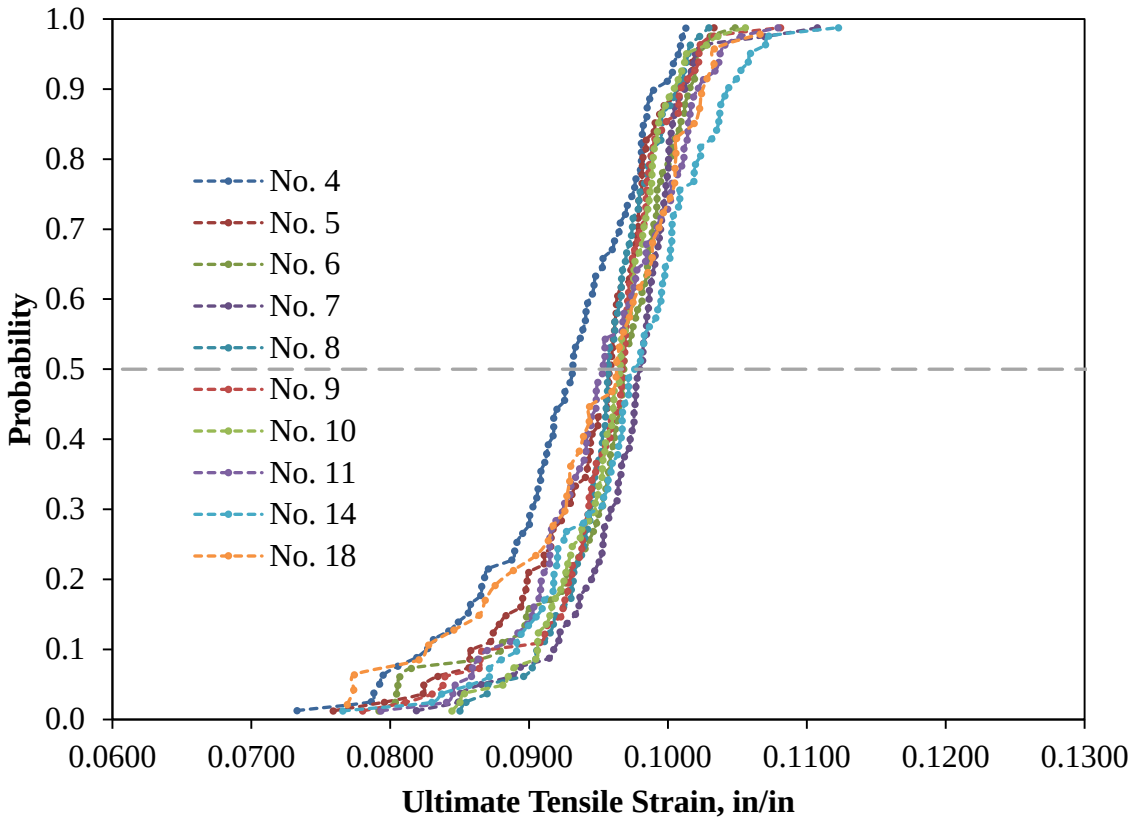

Figure 4-17. Ultimate tensile strain empirical CDFs for individual bar sizes

4.2.3.9.Tensile to Yield Ratio

Three possible methods for defining the tensile strength to yield strength ratio could be presented as three methods of defining the yield strength were investigated. The ADM yield strength is chosen as it is the parameter used for the final recommendations presented in Chapter 6. The yield strength values used in the development of this parameter included the 5% adjustment and the tensile strength value included the 6% adjustment, as described in Chapter 3.

The gamma and empirical CDF curves for the tensile-to-yield ratio considering all bar sizes are presented in Figure 4-18. The gamma and beta distributions were found to be acceptable fits to the yield strength data at a 5 percent significance level based on the Kolmogorov-Smirnov test statistic; however, the gamma distribution was identified as the best fitting distribution.

The mean value of the empirical data is 1.32. The standard deviation and coefficient of variation are 0.003 and 2.2% respectively. Also included in the graph is the ASTM minimum allowable tensile-to-yield ratio of 1.25 (ASTM, 2016). Because both the ADM yield strength and the tensile strength are based on load cell readings as opposed to Optotrak readings, there is only one fitted and one empirical distribution for this parameter.

Figure 4-19 illustrates the breakdown of the tensile strength to yield strength ratio data according to bar size. The mean values ranged from 1.29 to 1.34 with the No. 5 bars having the lowest mean value and the No. 10 bars having the highest. Overall, the No. 4 and No. 5 bars had the lowest tensile-to-yield ratios. The ratio increased with increasing bar size until peaking at the No 10 bars. The No. 7, 8, 9, 11, 14, and 18 bars all averaged the mean ratio of 1.32. Table 4-5 summarizes the mean values of each parameter according to bar size.

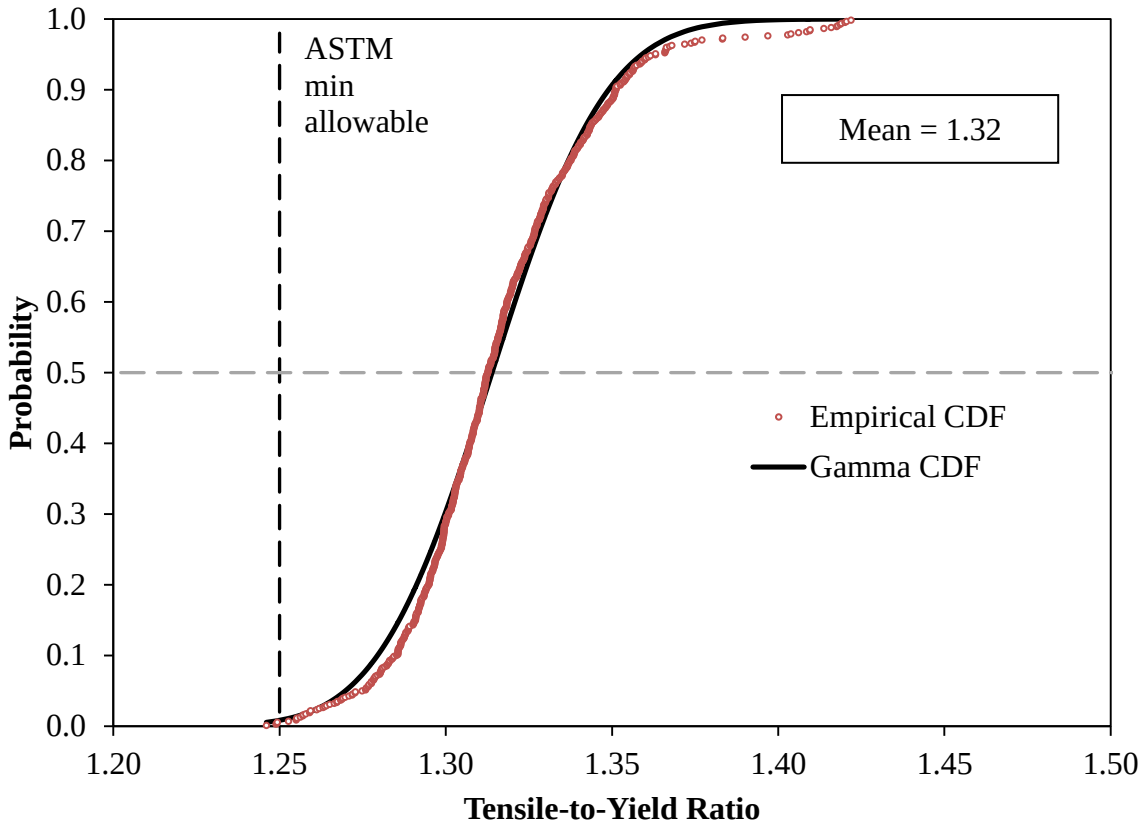

Figure 4-18. Tensile-to-yield ratio gamma and empirical CDFs including all bar sizes

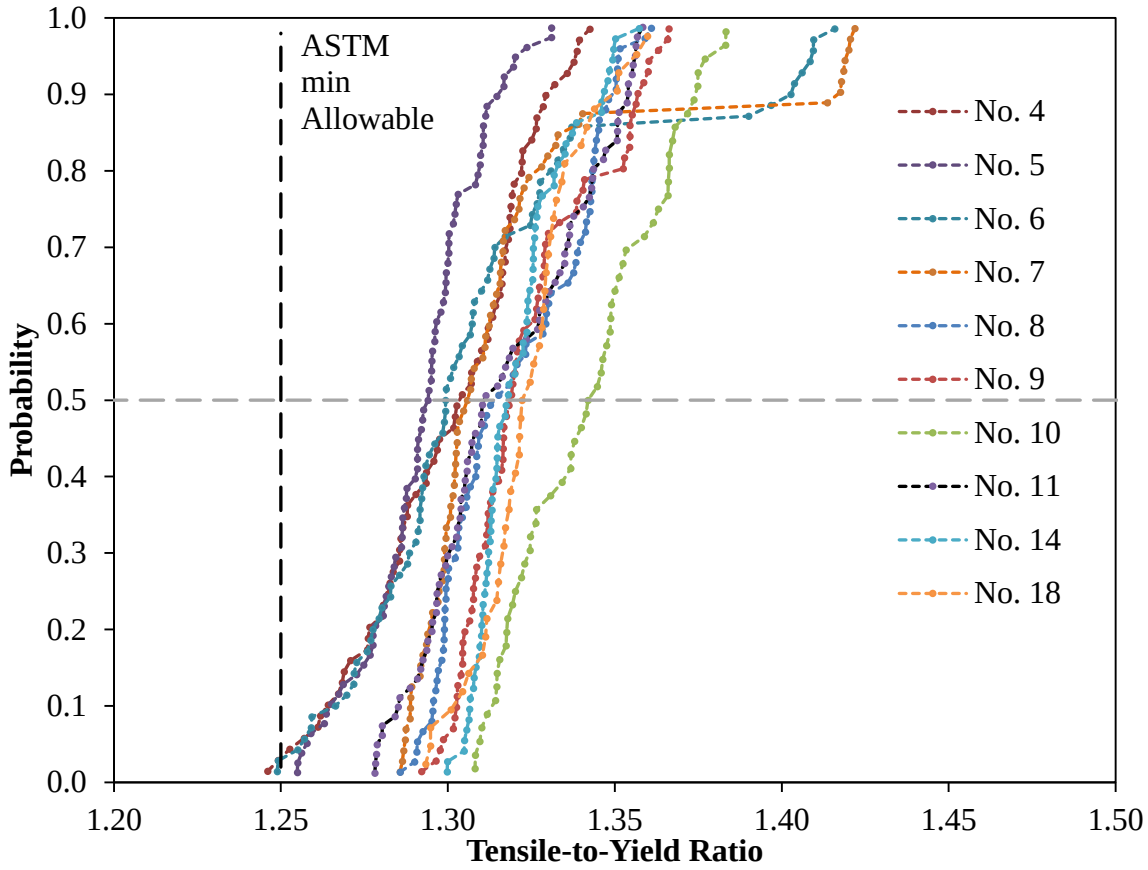

Figure 4-19. Tensile-to-yield ratio empirical CDFs for individual bar sizes

4.2.3.10. Summary of Tensile Test Results

Table 4-4 provides the summary statistics from the tensile testing portion of the experimental program. The values in the table represent the combined results of all 788 tests for each parameter. Table 4-5 breaks the findings down according to the individual bar sizes. The stated recommendations for each parameter coincide with the mean value obtained for that parameter.

Table 4-4. Summary of tensile testing results and design recommendations by parameter (1 ksi = 6.9 MPa).

	Yield Strength (ksi)			Yield Strain	Strain at onset of Strain Hardening	Tensile Strength (ksi)	Ultimate Tensile Strain	Tensile-to-Yield Ratio
	ADM	EUL	0.2% OM					
Mean	85.0	84.3	85.1	0.0033	0.0074	112.5	0.0954	1.32
St. Dev.	3.03	3.20	2.93	0.0003	0.0019	3.65	0.0055	0.03
COV	3.56%	3.79%	3.45%	9.03%	26.17%	3.24%	5.80%	2.19%
95th Percentile	89.2	88.7	89.4	0.0038	0.0109	118.9	0.1024	1.36
5th Percentile	79.0	78.5	79.4	0.0029	0.0048	106.4	0.0845	1.28
Recommendations		85.0		0.0033	0.0074	112.5	0.0954	1.32

Table 4-5. Summary of tensile testing means and standard deviations by bar size (1 ksi = 6.9 MPa).

Bar Size	Yield Strength (ksi)		Yield Strain		Onset of Strain Hardening		Tensile Strength (ksi)		Ultimate Tensile Strain	
	Mean	St. Dev.	Mean	St. Dev.	Mean	St. Dev.	Mean	St. Dev.	Mean	St. Dev.
No. 4	88.0	2.48	0.0034	0.0003	0.0072	0.0020	114.2	2.59	0.0922	0.0062
No. 5	86.7	2.14	0.0032	0.0002	0.0084	0.0015	112.1	2.04	0.0945	0.0055
No. 6	86.1	2.06	0.0031	0.0002	0.0085	0.0025	113.5	2.84	0.0958	0.0057
No. 7	86.3	3.01	0.0033	0.0004	0.0078	0.0012	114.2	3.28	0.0971	0.0045
No. 8	86.0	1.38	0.0032	0.0002	0.0069	0.0017	113.9	2.50	0.0957	0.0037
No. 9	85.1	1.48	0.0031	0.0003	0.0065	0.0015	113.6	3.53	0.0956	0.0051
No. 10	84.2	1.55	0.0031	0.0002	0.0056	0.0012	114.6	3.44	0.0959	0.0041
No. 11	83.6	2.85	0.0034	0.0003	0.0084	0.0023	110.1	2.69	0.0955	0.0056
No. 14	81.7	1.63	0.0034	0.0003	0.0076	0.0014	108.7	2.43	0.0971	0.0062
No. 18	80.7	2.51	0.0033	0.0003	0.0076	0.0014	107.6	3.35	0.0945	0.0073

4.2.4. Shape of the Strain Hardening Curve

One of the expressed objectives of the present research was to assess the shape of the stress-strain curve for A706 grade 80 rebar, in particular, the transition from elastic to

inelastic behavior and the curvature of the strain hardening region. Identification of the stress and strain values at yielding and the onset of strain hardening necessarily resolves the first of these issues; however, the shape of the strain hardening region is not as readily determined from stress-strain parameters alone.

While not as critical as the expected values of stress and strain at yield and ultimate and the strain at the onset of strain hardening, the shape of the strain hardening curve is important in modeling applications such as moment curvature analysis. As such, it becomes important to assess the ability of existing rebar models, formulated for a different grade of steel, to accurately describe this region.

This section offers a largely qualitative assessment of the shape of the strain hardening portion of the monotonic stress-strain curve. Two existing monotonic rebar models, the King Model (King et al. 1986) and the Raynor Model (Raynor et al. 2002), are evaluated by first defining them in terms of the recommended (mean) stress-strain parameter values presented in Section 4.2.3 and summarized in Chapter 6 and then overlaying the results on a plot containing all of the experimental stress-strain curves. An additional comparison is made by overlaying an A706 grade 60 curve on the same plot to visually compare the shape of the respective stain hardening regions. The remainder of this section discusses the results of these efforts.

Figure 4-20 provides a plot of all stress-strain curves generated during the tensile testing phase of the project overlaid one on top of another. The plot was generated using the as-measured No. 4 through No. 10 bar tests and the adjusted No. 11 through No. 18 bars tests. All curves have been plotted to their ultimate tensile strains but no further. Clearly

illustrated by the figure is the variability across the different tests and the consistency in the shape of the strain hardening region.

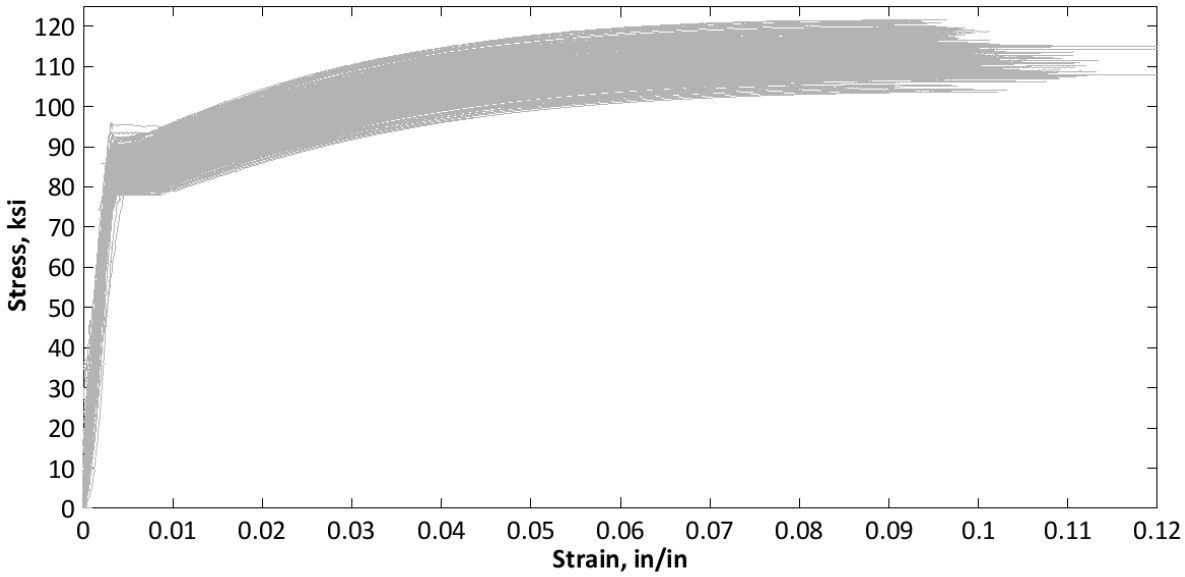

Figure 4-20. A706 grade 80 stress-strain curves for all tensile tests

Figure 4-21 provides a visual demonstration of the King model's (King et al., 1986) ability to represent the strain hardening portions of the curves. The parameters required to define the model and the values used are also provided in the figure. It is clear that the model overestimates the curvature of the initial portion of the strain hardening curve.

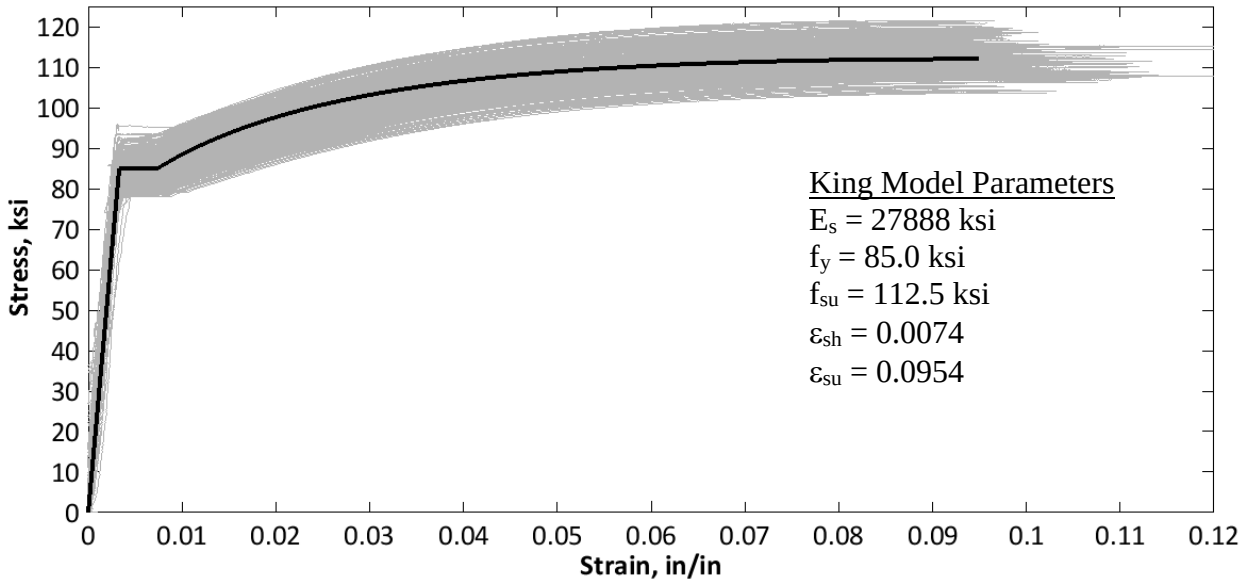

Figure 4-21. Overlay of King Model on all stress-strain curves using recommended parameter values (King et al., 1986)

Figure 4-22 provides a visual demonstration of the Raynor model's (Raynor et al., 2002) ability to represent the strain hardening portions of the curves. The parameters required to define the model and the values used are also provided in Figure 4-22. Distinct from the King model is the Raynor model's ability to define the slope of the yield plateau as well as adjust the curvature of the strain hardening region. A slope of zero for the yield plateau and a strain hardening exponent of 3 were used in the model shown in the figure. It is clear that the Raynor model, when defined with the given parameters, can reliably capture the shape of the A706 grade 80 stress-strain curve.

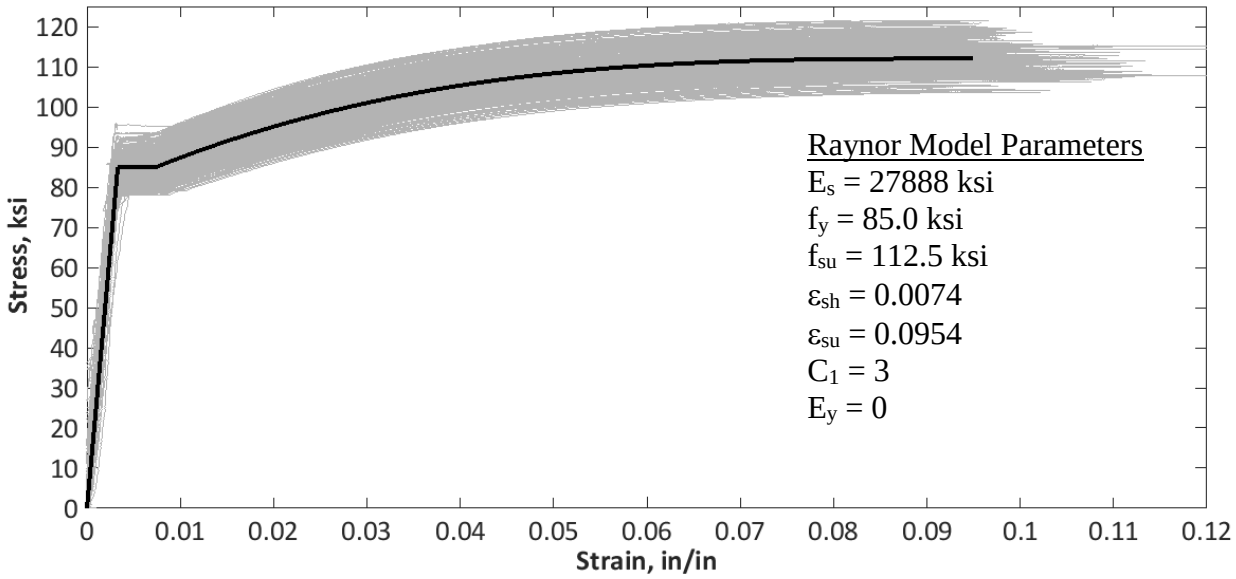

Figure 4-22. Overlay of Raynor Model on all stress-strain curves using recommended parameter values (Raynor et al., 2002)

Figure 4-23 provides a visual comparison between the shape of an A706 grade 60 stress-strain curve and the A706 grade 80 stress-strain curves. As indicated in the figure, the shape of the strain hardening region is essentially the same for both grades of steel. This lends support to the notion that existing monotonic stress-strain models commonly used in the analysis of reinforced concrete sections using A706 grade 60 rebar can be reliably used to perform the same tasks using A706 grade 80 rebar.

age

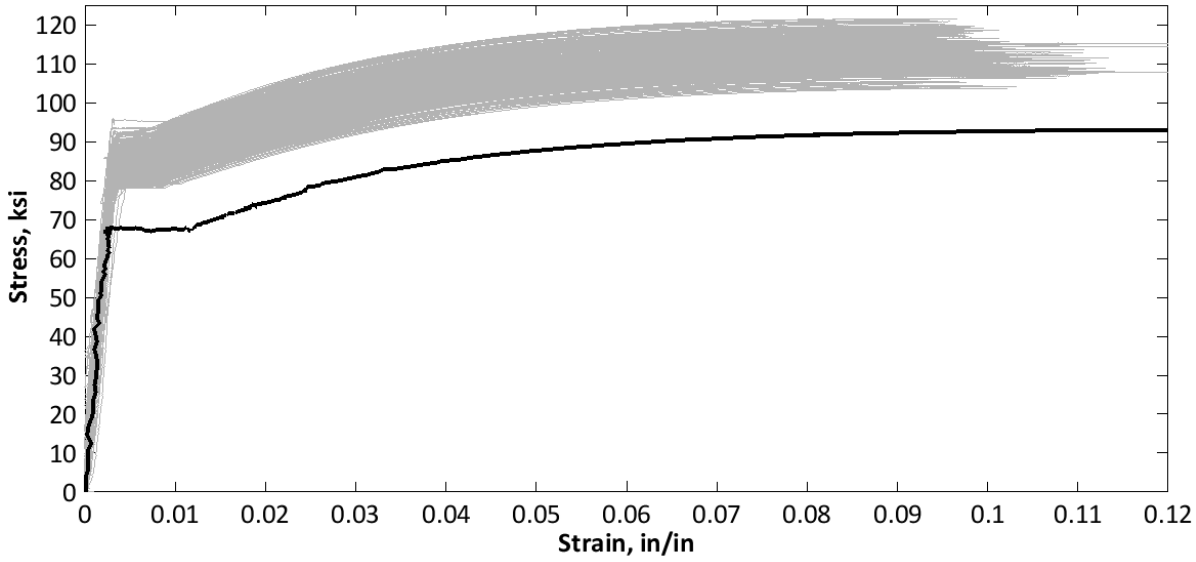

Figure 4-23. Overlay of an A706 grade 60 curve on all experimental stress-strain curves

4.3. Strain Age Testing

This section presents the results of the strain aging portion of the experimental program. As demonstrated in Chapter 2, the three primary indicators of strain aging in monotonically tested reinforcing steel are an increase in yield strength, an increase in tensile strength, and a reduction in ultimate tensile. Reemergence of a yield plateau is also an indicator of strain aging. The consensus from the literature is that not all of these indicators need to be present concurrently in a specimen exhibiting strain aging. For this research, the change in tensile strength and ultimate tensile strain are used as the measures of strain aging. The change in yield strength was not used for the following two reasons: (1) very little change in yield strength was observed to occur in any of the tests (See Appendix H) and (2)

as there was no indication of a re-emergent yield plateau in any of the tests, thus making identification of a new yield point highly subjective.

As described in Section 3.5.2, all of the tests originated from the same heat and producing mill. The average and standard deviation of the No. 5 and No. 7 bar tensile test results from this heat where therefore used in determining the significance of changes observed in the strain aging tests of the same steel.

4.3.1. Impact of Aging Period

Four aging periods were evaluated, based on the findings of the literature review, in order to assess the strain aging susceptibility of A706 grade 80 rebar. Figures 4-24 and 4-25 present the variation in the No. 5 and No. 7 bar tensile strengths, respectively, with time for the three pre-strain levels. Figures 4-26 and 4-27 present the variation in the No. 5 and No. 7 bar ultimate tensile strains, respectively, with time for the three pre-strain levels. The results in the figures were obtained by plotting the re-test values for tensile strength and ultimate tensile strain against a benchmark value (solid black line) for that bar size which was obtained from the tensile testing program results. Specifically, the benchmark represents the average of the nine Mill 1 Heat 1 tensile tests corresponding to each of the two bar sizes. Also shown in the figures are dashed lines indicating the extent of one standard deviation above and below the benchmark value to provide a point of reference. Actual monotonic stress-strain curves from the testing are available in Appendix H.

The results in Figure 4-24 illustrate a general decrease in tensile strength of the No. 5 bars between the 2 and 60 day tests followed by an increase in tensile strength between the

60 and 180 day tests. Despite this, there does not seem to be any significant trend as the lowest pre-strain level and the shortest aging period illustrate the highest tensile strength above the average while two of the 6 month tests showed tensile strengths just below the heat average.

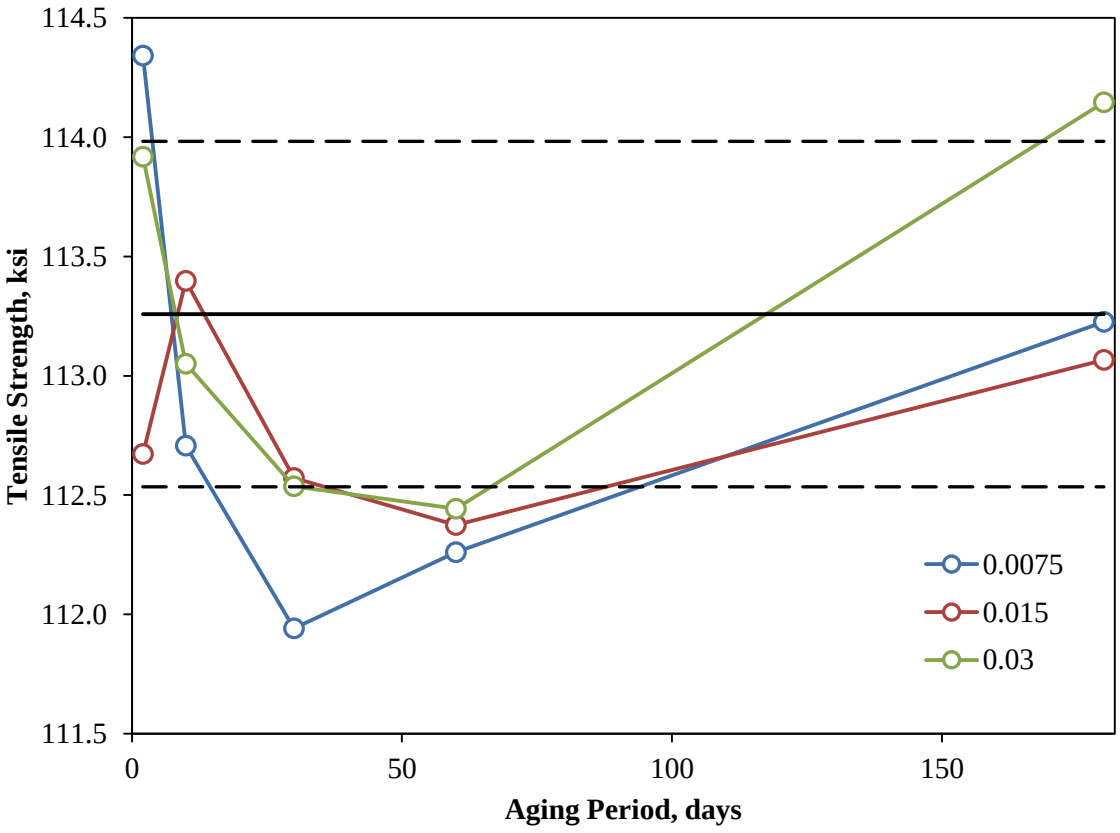

Figure 4-24. Impact of aging period on tensile strength of No. 5 bars

The results in Figure 4-25 illustrate a general decrease in tensile strength of the No. 7 bars between the 2 day tests and the 6 month tests. The results would seem to indicate a reversal of the anticipated trend if strain aging were to be significantly affecting the steel: an

increase in tensile strength with increased aging period. Nearly all of the results fell within one standard deviation of the mean.

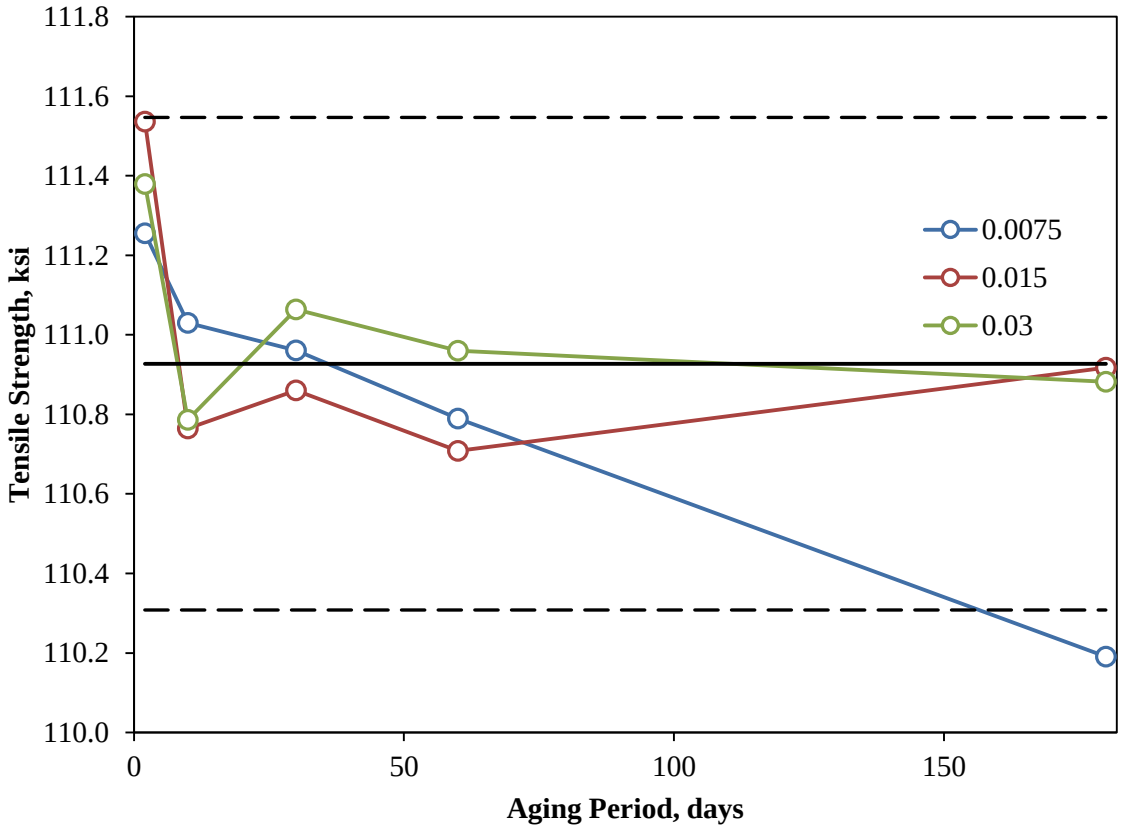

Figure 4-25. Impact of aging period on tensile strength of No. 7 bars

The results in Figure 4-26 illustrate a general decrease in ultimate tensile strain of the No. 5 bars between the 2 day tests and the 30 day tests followed by an increase in ultimate tensile strain between the 60 and 180 day tests. Observing that all three of the 6 months tests fell above one standard deviation of the heat mean for all three pre-strain levels, there again seems to be a reversal of the anticipated trend. Otherwise, nearly all of the results fell within one standard deviation of the mean.

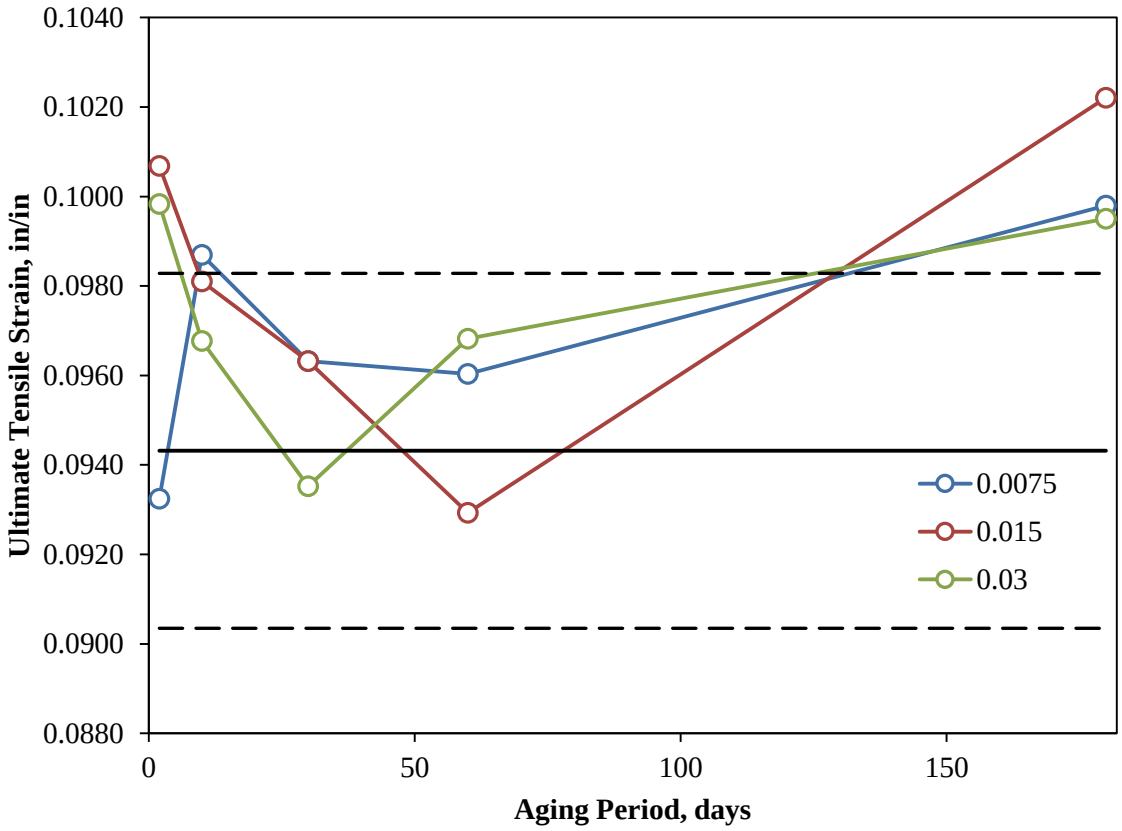

Figure 4-26. Impact of aging period on ultimate tensile strain of No. 5 bars

The results of the No. 7 bar tests do not seem to indicate any effect of aging period on the ultimate tensile strain. There were nearly identical results between the 2 day and the 180 day tests.

The results in Figure 4-27 show a rapid decrease in ultimate tensile strain of the No. 7 bars between the 2 day tests and the 30 day tests followed by an equivalently rapid increase in ultimate tensile strain between the 30 day and 60 day tests. The 180 day tests were distributed about the mean in either direction with the highest pre-strain level indicating the highest retested ultimate tensile strain. As such, there does not seem to be a definable trend.

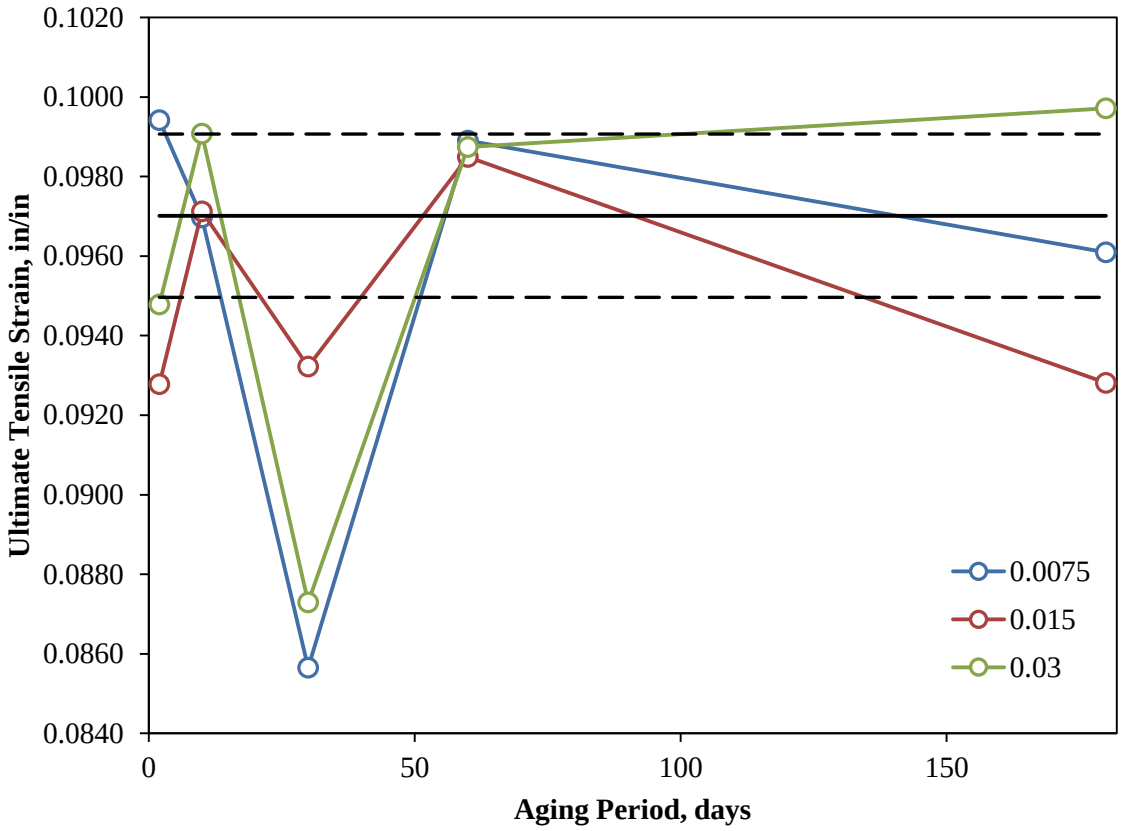

Figure 4-27. Impact of aging period on ultimate tensile strain of No. 7 bars

4.3.2. Impact of Pre-Strain Level

Three pre-strain levels were evaluated, based on the literature presented in Chapter 2, in order to assess the strain aging susceptibility of A706 grade 80 rebar. Figures 4-28 and 4-29 present the variation in the No. 5 and No. 7 bar tensile strengths, respectively, with pre-strain level for the four aging periods. Figures 4-30 and 4-31 present the variation in the No. 5 and No. 7 bar ultimate tensile strains, respectively, against pre-strain level for the four aging periods.

The results in Figure 4-28 illustrate little to no increase in tensile strength with increasing pre-strain level for the No. 5 bars. Most of the tests fell within one standard deviation of the heat average for this bar size.

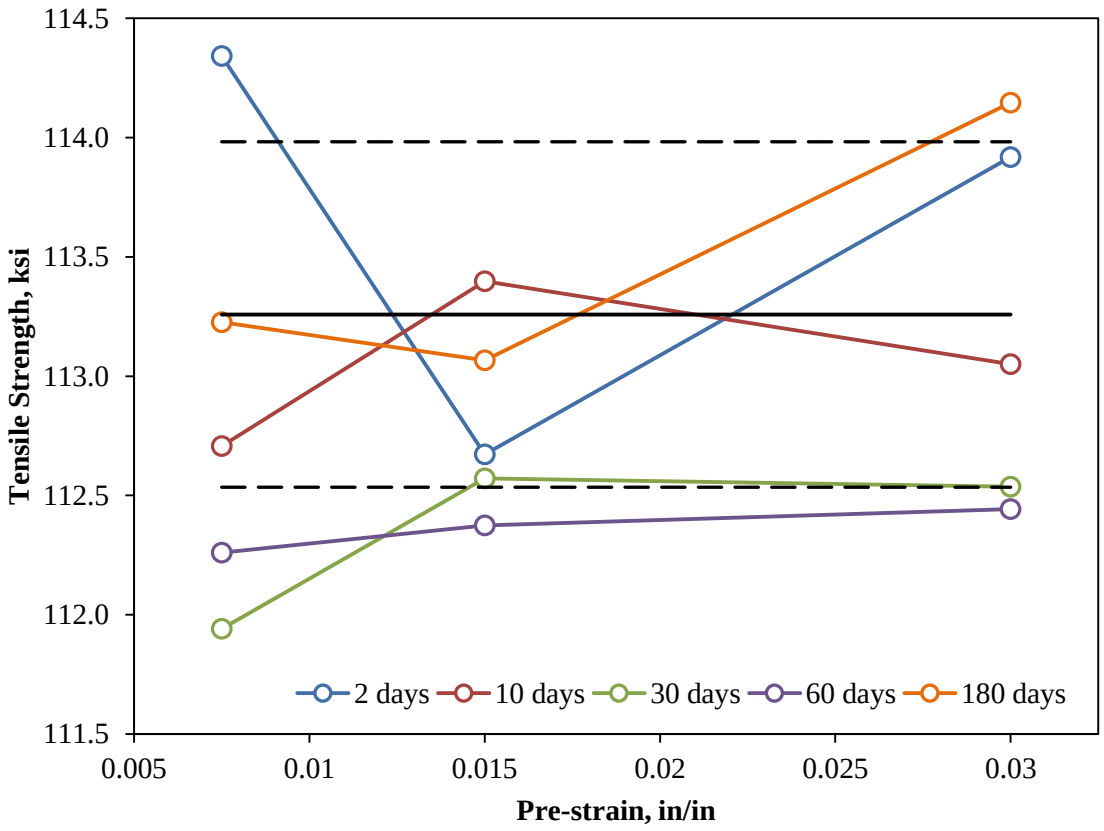

Figure 4-28. Impact of pre-strain level on tensile strength of No. 5 bars

The results in Figure 4-29 illustrate very limited variability in the re-test tensile strengths. As well, there does not seem to be any trend between tensile strength and pre-strain level. Nearly all of the tests fell within one standard deviation of the heat average for this bar size.

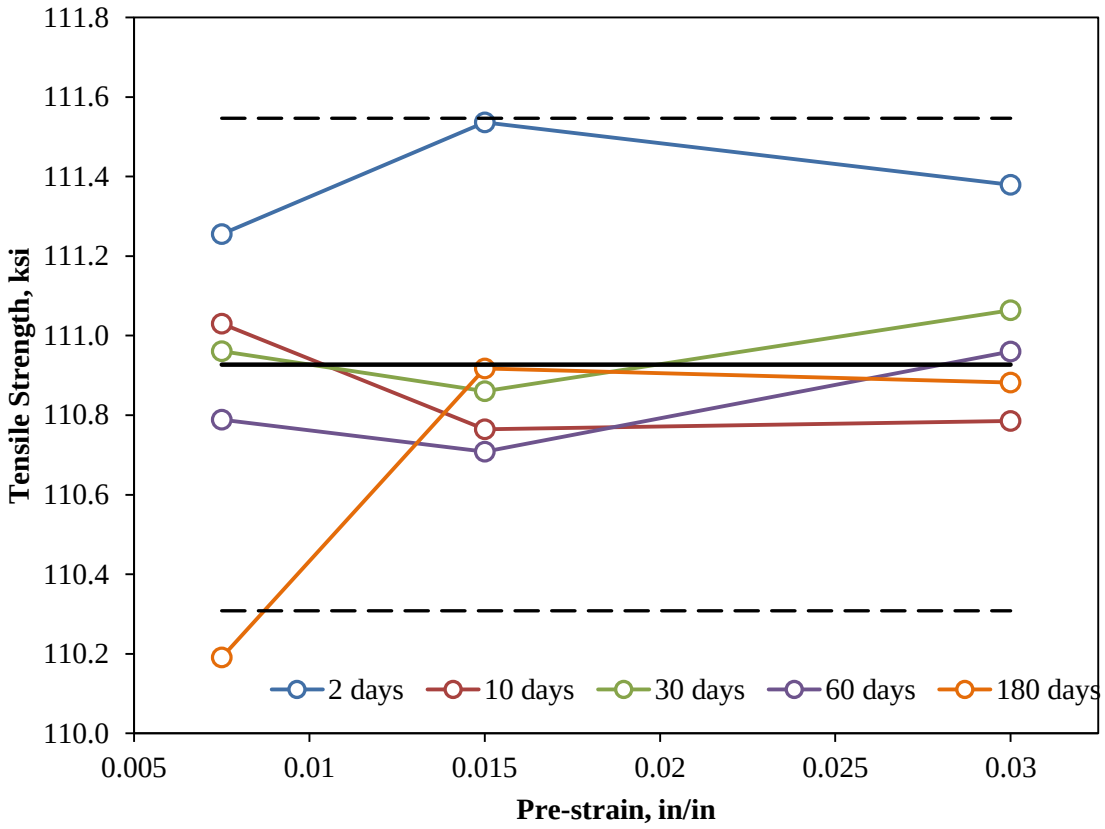

Figure 4-29. Impact of pre-strain level on tensile strength of No. 7 bars

The results in Figure 4-30 indicate that there was no effect of pre-strain level on the ultimate tensile strain for the No. 5 bars. The majority of the tests fell within or above one standard deviation above the heat average for this bar size.

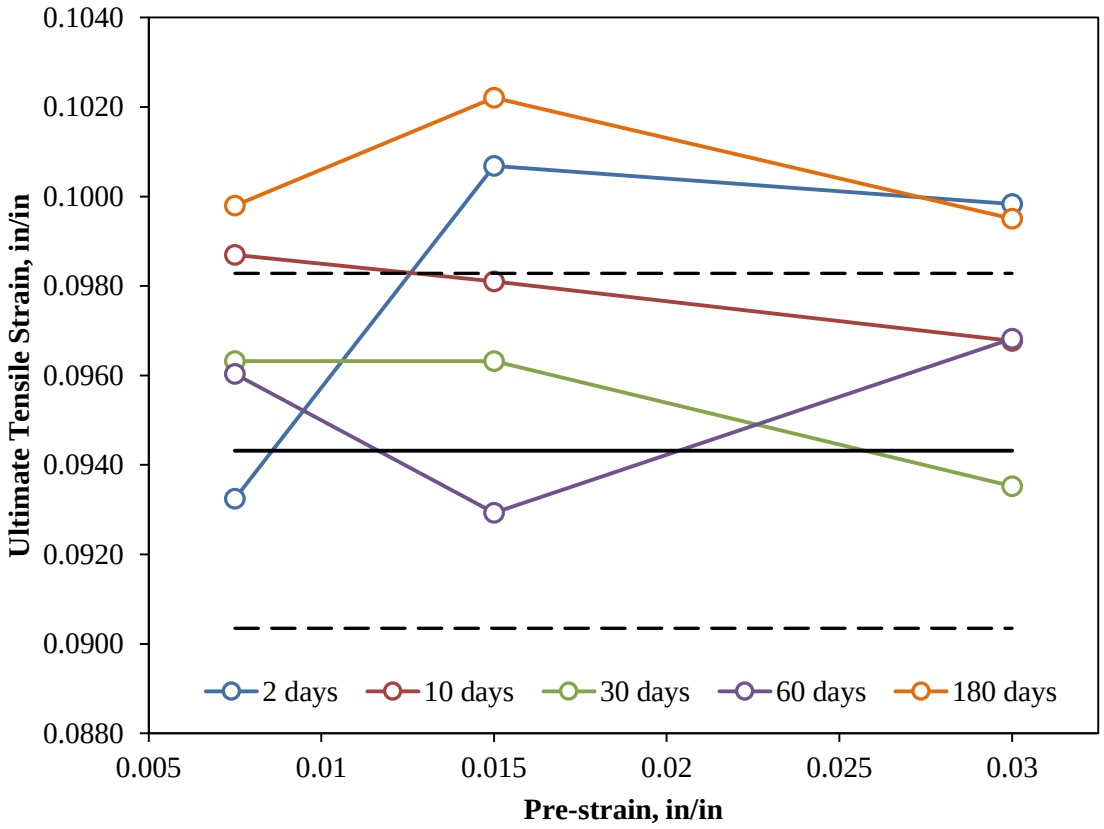

Figure 4-30. Impact of pre-strain on ultimate tensile strain of No. 5 bars

The results in Figure 4-31 do not indicate any effect of pre-strain level on the ultimate tensile strain for the No. 7 bars. All three of the 30 day tests showed very low ultimate tensile strains; however, this was not typical of the other aging period tests.

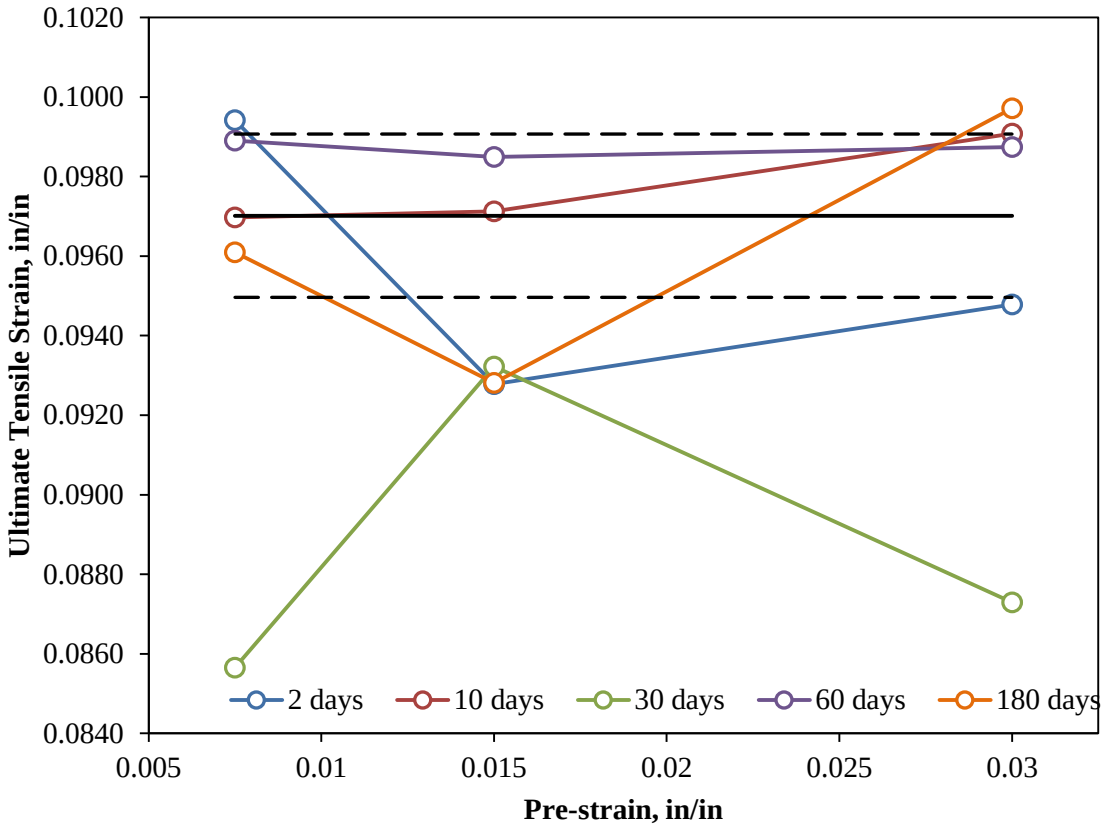

Figure 4-31. Impact of pre-strain on ultimate tensile strain of No. 7 bars

4.3.3. Impact of Bar Size

Two bar sizes (No. 5 and No. 7) were considered for the strain aging program. Figures 4-32 and 4-33 illustrate the influence of bar size on the change in tensile strength and ultimate tensile strain, respectively, for each of the pre-strain levels and aging periods. The values in the figures represent the difference between the re-test value and the reference value for the two parameters. Also included in each of the figures is the standard deviation of that parameter for each of the bar sizes.

The results in Figure 4-32 indicate that, overall, the No. 5 bars tended to show a reduction in tensile strength as a result of strain aging while the No. 7 bars were about evenly distributed between an increase and a decrease. In all cases, the effects are negligibly small (typically less than 1 ksi) and scarcely exceed 1 standard deviation from the benchmark value.

The results in Figure 4-33 indicate that, overall, the No. 5 bars tended to show an increase in ultimate tensile strain as a result of strain aging while the No. 7 bars again seemed to be evenly distributed between an increase and a decrease from the reference value. Several of the No. 7 bar re-tests did show a distinct reduction in ultimate tensile strain from the reference value (well below one standard deviation), however, as already mentioned and clearly shown in Figure 4.31, there is no indication that this was influenced by either the pre-strain level or the aging period.

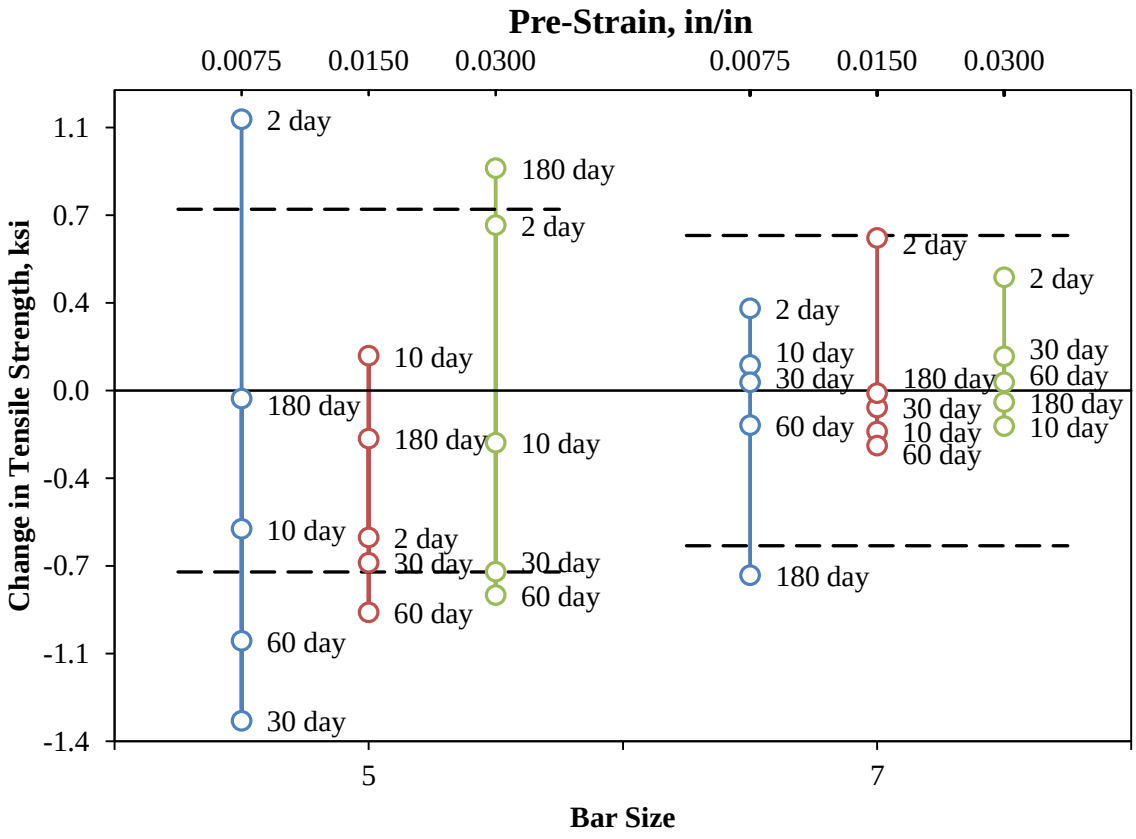

Figure 4-32. Impact of bar size on tensile strength after strain aging

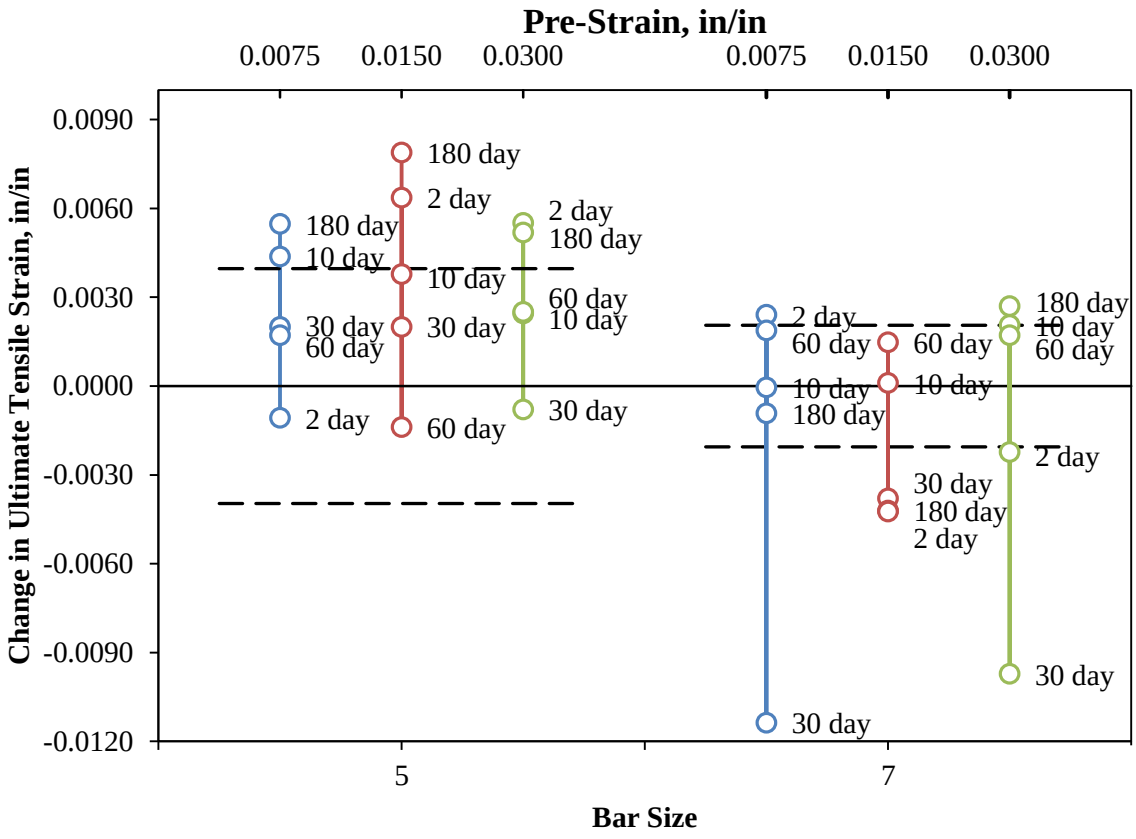

Figure 4-33. Impact of bar size on ultimate tensile strain after strain aging

4.3.4. Impact of Temperature

A subset of the No. 7 bars were used to investigate the effect of freezing temperatures on the rate of strain aging. Figures 4-34 and 4-35 compare the results of these tests with the results of the No. 7 bar tests that were aged at ambient temperatures. As there were no obvious indications of strain aging in any of the ambient temperature tests, the benefit of the low temperature tests is largely negated; nonetheless, the findings are summarized below.

Figure 4-34 is a reproduction of Figure 4-29 with the addition of the low temperature tests for the 30, 60, and 180 day aging periods which are shown as dashed lines. All of the

low temperature re-test values fell within one standard deviation of the heat average. The effects of the cold temperature aging did not seem to be significant as the tensile strengths were sometimes lower and sometimes higher than the ambient temperature results with no apparent trend. The maximum deviation from the benchmark was a reduction of 0.43 ksi which occurred in the 6 month tests after a pre-strain of 0.0150. The maximum deviation between an ambient temperature test and a low temperature tests was an increase of 0.42 ksi (freezing higher than ambient) for the 6 month test with a pre-strain of 0.0150.

Figure 4-35 is a reproduction of Figure 4-31 with the addition of the low temperature tests for the 30, 60, and 180 day aging periods which are shown as dashed lines. The maximum deviation from the benchmark was a reduction of 0.0058 strain which occurred in the 6 month tests after a pre-strain of 0.0075. The maximum deviation between an ambient temperature test and a low temperature tests was a reduction of 0.0130 strain (freezing lower than ambient) for the 30 day test with a pre-strain of 0.0075.

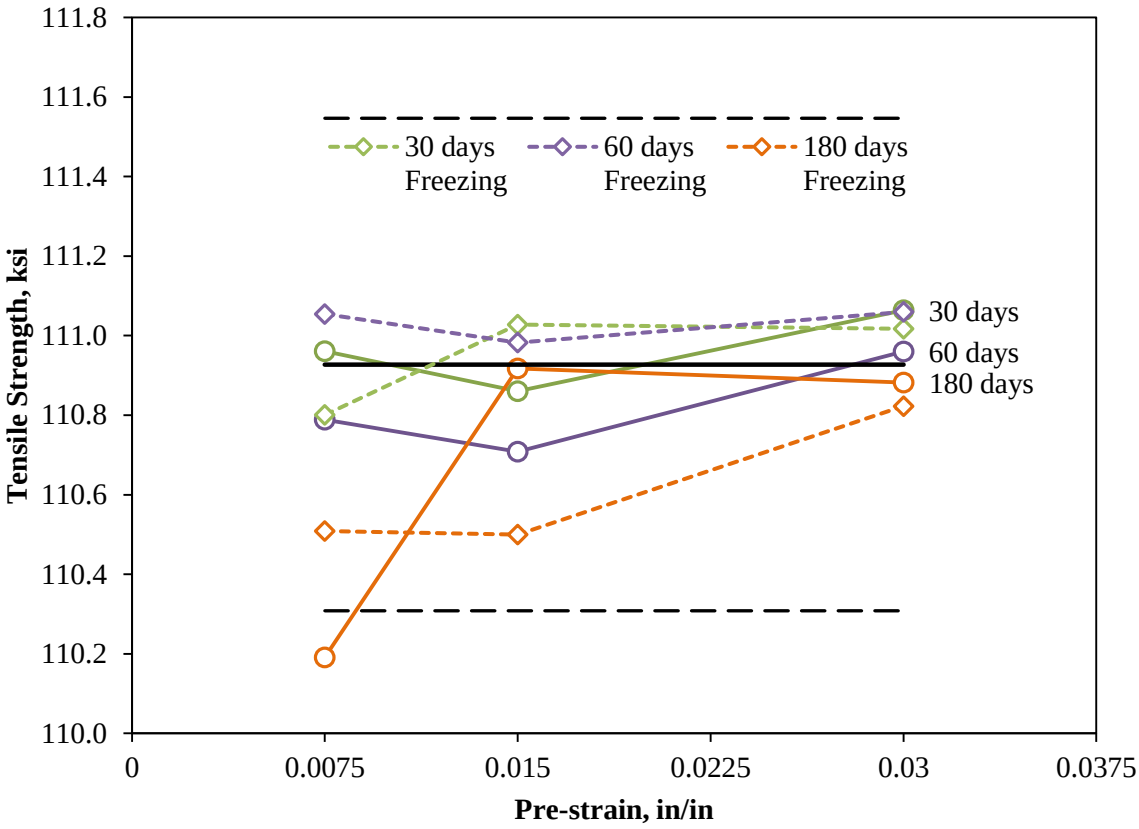

Figure 4-34. Impact of temperature on tensile strength of No. 7 bars

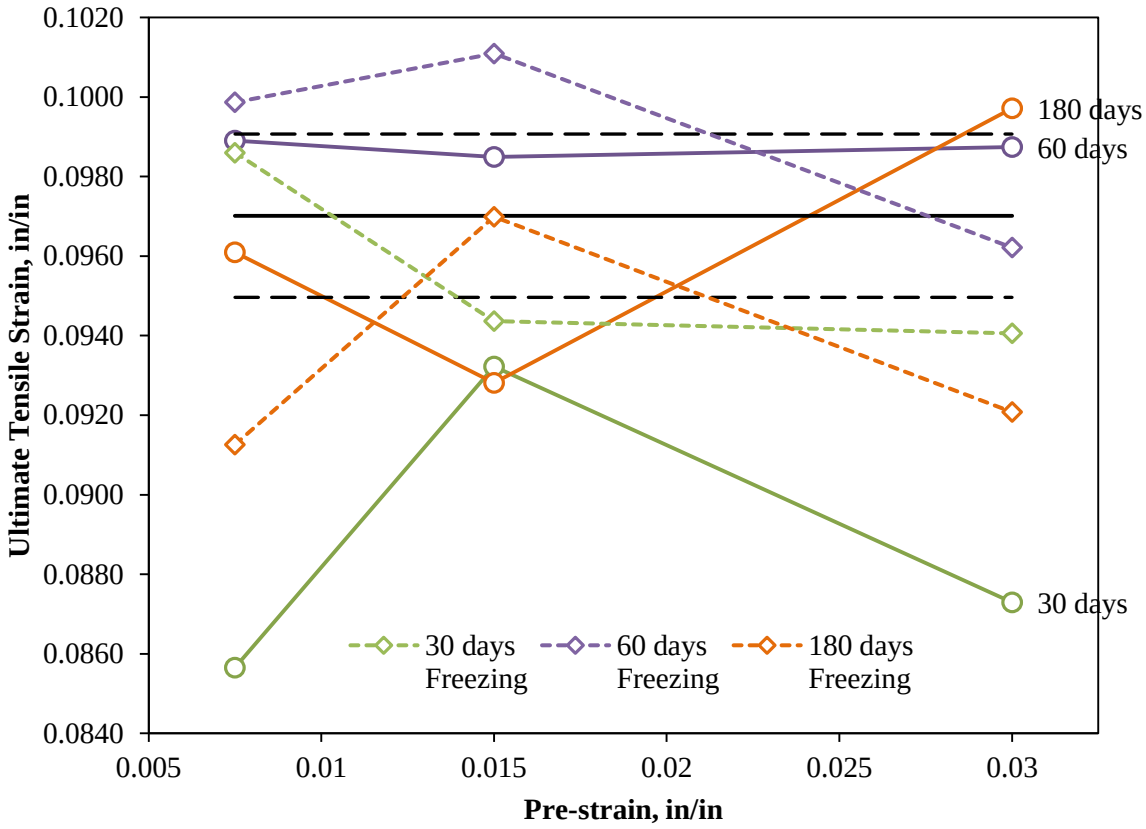

Figure 4-35. Impact of temperature on ultimate tensile strain of No. 7 bars

4.4. Cyclic Testing

A limited number of cyclic tests on No. 5 and No. 7 bars were conducted for the purpose of evaluating the capability of existing rebar models to characterize the A706 grade 80 cyclic material behavior and to investigate the effect of cyclic load history on the ultimate tensile strain (strain at max stress). This section summarizes the findings of these tests.

4.4.1. Model Comparison

Two No. 7 bars were tested in manual control with random load history in order to evaluate an existing stress strain model. The OpenSees uniaxial model Reinforcing Steel Material (Mazzoni et al. 2007) was used to characterize the experimental data from one of the tests. This model is based on the Chang and Mander (1994) model presented in Chapter 2 with the addition of optional buckling rules after either Gomes and Appleton (1997) or Dhakal and Maekawa (2002). Figure 4-36 shows the comparison between the experimental and the theoretical curves for one of the tests. From the figure, it is evident that the model is able to characterize the shape of the cyclic test results reasonably well except for the last compression cycle which was marked by obvious bar buckling.

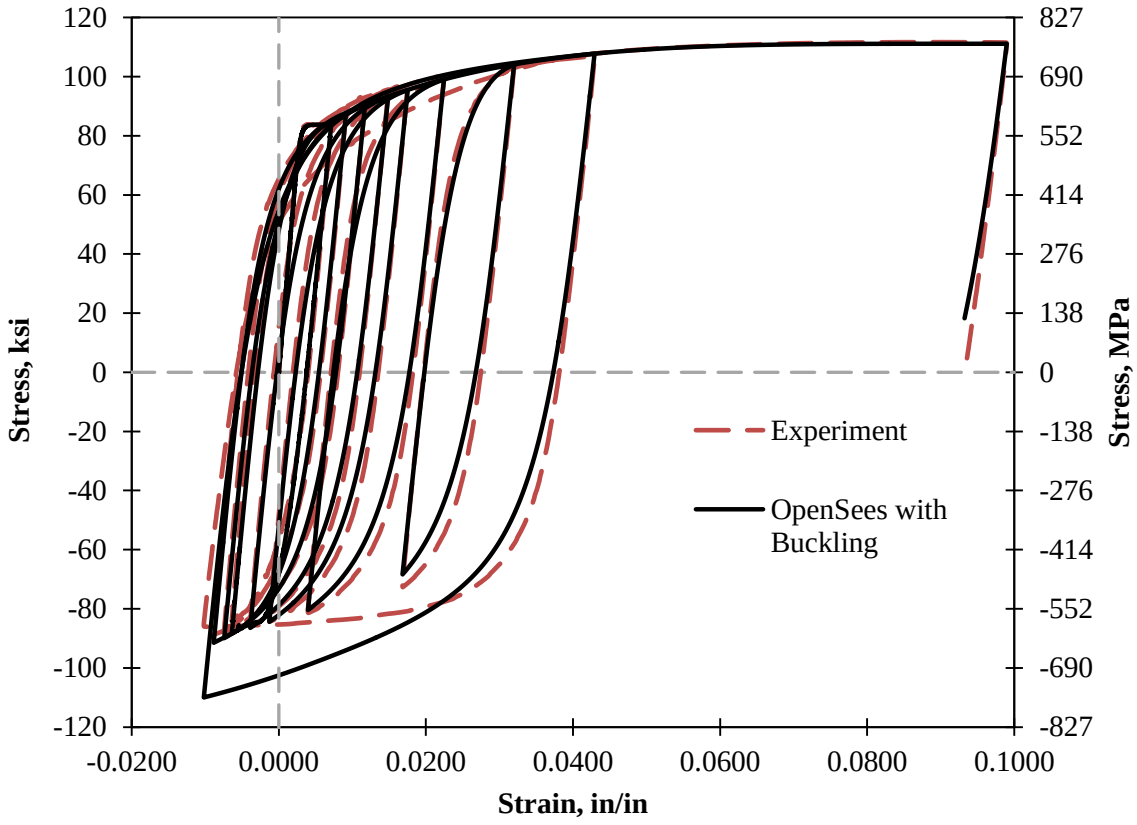

Figure 4-36. Comparison of cyclic test of No. 7 bar with OpenSees Reinforcing Steel Material (Mazzoni et al. 2007) model

4.4.2. Effects of Load History on Ultimate Tensile Strain

The remainder of the cyclic testing was used to investigate the effect of load history on the ultimate tensile strain. As indicated in Chapter 3 and further explained here, difficulties with the testing grips hindered the scope of this portion of the research.

The initial tests, which were aimed at achieving a strain history of -0.005 to 0.02 strain for a limited number of cycles before tensioning to failure, suffered from two problems. The first of these was that the strains "drifted" with each cycle, such that the

compressive strains reduced while the tensile strains increased. Figure 4-37 illustrates this phenomenon for a No. 5 bar tested in force control for 100 cycles. Figure 4-38, which shows the associated stress vs. time graph, confirms that the strains drifted despite the forces remaining consistent. This behavior can be associated with slipping of the bar in the grips.

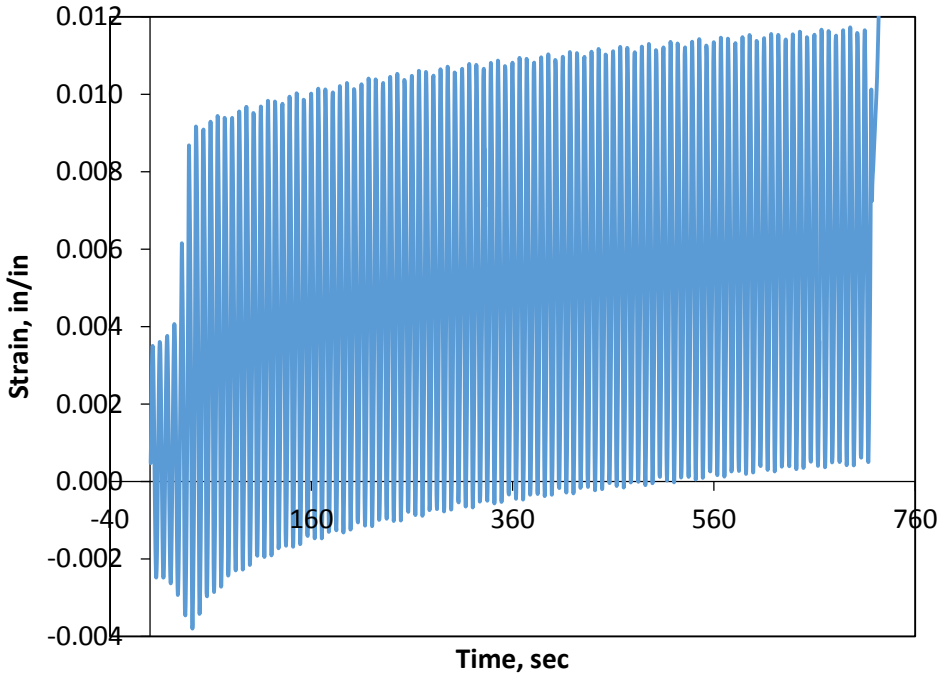

Figure 4-37. Strain history of a No. 5 bar (12547) tested in force-control mode showing obvious strain "drifting"

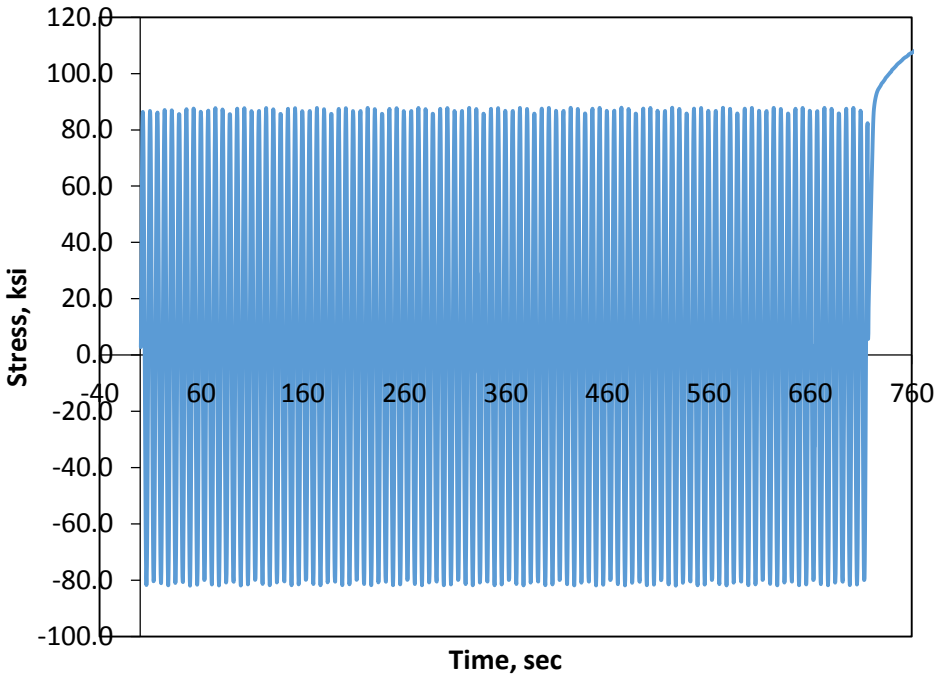

Figure 4-38. Stress history of the same No. 5 bar tested in force-control mode showing constant stress while strains "drifted"

The second problem that arose was buckling of the bars at lower-than-expected strains. A subset of monotonic compression tests on five No. 7 bars having unbraced lengths of 4, 5, 6, 7, and 8 times the bar diameter were conducted as part of an investigation into this issue. Figure 4-39 shows the buckled shape of one of the bars having an unbraced length of 5 bar diameters. From the picture, it is immediately obvious that the buckled shape of the bar is not representative of a fixed-fixed boundary condition. This observation demonstrated that (1) taking the theoretical unbraced length as the distance between the grips would underestimate the actual unbraced length and (2) assuming the bar to be fixed at both ends was not a viable assumption for the test setup used. Figure 4-40 shows the buckled shapes of

the five compression test bars. From the figure, it is evident that the bars did not take the theoretical buckled shape until a theoretical unbraced length of 7 bar diameters.

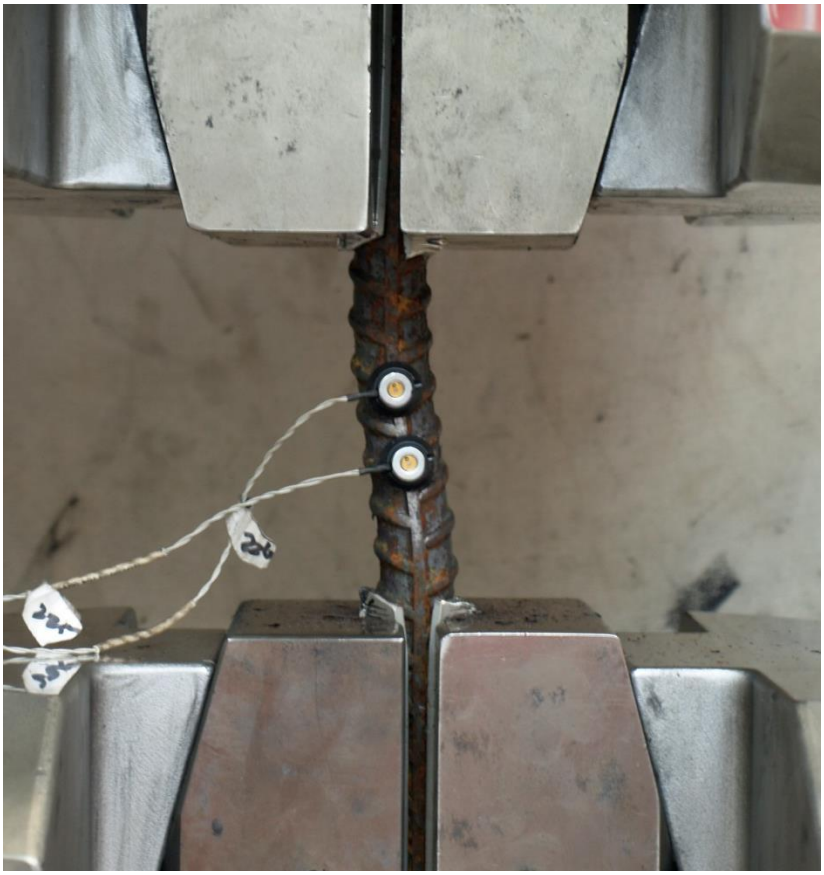

Figure 4-39. Unexpected buckled shape of a No. 7 bar tested in pure compression ($L/d_{bl} = 5$)

Figure 4-40. Buckled shapes of No. 7 bars tested in pure compression (L/d_{bl} = 8 to L/d_{bl} = 4) indicating poor fixity of the boundary conditions (MTS machine grips)

As a result of the problems just described, it was not possible to specify a cyclic strain history that could be maintained for multiple cycles, despite several attempts to do so. As such, there was no way to develop a relationship between load history and reduction in ultimate tensile strain. Nonetheless, a qualitative assessment could still be performed to investigate the impact of cycling on the ultimate tensile strain. The results of six No. 5 bar tests and 1 No. 7 bar tests are presented next.

4.4.2.1.Test ID: 12544

Figure 4-41 presents the results of a No. 5 bar tested for 100 cycles in displacement-control and then pulled to failure in tension. The displacement limits were established to generate strains between 0.01 in tension and -0.001 in compression which would have correlated to cycling within the yield plateau. As evidenced by the figure, the actual strain

history between 0.0025 in tension and -0.002 in compression resulted in fully elastic cycling before pulling to failure. An ultimate tensile strain of 0.1008 was achieved during the tensile test. Table 4-6 summarizes the ultimate tensile strains for each of the tests.

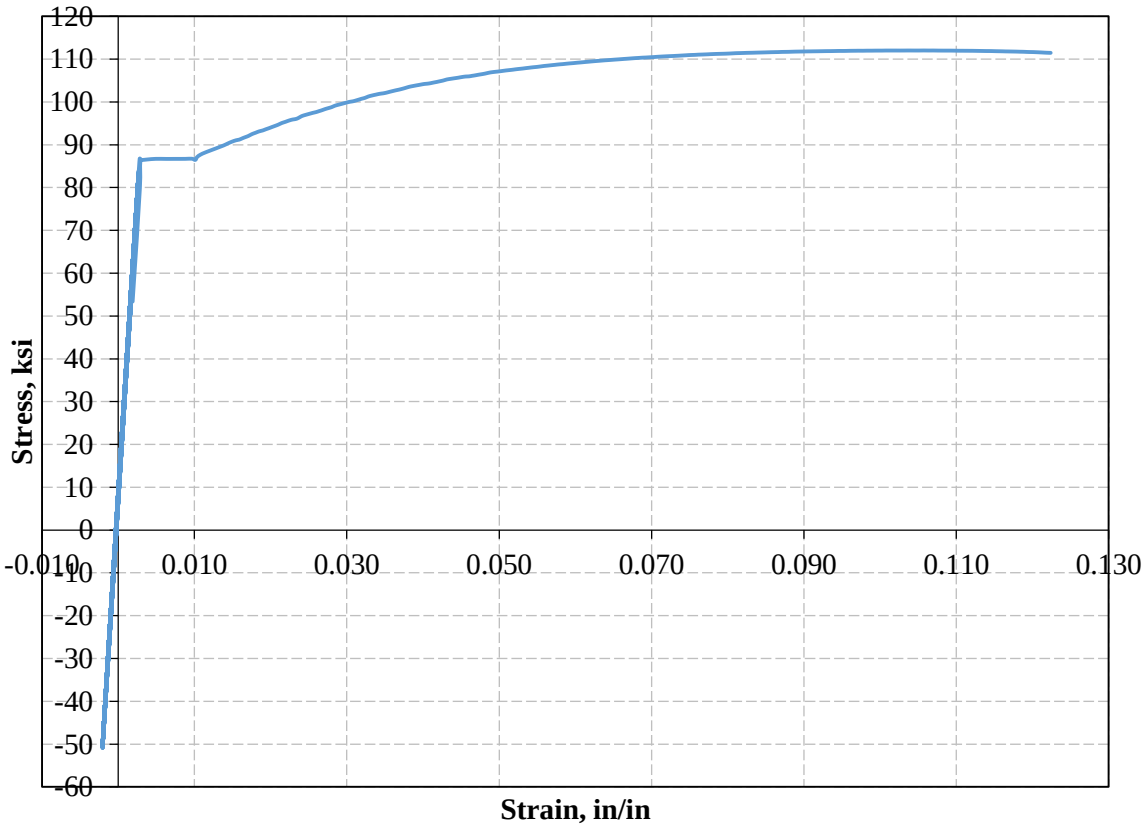

Figure 4-41. Cyclic test of a No. 5 bar (12544) followed by tensile test to failure

4.4.2.2.Test ID: 12547

Figure 4-42 presents the results of a No. 5 bar tested for 100 cycles in force-control and then pulled to failure in tension. The force limits were established based on the findings of the tensile testing program to generate strains between 0.01 in tension and -0.001 in compression which would have correlated to cycling within the yield plateau. As evidenced

by the figure, the actual strain history varied from a tension-compression pair of 0.0086 and -0.003 in the first cycle to 0.012 and 0.0005 by the last cycle. An ultimate tensile strain of 0.1049 was achieved during the tensile test. Table 4-6 summarizes the ultimate tensile strains for each of the tests.

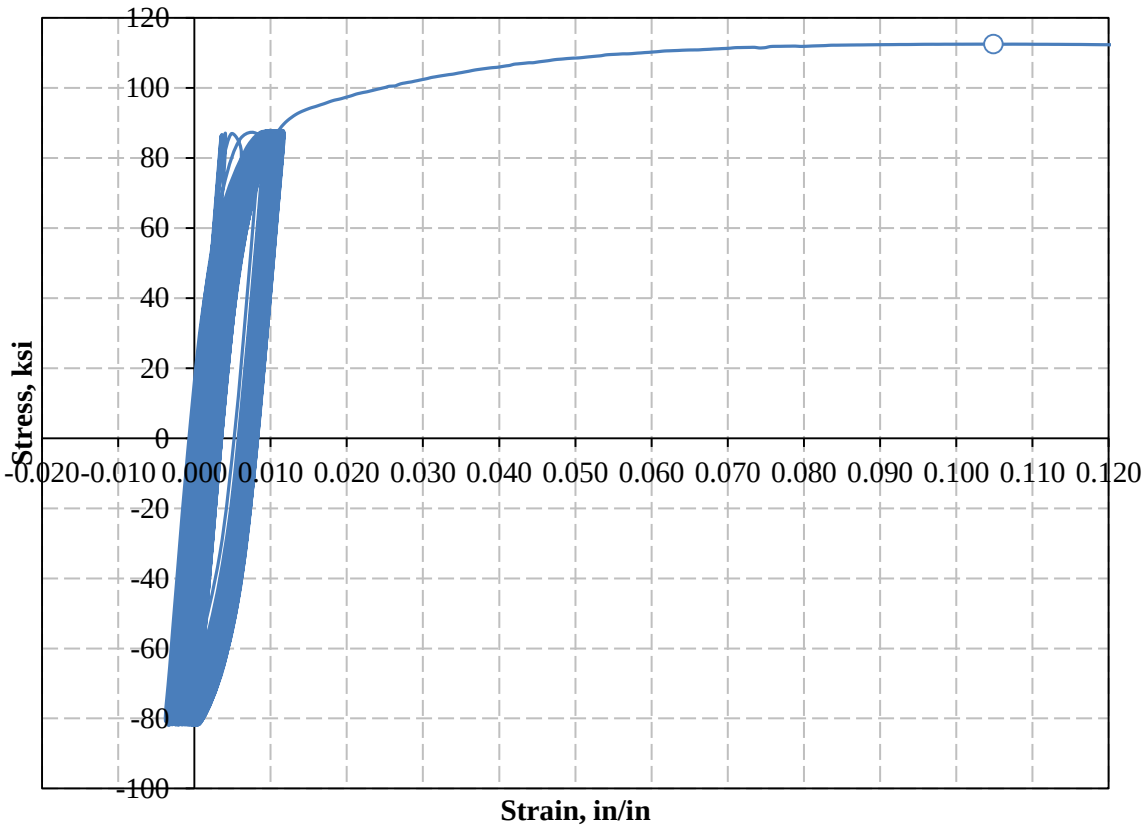

Figure 4-42. Cyclic test of a No. 5 bar (12547) followed by tensile test to failure

4.4.2.3.Test ID: 12548

Figure 4-43 presents the results of a No. 5 bar tested for 60 cycles in displacement-control and then pulled to failure in tension. The displacement limits were established based on the findings of the tensile testing program to generate strains between 0.02 and 0.017 in

tension such that the bar remained in a state of tensile stress for the duration of the test. As evidenced by the figure, the actual strain history between 0.009 and 0.0076 in tension resulted in nearly elastic cycling within the yield plateau before pulling to failure. An ultimate tensile strain of 0.1000 was achieved during the tensile test. Table 4-6 summarizes the ultimate tensile strains for each of the tests.

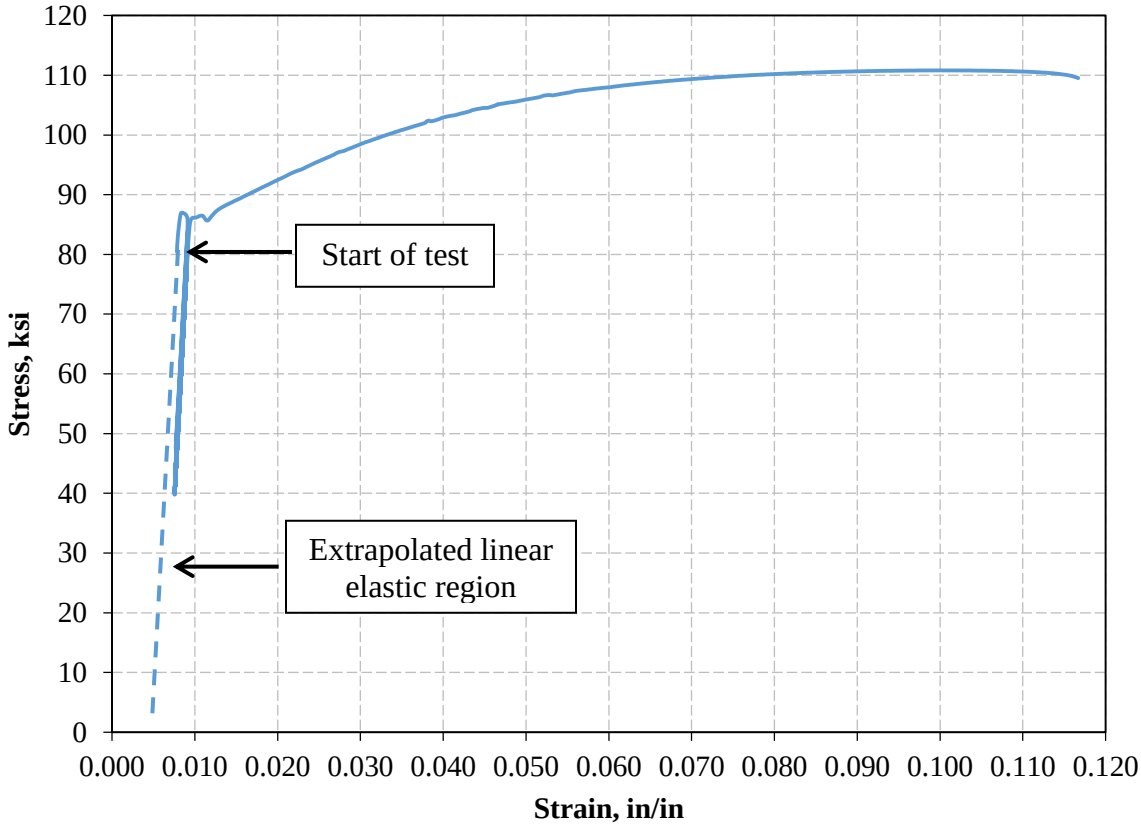

Figure 4-43. Cyclic test of a No. 5 bar (12548) followed by tensile test to failure

4.4.2.4.Test ID: 12549

Figure 4-44 presents the results of a No. 5 bar tested for 50 cycles in force-control and then pulled to failure in tension. The force limits were established based on the findings

of the tensile testing program to generate strains between 0.02 and ε(σ=0) in tension such that the bar remained in a state of tensile stress for the duration of the test. As evidenced by the figure, the actual strain history varied from a tension-compression pair of 0.017 and 0.013 in the first cycle to 0.025 and 0.021 by the last cycle. An ultimate tensile strain of 0.0949 was achieved during the tensile test. Table 4-6 summarizes the ultimate tensile strains for each of the tests.

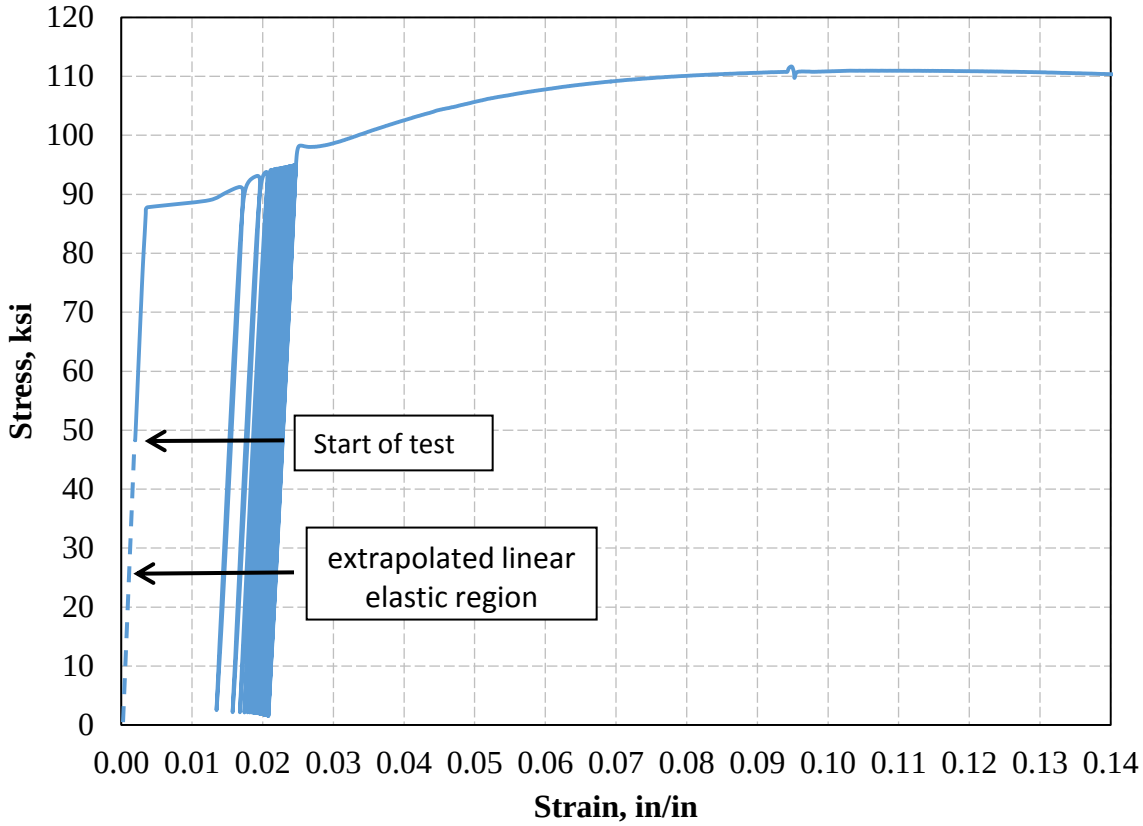

Figure 4-44. Cyclic test of a No. 5 bar (12549) followed by tensile test to failure

4.4.2.5.Test ID: 125410

Figure 4-45 presents the results of a No. 5 bar tested for 10 cycles and then pulled to failure in tension. The test was controlled manually to ensure the reversals occurred at the desired strains. Eight cycles were performed between strains of 0.00 and 0.01 followed by two cycles between strains of 0.00 and 0.02 before the tensile test to failure. Visible buckling was observed in the last compressive cycle before pulling to failure. An ultimate tensile strain of 0.0965 was achieved during the tensile test. Table 4-6 summarizes the ultimate tensile strains for each of the tests.

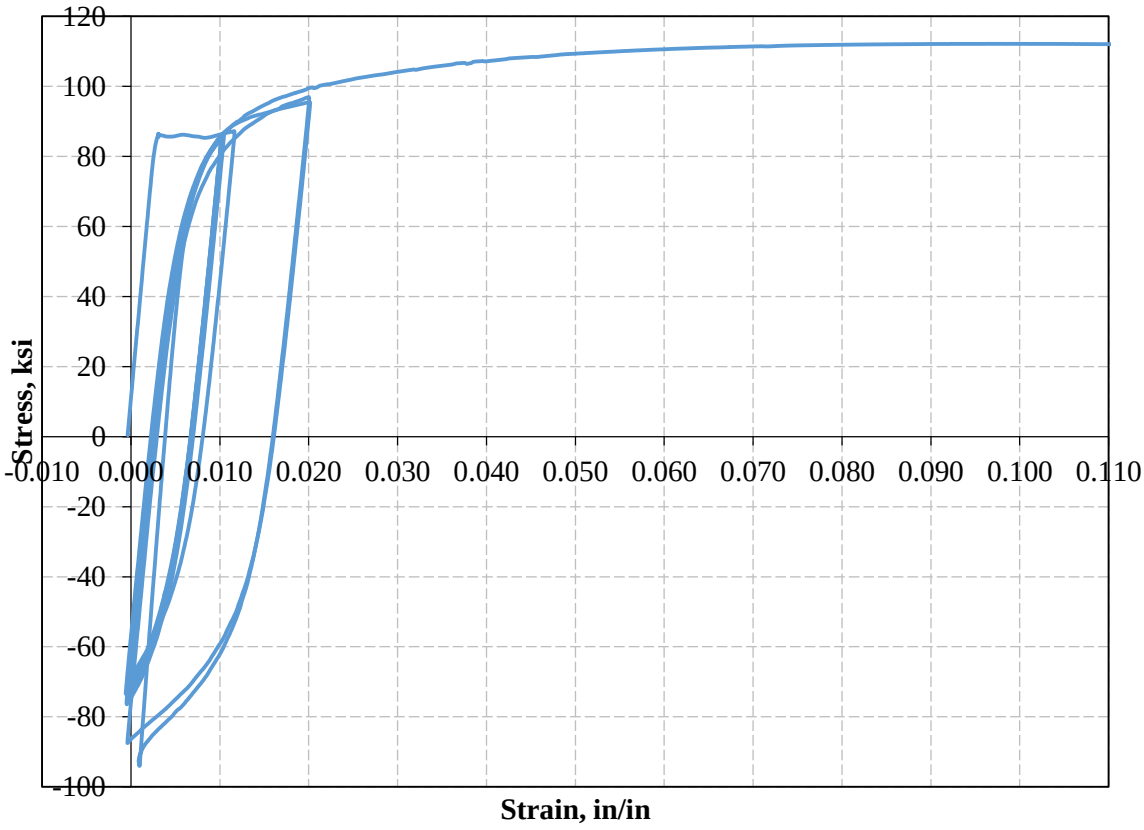

Figure 4-45. Cyclic test of a No. 5 bar (125410) followed by tensile test to failure

4.4.2.6.Test ID: 125411

Figure 4-46 presents the results of a No. 5 bar tested for 30 cycles and then pulled to failure in tension. The test was controlled manually to ensure the reversals occurred at the desired strains. Ten cycles were performed between 0.00 and 0.01 strain followed by 10 cycles between 0.01 and 0.02 strain followed by 10 cycles between 0.02 and 0.03 strain followed by a reversal back to 0.01 strain before the tensile test to failure. Visible buckling was observed in the last compressive cycle before pulling to failure. An ultimate tensile strain of 0.1055 was achieved during the tensile test. Table 4-6 summarizes the ultimate tensile strains for each of the tests.

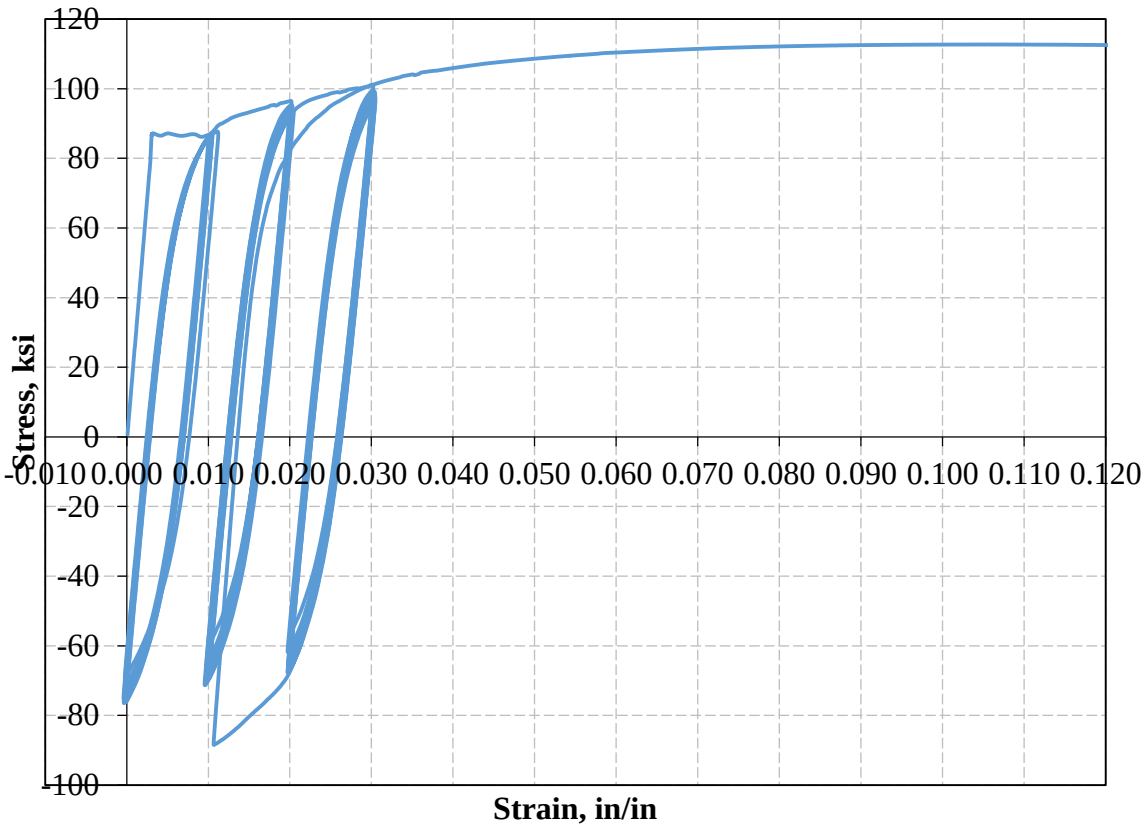

Figure 4-46. Cyclic test of a No. 5 bar (125411) followed by tensile test to failure

4.4.2.7.Test ID: 12746

Figure 4-47 presents the results of a No. 7 bar tested for 20 cycles in displacement-control and then pulled to failure in tension. The displacement limits were established based on the findings of the tensile testing program to generate strains between 0.02 in tension and -0.005 in compression. The displacement limits for the first 10 cycles resulted in an actual strain history that varied from 0.008 to 0.007 in tension while consistently reversing at -0.003 in compression. An adjustment to the displacement limits for the next 10 cycles resulted in an actual strain history that varied from 0.02 to 0.01 in tension and -0.02 to -0.03 in

compression. Obvious buckling of the bar was observed in second set of 10 cycles. An ultimate tensile strain of 0.0857 was achieved during the tensile test. Table 4-6 summarizes the ultimate tensile strains for each of the tests.

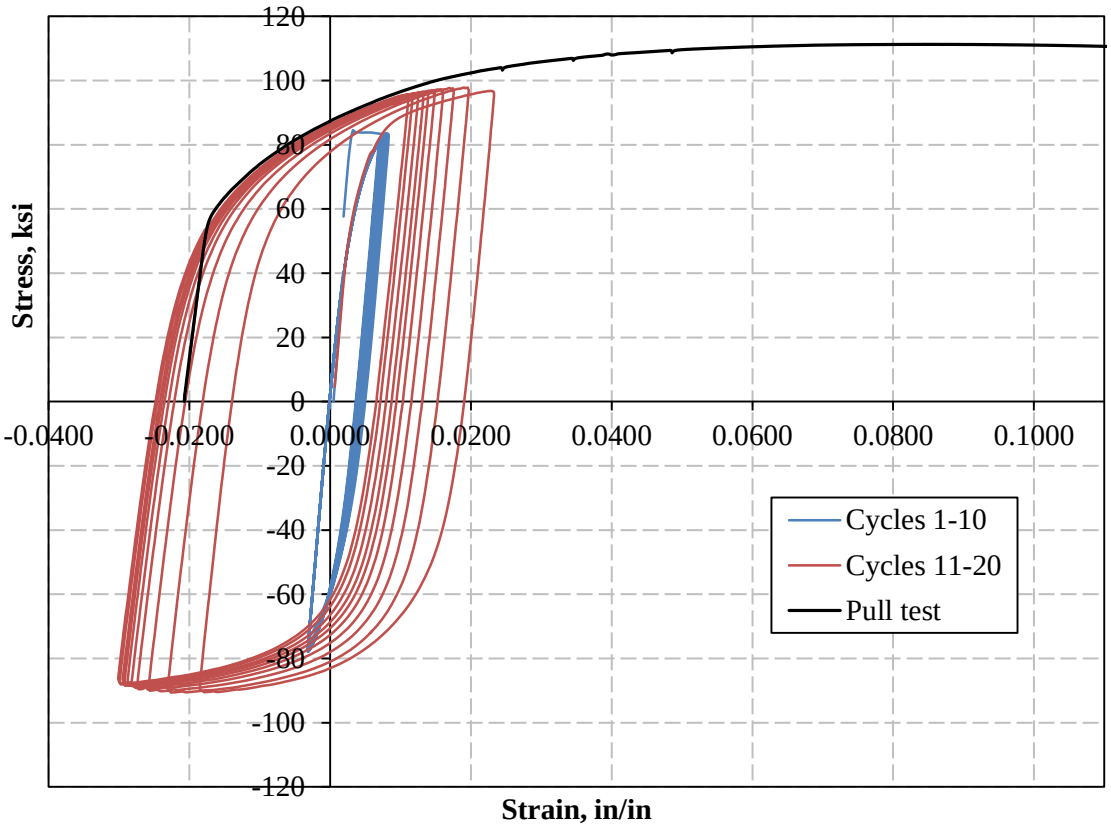

Figure 4-47. Cyclic test of a No. 7 bar (12746) followed by tensile test to failure

4.4.2.8.Summary Table

Table 4-6. Ultimate tensile strain occurring during tensile test following cyclic loading

ID	Bar Size	L/d_{bl}	Control Mode	Ultimate Tensile Strain
12544	5	6	displ.	0.1008
12547	5	6	force	0.1049
12548	5	6	displ.	0.1000
12549	5	6	force	0.0949
125410	5	6	manual	0.0965
125411	5	6	manual	0.1055
Mill 1, Heat 2, No. 5 bar average:				0.0917
12746	7	6	displ.	0.0857

5. DISCUSSION

5.1. Tensile Tests

5.1.1. Comparison with Literature Results

As demonstrated in Chapter 2, several of the literature papers presenting numerical stress-strain data on A706 grade 80 rebar additionally presented the associated stress-strain curves. A graphical comparison between these curves and those generated as part of the current research can be accomplished by superimposing the graphs on top of one another. In addition to illustrating the similarities in the shape of the strain hardening region, this exercise also serves as a means of validating the experimental findings.

The results indicate that the experimental findings are consistent with currently available literature data with respect to the shape of the stress-strain curve. Figure 5-1 highlights the consistency in the length of the yield plateau and the initial slope of the strain hardening region. Note that the project data curves have been plotted to ε_u in Figures 5-2 and 5-3. Figure 5-2 illustrates a consistency in shape of the strain hardening curve and ultimate tensile strain. An interesting observation from Figure 5-2 is the fact that the No. 18 bar stress-strain curve lies near the bottom of the experimental stress-strain curves. This trend for the larger bars to have lower strength was illustrated in Chapter 3. Figure 5-3 illustrates a consistency in length of the yield plateau and shape of the strain hardening curve but a difference in the ultimate tensile strains.

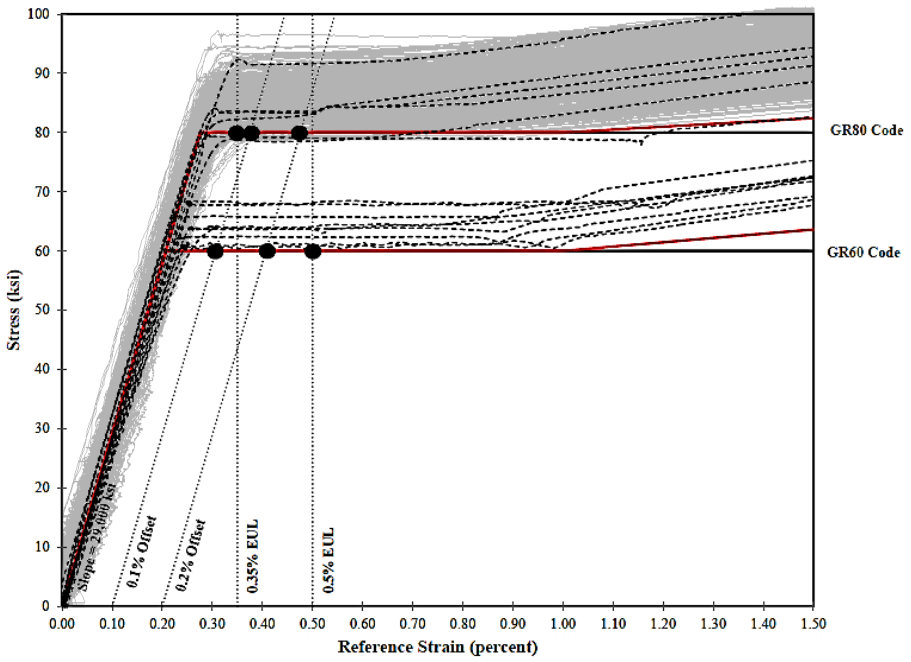

Figure 5-1. WJE (2013) stress-strain curves superimposed over project data

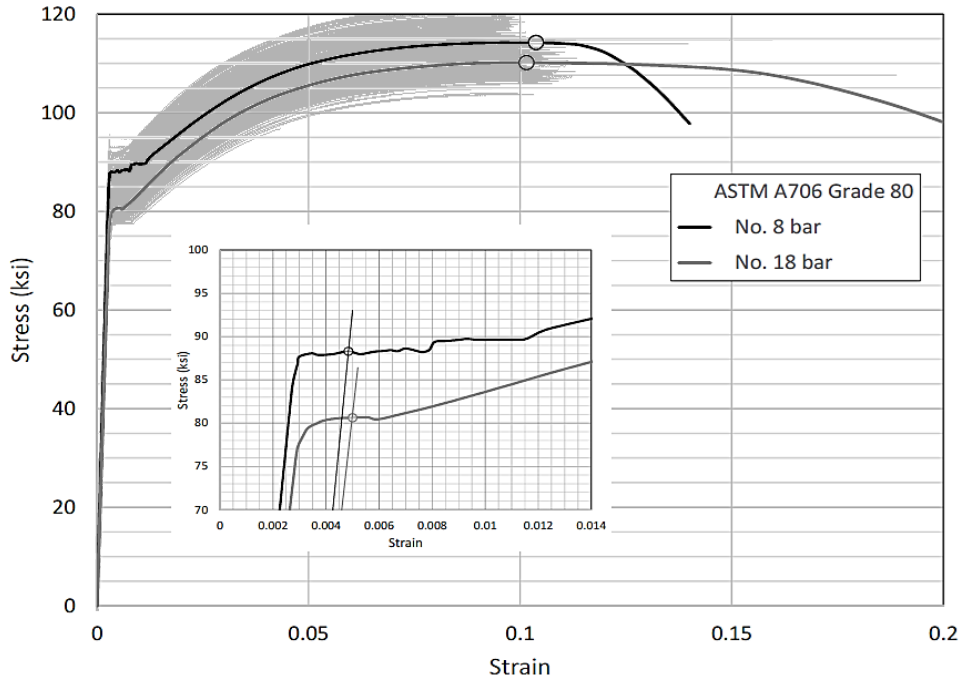

Figure 5-2. GCR (2014) stress-strain curves superimposed over project data (plotted up to ε_{su})

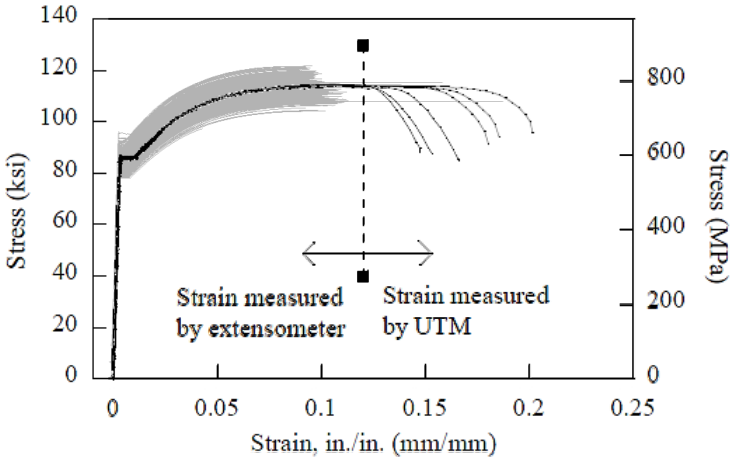

Figure 5-3. Trejo et al. (2014) stress-strain curves superimposed over project data (plotted up to ε_{su})

5.1.2. Comparison with Mill and CRSI Data

As described in Chapter 2, there seems to be a trend for steel mill rebar-test results to differ from research laboratory tests of the same batch of steel. This section presents a comparison of the tensile test results acquired through the current project with the corresponding certificate values from the three mills providing steel in support of this trend. Additional mill-derived data taken from the CRSI mill database is included in the comparison. The parameters available for comparison are the yield strength, the tensile strength, percent elongation at fracture, and tensile-to-yield ratio.

5.1.2.1.Yield Strength

Figure 5-4 presents the empirical CDF curves from the three datasets for the yield strength parameter. The mill certificate values provided with the steel supplied to the current project lie along the empirical CDF curve derived from the CRSI mill database which is composed of mill test results submitted to CRSI. As illustrated in the figure, the yield strength results from the tensile testing program are consistently lower than the mill-based values. There is an approximate 2.2% difference in the means. Table 5-1 summarizes the mean values for each of the four parameters.

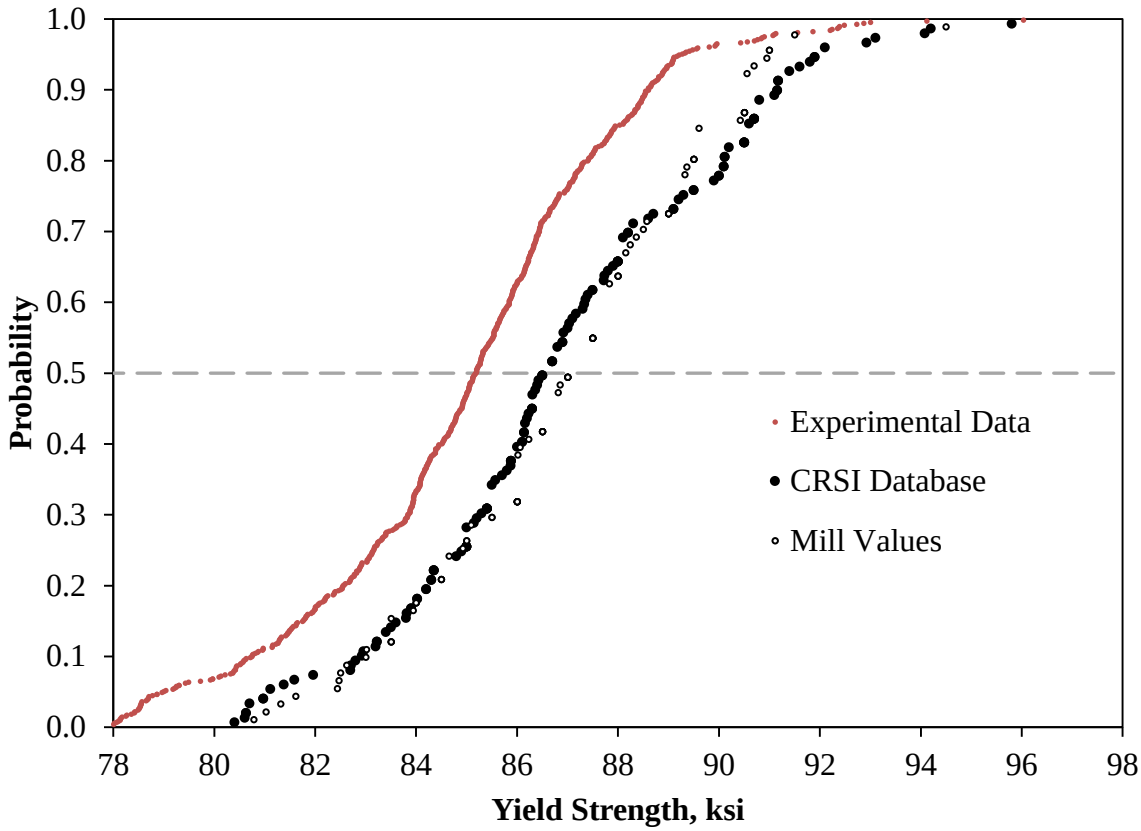

Figure 5-4. Empirical CDFs comparing project, CRSI, and mill certificate yield strength data

5.1.2.2.Tensile Strength

Figure 5-5 presents the empirical CDF curves from the three datasets for the tensile strength parameter. As with the yield strength graphs, the mill cert values related to the current project tend to follow along the CRSI mill database values. There is an approximate 1.8% difference in the mean tensile strengths with the mill values being higher than the experimental results.

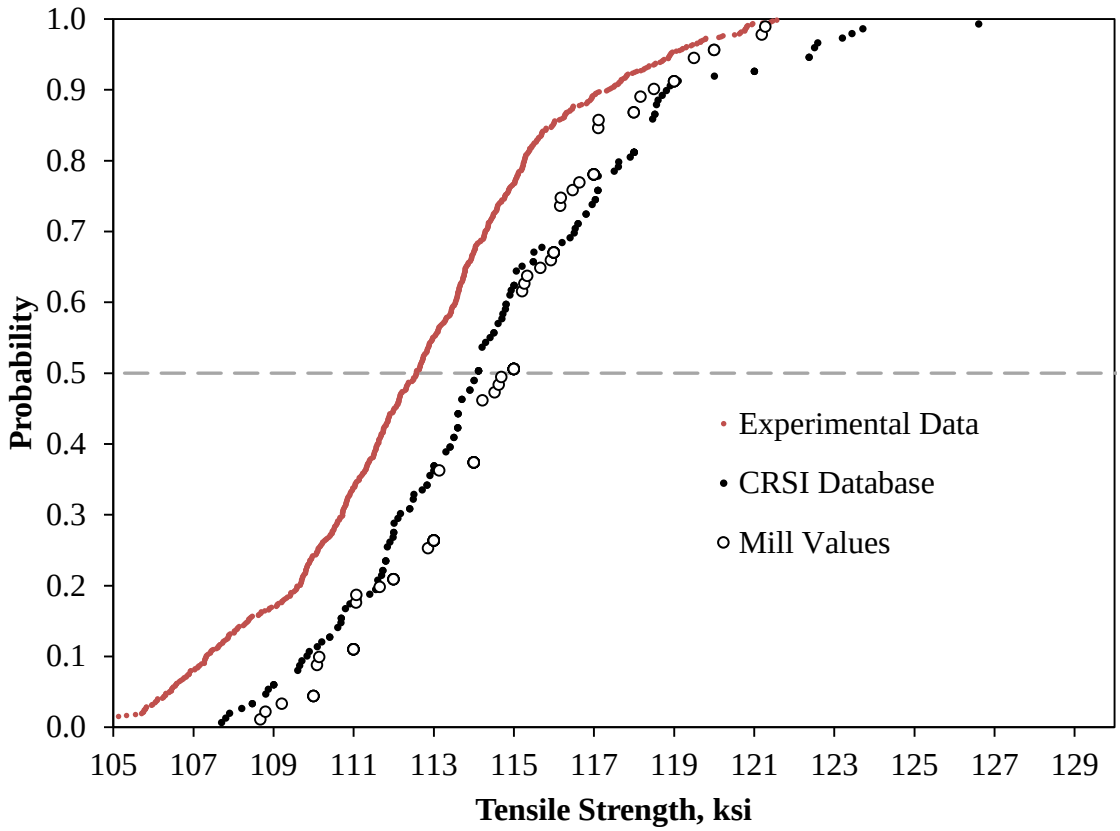

Figure 5-5. Empirical CDFs comparing project, CRSI, and mill certificate tensile strength data

5.1.2.3.Percent Elongation at Fracture

Figure 5-6 presents the empirical CDF curves from the three datasets for the percent elongation at fracture. The CRSI mill database values essentially coincide with the mill certificate values; however, unlike with the previous two parameters, the experimental program data lies consistently higher than the mill-based values. A possible reason for this trend is discussed in Section 5.1.4.6. There is an approximate 8.6% difference in the means.

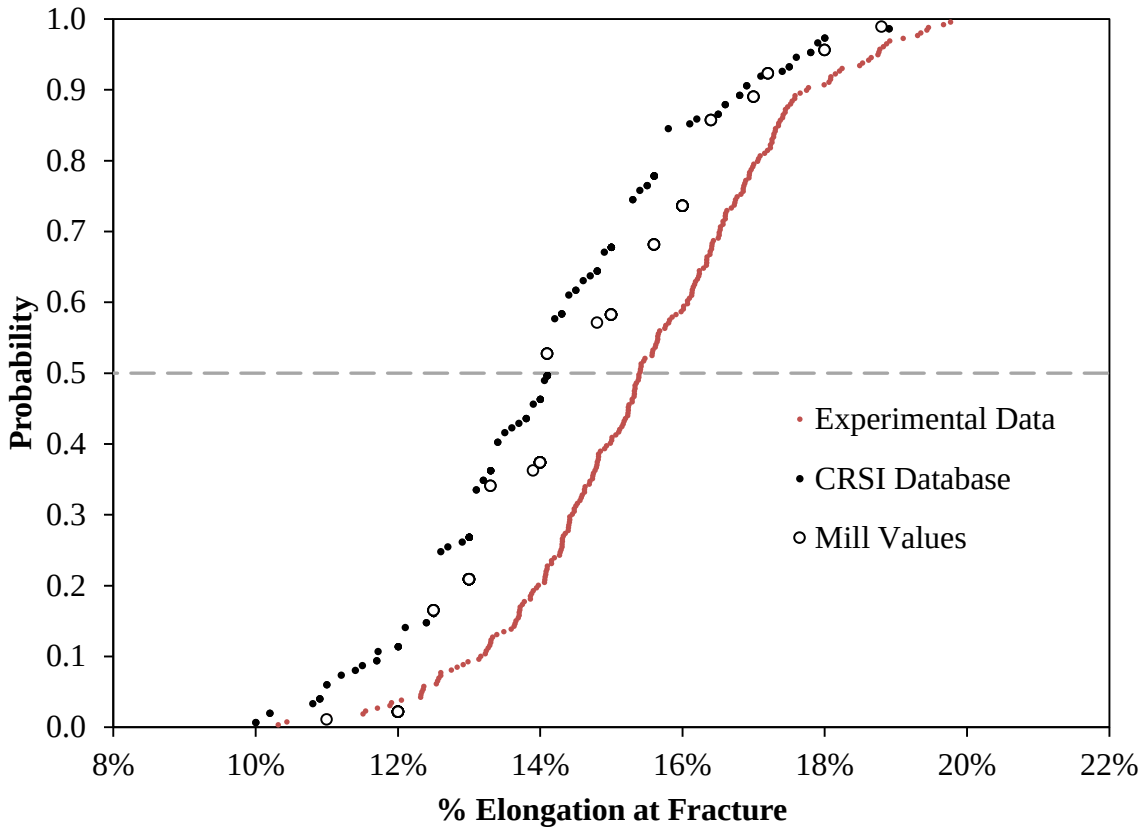

Figure 5-6. Empirical CDFs comparing project, CRSI, and mill certificate elongation at fracture data

5.1.2.4.Tensile-to-Yield Ratio

Figure 5-7 presents the empirical CDF curves from the three datasets for the tensile-to-yield ratio. In this case, all three datasets follow the same trend with the mill certificate values closely aligning with the experimental results. These results indicate that, while the mill-acquired yield and tensile strength values are higher than what was found experimentally, the ratio between the two is equivalent in both cases. There is an approximate 0.2% difference in the means.

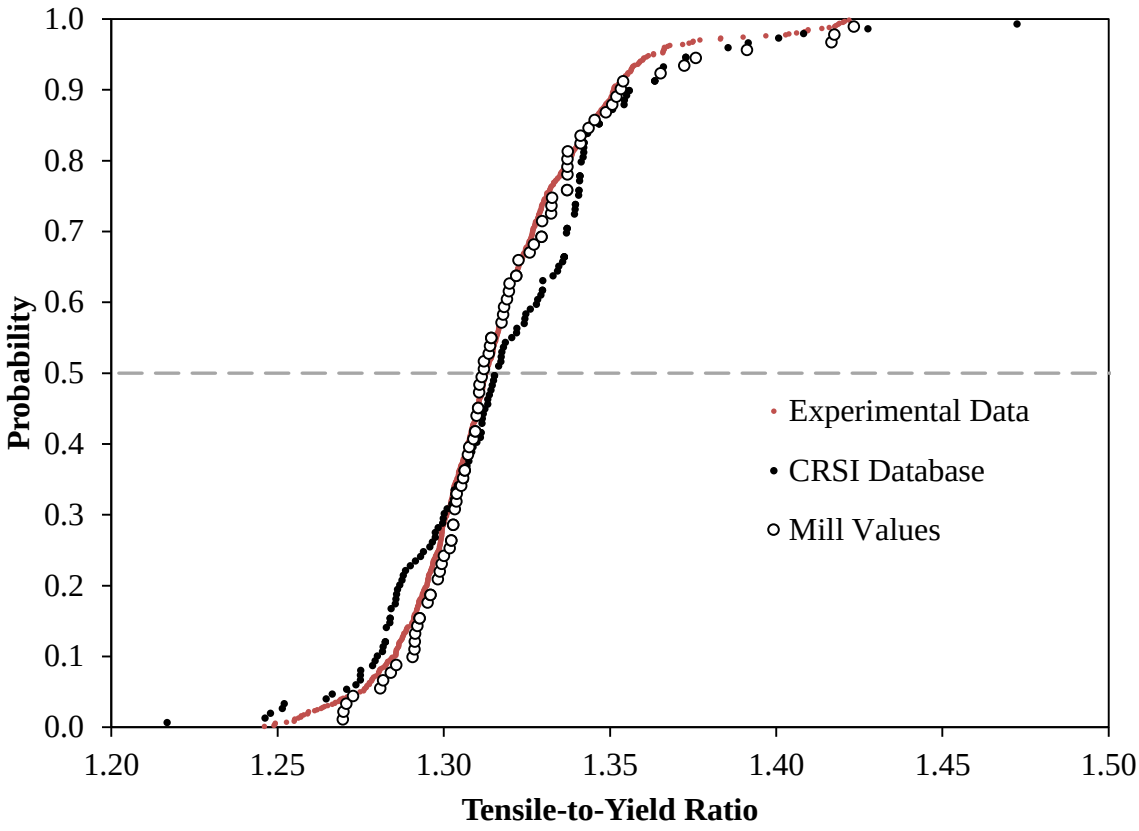

Figure 5-7. Empirical CDFs comparing project, CRSI, and mill certificate tensile-to-yield ratio data

Table 5-1. Percent difference between experimental and mill-based data

Averages	Experimental Data	Combined Mill & CRSI Data	%Difference
f_{ye} [ksi]	85.0	86.9	2.20%
f_{ue} [ksi]	112.5	114.5	1.78%
%elong	15.5%	14.2%	8.62%
f_{ue}/f_{ye}	1.32	1.32	0.20%

5.1.3. Analysis of Variabilities

As stated in Section 3.4.2., each test specimen was given a unique identification number indicating its mill, heat, and 20-foot bar of origin. Not only does this allow the data to be filtered on the basis of one or more common variables (ex: tensile strengths of all No. 6 bar tests from Mill 2 Heat 3), but it also permits the data to be interpreted in terms of those common variables (ex: standard deviation for all No. 6 bar tests from Mill 2 Heat 3). An advantage of this is the increased ability to identify trends in the dataset and to detect and/or explain anomalies.

This section specifically addresses the degree of variability associated with each of the five main stress-strain parameters in terms of three variables: producing mills, heats within a mill, and twenty-foot bars within a heat. The coefficient of variation (CV) is used as the primary indicator of variability. The following eight topics are addressed: variability between the three mills, average variability within a mill, average variability between heats from a common mill, average variability between heats from a common mill by bar size, average variability within a heat, average variability within a heat by bar size, average variability between three 20’ bars from a common heat, and average variability within a 20-foot bar (between three specimens from a common 20-foot bar).

5.1.3.1.Mills

Table 5-2 provides the average experimental values corresponding to each of the three mills and the five main stress-strain parameters. Included at the bottom of the table are the standard deviation and coefficient of variation (CV) of the mill averages for each of the

five parameters. In words, these describe the variability between the three mills. The low coefficient of variation values imply that specimens tested from any of the three mills generally behaved in the same way. Mill CDFs for each of the five parameters may be found in Appendix C.

Table 5-2. Mill averages and variability between mills

Avg	f_{ye}	ε_{ye}	ε_{sh}	f_{ue}	ε_{su}
Mill 1	84.99	0.0032	0.0078	111.16	0.0965
Mill 2	85.42	0.0034	0.0069	113.29	0.0934
Mill 3	84.54	0.0032	0.0077	112.84	0.0965
St. Dev	0.44	0.0001	0.0005	1.12	0.0018
CV	0.51%	3.00%	6.93%	1.00%	1.89%

Table 5-3 provides the coefficients of variation of the experimental data corresponding to each of the three mills and the five main stress-strain parameters. At the bottom of the table are the averages of the mill coefficients of variation for each of the parameters. In words, these describe the average variability within each mill. The high coefficient of variation values imply that even within a single mill, specimens tended to exhibit a wide range of responses, particularly in the length of the yield plateau as indicated by the onset of strain hardening parameter. This general trend can be attributed to the fact that multiple heats were represented for each mill as described in the next section.

Table 5-3. Mill coefficients of variation and average CV across the mills

CV	f_{ye}	ε_{ye}	ε_{sh}	f_{ue}	ε_{su}
Mill 1	3.14%	7.74%	20.23%	2.28%	4.98%
Mill 2	3.67%	10.37%	24.67%	3.17%	6.73%
Mill 3	3.82%	7.87%	30.20%	3.74%	4.93%
Averages	3.54%	8.66%	25.03%	3.06%	5.55%

5.1.3.2.Heats

A similar approach to that just described for mills can be used to determine the variability between and within heats. Note that it would not make sense to compare all 25 heats with one another directly as they are associated with different producing mills. As such, the variability "between" heats is defined as the average variability between heats from a common mill. The average variability within a heat, however, is defined the same as for the mills: average of the coefficients of variation of all the tests associated with each heat.

Two tables of heats analogous to Tables 5-2 and 5-3 for mills could be presented but would be too large to comfortably fit into the body of the report. Nonetheless, Tables 5-6 and 5-7 summarize what would have been the bottom lines of these tables. The values in Table 5-6 illustrate that even within a single mill the variability between different heats can be somewhat high. Compared to the average variability within a mill, the average variability within a heat is noticeably lower (Table 5-7). It should be noted that it is difficult to make broad, substantive claims about variation between heats as different heats contained different bar sizes (refer Appendix A). Section 5.1.3.4 addresses this issue by defining the variability within and between heats in terms of individual bar sizes. Heat CDFs for each of the five parameters may be found in Appendix D.

5.1.3.3.Twenty-foot Bars

Table 5-6 summarizes the average variability between twenty-foot bars from a common heat in terms of the coefficient of variation. Table 5-7 summarizes the average variability within a single twenty-foot bar. The coefficients of variation presented in these

two tables for the twenty-foot bars were defined in the same way as just described for the heats. At this level of detail, the coefficients of variation for the yield strength, tensile strength, and onset of strain hardening are lower than in any of the other methods of comparison.

5.1.3.4.Heats by Bar Size

The primary purpose of this section is to expand on the observations presented in section 5.1.3.2 by evaluating the variability between and within heats in terms of individual bar sizes as this offers a more practical interpretation of the data. Table 5-4 summarizes the variability between heats from a common mill for each bar size. The values in the table are obtained by finding the coefficient of variation of the heat averages within a mill (ex: M1H1, M1H2, M1H3 – 9 tests in each) for a given bar size and then taking the average coefficient of variation across the three mills for that bar size. This represents the case in which a shipment of steel from a single manufacturer includes multiples heats for a given bar size, and the variability between those heats is of interest.

Table 5-5 summarizes the average variability within a single heat for each bar size. The values in this table where obtained by determining the coefficient of variation for each combination of mill, heat, and bar size (ex: M1H1 No. 4 bars – 9 tests in each) and averaging across all the heats for that bar size (9 heats for each bar size). This represents the case in which a shipment of steel includes bars from only one heat, and the variability within that heat and for a given bar size is of interest.

Table 5-4. Coefficients of variation of averages - variability "between" (heats from a common mill for each bar size)

CV	f_{ye}	ε_{ye}	ε_{sh}	f_{ue}	ε_{su}
No. 4	1.64%	3.62%	10.59%	1.60%	3.20%
No. 5	2.39%	2.40%	11.59%	1.62%	1.79%
No. 6	1.54%	5.36%	21.10%	2.29%	3.41%
No. 7	2.99%	5.08%	6.06%	1.49%	1.79%
No. 8	1.30%	3.63%	11.22%	1.33%	0.87%
No. 9	0.94%	5.66%	13.66%	1.86%	3.11%
No. 10	1.74%	4.45%	9.75%	1.57%	1.75%
No. 11	3.35%	5.07%	22.79%	2.09%	1.57%
No. 14	1.70%	5.17%	18.32%	2.09%	2.62%
No. 18	4.00%	7.42%	14.50%	3.44%	2.00%

Table 5-5. Averages of coefficient of variation - variability "within" (a heat for a given bar size)

AVG CV	f_{ye}	ε_{ye}	ε_{sh}	f_{ue}	ε_{su}
No. 4	1.46%	5.50%	12.36%	1.28%	5.72%
No. 5	1.11%	4.69%	12.02%	0.86%	5.37%
No. 6	1.06%	5.02%	10.82%	1.11%	4.49%
No. 7	1.03%	6.87%	8.91%	0.62%	3.95%
No. 8	0.60%	5.25%	7.34%	0.45%	3.71%
No. 9	0.58%	6.28%	8.44%	0.58%	3.82%
No. 10	0.68%	5.15%	6.93%	0.78%	3.81%
No. 11	1.26%	5.57%	8.53%	0.86%	5.57%
No. 14	0.66%	6.44%	9.02%	0.66%	5.87%
No. 18	1.19%	6.23%	11.89%	1.31%	6.43%

5.1.3.5.Summary

The results follow what would be expected in that there is more variability between tests within a heat than tests within a single twenty-foot bar and more variability between tests within a mill than tests within a heat. Past studies of reinforcing steel mechanical

properties have indicated similar results (Allen, 1972). The high variability in the length of the yield plateau likely results from the fact that this parameter is sensitive to a number of factors related to the manufacturing process (grain refinement due to rolling, cooling, etc.) as well as chemical composition (Lim, 1991; Pussegoda, 1978). As such, high variability in this parameter is not unexpected.

Table 5-6. Coefficients of variation of averages - variability "between"

CV	f_{ye}	ε_{ye}	ε_{sh}	f_{ue}	ε_{su}
Mills	0.51%	3.00%	6.93%	1.00%	1.89%
Heats	3.34%	5.44%	20.51%	2.82%	2.25%
20’ Bars	1.77%	5.50%	14.77%	1.75%	3.83%

Table 5-7. Averages of coefficient of variation - variability "within"

AVG CV	f_{ye}	ε_{ye}	ε_{sh}	f_{ue}	ε_{su}
Mills	3.54%	8.66%	25.03%	3.06%	5.55%
Heats	1.72%	7.08%	14.79%	1.74%	5.18%
20’ Bars	0.34%	4.40%	3.56%	0.25%	3.82%

5.1.4. Parameter Interactions

The current industry practice is for producing mills to provide with their steel shipments a certified test report indicating the mechanical and chemical properties of the steel being provided. Three of these properties that are readily available are the yield strength, the tensile strength, and the percent elongation at fracture; however, without the associated strains, these values alone are insufficient to fully characterize the stress-strain profile of the steel they represent. Should it be possible to establish a reliable correlation between the parameters provided by mills and the associated but unknown strain parameters,

for example, percent elongation at fracture and ultimate tensile strain, then such a relationship could later be used to relate project-specific mill cert values to expected stress-strain performance.

This section summarizes the relationships between a few of the parameters of interest obtained from the A706 grade 80 rebar tensile tests. The relationships are presented qualitatively in the form of scatter plots with some accompanying discussion. No correlations were established for any of the comparisons as will be discussed below.

5.1.4.1.f_{ye} vs ε_{sh}

The graph containing all of the A706 grade 80 experimental stress-strain curves presented in Figure 4-20 seems to indicate an increased likelihood for the onset of strain hardening to occur at higher strains as the yield strength of the material decreases. Figure 5-8, however, reveals that this is not the case and that no distinguishable trend exists between the yield strength and the onset of strain hardening. Therefore, mill-specified values of yield strength cannot be used as an indicator of the onset of strain hardening for this type and grade of steel.

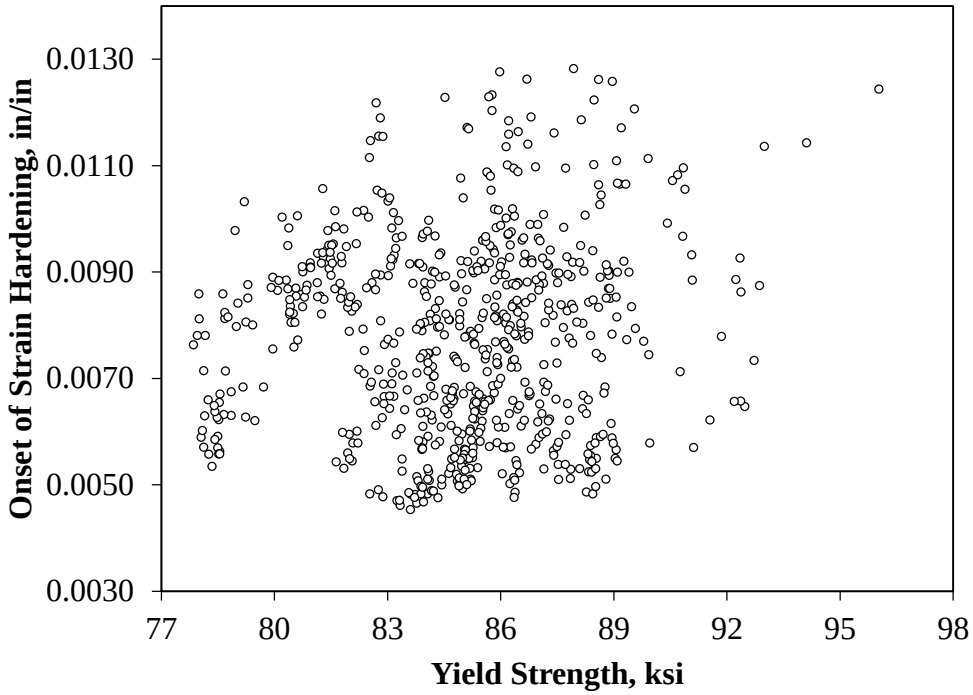

Figure 5-8. Interaction between yield strength and onset of strain hardening strain

5.1.4.2.f_{ye} vs f_{ue}

Figure 5-9 illustrates the interaction between the yield strength and tensile strength. As expected, the two parameters are positively correlated. A linear trend through the data reveals an R squared value of 0.62.

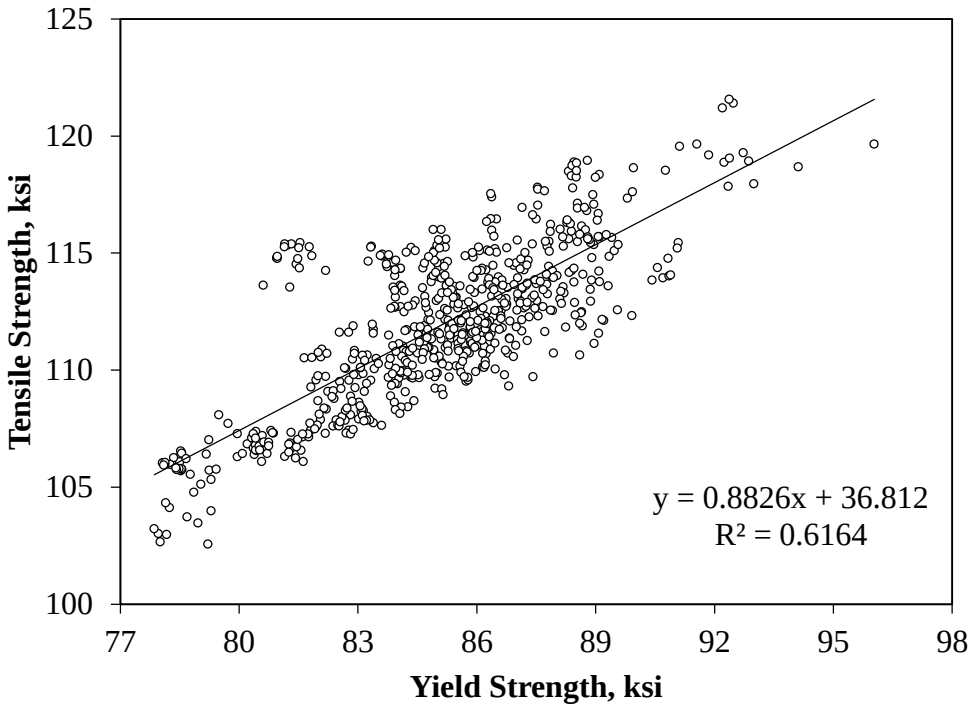

Figure 5-9. Interaction between yield strength and tensile strength

5.1.4.3.f_{ye} vs ε_{su}

Figure 5-10 illustrates the interaction between the yield strength and ultimate tensile strain. No apparent trend existed between these parameters.

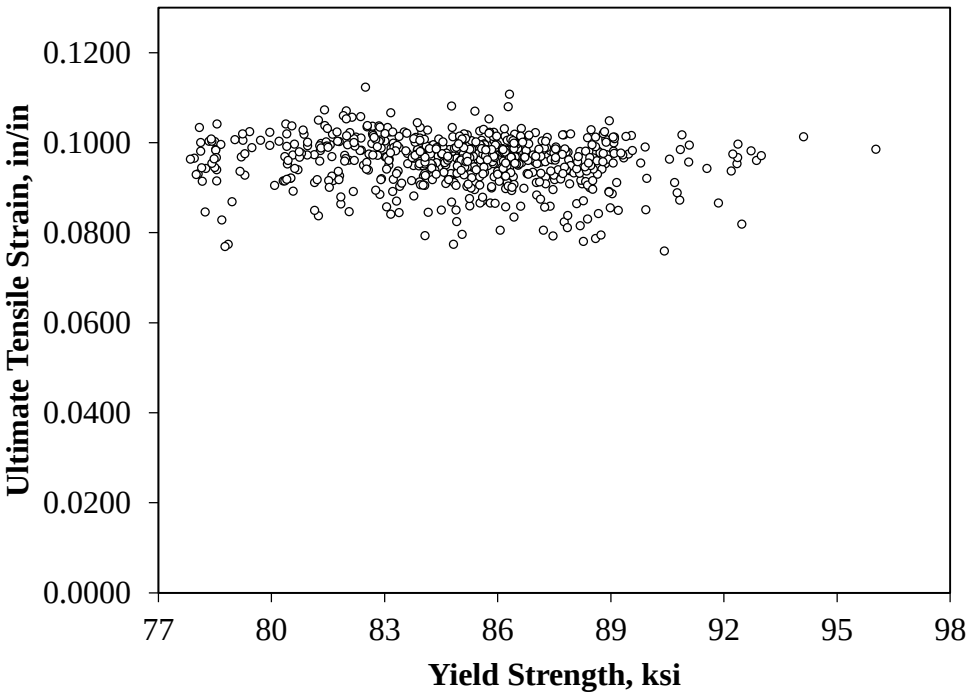

Figure 5-10. Interaction between yield strength and ultimate tensile strain

5.1.4.4.f_{ue} vs ε_{su}

Figure 5-11 illustrates the interaction between the tensile strength and ultimate tensile strain. The figure indicates a slight negative trend.

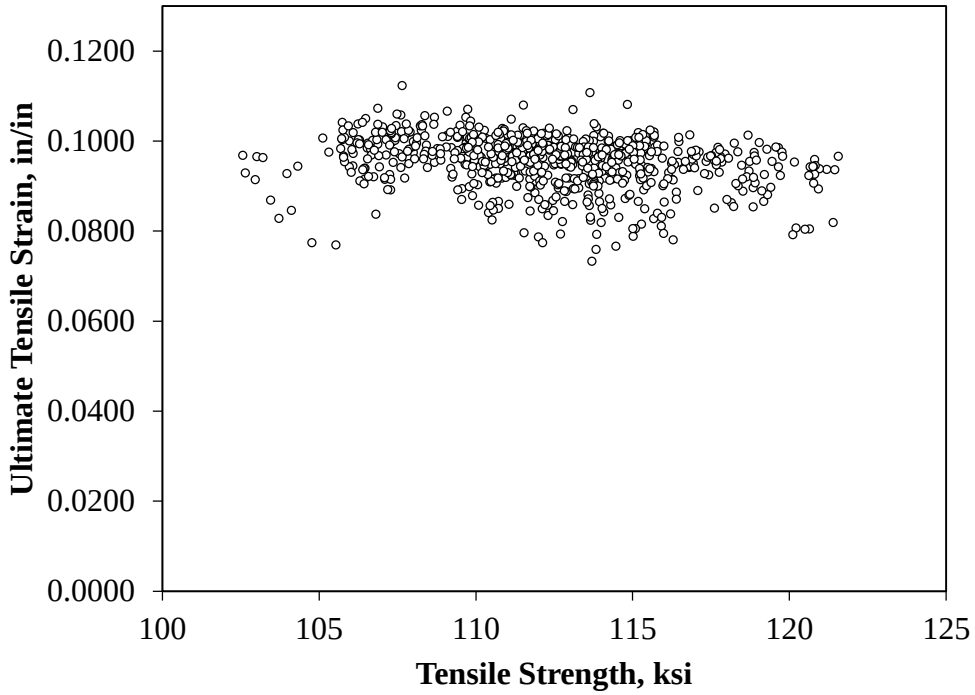

Figure 5-11. Interaction between tensile strength and ultimate tensile strain

5.1.4.5. ε_{sh} *vs* ε_{su}

Figure 5-12 illustrates the interaction between the strain at the onset of strain hardening and ultimate tensile strain. A slight positive trend appears to exist between these parameters.

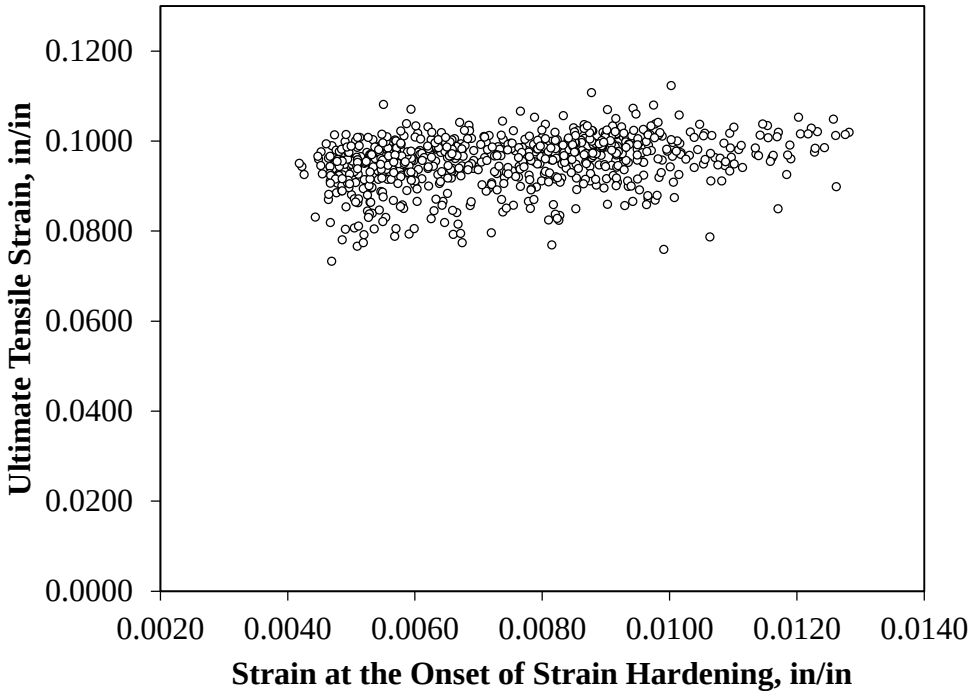

Figure 5-12. Interaction between strain at the onset of strain hardening and ultimate tensile strain

5.1.4.6.percent elongation vs ε_{su}

The percent elongation at fracture and the ultimate tensile strain are both meant to serve as measures of ductility. While the ultimate tensile strain, sometimes referred to as the strain at max stress, is generally required in the calibration of reinforcing steel models, oftentimes the only material-specific parameter related to ductility is the percent elongation at fracture provided by the mill supplying the steel. The ability to confidently define a correlation between these two parameters would be of great value to a designer or analyst attempting to use project-specific material properties to define reinforcing steel models where other data was lacking.

Figure 5-13 presents a comparison between the A706 grade 80 ultimate tensile strain values and Optotrak-based percent elongation at fracture values. The figure indicates a slight correlation between the two parameters; however, no effort to quantify this correlation has been made for reasons discussed next.

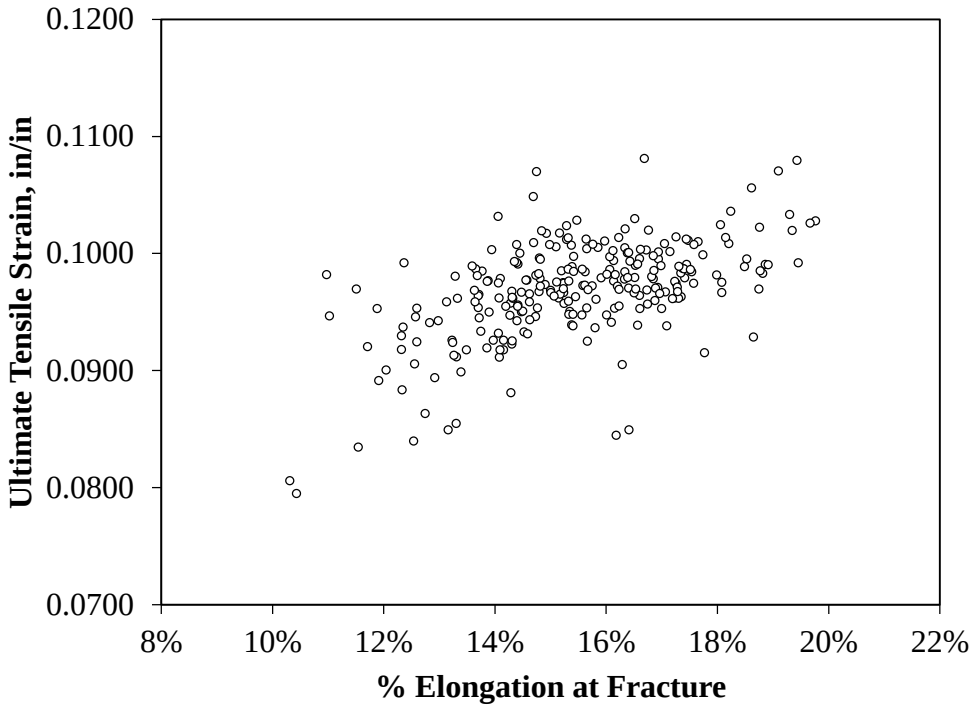

Figure 5-13. Interaction between Optotrak-based percent elongation at fracture and ultimate tensile strain measurements

The percent elongation at fracture values used in Figure 5-13 have been based on Optotrak strain measurements in which the final reading from the markers just before bar fracture is used to calculate the percent elongation at fracture. Recall from Section 3.4.3 that not all of the tests were taken fully to fracture of the bar; therefore, only a portion of the dataset is available to make this comparison. All of the data points in Figure 5-13 represent

fractured bars. A limited number of additional percent elongation at fracture values were obtained using the conventional method of measuring a predefined 8" gage length prior to the test and then re-measuring the same gage length after the test in the event that fracture occurred within the gage length. A comparison of these hand measurements to the Optotrak-based values reveals that, on average, there is a 14 percent-difference in the percent elongation measurements. To clarify, this translates into Optotrak-based percent elongation at fracture values that are, on average, 1.8 percentage points higher than their corresponding hand measured values. An attempt to explain this observation is provided in the next paragraph.

Prior to the onset of necking, a tensile test specimen is in a state of combined plastic and elastic strain. As necking commences (a concentration of plastic deformation) the non-necked regions of the bar can be observed to relax, essentially recovering some of the existing elastic strains. Upon fracture of the test specimen, any remaining elastic strains are recovered and the combined length of the two fractured ends represents the total plastic elongation. The traditional hand measurement approach to determining percent elongation at fracture by fitting the fractured ends together and re-measuring the elongated gage length necessarily captures the plastic strain in the bar. The Optotrak-based method of determining the percent elongation at fracture by taking the last recording of strain before fracture necessarily captures the plastic strain in addition to any remaining elastic strains. For this reason, it can be expected that the Optotrak-based approach would predict a higher percent elongation at fracture value than the traditional approach, hence the hesitancy to define a

quantitative relationship between the percent elongation at fracture values provided in the mill certificates and those obtained using the Optotrak system.

5.1.5. Yield Strengths Falling Below 80 ksi

As stated in Section 4.2.3.2, a number of the No. 11, 14, and 18 bars had yield strengths falling below the ASTM lower limit of 80 ksi after accounting for pressure losses occurring in the large bar testing rig. The additional tests of nine No. 11 bars and nine No. 14 bars described in Section 3.4.4 confirmed that this was an accurate assessment and not a by-product of the adjustment factor. While no definitive explanation is offered as to why this behavior revealed itself exclusively in the No. 11, 14, and 18 bar tests, the remainder of this section describes the extent of the phenomenon.

The number of No. 11 bar tests having yield strength below 80 ksi was limited to a single heat from Mill 1 (heat 5). In this specific case, there were no other bar sizes represented in this heat (see Appendix A); therefore, no comparison can be made to determine if the behavior was related to the bar size or the entire heat. Following the adjustment, all nine of the test specimens from this heat had yield strengths below 80 ksi with 78.1 ksi being the minimum and 78.6 ksi the maximum.

Similar to the No. 11 bars, the number of No. 14 bar tests having yield strength below 80 ksi was also limited to a single heat, this time from Mill 3 (heat 7). However, unlike the previous case, there were additional bar sizes represented in this heat. The average yield strength of Mill 3 Heat 7, which was comprised of No. 10-No. 18 bars (Appendix A), was 80.35 ksi. Table 5-8 summarizes the averages by bar size. From the table, it is clear that

between the No. 10 and No. 14 bars there is a decrease in average yield strength with increase in bar size. This pattern did not hold for the No. 18 bars. The minimum No. 14 bar yield strength was 78.1 ksi and the maximum was 78.7 ksi.

Table 5-8. Mill 3 Heat 7 mean yield strengths by bar size

Mill 3 Heat 7	No. 10	No. 11	No. 14	No. 18
Averages	83.8	80.5	78.5	79.0

Four heats of No. 18 bars contained tests having yield strength below 80 ksi. These included two heats from Mill 3 (heats 6 and 7) and two heats from Mill 2 (heats 1 and 7). While at least one specimen was tested from each of the three Mill 1 heats containing No. 18 bars, it is uncertain whether additional testing would have resulted in any specimens yielding below 80 ksi. Recall that only a subset of the Mill 1 No. 18 bars could be tested because of the "bamboo-style" transverse ribs on the bars which caused the wedge grips to crack and fracture within one to three tests. All No. 18 specimens tested from Mill 2 Heat 1 and Mill 3 Heat 7 had yield strengths below 80 ksi. Each of these heats contained additional bar sizes (Appendix A). Mill 2 Heat 7 had seven out of nine specimens falling below the yield limit, and Mill 3 Heat 6 had three out of nine specimens falling below the yield limit. Mill 2 Heat 7 did not contain any additional bar sizes. Mill 3 Heat 6 did contain additional bar sizes.

5.1.6. Variability in Strain Over Bar Length

As demonstrated in Section 3.3.2, one of the unique traits of the Optotrak is the ability to track multiple markers simultaneously. Because this permits multiple gage lengths to be established on a single specimen, it is possible to assess the distribution of strain over

the entire instrumented region of the specimen at each reading of the data. This poses an advantage over traditional methods of capturing bar strains such as with strain gages and extensometers which, while reliable, are limited to a single gage length.

An unanticipated consequence of using this type of instrumentation was the realization that the strains varied over the length of the test specimens at a given instant in time and that the variability between gage lengths seemingly increased with increasing strain. It is perhaps not surprising that the strains should vary over the length of the bar as it is neither a homogeneous material or of a continuous cross-section (as a result of the longitudinal and transverse ribs). Additionally, some degree of variability in the different gage lengths can be attributed to the precision of the instrumentation. Table 5-9 summarizes the average variation between the six 2" gage lengths for the yield strain, onset of strain hardening, and ultimate tensile strain considering all tests which is calculated by finding the coefficient of variation between the six gage lengths for each test and then averaging all of the coefficients of variation.

Table 5-9 and Figure 5-14 both indicate that the highest variability in the strains was at the yield point while the lowest was shortly thereafter at the onset of strain hardening. This trend for the variability to be high towards the beginning of the tests, lowest near the middle, and high again near the end may be the result of low variability in the strains while they are small and the precision of the Optotrak is lower coupled with an increased variability in the strains when they are large and the precision of the Optotrak is higher. This would imply that the higher variability at the yield point is more a result of instrumentation than actual variation in the strains. In any case, the point to be emphasized is not so much that the strains

are not uniform over the length of the test specimen at a given instant in time, but that the strains will typically be measured at only one location on the bar at a given instant in time. Such knowledge may be useful in directing future tensile testing efforts.

Table 5-9. Average variabilities in the six strain values recorded for each parameter from each test

Parameter	Average coefficient of variation
ε_{ye}	9.57%
ε_{sh}	6.74%
ε_{su}	9.10%

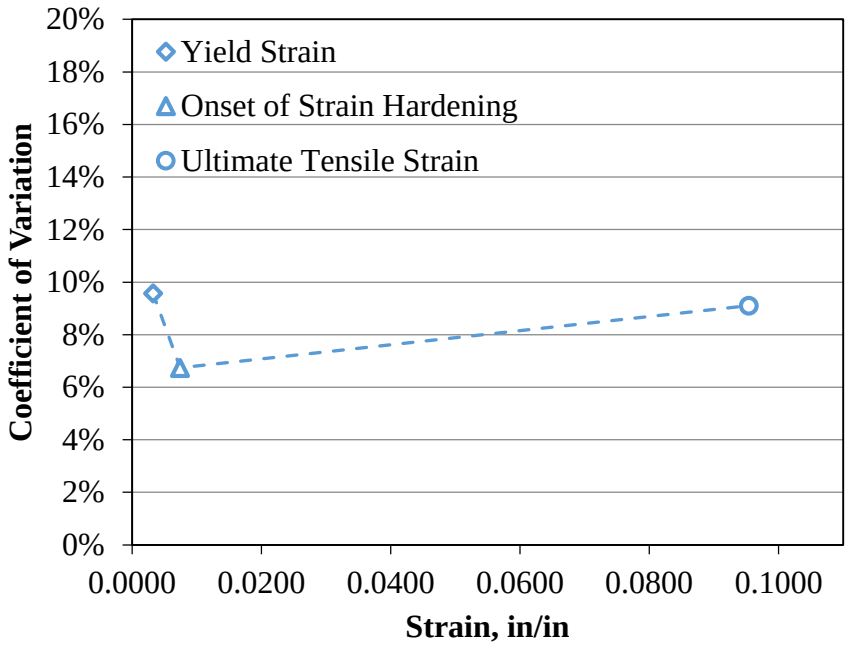

Figure 5-14. Change in variation between gage lengths with increasing strain

5.1.7. Future Tensile Testing

A similar analysis as that presented in Section 5.1.3 can be used to determine the extent to which reducing the breadth of testing performed in this project would have influenced the final recommended values for the key parameters presented in the next chapter. Should it be the case that sampling only 1 specimen per bar or just 1 specimen per heat resulted in nearly identical mean values for each stress-strain parameter and with similar variability, then future tensile testing programs could be designed around this knowledge to acquire comparably reliable results from fewer total tests.

5.1.7.1.Effect of Testing 1 Specimen per Bar

Testing only 1 specimen per twenty-foot bar would have decreased the total possible number of tests from 810 to 270. Table 6-2 summarizes the impact of such a testing program on the final recommended values. In order to generate the results presented in Table 5-10, a separate dataset containing only the first test specimen from each of the three twenty-foot bars sampled for every heat, bar size, and mill (ID: "x x x x 1") was compiled and analyzed the same as the full dataset.

It is clearly evident from Table 5-10 that there was little difference in the final outcome between the two approaches. In particular, the yield and tensile strengths differed by less than 0.1 percent between the two datasets. While the strains tended to differ by a larger amount, this was still limited to a percent difference of less than 0.2 percent. The 95th percentile tensile strengths differed by less than 0.01 percent. The 5th percentile ultimate tensile strains differed by the largest margin of about 0.5 percent with the reduced dataset

predicting a lower value. From these results, it is clear that reducing the dataset by a factor of 3 had little impact on the final mean values that would have gone into the final recommendations.

Table 5-10. Impact on recommendations considering only 1 specimen per 20' bar

	All Tests	**1/Bar**	**% Diff.**
E_s	27888	27871	0.06%
f_{ye}	85.0	84.9	0.07%
ε_{ye}	0.0033	0.0033	0.19%
ε_{sh}	0.0074	0.0074	0.14%
f_{ue}	112.5	112.4	0.01%
ε_{su}	0.0954	0.0956	0.14%
$f_{ue\ (95\%)}$	118.9	118.9	0.00%
$\varepsilon_{su\ (5\%)}$	0.0845	0.0840	0.54%

5.1.7.2.Effect of Testing 1 Specimen per Bar per Heat

Testing only 1 specimen per heat would have decreased the total possible number of tests from 810 to 90. Table 5-11 summarizes the impact of such a testing program on the final recommended values. In order to generate the results presented in Table 5-11, a separate dataset containing only the first test specimen from the first of the three twenty-foot bars sampled for every heat, bar size, and mill (ID: “x x x 1 1”) was compiled and analyzed the same as the full dataset.

As with the case of testing 1 specimen per twenty-foot bar, there was little difference in the final outcome between the two approaches; however, the percent differences did increase as the size of the dataset was reduced. The yield and tensile strengths differed the least between the two datasets – again, less than 0.1 percent each. Excluding the yield strain

parameter, the expected onset of strain hardening strains and the ultimate tensile strains differed between the two datasets by less than 1 percent. The 95th percentile tensile strengths differed by less than 0.1 percent. The 5th percentile ultimate tensile strains differed by less than 0.01 percent with the reduced dataset now predicting a slightly higher value. Reducing the dataset by a factor of 9 had some impact on the final mean values that would have gone into the final recommendations; however, the largest percent difference between any two parameters was still below 1.5 percent. It should be noted that these percentages are extremely small and, for several of the parameters, no observable difference between the two datasets is even distinguishable at the provided number of decimal places.

Table 5-11. Impact on recommendations considering only 1 specimen per 20' bar and 1 20' bar per heat

	All Tests	**1/Bar/Heat**	**% Diff.**
E_s	27888	27970	0.29%
f_{ye}	85.0	84.9	0.03%
ε_{ye}	0.0033	0.0033	1.26%
ε_{sh}	0.0074	0.0074	0.49%
f_{ue}	112.5	112.5	0.06%
ε_{su}	0.0954	0.0961	0.67%
$f_{ue\ (95\%)}$	118.9	119.0	0.09%
$\varepsilon_{su\ (5\%)}$	0.0845	0.0845	0.01%

5.2. Strain Age Tests

5.2.1. Comparison with Literature Results

Based on the strain age test results presented in Chapter 4, it was concluded that A706 grade 80 rebar did not display identifiable susceptibility to the strain aging phenomenon. This

claim is substantiated based on the following three observations: (1) the anticipated trends of an increase in yield and tensile strength and/or a decrease in the ultimate tensile strain with increasing pre-strain and aging period failed to appear in the results plotted in Section 4.3, (2) the magnitude of the deviations of the strain age test results from the benchmark tests was negligibly small as compared to the magnitudes presented in the literature (compare Tables 2.6-2.8 with Figures 4.32-4.33), and (3) the difference between the strain age tests and the benchmark values rarely exceeded the standard deviation of the tensile test represented by the benchmark value, thus making the effects of strain aging nearly indistinguishable from variation already present in the tensile test data.

A limitation of the current investigation into the strain aging susceptibility of A706 grade 80 rebar was the inability to define a vanadium to nitrogen (V/N) ratio for the steel as the percentage of nitrogen is not provided with the mill test certificates. The literature review demonstrated that microalloying elements such as vanadium, which provides increased strength to the rebar while still maintaining high ductility, have been shown to inhibit strain aging in reinforcing steels through bonding with nitrogen, which is a known contributor to strain aging. Therefore, despite chemical composition playing a major role in the strain aging susceptibility of reinforcing steel, it could not be properly evaluated within the current research effort.

5.2.2. Future Strain Age Testing

Based on the literature review observations and the points addressed in the previous section, two areas of future research into the strain aging susceptibility of A706 grade 80

rebar stand out: (1) perform chemical analysis to identify the nitrogen percentage such that a V/N ratio may be determined and compared with additional tests and (2) investigation of strain aging embrittlement in bent reinforcing bars used as hooks or transverse reinforcement. The latter of these items is particularly relevant to earthquake structural engineering as the current design philosophy relies on the structures ability to dissipate energy through the ductile behavior of inelastic mechanism strategically located to prevent sudden, brittle failures. Anchorage and confinement failures resulting from strain aging and early fracture of bent bars should therefore be avoided.

5.3. Cyclic Tests

5.3.1. Future Cyclic Testing

The two main objectives of the cyclic testing program were the evaluation of existing reinforcing steel models to be able to characterize the A706 grade 80 cyclic stress-strain curve and the impact of bar strain history on the ultimate tensile strain. As illustrated in the previous chapter, the extent of the cyclic testing program was greatly limited by the type and condition of the testing equipment used. Nonetheless, it was demonstrated that an existing reinforcing steel model was able to characterize the shape of the stress-strain curve for a randomly cycled A706 grade 80 rebar specimen. Further research in this area could be largely analytical and involve the evaluation of additional stress-strain models to the cyclic data already collected and presented in Chapter 4.

Based on the stated limitations, the impact of load history on the ultimate tensile strain of the rebar deserves some further investigation. The results in Table 4-6 indicate that

the imposed load histories did not cause a reduction in the strain at max stress values for the No. 5 bars. In fact, it appears that the cyclic tests showed higher ultimate tensile strains than the tensile test mill-heat-size average. Two possible explanations for this observation are that (1) the benchmark value was based on nine tests originating from three 20’ bars while the cyclic tests originated from a fourth 20’ bar from the same heat or (2) the fact that the benchmark value is based on Optotrak strain readings while the cyclic test strains were obtained with an extensometer as stated in Section 3.3.2. Thus, the difference could be a result of difference in instrumentation.

The more strenuous load history of the No. 7 bar in Table 4-6, however, which included multiple cycles in with the bar visibly buckled, does indicate a reduction in the ultimate tensile strain during the pull test. As this only represents one data point, future research could reconsider this issue and address a larger number of bars sizes and load histories to either confirm or reject this trend.

6. CONCLUSIONS

6.1. Summary

An assessment of the stress-strain behavior of ASTM A706 grade 80 reinforcement was conducted at NC State University through experimental testing and analysis. A total of 788 tensile tests of No. 4 through No. 18 bars, in the as-rolled condition, originating from three different producing mills and including multiple heats of steel from each mill provided a substantial dataset of test results that was otherwise lacking in the literature. These results were used to identify the expected values of key parameters necessary to define the monotonic stress-strain curve of A706 grade 80 rebar: the yield strength, yield strain, strain at onset of strain hardening, tensile strength, and ultimate tensile strain. Two subsets of tests focused on the cyclic and strain aging performance of the steel. Based on the work just described, the following conclusions are presented:

- The current work increased the body of publically available A706 grade 80 stress-strain data by over 650%. The recommendations for yield stress, yield strain, strain at the onset of strain hardening, ultimate tensile strain, and tensile strength provided in Table 6-1 may be used as the basis for future building code requirements.
- Best-fit probability distributions were presented for both of the strength parameters as well as the strain parameters based on the Kolmogorov-Smirnov goodness-of-fit test.
- The yield strength values were shown to be well represented by the beta distribution, while the yield strain values were shown to be well represented by the gamma distribution. The strain at the onset of strain hardening values showed the highest

degree of variability and were not found to be well represented by any of the considered distributions. The tensile strength values were shown to be well represented by the lognormal distribution, and lastly, the ultimate tensile strain values were shown to be well represented by the Weibull distribution.

- The A706 grade 80 stress-strain curve is nearly identical in shape to the A706 grade 60 curve.
- The cyclic stress-strain curve was accurately predicted using a currently available cyclic reinforcing steel material model.
- The shape of the strain hardening curve may be accurately characterized using currently available monotonic rebar models.
- About 7% of the tests failed to meet the ASTM minimum yield strength requirement of 80 ksi. This behavior was limited to the No. 11, 14, and 18 bars.
- The No. 11, 14, and 18 bars, overall, had lower yield and tensile strength than the No. 4 through No. 10 bars. However, no trends were evident for any other parameters as a function of bar size.
- A706 grade 80 rebar did not show susceptibility to strain aging for any of the considered pre-strain levels, even up to an aging period of 6 months, however, further studies on larger bar sizes may be worthwhile.
- A706 grade 80 rebar may be reliably specified for capacity protected members and, as a result, may reduce congestion in joints and provide a potential savings in terms of reduced material and labor costs.

- Future research will focus on behavior of plastic hinge regions reinforced with A706 grade 80 rebar as spread of plasticity and limit state strains may be influenced by the different material response.

6.2. Recommendations

Table 6-1 summarizes the A706 grade 80 monotonic stress-strain recommendations. Included in the table are both the specified and the expected material properties. Specified values are taken from the ASTM A706/A706M specification (ASTM A706/A706M, 2016). Expected values are based on the experimental results presented in Section 4.2.3. Also included are the 95th percentile tensile strength and the 5th percentile ultimate tensile strain as these may offer the most benefit to designers.

Table 6-1. Recommendations for A706 grade 80 monotonic stress-strain parameters

Parameter	**Notation**	**Value**	**Units**
Modulus of elasticity	E_s	29000	ksi
Specified minimum yield strength	f_y	80	ksi
Expected yield strength	$f_{ye\ (mean)}$	85	ksi
Nominal yield strain	ε_y	0.0028	
Expected yield strain	$\varepsilon_{ye\ (mean)}$	0.0033	
Specified minimum tensile strength	f_u	100	ksi
Expected tensile strength	$f_{ue\ (mean)}$	112	ksi
95^{th} percentile tensile strength	$f_{ue\ (95\%)}$	119	ksi
Ultimate tensile strain	$\varepsilon_{su\ (mean)}$	0.0954	
5^{th} percentile ultimate tensile strain	$\varepsilon_{su\ (5\%)}$	0.0845	
Onset of strain hardening	$\varepsilon_{sh\ (mean)}$	0.0074	

7. REFERENCES

AASHTO. 2011. Guide Specification for LRFD Seismic Bridge Design, Second Edition with 2012 Interim Revisions. American Association of State Highway and Transportation Officials, Washington, DC.

AASHTO. 2014. AASHTO LRFD Bridge Design Specifications, Customary U.S. Units, Seventh Edition with 2016 Interim Revisions. American Association of State Highway and Transportation Officials, Washington, DC.

ACI Committee 318, "Building Code Requirements for Structural Concrete (ACI318-11) and Commentary," American Concrete Institute, Farmington Hills, MI, 2011, 503 pp.

ACI Committee 318, "Building Code Requirements for Structural Concrete (ACI 318-14) and Commentary," American Concrete Institute, Farmington Hills, MI, 2014.

Allen, D. E. 1972. "Statistical Study of the Mechanical Properties of Reinforcing Bars," Building Research Note No. 85, Division of Building Research, National Research Council, Ottawa, Canada, April, 8 pp.

ASTM A370 (2015), "Standard Test Methods and Definitions for Mechanical Testing of Steel Products," American Society for Testing and Materials, West Conshohocken, PA, 50 pp.

ASTM A615/A615M-16, "Standard Specification for Deformed and Plain Carbon-Steel Bars for Concrete Reinforcement," ASTM International, West Conshohocken, PA, 2016, 8 pp.

ASTM A706/A706M-16, “Standard Specification for Deformed and Plain Low-Alloy Steel Bars for Concrete Reinforcement,” ASTM International, West Conshohocken, PA, 2016, 7 pp.

Barbosa, A.R., T. Link, and D. Trejo. 2015. "Seismic Performance of High-Strength Steel RC Bridge Columns." J. Bridge Eng., 10.1061/(ASCE)BE.1943-5592.0000769 , 04015044.

Bournonville, M., J. Dahnke, and D. Darwin. 2004. “Statistical Analysis of the Mechanical Properties and Weight of Reinforcing Bars.” Research Report SL 04-1. University of Kansas.

CALTRANS. 2013. CALTRANS Seismic Design Criteria. Version 1.7. California Department of Transportation.

Chang, G.A. and J.B., Mander. 1994. “Seismic energy based fatigue damage analysis of bridge columns: Part 1 – Evaluation of seismic capacity.” Tech. Rep. Multidisciplinary Center for Earthquake Engineering Research, University at Buffalo, State University of New York.

Coffin, L.F., Jr. 1955. “Design Aspects of High Temperature Fatigue with Particular Reference to Thermal Stresses, ASME Transactions, V. 78, pp. 527-532.

Cottrell, A.H., and B.A. Bilby. 1949. “Dislocation theory of yielding and strain ageing of iron.” Proc., Physical Soc., Section A, 62(1), pp. 49-62.

Dhakal, R. and K. Maekawa. 2002. “Modeling of post-yield buckling of reinforcement.” Tech. Rep. University of Canterbury, Civil and Natural Resources Engineering.

Filippou, F.C., V.V. Bertero, and E.P. Popov. 1983. “Effects of Bond Deterioration on Hysteretic Behavior of Reinforced Concrete Joints.” Report No. UCB/EERC-83/19, Univ. of California, Berkeley, Calif.

Giuffre, A. and P. Pinto. 1970. “Il Comportamento del Cemento Armato per Sollecitazioni Cicliche di Forte Intensita.” Giornale del Genio Civile, pp. 391-408.

Goldberg, J. and R. Richard. 1963. “Analysis of Nonlinear Structures.” Journal of the Structural Division, Proceedings of the American Society of Civil Engineers, pp. 333-351.

Gomes, A. and J. Appleton. 1997. “Nonlinear cyclic stress strain relation of reinforcing bars including buckling.” Eng. Struct. V. 19, No. 10, pp. 822-826.

Gustafson, D.P. 2010. “Raising the Grade.” Concrete International V. 32, No. 4, April 2010, pp. 59-62.

Kent, D.C. and R. Park. 1973. “Cyclic load behavior of reinforcing steel.” Strain V. 9, No. 3, pp. 98-103.

King, D.J, M. Priestley, and R. Park. 1986. “Computer Programs for Concrete Column Design.” Research Report 86/12, Department of Civil Engineering University of Canterbury, New Zealand.

Lim, W. T., “Statistical Analysis of Reinforcing Steel Properties,” Master’s Thesis, University of Canterbury, Christchurch, New Zealand, June 1991, 151 pp.

Ma, S.M., V.V., Bertero, and E.P, Popov. 1976. “Experimental and Analytical Studies on the Hysteretic Behavior of Reinforced Concrete Rectangular and T-beams.” Technical Report Earthquake Engineering Research Center, University of California

Mander, J.B. 1983. “Seismic Design of Bridge Piers.” PhD thesis. University of Canterbury.

Mazzoni, S., F. McKenna, M.H. Scott, and G.L. Fenves. 2007. OpenSees command language manual. Pacific Earthquake Engineering Research (PEER) Center.

Mendez, L. and L. Castro. 2014. “A simplified reinforcing steel model suitable for cyclic loading including ultra-low-cycle fatigue effects.” Engineering Structures V. 68, pp. 155-164.

Menegotto, M. and P. Pinto. 1973. “Method of Analysis for Cyclically Loaded Reinforced Concrete Plane Frames Including Changes in Geometry and Non-elastic Behavior of Elements Under Combined Normal Force and Bending.” IABSE Symposium of Resistance and Ultimate Deformability of Structures Acted on by Well-Defined Repeated Loads, International Association of Bridge and Structural Engineering, Lisbon, Portugal, V. 13, pp. 15-21

Milbourn, D. and L. Yu. 2010. “Metallurgical Benefits of Vanadium Microalloying in Producing High Strength Seismic Grade Rebar.” Proceedings of International Seminar on Production and Application of High Strength Seismic Grade Rebar Containing Vanadium, Beijing, China, pp. 32-43.

Mirza, S.A. and J. MacGregor. 1979. “Variability of Mechanical Properties of Reinforcing Bars.” Journal of the Structural Division, ASCE, V. 105, pp. 921-937.

Momtahan, A., R.P. Dhakal, and A. Reider. 2009. “Effects of Strain-Ageing on New Zealand Reinforcing Steel Bars.” Bulletin of the New Zealand Society for Earthquake Engineering V. 42, No. 2, September 2009, pp. 179-186.

Monti, G. and C. Nuti. 1992. “Nonlinear cyclic behavior of reinforcing bars including buckling.” J. Struct. Eng. V. 118, No. 12, pp. 3268-3284.

NDI. 2011. Optotrak Certus User Guide. Rev. 5. May 2011. Northern Digital Inc.

NEES. 2009. NEES Project Warehouse. http://nees.org/warehouse/project/904. (last accessed Aug. 21, 2015)

NIST. 2014. “Use of High-Strength Reinforcement in Earthquake-Resistant Concrete Structures.” NIST GCR 14-917-30 Report, prepared by the NEHRP Consultants Joint Venture, a partnership of the Applied Technology Council and the Consortium of Universities for Research in Earthquake Engineering, for the National Institute of Standards and Technology, Gaithersburg, Maryland.

Nowak, A.S. and M. Szerszen. 2003. “Calibration of Design Code for Buildings (ACI318): Part 1-Statistical Models for Resistance.” ACI Structural Journal, V. 100, pp. 377-382.

ODOT. 2015. Bridge Design and Drafting Manual. 2015, rev. April 2015. Oregon Department of Transportation.

Panthaki, F.D. 1991. “Low cycle fatigue behavior of high strength and ordinary reinforcing steels.” MS thesis, Dept. of Civil Eng., State Univ. of New York at Buffalo, N.Y.

Paulay, T. and M.J.N. Priestley. 1992. “Seismic Design of Reinforced Concrete and Masonry Buildings” Wiley, New York, 744 pp.

Pussegoda, L.N. 1978. "Strain Age Embrittlement in Reinforcing Steels." Ph.D. Thesis, Dept. of Mechanical Eng., University of Canterbury, New Zealand.

Ramberg, W. and W. Osgood.1943. “Description of Stress-Strain Curves by Three Parameters.” NACA Rep. TN-902, National Advisory Committee on Aeronautics, Washington, D.C. 27 pp.

Rautenberg, J. M. 2011. “Drift Capacity of Concrete Columns Reinforced with High-Strength Steel.” PhD dissertation, Purdue University, West Lafayette, IN, May 2011, 263 pp.

Rautenberg, J.M., S. Pujol, H. Tavallali, and A. Lepage. 2013. “Drift Capacity of Concrete Columns Reinforced with High-Strength Steel.” ACI Structural Journal V. 110, No. 2, March-April 2013, pp. 307-317.

Raynor, D. J., D. Lehman, and J. Stanton. 2002. “Bond Slip Response of Reinforced Bars Grouted in Ducts.” ACI Structural Journal V. 99, No. 5, 2002.

Restrepo-Posada, J.I., L.L. Dodd, R. Park, and N. Cooke. 1994. “Variables Affecting Cyclic Behavior of Reinforcing Steel.” J. Struct. Eng. V. 120, No. 11, pp. 3178-3196.

Russwurm, D. and P. Wille. 1995. “High Strength, Weldable Reinforcing Bars.” Microalloying 95: Proceedings of the International Conference, Pittsburgh, USA, pp. 377-393.

Shahrooz, B.M., R.A. Miller, K.A. Harries, and H.G. Russell. 2011. “Design of Concrete Structures Using High-Strength Reinforcement.” NCHRP Report 679. Transportation Research Board, National Research Council, Washington, DC.

Stanton, J.F and H.D. McNiven. 1979. “The development of a mathematical model to predict the flexural response of R.C. beams to cyclic loads, using system identification.” Report No. UCB/EERC-79/02, Univ. of California, Berkeley, Calif.

Trejo, D., A.R. Barbosa, and T. Link. 2014. “Seismic Performance of Circular Reinforced Concrete Bridge Columns Constructed with Grade 80 Reinforcement.” Research Project SRS 500-610, March 2014.

Wiss, Janney, Elstner and Associates, Inc. (WJE). 2013. “Determination of Yield Strength for Nonprestressed Steel Reinforcement.” WJE Project No. 2013.4171, Dec. 31.

WSDOT. 2015. Bridge Design Manual LRFD. M 23-50.15. Washington Department of Transportation.

APPENDICES

8. APPENDIX A: SUMMARY OF BAR SIZES BY HEAT AND MILL

8.1. Mill 1

Heat 1	Heat 2	Heat 3	Heat 4	Heat 5	Heat 6	Heat 7	Heat 8	Heat 9
No. 4	No. 4	No. 4	No. 18	No. 11	No. 11	No. 11	No. 18	No. 18
No. 5	No. 5	No. 5						
No. 6	No. 6	No. 6						
No. 7	No. 7	No. 7						
No. 8	No. 8	No. 8						
No. 9	No. 9	No. 9						
No. 10	No. 10	No. 10						
No. 14	No. 14	No. 14						

8.2. Mill 2

Heat 1	Heat 2	Heat 3	Heat 4	Heat 5	Heat 6	Heat 7
No. 4	No. 6	No. 5	No. 4	No. 7	No. 4	No. 18
No. 5	No. 7	No. 6	No. 8	No. 9	No. 5	
No. 6	No. 9	No. 8	No. 9	No. 10	No. 7	
No. 8	No. 10				No. 10	
No. 11	No. 11				No. 11	
No. 14	No. 14				No. 14	
No. 18	No. 18					

8.3. Mill 3

Heat 1	Heat 2	Heat 3	Heat 4	Heat 5	Heat 6	Heat 7	Heat 8	Heat 9
No. 5	No. 5	No. 4	No. 4	No. 4	No. 10	No. 10	No. 10	No. 5
No. 6	No. 6	No. 8	No. 8	No. 8	No. 11	No. 11	No. 11	No. 6
No. 7	No. 7	No. 9	No. 9	No. 9	No. 14	No. 14	No. 14	No. 7
					No. 18	No. 18	No. 18	

9. APPENDIX B: DETERMINATION OF STRESS-STRAIN PARAMETERS

9.1. Modulus of Elasticity

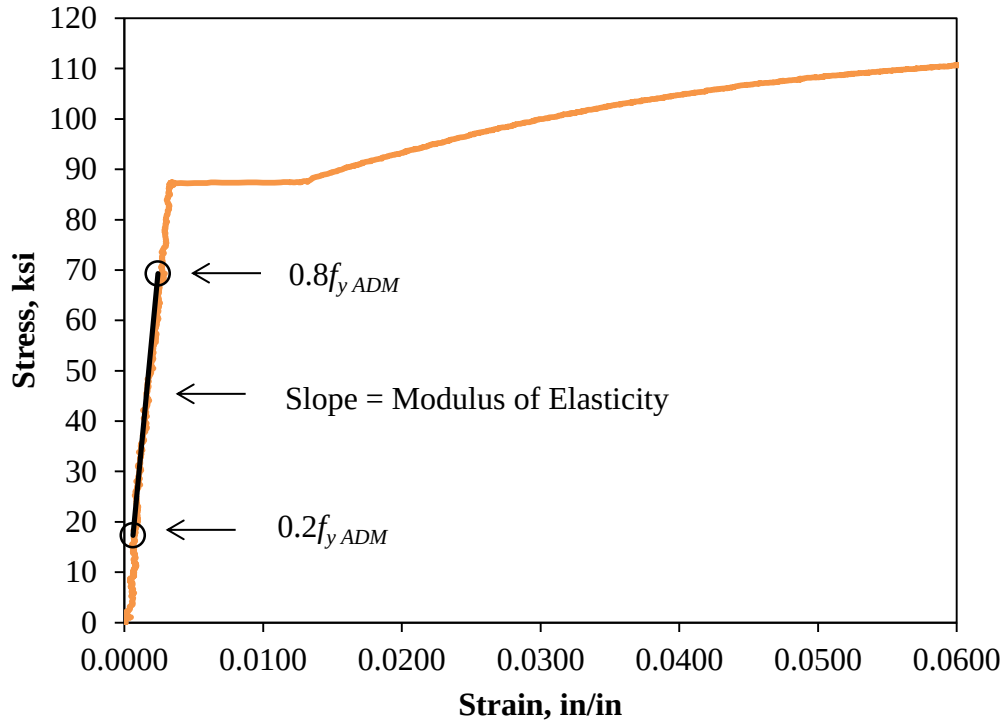

9.2. Yield Strength

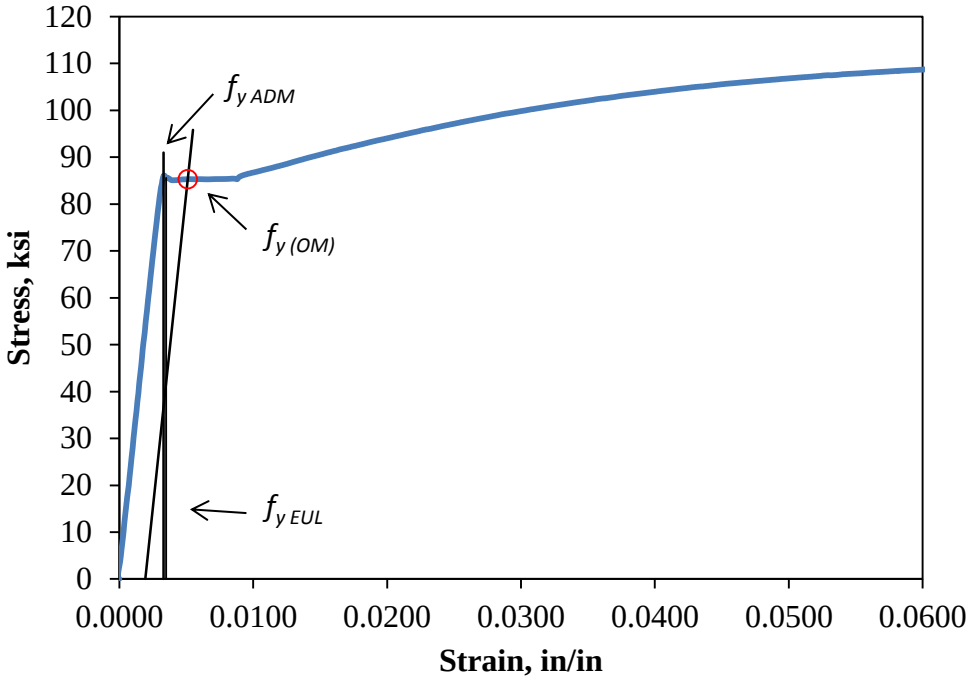

9.3. Onset of Strain Hardening

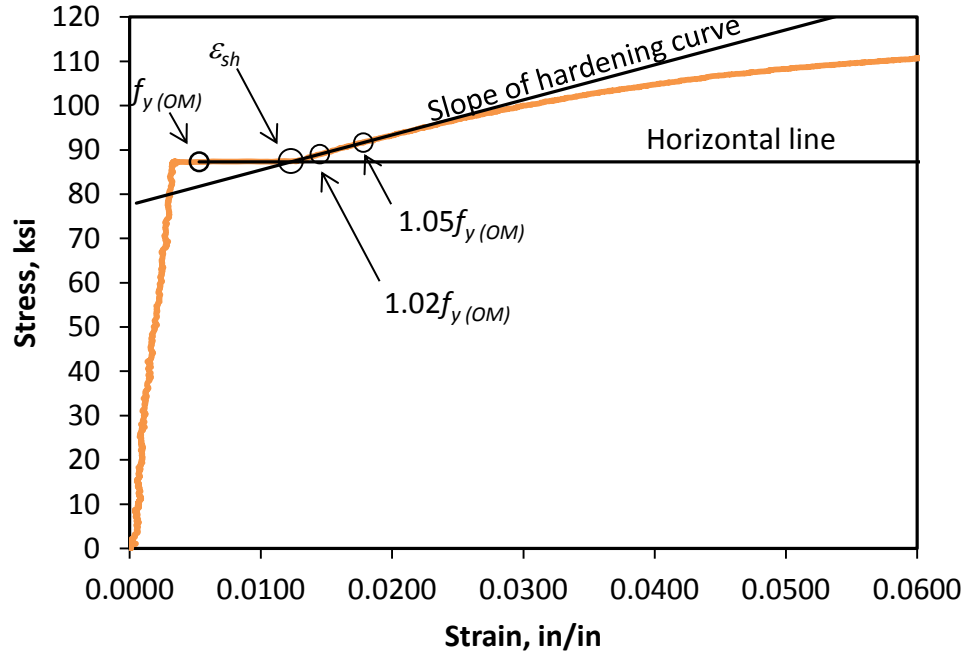

10. APPENDIX C: MILL CUMULATIVE DISTRIBUTION FUNCTIONS

10.1. ADM Yield Strength

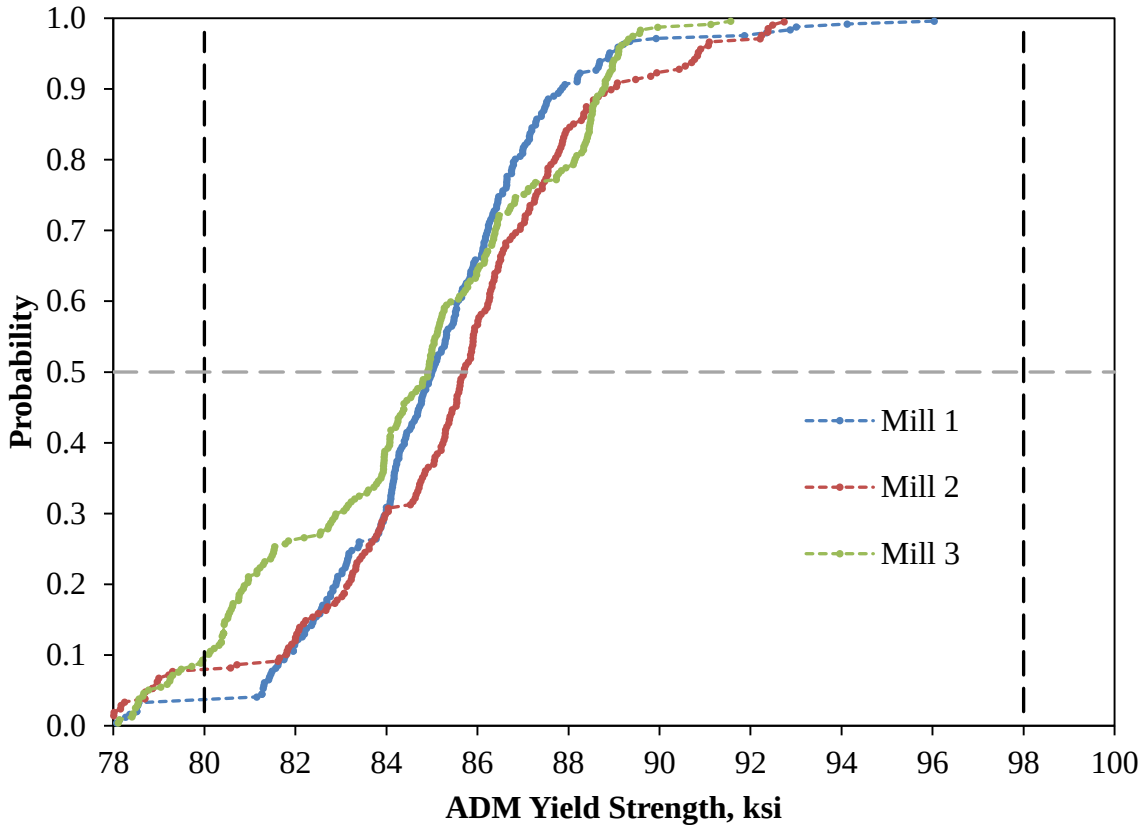

10.2. Yield Strain

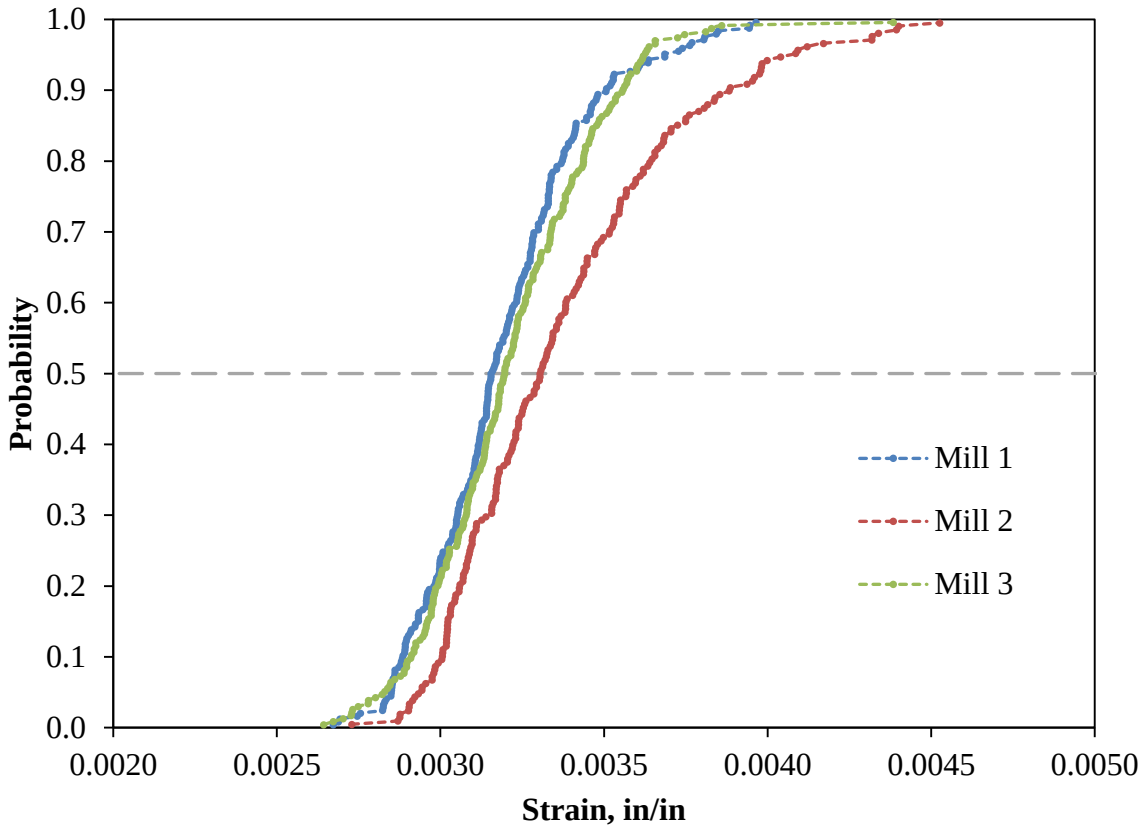

10.3. Onset of Strain Hardening

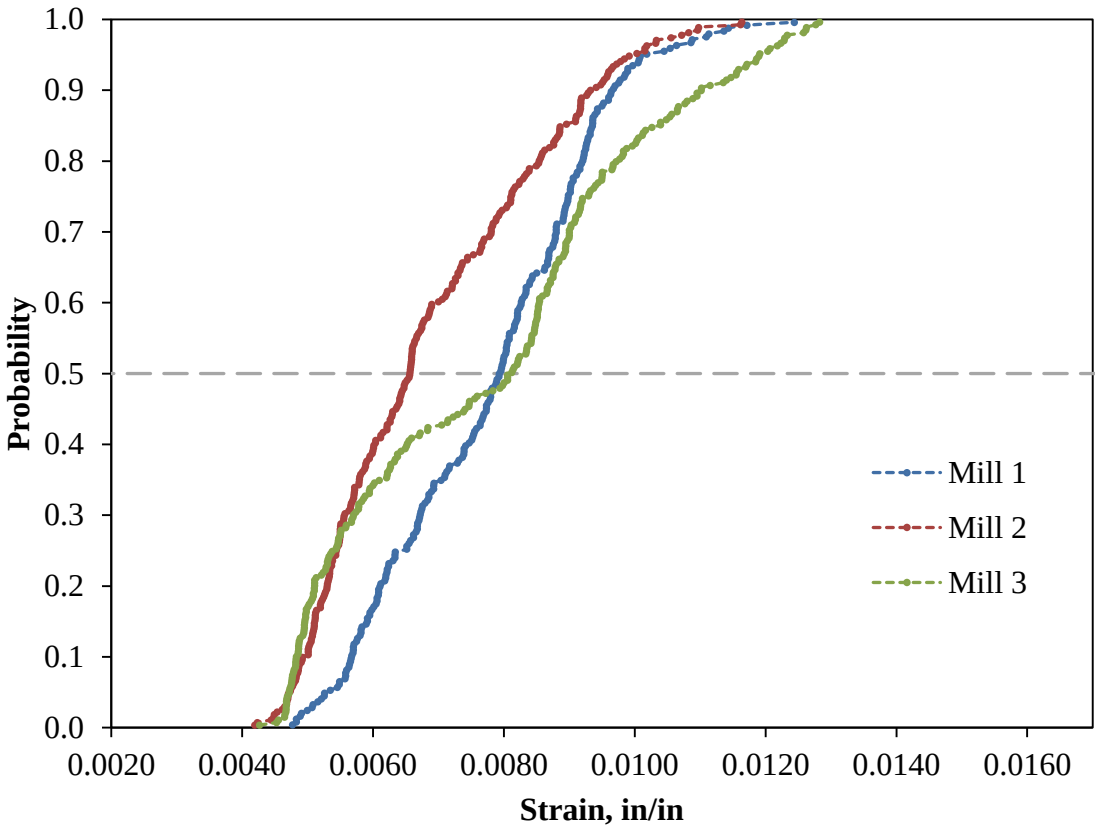

10.4. Tensile Strength

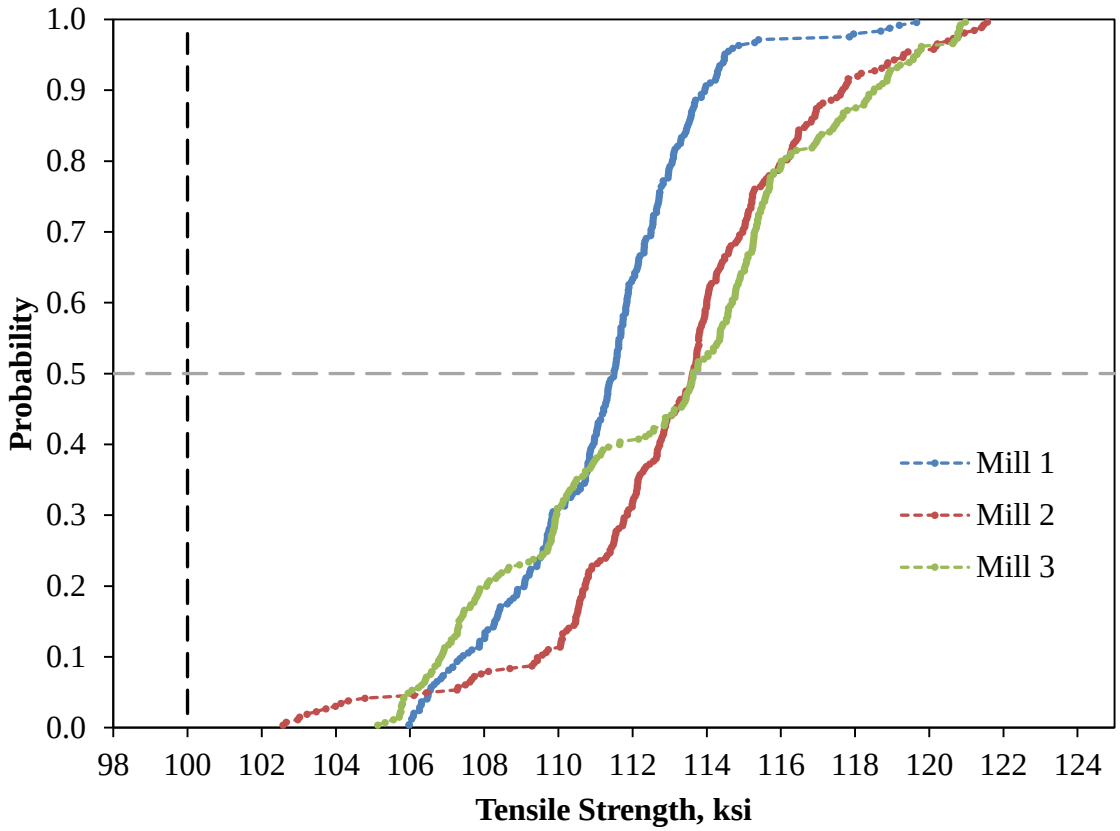

10.5. Ultimate Tensile Strain

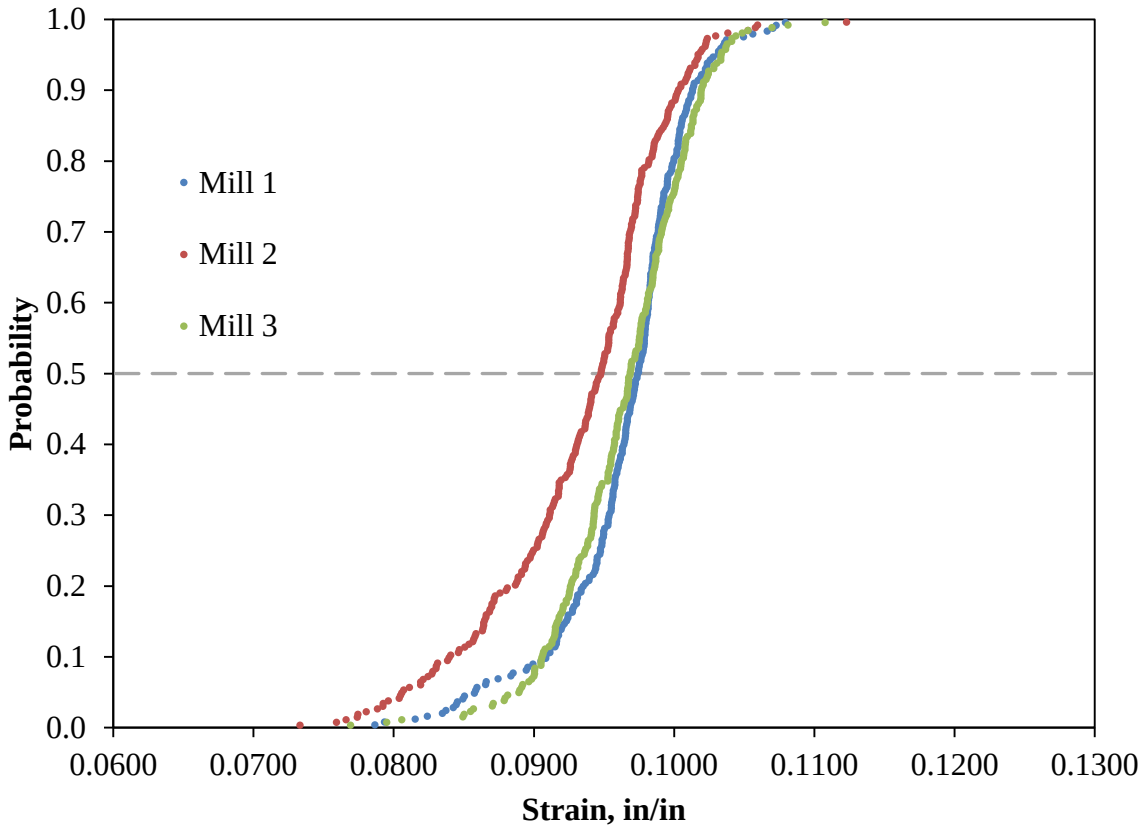

10.6. Tensile-to-Yield Ratio

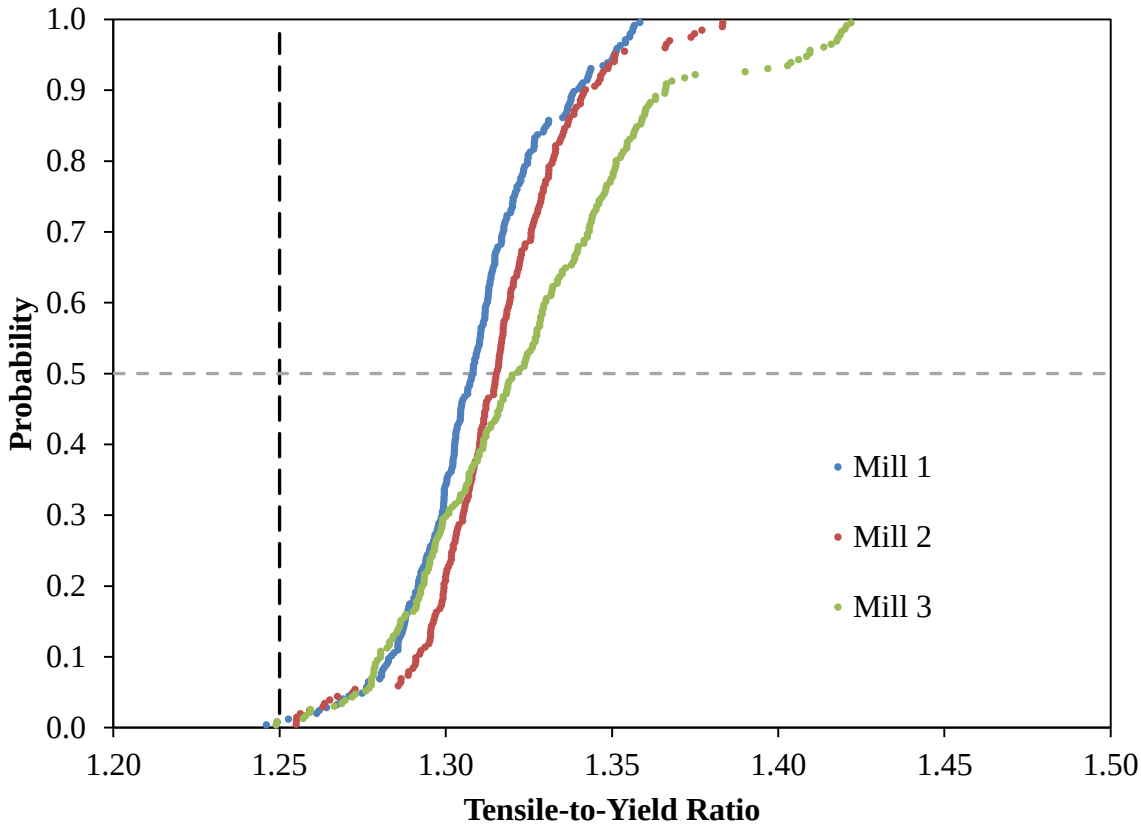

11. APPENDIX D: HEAT CUMULATIVE DISTRIBUTION FUNCTIONS

11.1. Yield Strength

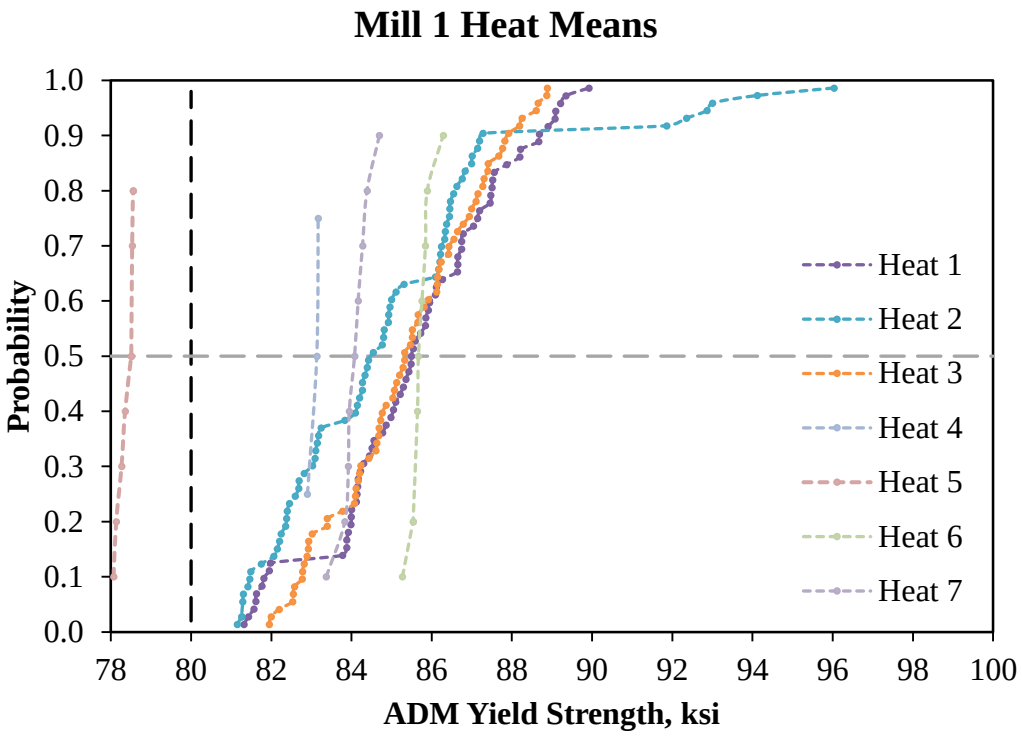

Mill 2 Heat Means

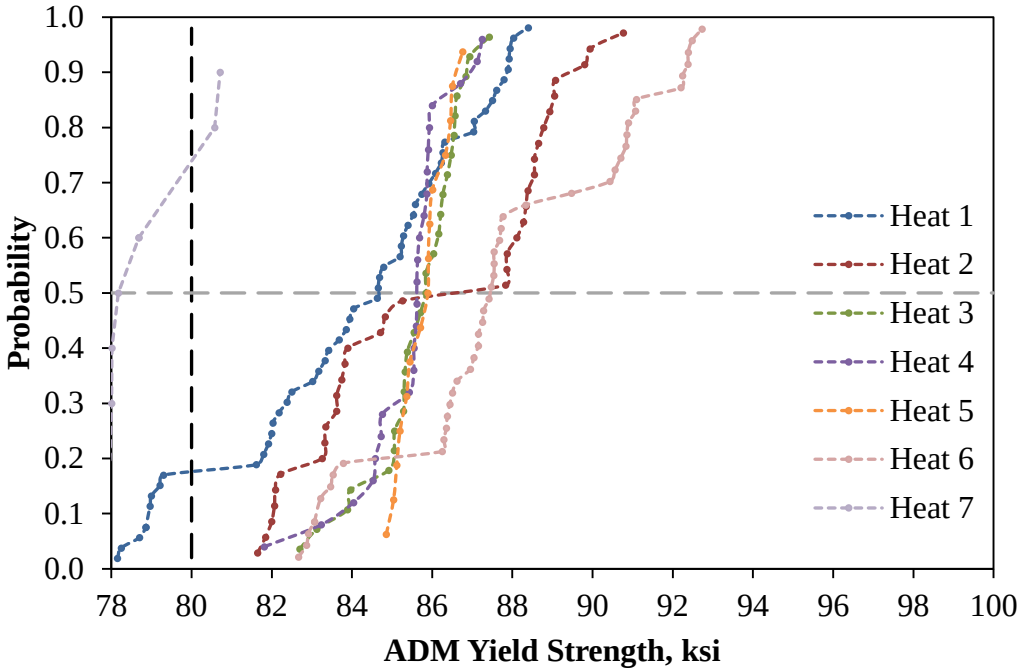

Mill 3 Heat Means

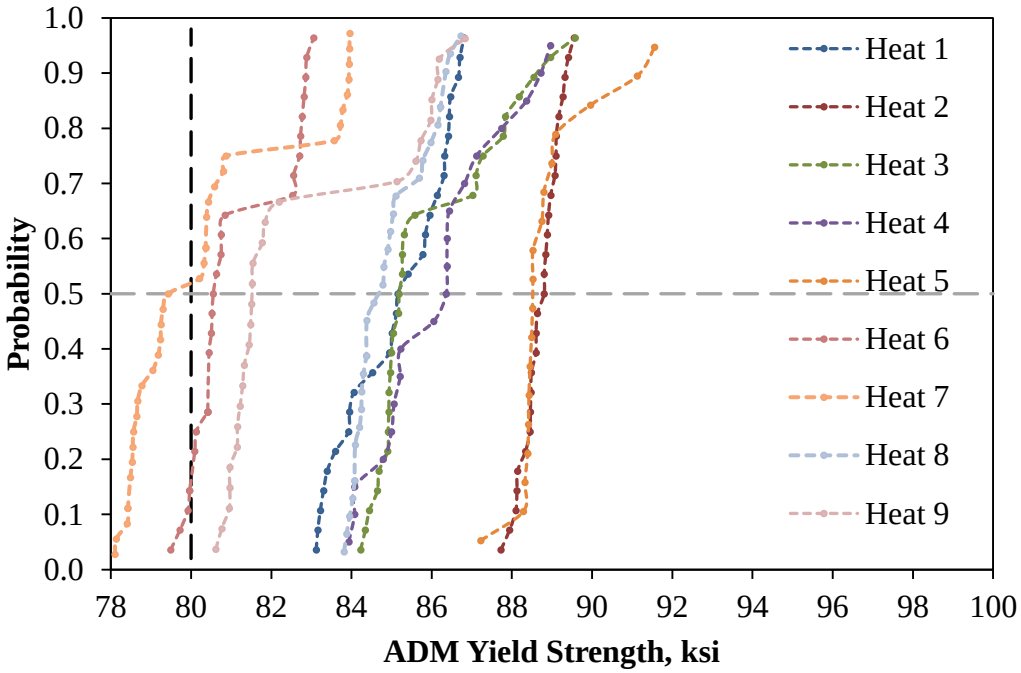

11.2. Yield Strain

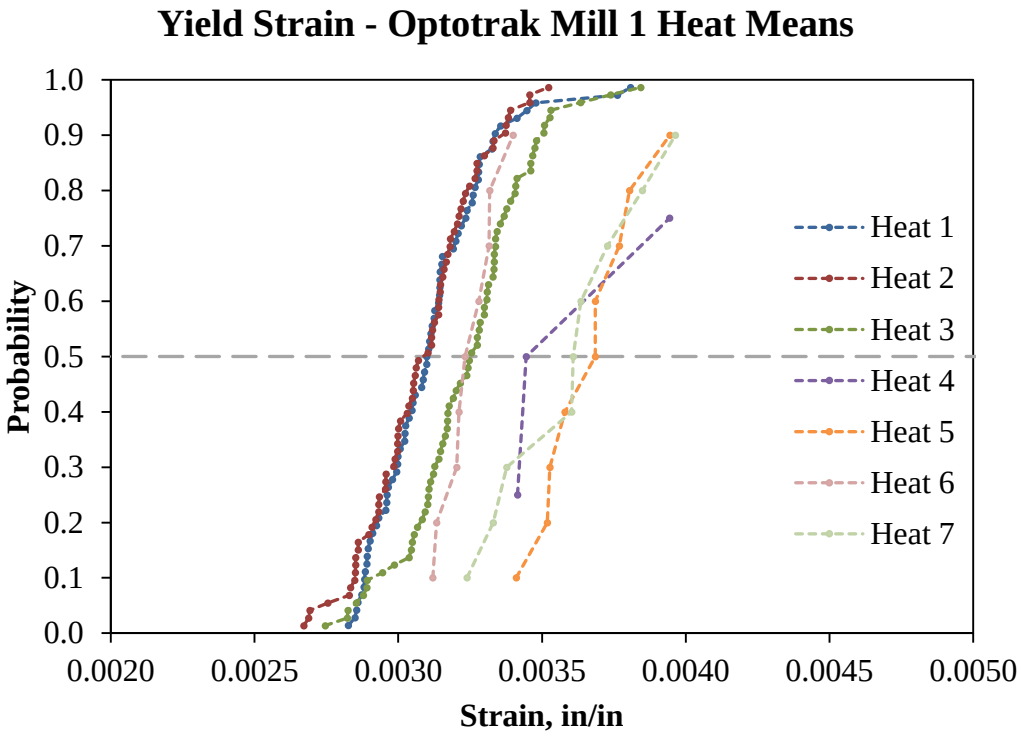

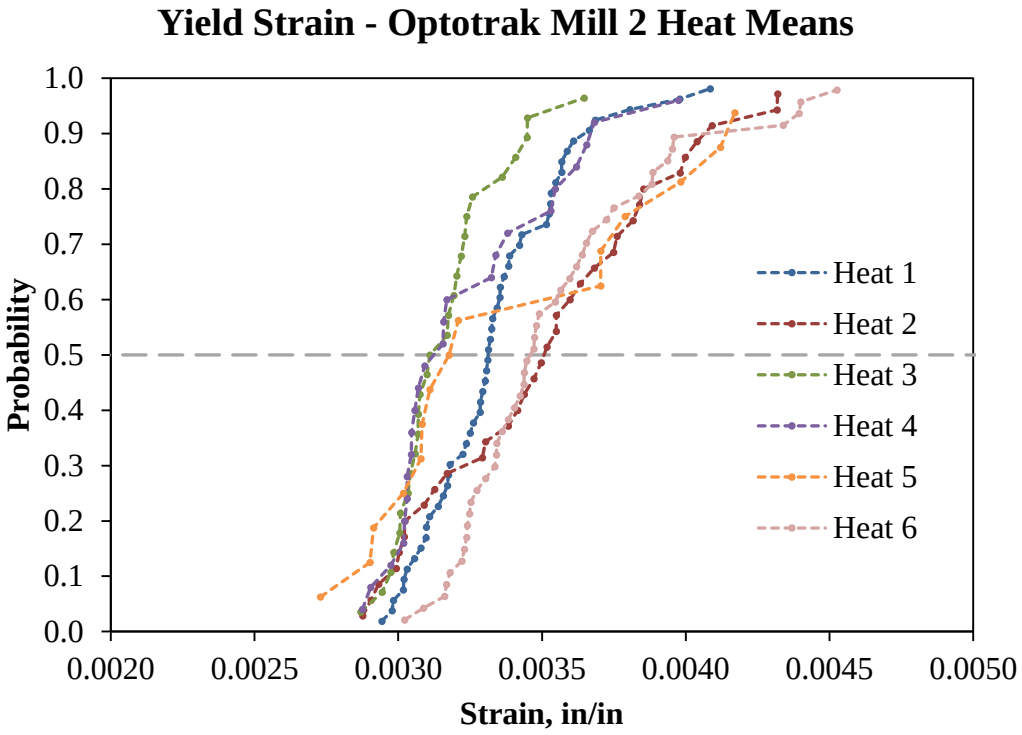
Yield Strain - Optotrak Mill 2 Heat Means
Probability
1.0
0.9
0.8
0.7
0.6
0.5
0.4
0.3
0.2
0.1
0.0
0.0020
0.0025
0.0030
0.0035
0.0040
0.0045
0.0050
Strain, in/in
Heat 1
Heat 2
Heat 3
Heat 4
Heat 5
Heat 6

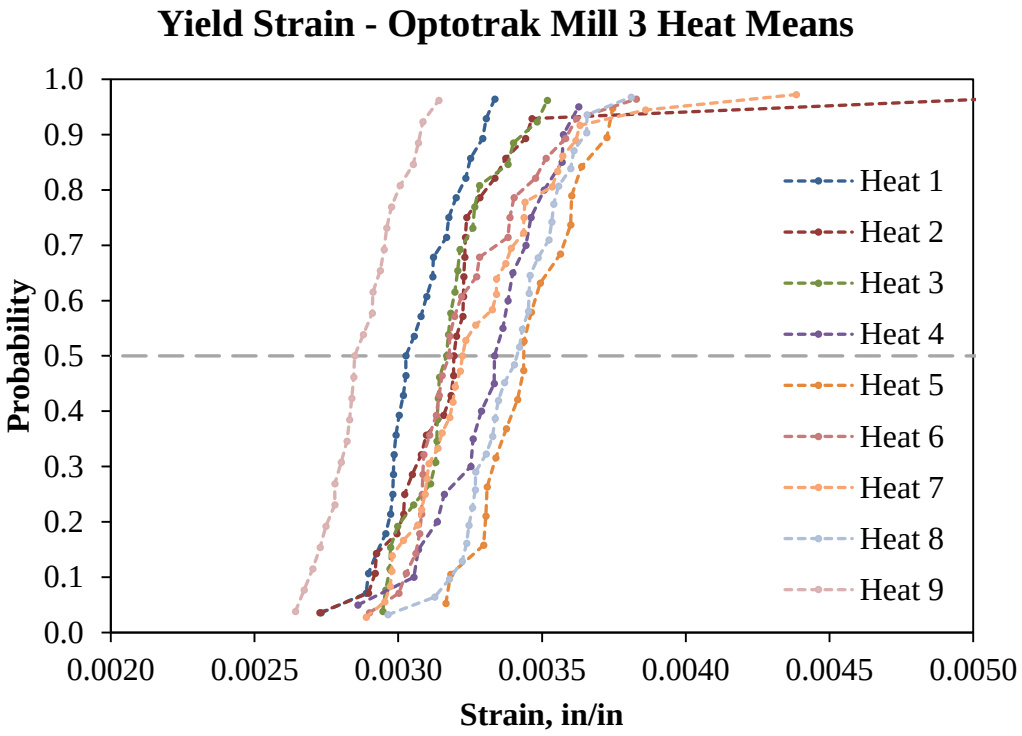
Yield Strain - Optotrak Mill 3 Heat Means
Probability
1.0
0.9
0.8
0.7
0.6
0.5
0.4
0.3
0.2
0.1
0.0
0.0020
0.0025
0.0030
0.0035
0.0040
0.0045
0.0050
Strain, in/in
Heat 1
Heat 2
Heat 3
Heat 4
Heat 5
Heat 6
Heat 7
Heat 8
Heat 9

11.3. Onset of Strain Hardening

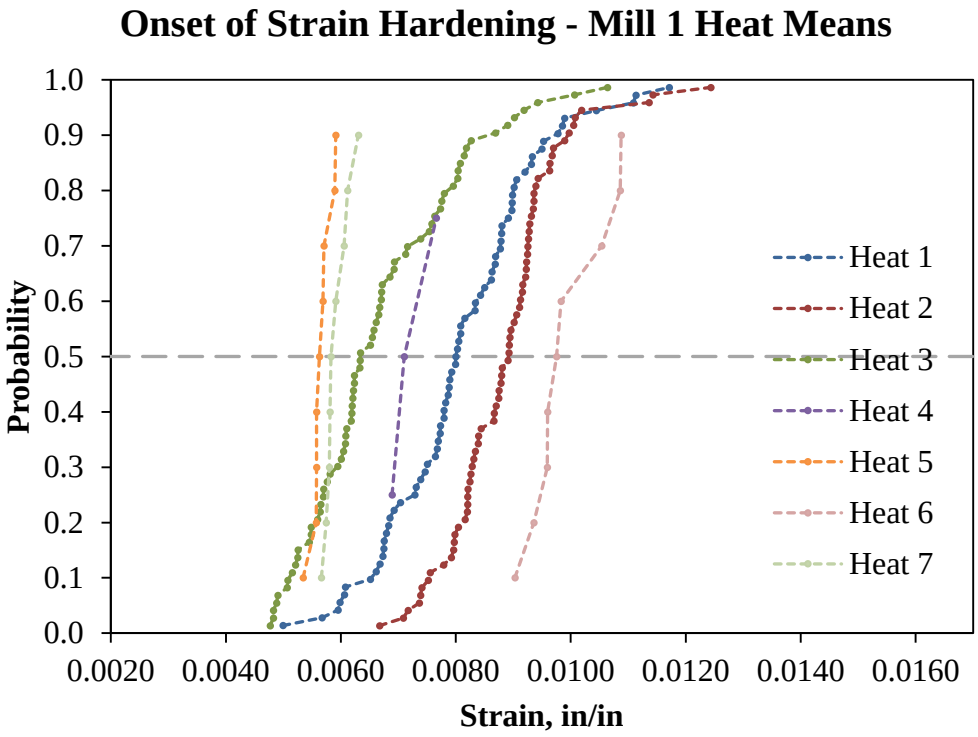

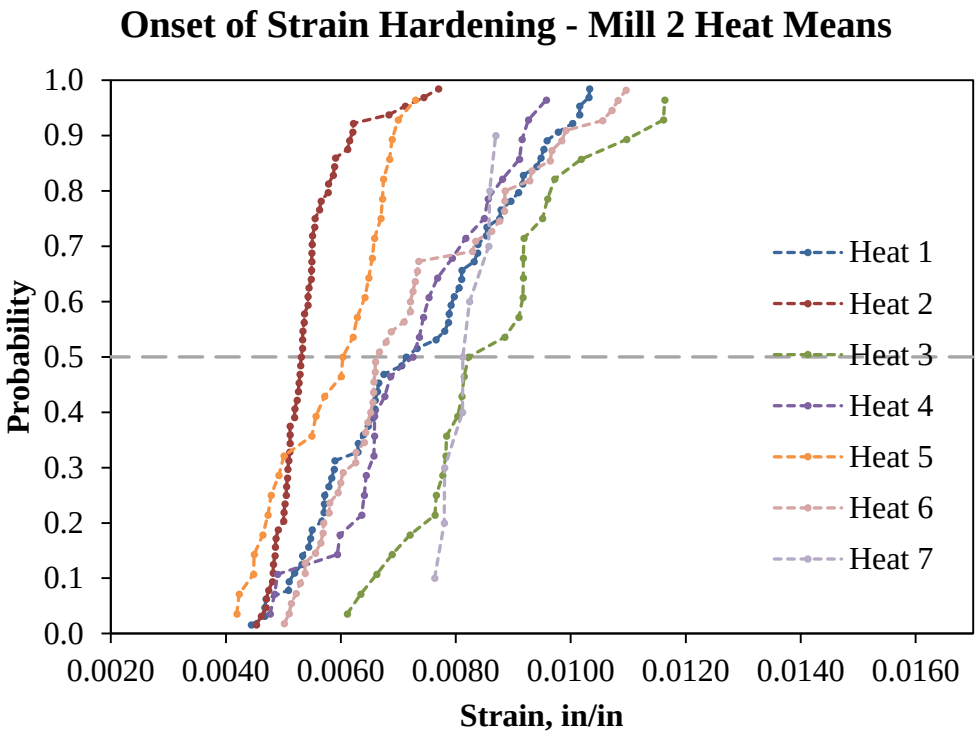
Onset of Strain Hardening - Mill 2 Heat Means
Probability
1.0
0.9
0.8
0.7
0.6
0.5
0.4
0.3
0.2
0.1
0.0
0.0020
0.0040
0.0060
0.0080
0.0100
0.0120
0.0140
0.0160
Strain, in/in
Heat 1
Heat 2
Heat 3
Heat 4
Heat 5
Heat 6
Heat 7

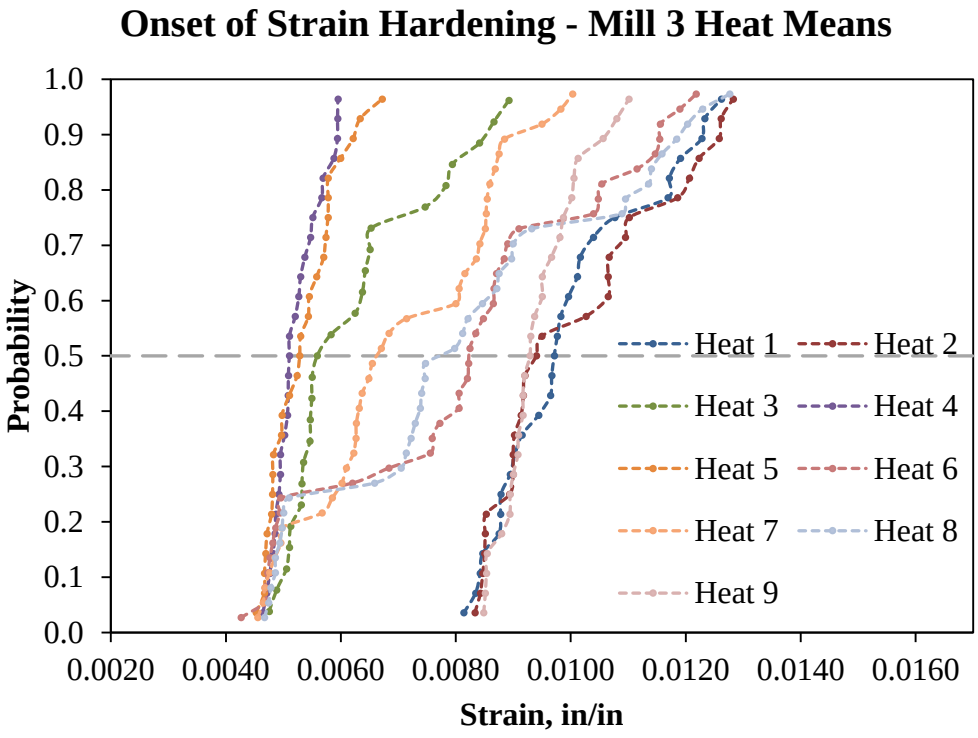
Onset of Strain Hardening - Mill 3 Heat Means
Probability
1.0
0.9
0.8
0.7
0.6
0.5
0.4
0.3
0.2
0.1
0.0
0.0020
0.0040
0.0060
0.0080
0.0100
0.0120
0.0140
0.0160
Strain, in/in
Heat 1
Heat 2
Heat 3
Heat 4
Heat 5
Heat 6
Heat 7
Heat 8
Heat 9

11.4. Tensile Strength

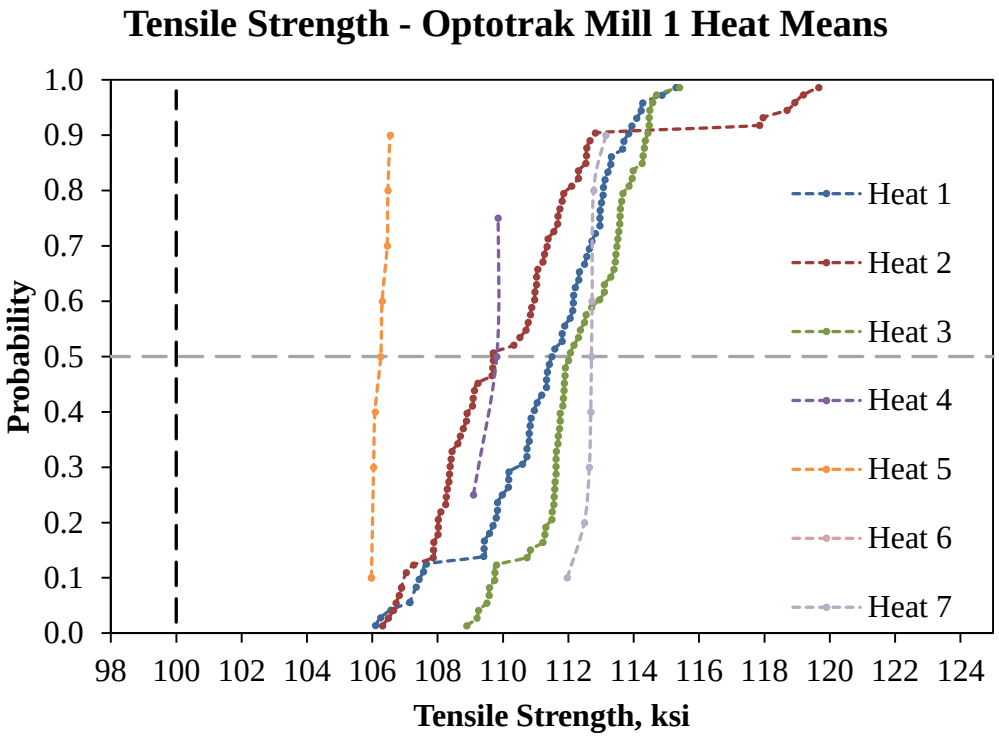

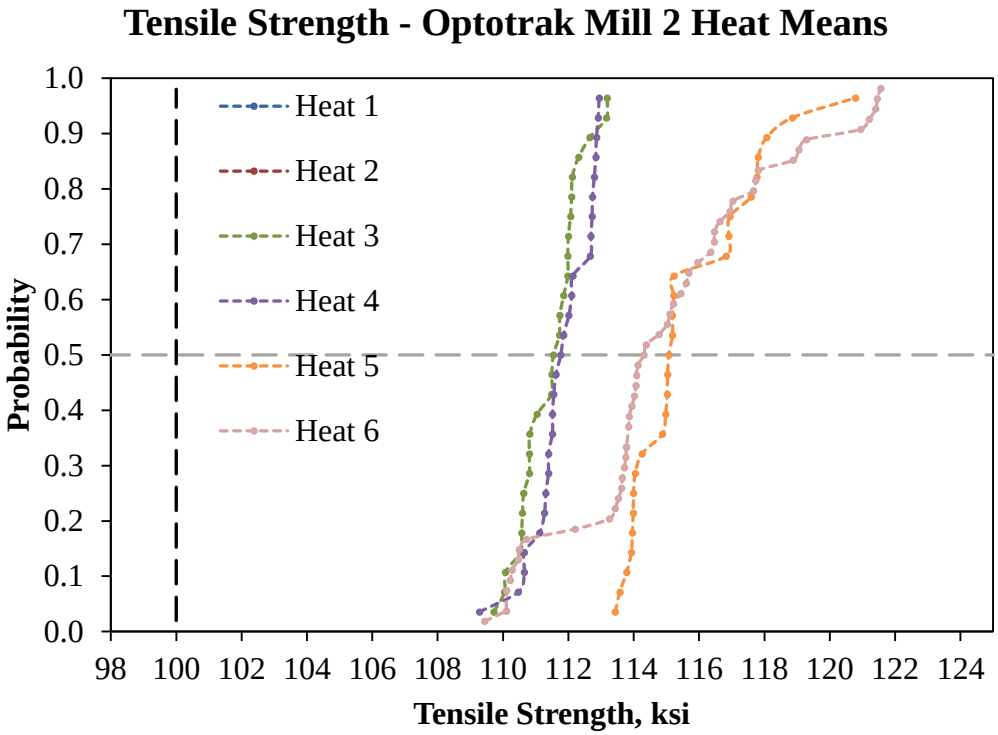
Tensile Strength - Optotrak Mill 2 Heat Means
Probability
1.0
0.9
0.8
0.7
0.6
0.5
0.4
0.3
0.2
0.1
0.0
Heat 1
Heat 2
Heat 3
Heat 4
Heat 5
Heat 6
98 100 102 104 106 108 110 112 114 116 118 120 122 124
Tensile Strength, ksi

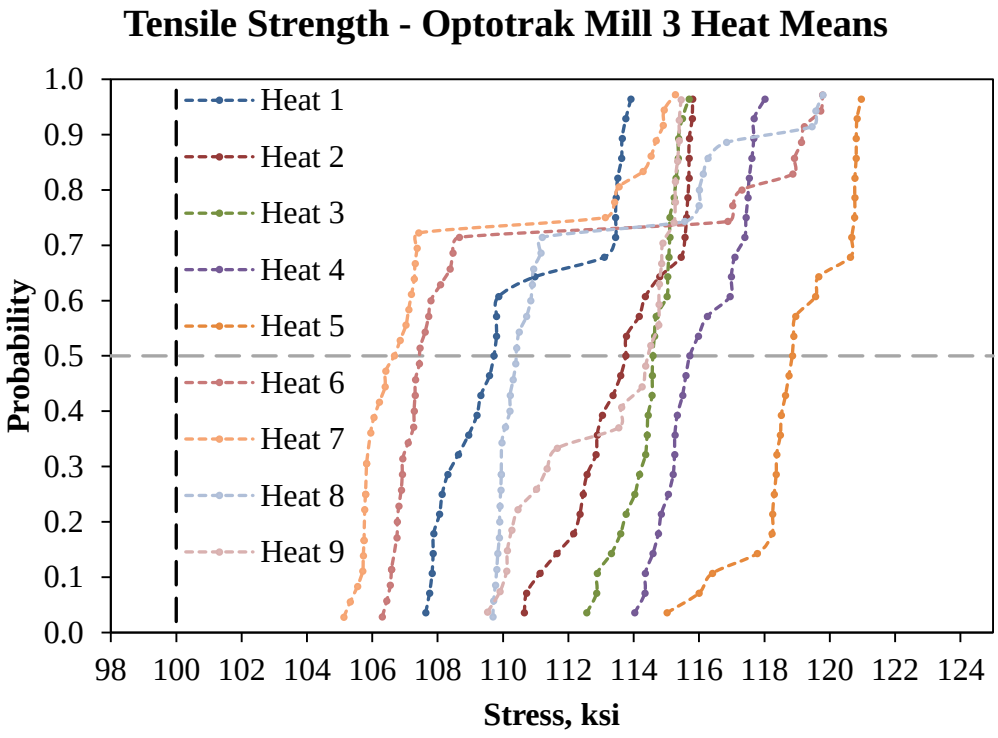
Tensile Strength - Optotrak Mill 3 Heat Means
Probability
1.0
0.9
0.8
0.7
0.6
0.5
0.4
0.3
0.2
0.1
0.0
Heat 1
Heat 2
Heat 3
Heat 4
Heat 5
Heat 6
Heat 7
Heat 8
Heat 9
98 100 102 104 106 108 110 112 114 116 118 120 122 124
Stress, ksi

11.5. Ultimate Tensile Strain

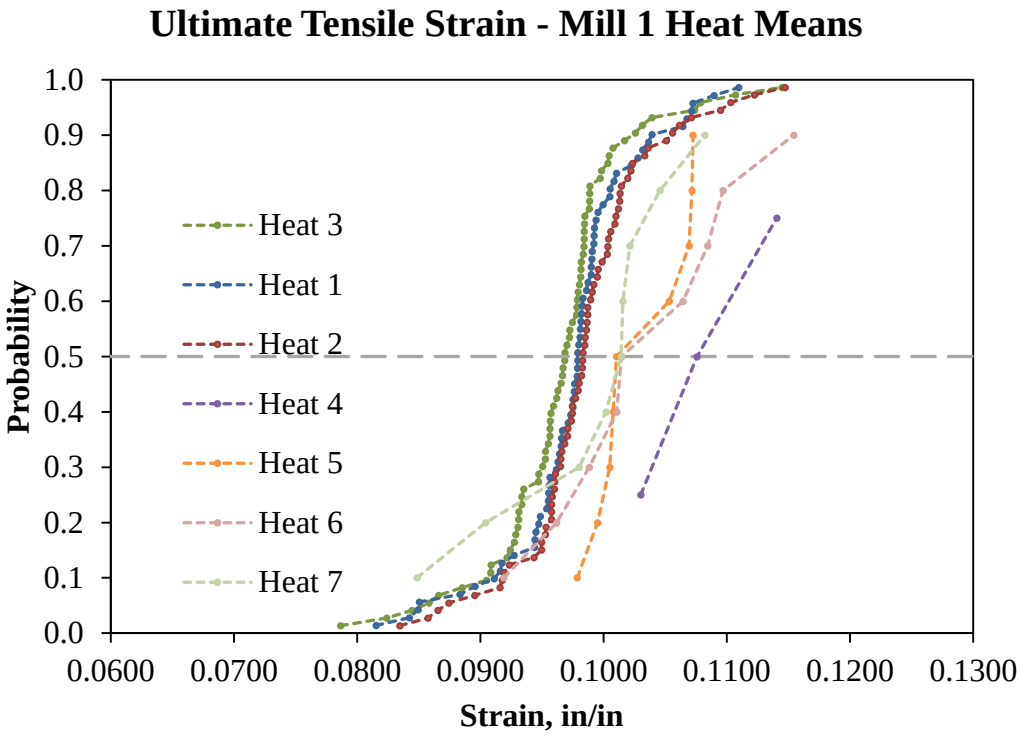

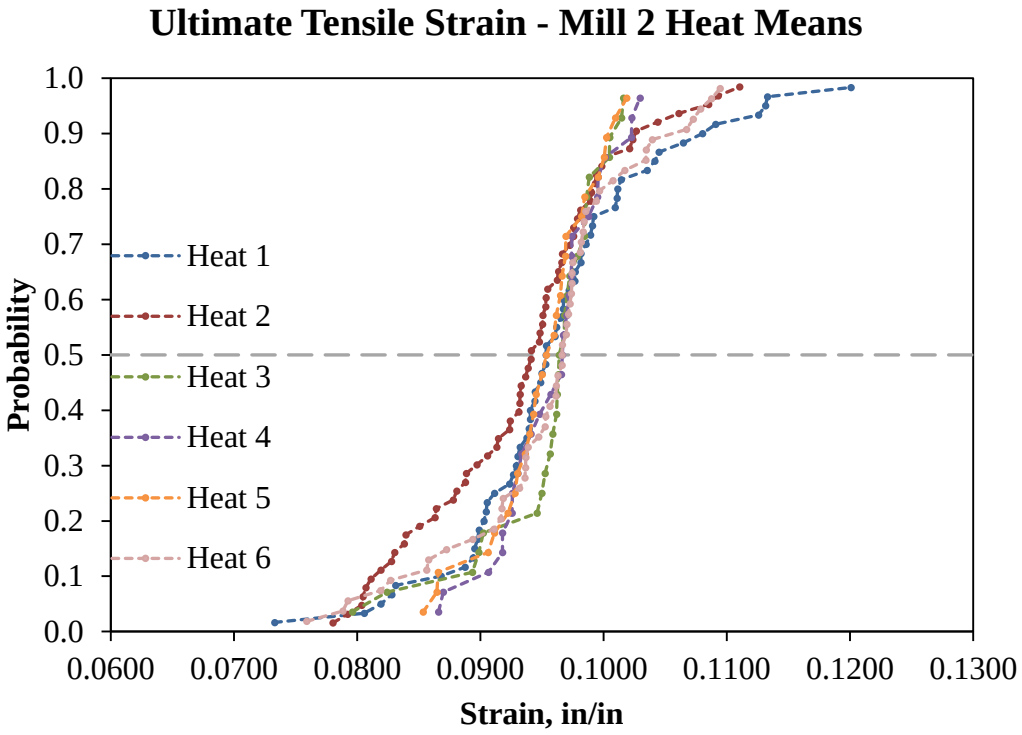
Ultimate Tensile Strain - Mill 2 Heat Means
Probability
1.0
0.9
0.8
0.7
0.6
0.5
0.4
0.3
0.2
0.1
0.0
Heat 1
Heat 2
Heat 3
Heat 4
Heat 5
Heat 6
0.0600
0.0700
0.0800
0.0900
0.1000
0.1100
0.1200
0.1300
Strain, in/in

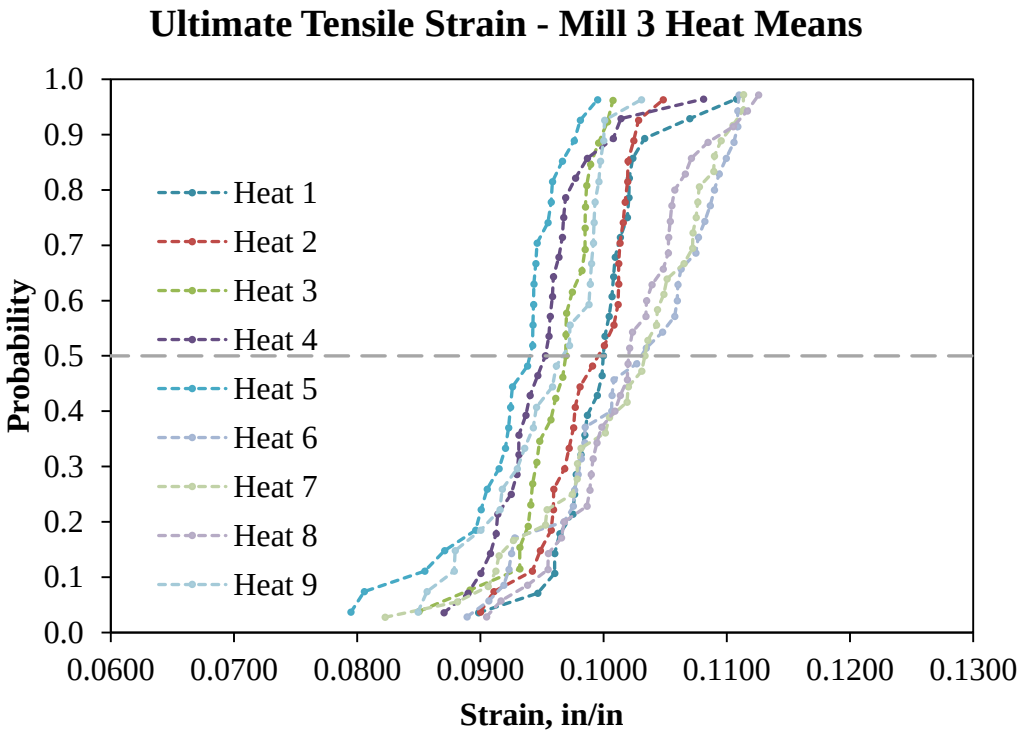
Ultimate Tensile Strain - Mill 3 Heat Means
Probability
1.0
0.9
0.8
0.7
0.6
0.5
0.4
0.3
0.2
0.1
0.0
Heat 1
Heat 2
Heat 3
Heat 4
Heat 5
Heat 6
Heat 7
Heat 8
Heat 9
0.0600
0.0700
0.0800
0.0900
0.1000
0.1100
0.1200
0.1300
Strain, in/in

12. APPENDIX E: 2” VS 8” GAGE LENGTH COMPARISON

12.1. Yield Strain

ε_y	Mean		St. Dev.		CV	
	2-inch	8-inch	2-inch	8-inch	2-inch	8-inch
No. 4	0.0034	0.0034	0.0003	0.0003	8.9%	8.8%
No. 5	0.0032	0.0032	0.0002	0.0002	5.8%	6.0%
No. 6	0.0031	0.0031	0.0002	0.0003	7.9%	8.6%
No. 7	0.0033	0.0033	0.0004	0.0005	12.6%	14.1%
No. 8	0.0032	0.0032	0.0002	0.0002	6.6%	6.6%
No. 9	0.0031	0.0031	0.0003	0.0003	8.9%	8.9%
No. 10	0.0031	0.0031	0.0002	0.0002	7.6%	7.4%
No. 11	0.0034	0.0033	0.0003	0.0003	8.6%	8.4%
No. 14	0.0034	0.0033	0.0003	0.0003	7.4%	7.5%
No. 18	0.0033	0.0033	0.0003	0.0003	8.0%	8.0%
Total	**0.0033**	**0.0032**	**0.0003**	**0.0003**	**9.0%**	**9.5%**

12.2. Onset of Strain Hardening

ε_{sh}	Mean		St. Dev.		CV	
	2-inch	8-inch	2-inch	8-inch	2-inch	8-inch
No. 4	0.0072	0.0072	0.0020	0.0020	27.7%	27.8%
No. 5	0.0084	0.0085	0.0015	0.0015	18.3%	18.2%
No. 6	0.0085	0.0085	0.0025	0.0025	28.9%	29.4%
No. 7	0.0078	0.0078	0.0012	0.0013	16.0%	16.1%
No. 8	0.0069	0.0068	0.0017	0.0017	24.9%	25.0%
No. 9	0.0065	0.0066	0.0015	0.0015	23.3%	23.0%
No. 10	0.0056	0.0055	0.0012	0.0012	22.0%	21.9%
No. 11	0.0084	0.0084	0.0023	0.0023	27.2%	27.3%
No. 14	0.0076	0.0075	0.0014	0.0014	18.5%	18.9%
No. 18	0.0076	0.0076	0.0014	0.0014	18.3%	19.0%
Total	**0.0074**	**0.0074**	**0.0019**	**0.0020**	**26.2%**	**26.3%**

12.3. Ultimate Tensile Strain

ε_u	Mean		St. Dev.		CV	
	2-inch	8-inch	2-inch	8-inch	2-inch	8-inch
No. 4	0.0922	0.0922	0.0062	0.0067	6.8%	7.3%
No. 5	0.0945	0.0945	0.0055	0.0058	5.8%	6.2%
No. 6	0.0958	0.0959	0.0057	0.0059	6.0%	6.2%
No. 7	0.0971	0.0973	0.0045	0.0047	4.6%	4.8%
No. 8	0.0957	0.0960	0.0037	0.0036	3.9%	3.8%
No. 9	0.0956	0.0956	0.0051	0.0054	5.3%	5.6%
No. 10	0.0959	0.0961	0.0041	0.0040	4.3%	4.2%
No. 11	0.0955	0.0954	0.0056	0.0060	5.9%	6.3%
No. 14	0.0971	0.0966	0.0062	0.0066	6.4%	6.8%
No. 18	0.0945	0.0946	0.0073	0.0069	7.8%	7.3%
Total	**0.0954**	**0.0955**	**0.0055**	**0.0057**	**5.8%**	**6.0%**

13. APPENDIX F: COMPARISON OF YIELD STRENGTH DETERMINATION METHODS

Means	$f_{y\ ADM}$	$f_{y\ OM}$	$f_{y\ EUL}$	CV
No. 4	88	87	87	0.82%
No. 5	87	86	86	0.43%
No. 6	86	86	85	0.86%
No. 7	86	86	86	0.38%
No. 8	86	86	86	0.15%
No. 9	85	85	85	0.27%
No. 10	84	86	85	0.78%
No. 11	84	84	82	1.34%
No. 14	82	82	81	0.96%
No. 18	81	81	80	0.44%
Total	85.0	85.1	84.3	0.52%

14. APPENDIX G: SUMMARY OF YIELD BEHAVIORS

Percent of Total	well-defined yield plateau	knee but no drop in stress	completely roundhouse
All Tests	87.6%	9.6%	2.8%
Mill 1 tests	100%	--	--
Mill 2 tests	75.9%	15.9%	8.1%
Mill 3 tests	87.8%	12.2%	--

15. APPENDIX H: STRAIN-AGING STRESS-STRAIN CURVES

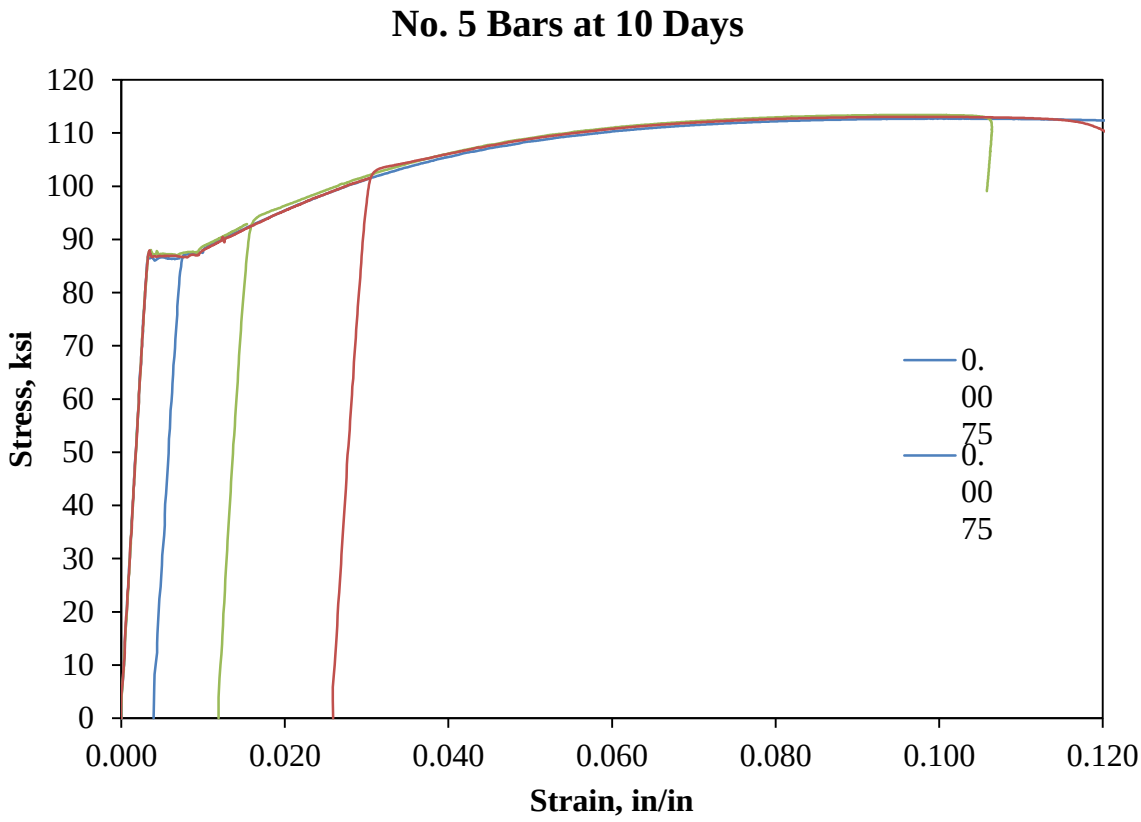

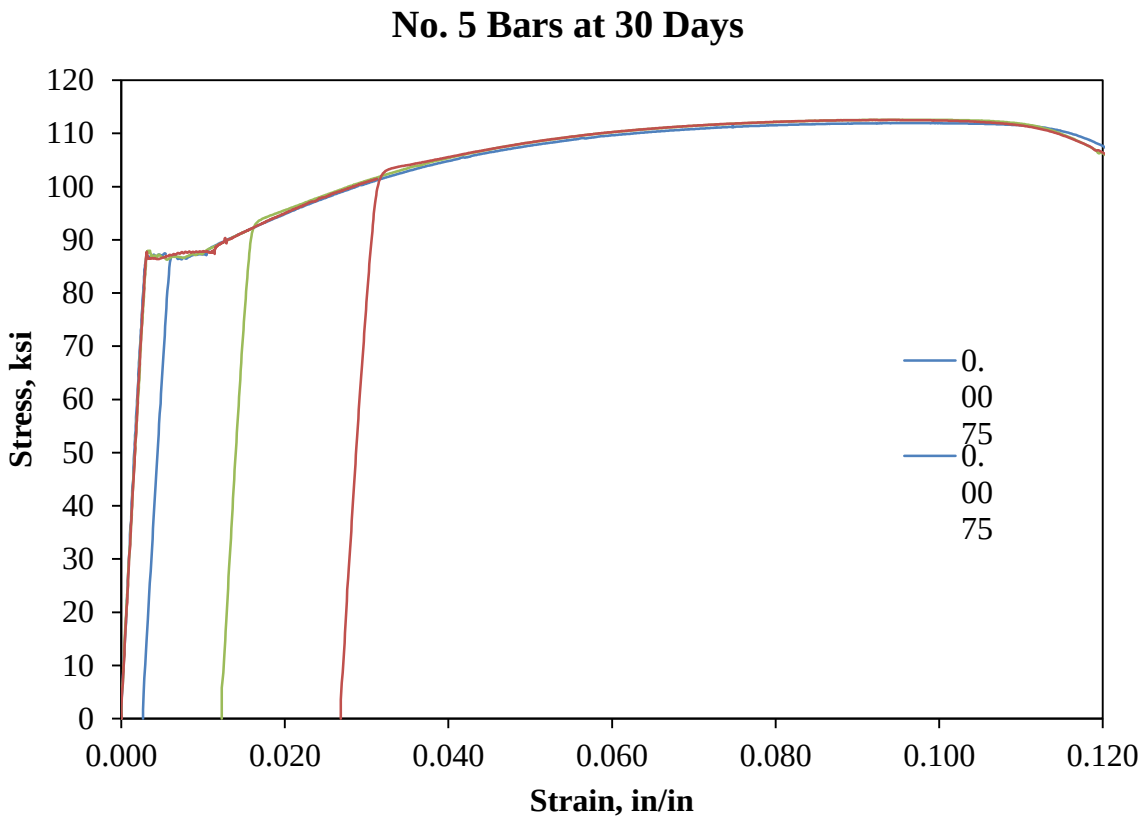
No. 5 Bars at 30 Days
Stress, ksi
120
110
100
90
80
70
60
50
40
30
20
10
0
0.000
0.020
0.040
0.060
0.080
0.100
0.120
Strain, in/in
0.00075
0.00075

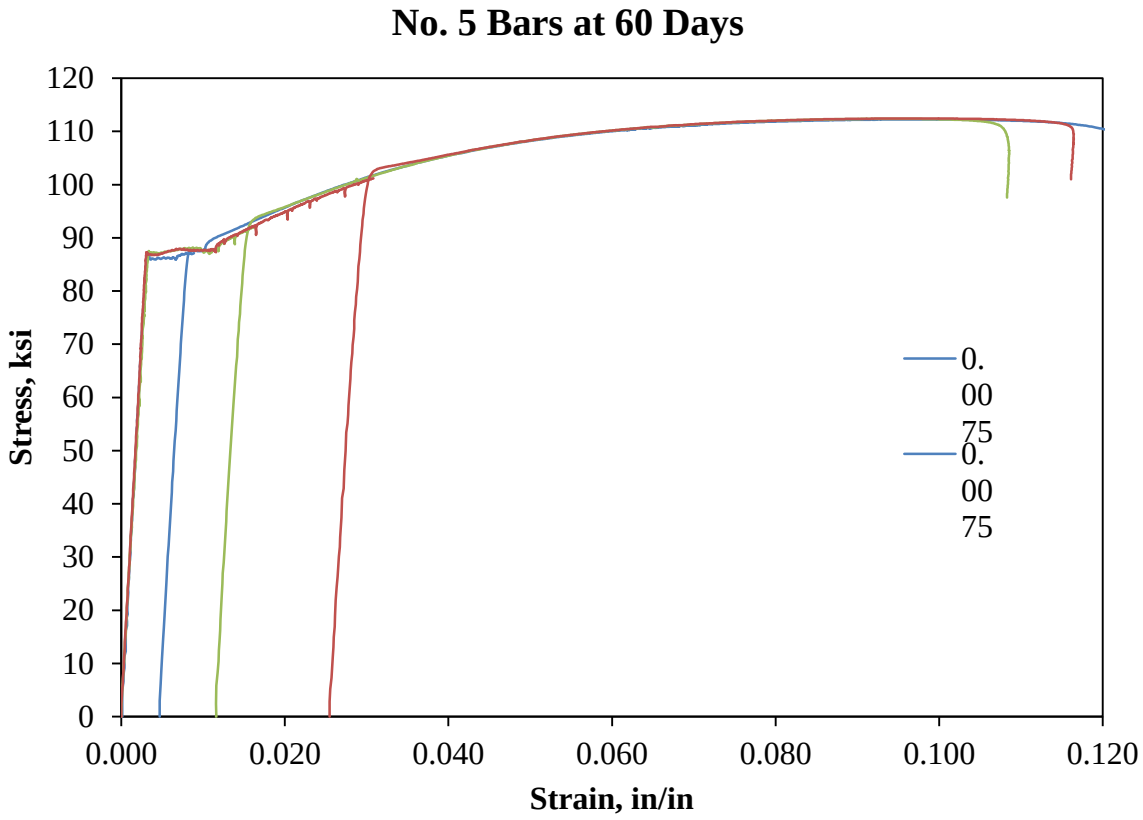
No. 5 Bars at 60 Days
Stress, ksi
120
110
100
90
80
70
60
50
40
30
20
10
0
0.000
0.020
0.040
0.060
0.080
0.100
0.120
Strain, in/in
0.00075
0.00075

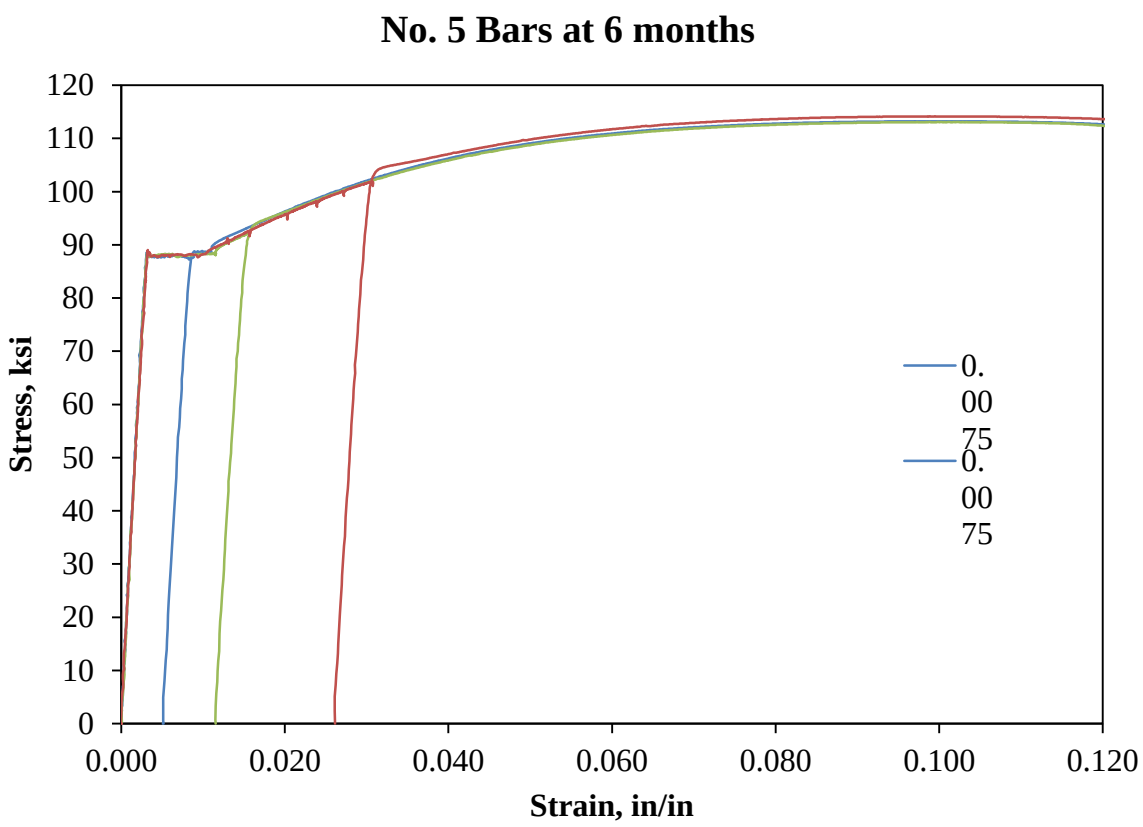
No. 5 Bars at 6 months
Stress, ksi
120
110
100
90
80
70
60
50
40
30
20
10
0
0.000
0.020
0.040
0.060
0.080
0.100
0.120
Strain, in/in
0.00075
0.00075

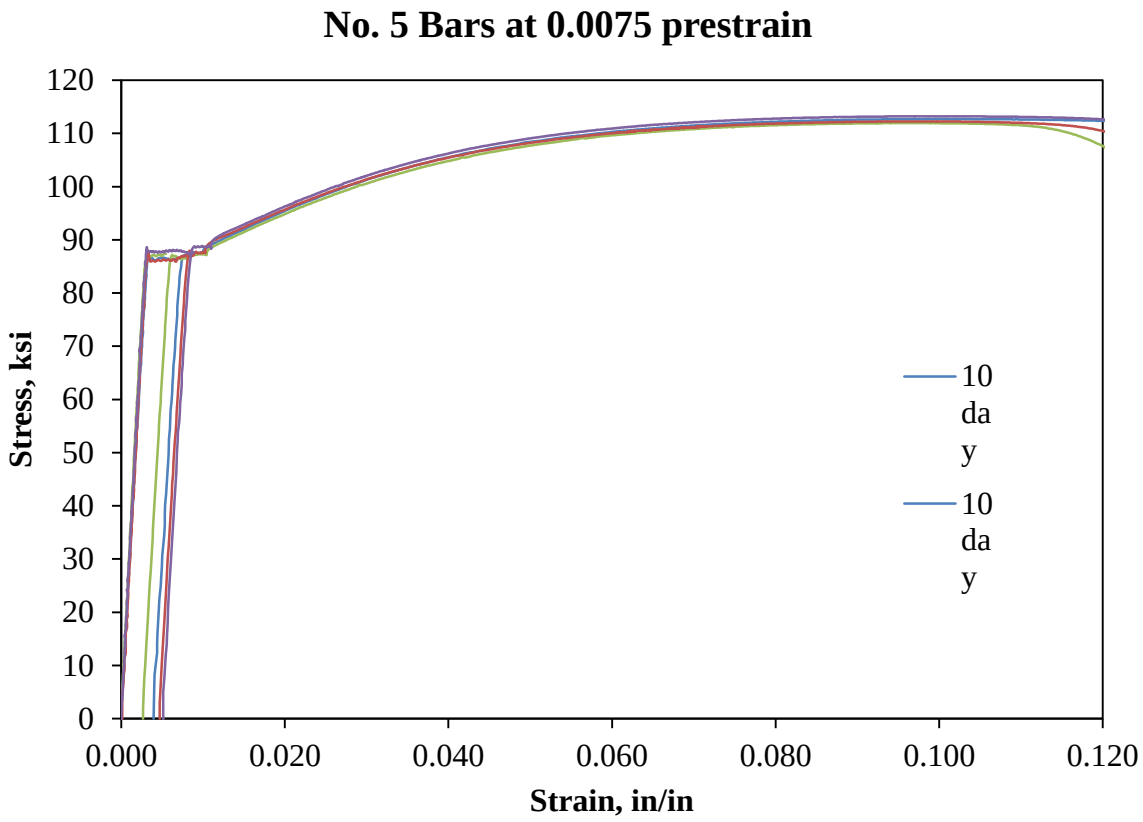
No. 5 Bars at 0.0075 prestrain
Stress, ksi
120
110
100
90
80
70
60
50
40
30
20
10
0
0.000
0.020
0.040
0.060
0.080
0.100
0.120
Strain, in/in
10 day
10 day

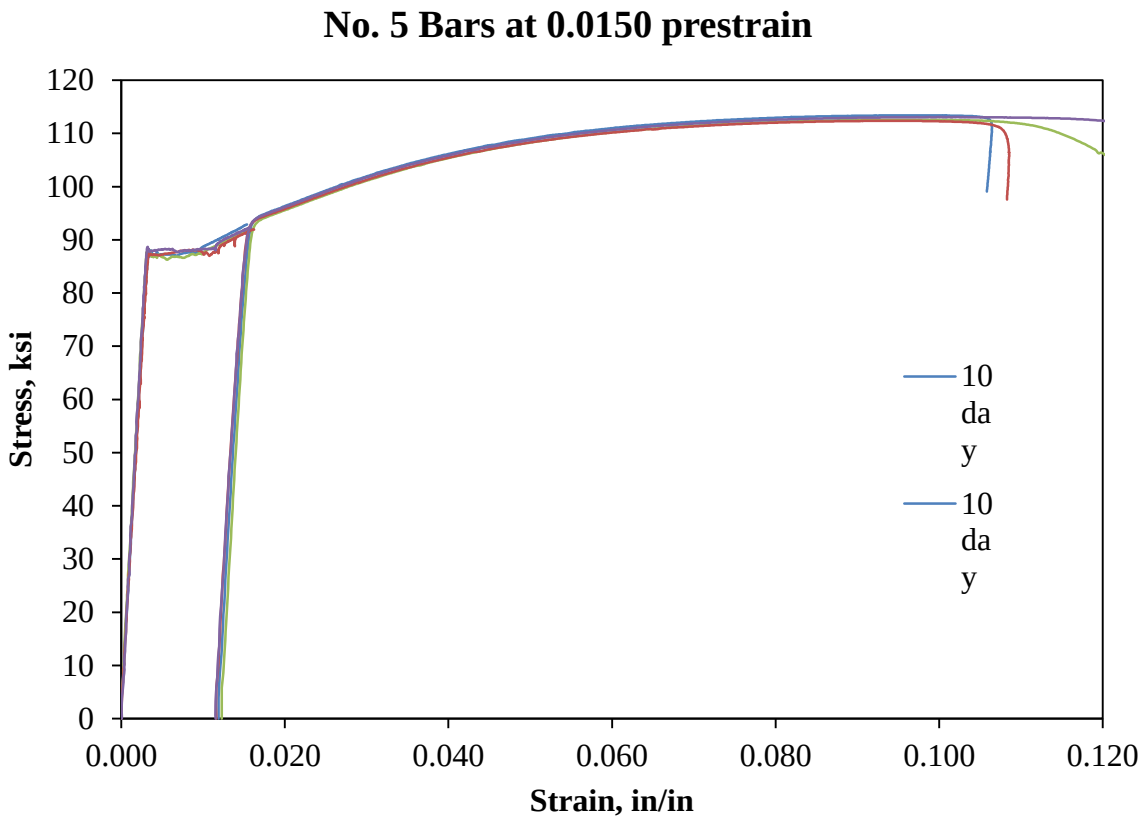
No. 5 Bars at 0.0150 prestrain
Stress, ksi
120
110
100
90
80
70
60
50
40
30
20
10
0
0.000
0.020
0.040
0.060
0.080
0.100
0.120
Strain, in/in
10 day
10 day

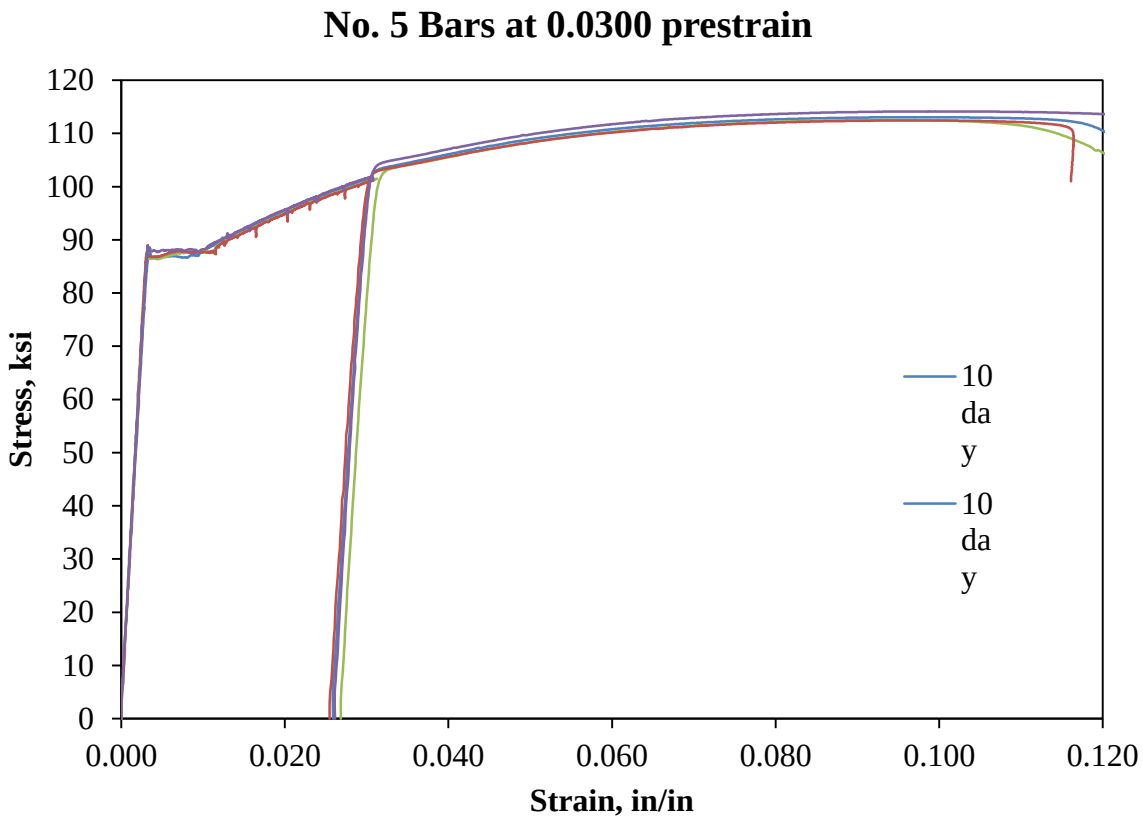
No. 5 Bars at 0.0300 prestrain
Stress, ksi
120
110
100
90
80
70
60
50
40
30
20
10
0
0.000
0.020
0.040
0.060
0.080
0.100
0.120
Strain, in/in
10 day
10 day

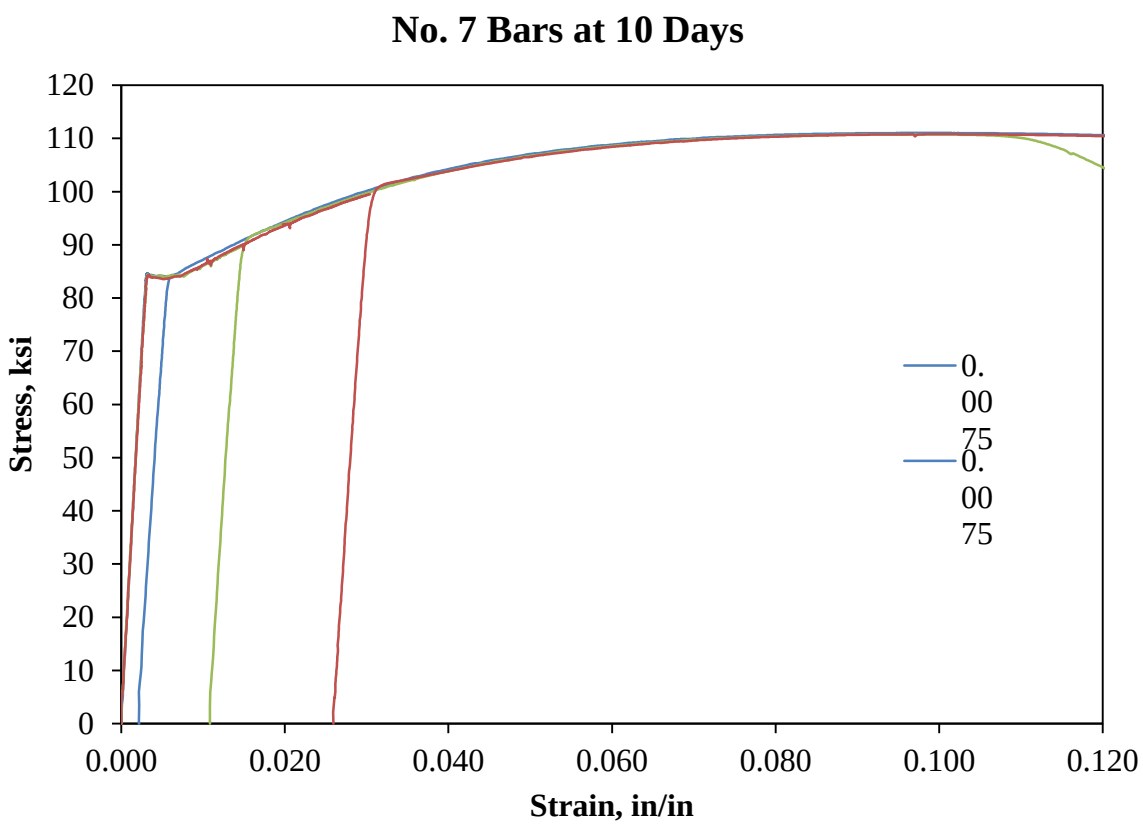
No. 7 Bars at 10 Days
120
110
100
90
80
70
60
50
40
30
20
10
0
Stress, ksi
0.000
0.020
0.040
0.060
0.080
0.100
0.120
Strain, in/in
0.
00
75
0.
00
75

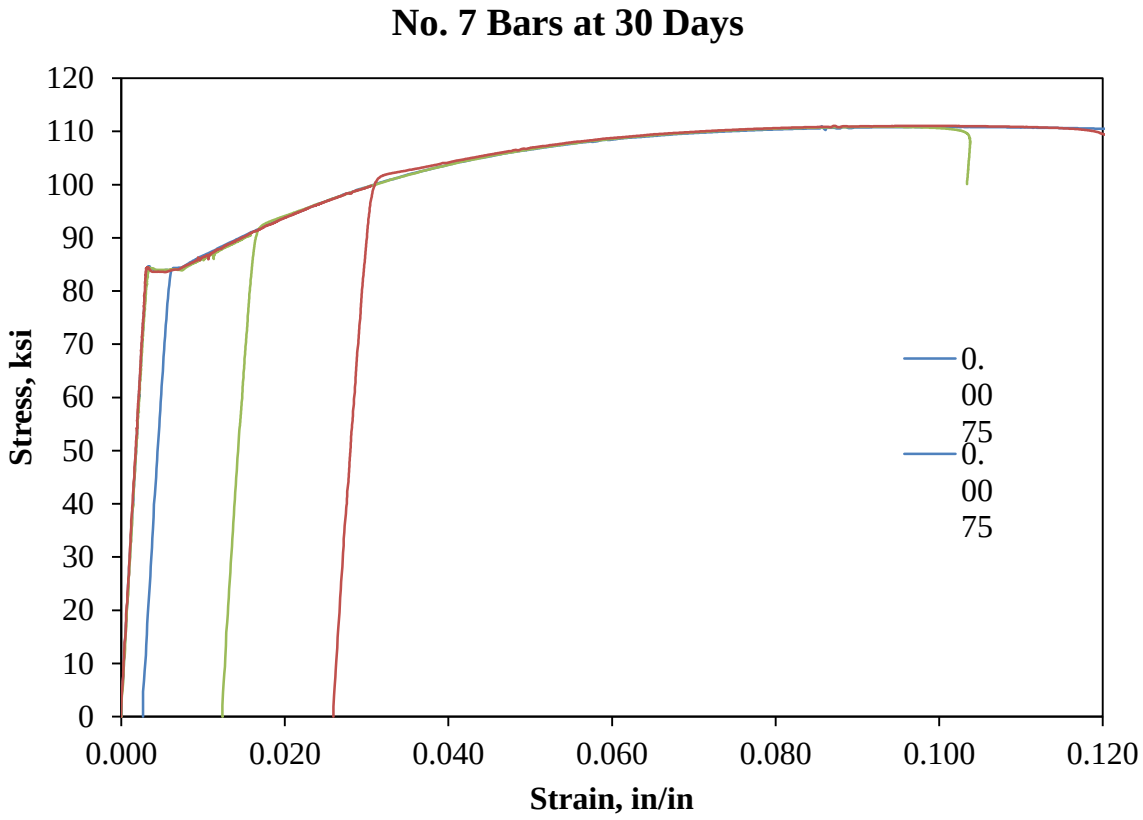
No. 7 Bars at 30 Days
120
110
100
90
80
70
60
50
40
30
20
10
0
Stress, ksi
0.000
0.020
0.040
0.060
0.080
0.100
0.120
Strain, in/in
0.
00
75
0.
00
75

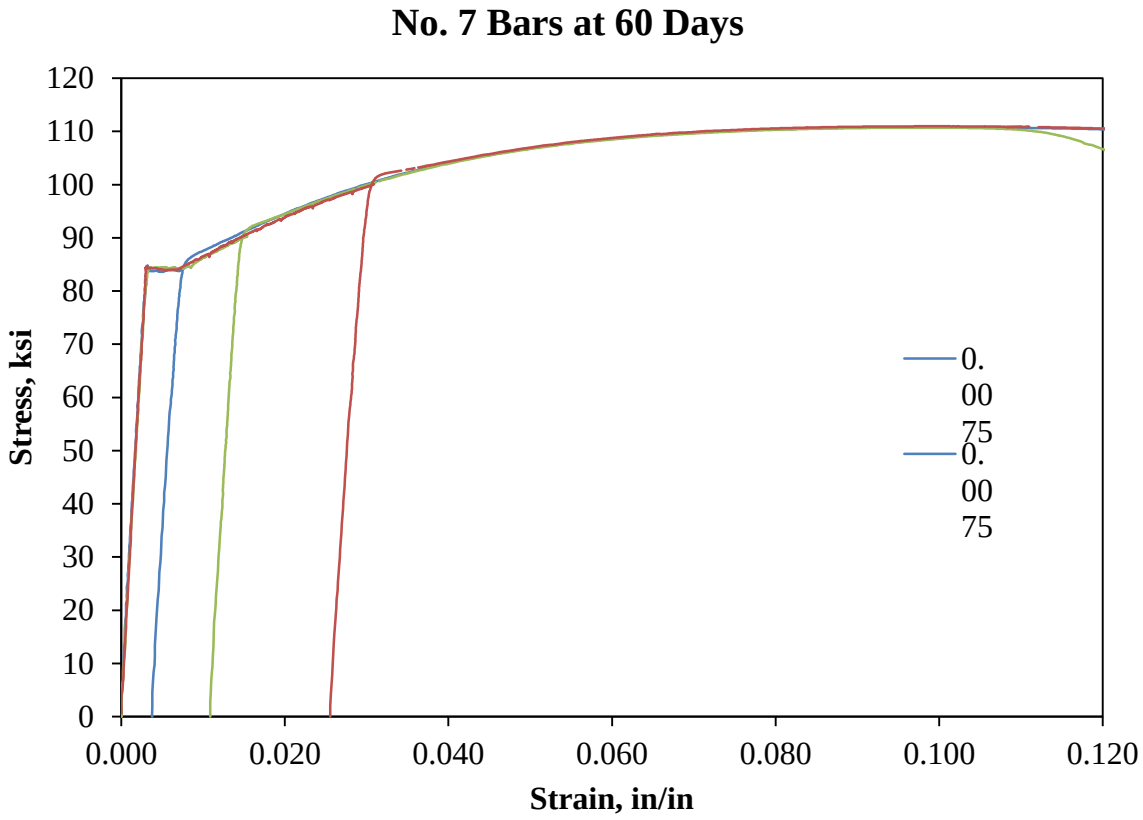
No. 7 Bars at 60 Days
120
110
100
90
80
70
60
50
40
30
20
10
0
Stress, ksi
0.000
0.020
0.040
0.060
0.080
0.100
0.120
Strain, in/in
0.00075
0.00075

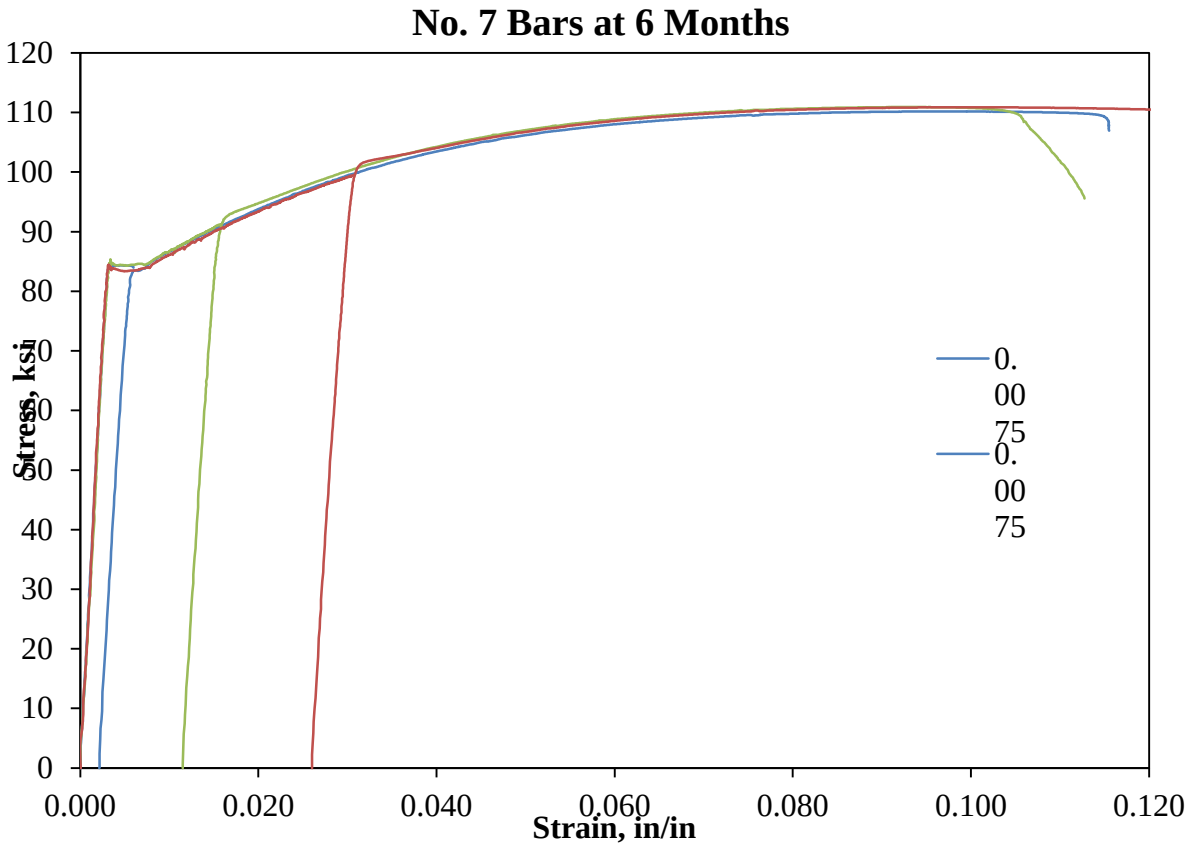
No. 7 Bars at 6 Months
120
110
100
90
80
70
60
50
40
30
20
10
0
Stress, ksi
0.000
0.020
0.040
0.060
0.080
0.100
0.120
Strain, in/in
0.00075
0.00075

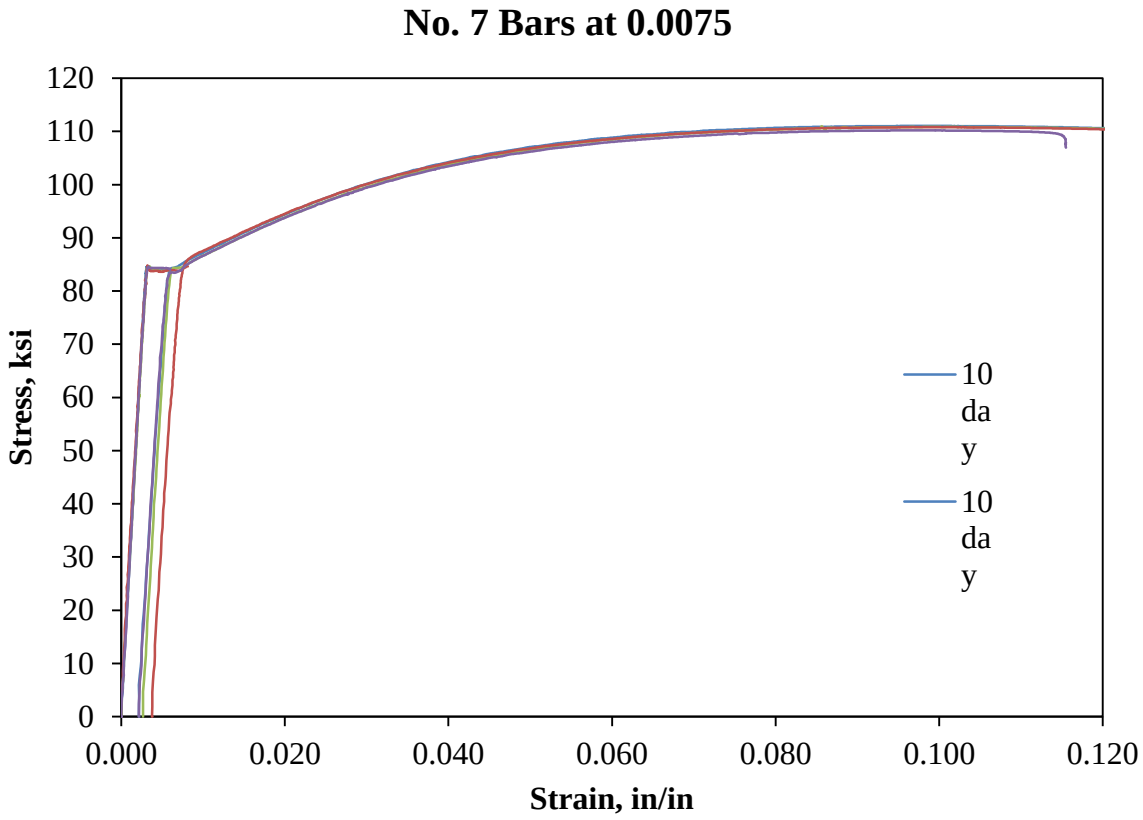
No. 7 Bars at 0.0075
120
110
100
90
80
70
60
50
40
30
20
10
0
Stress, ksi
0.000
0.020
0.040
0.060
0.080
0.100
0.120
Strain, in/in
10 day
10 day

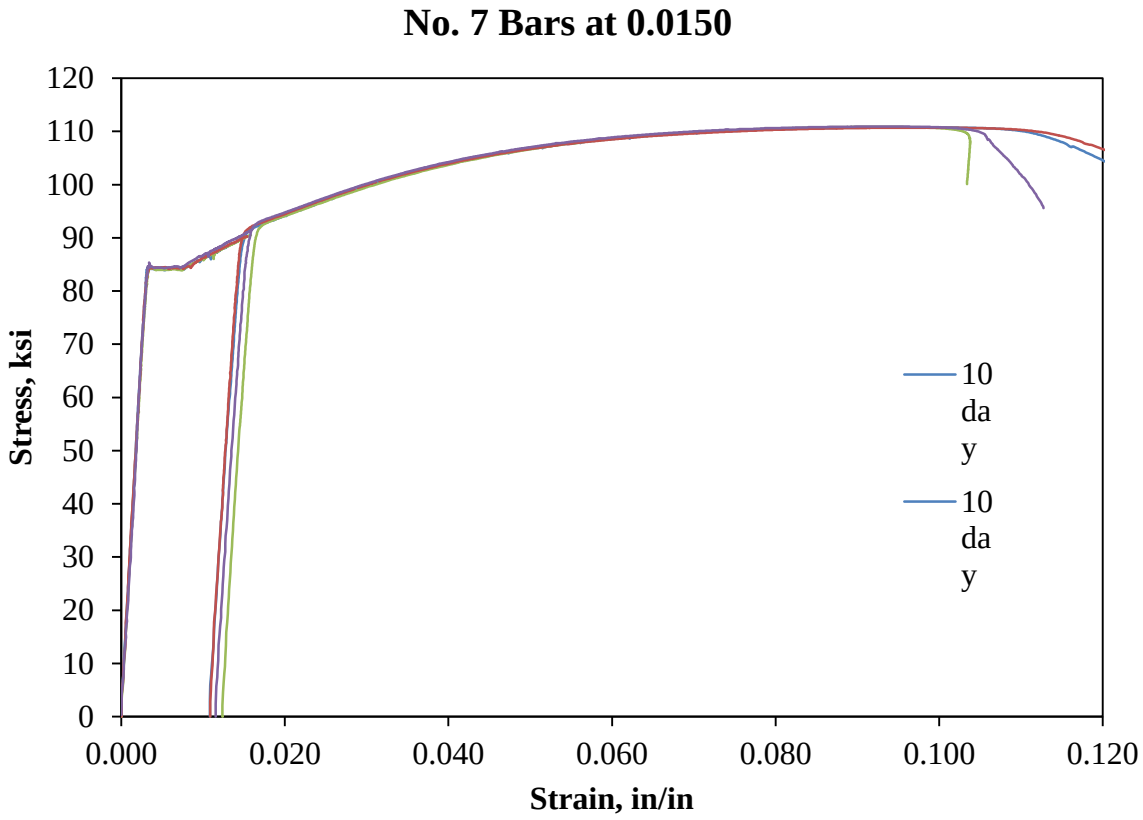
No. 7 Bars at 0.0150
Stress, ksi
120
110
100
90
80
70
60
50
40
30
20
10
0
0.000
0.020
0.040
0.060
0.080
0.100
0.120
Strain, in/in
10 day
10 day

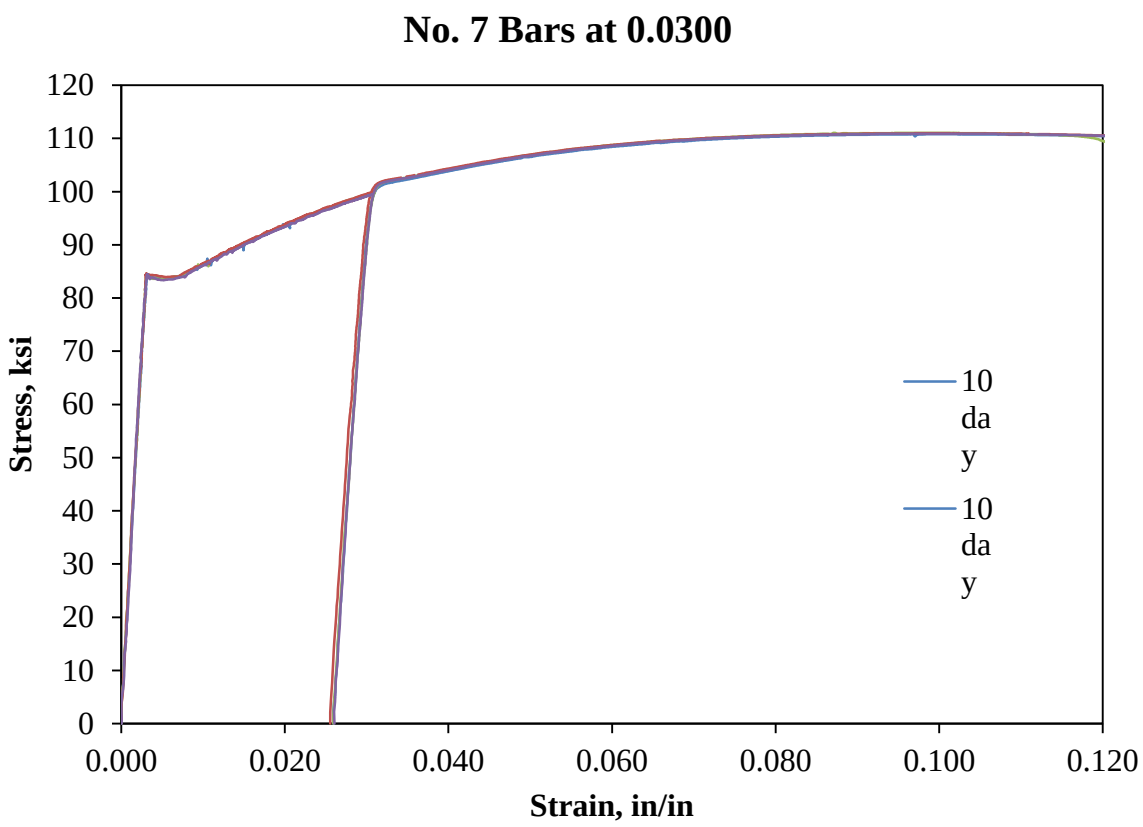
No. 7 Bars at 0.0300
120
110
100
90
80
70
60
50
40
30
20
10
0
Stress, ksi
0.000
0.020
0.040
0.060
0.080
0.100
0.120
Strain, in/in
10 day
10 day

16. APPENDIX I: ADDITIONAL NO. 7 BAR CYCLIC TEST

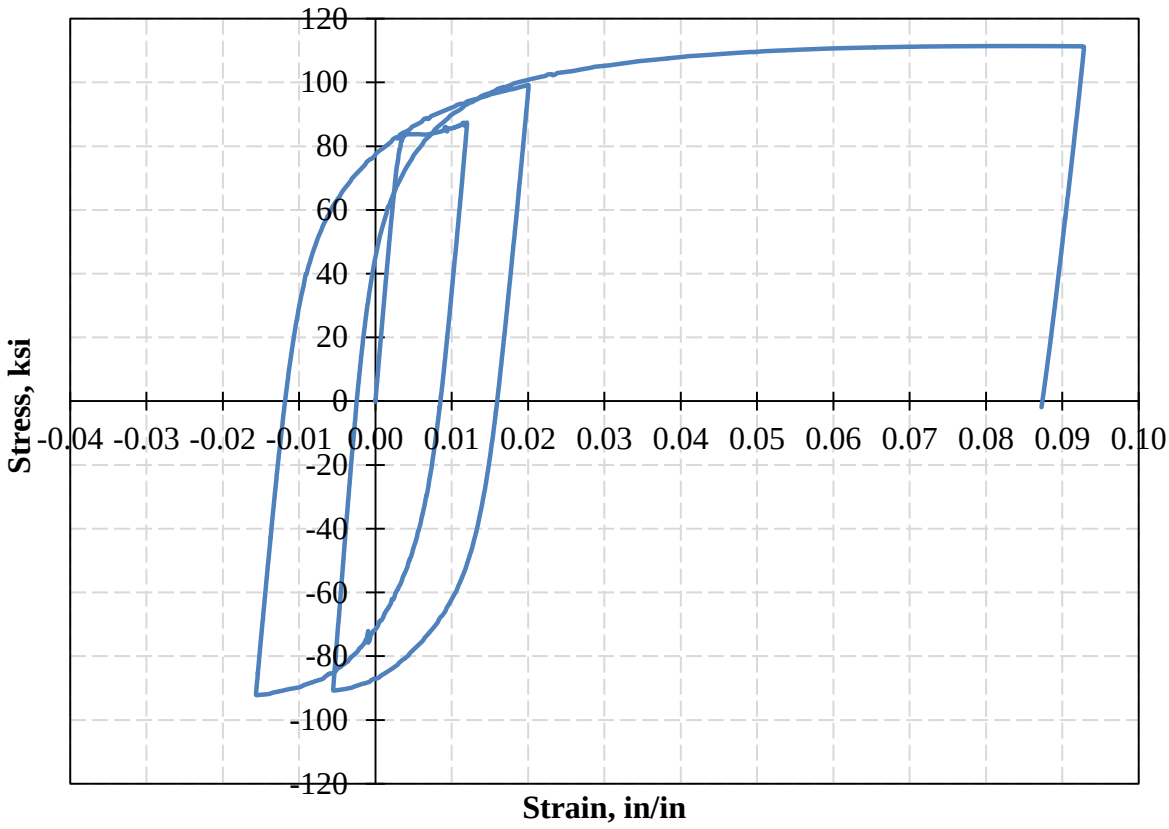

17. APPENDIX J: TEST PHOTOS

No. 4 Bars

No. 5 Bars – necked and untested

No. 6 Bars

No. 7 Bar

No. 8 Bar

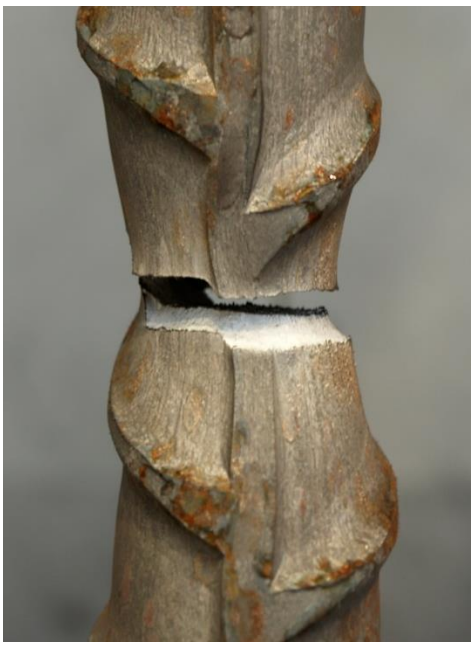

No. 9 Bar

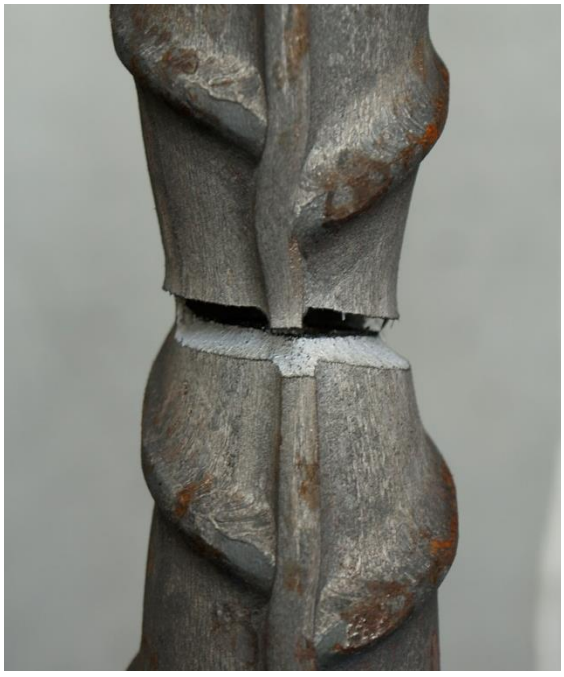

No. 10 Bar

No. 11 Bar

No. 14 Bar – mill stamp digitally removed for confidentiality

No. 18 Bar – brittle failure at grips early into necking